2008-01-01

Investigation of Millimetre Wave Generation by stimulated Brillouin scattering for Radio Over Fibre Applications

Markus Junker
Technological University Dublin

I4 Eye diagrams of back to back transmission.

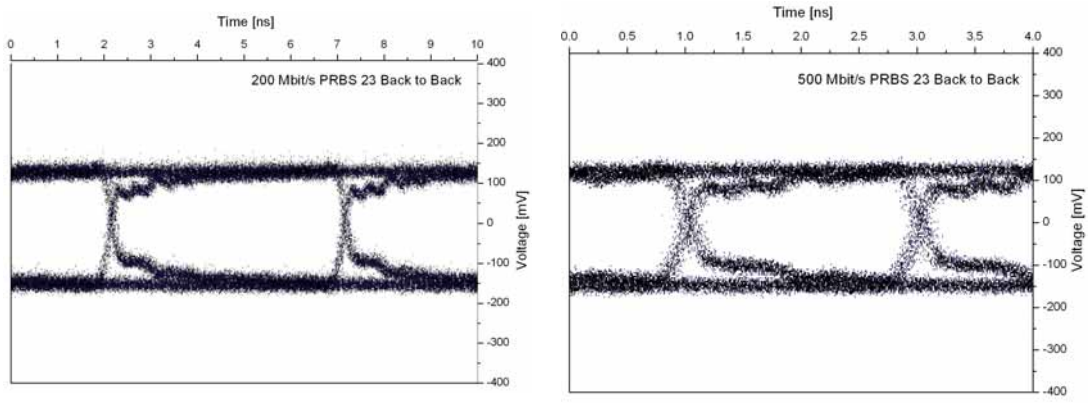

I5 Determination of standard deviation σ

Inset a: Probability Density Function (PDF) of logical "0" and "1" in the middle of the eye according to Fig. 8-7

Inset b: Gauss fit of PDF "0" with U_0 as the maximum magnitude and the standard deviation σ at the 68% area points around the centre line.

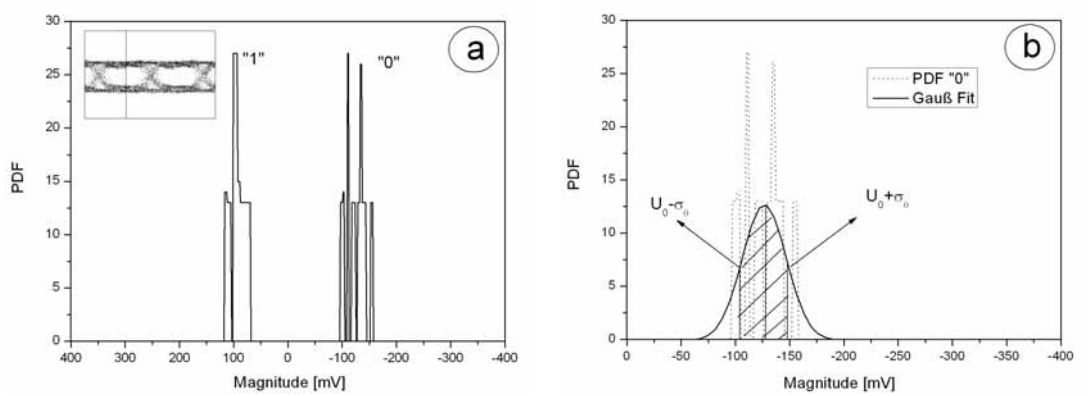

I6 Eye diagrams of 200 Mbit/s and 500 Mbit/s after radio propagation.

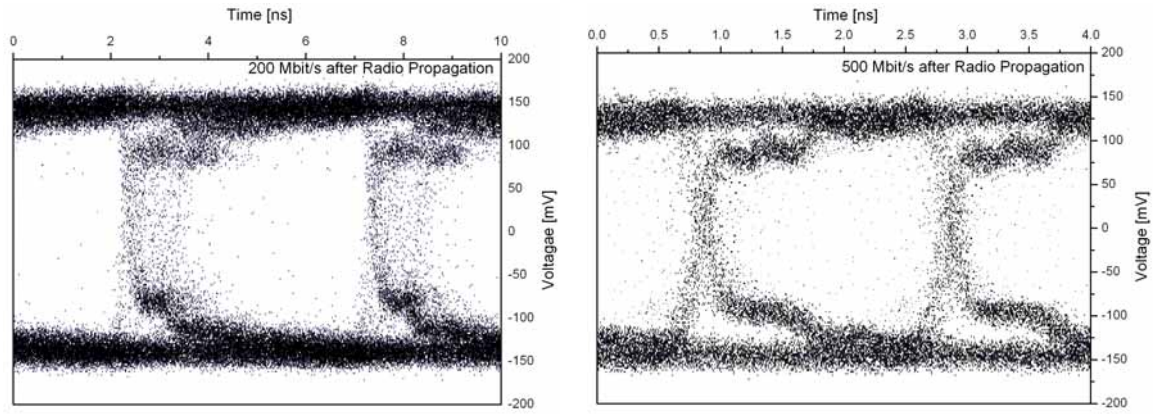

I Modulation

I1 Eye diagrams of the pulse pattern generator.

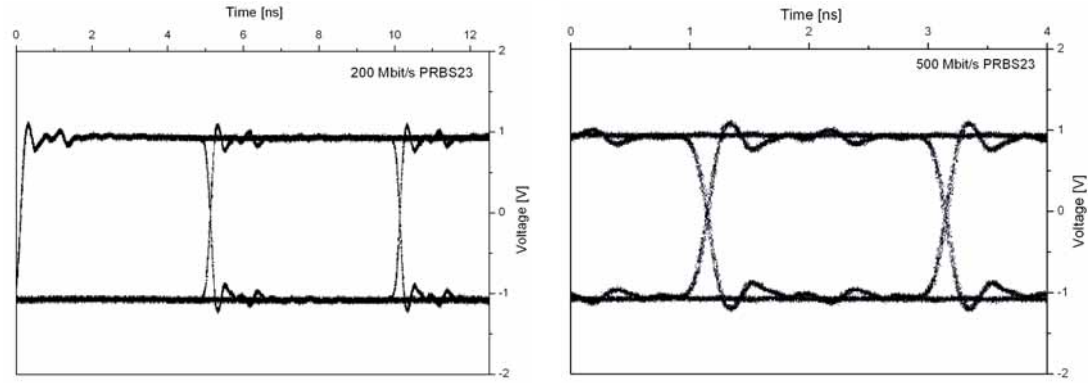

I2 Modulated RF signals at 32 GHz carrier.

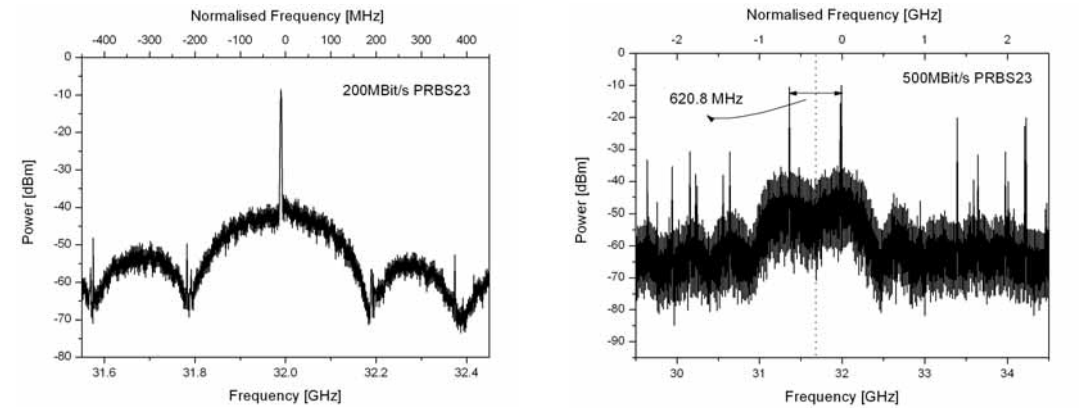

I3 Modulation signals in baseband after down conversion.

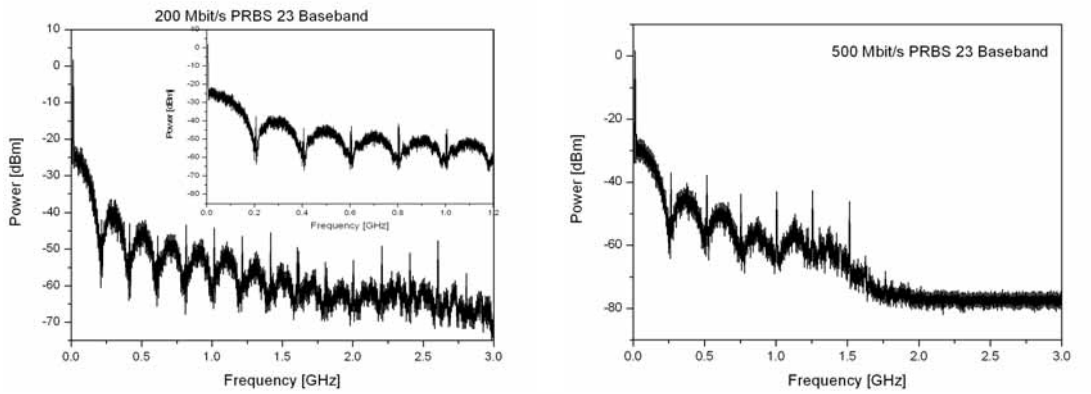

H Power fluctutains in the system set-up. The inset numbers correspond to the points in Fig. 7-16 in Sections 7.3.5.1.

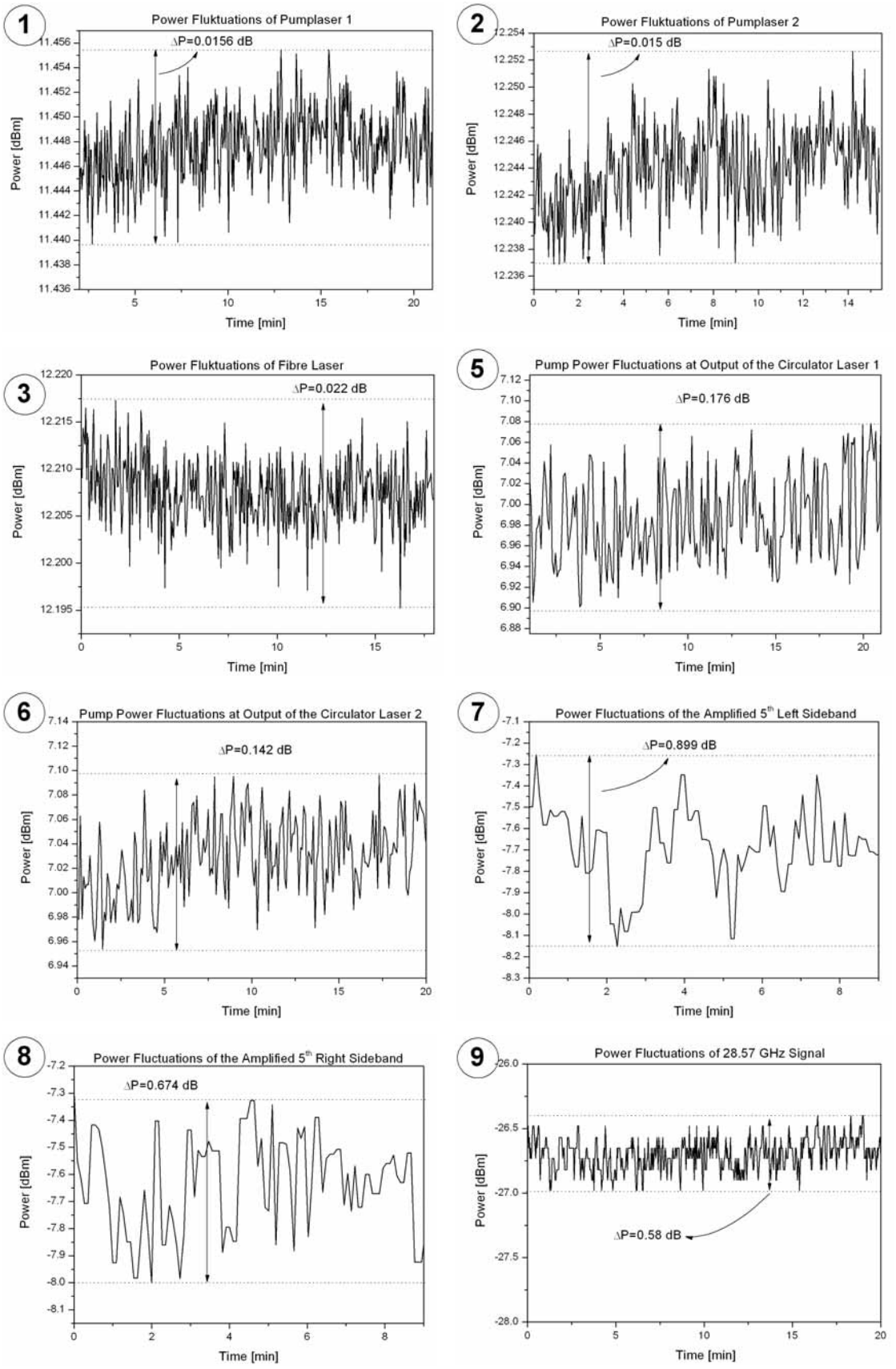

G7 Spectrum analysis of the 39.998 GHz signal (SBS amplified 7th order sidebands)

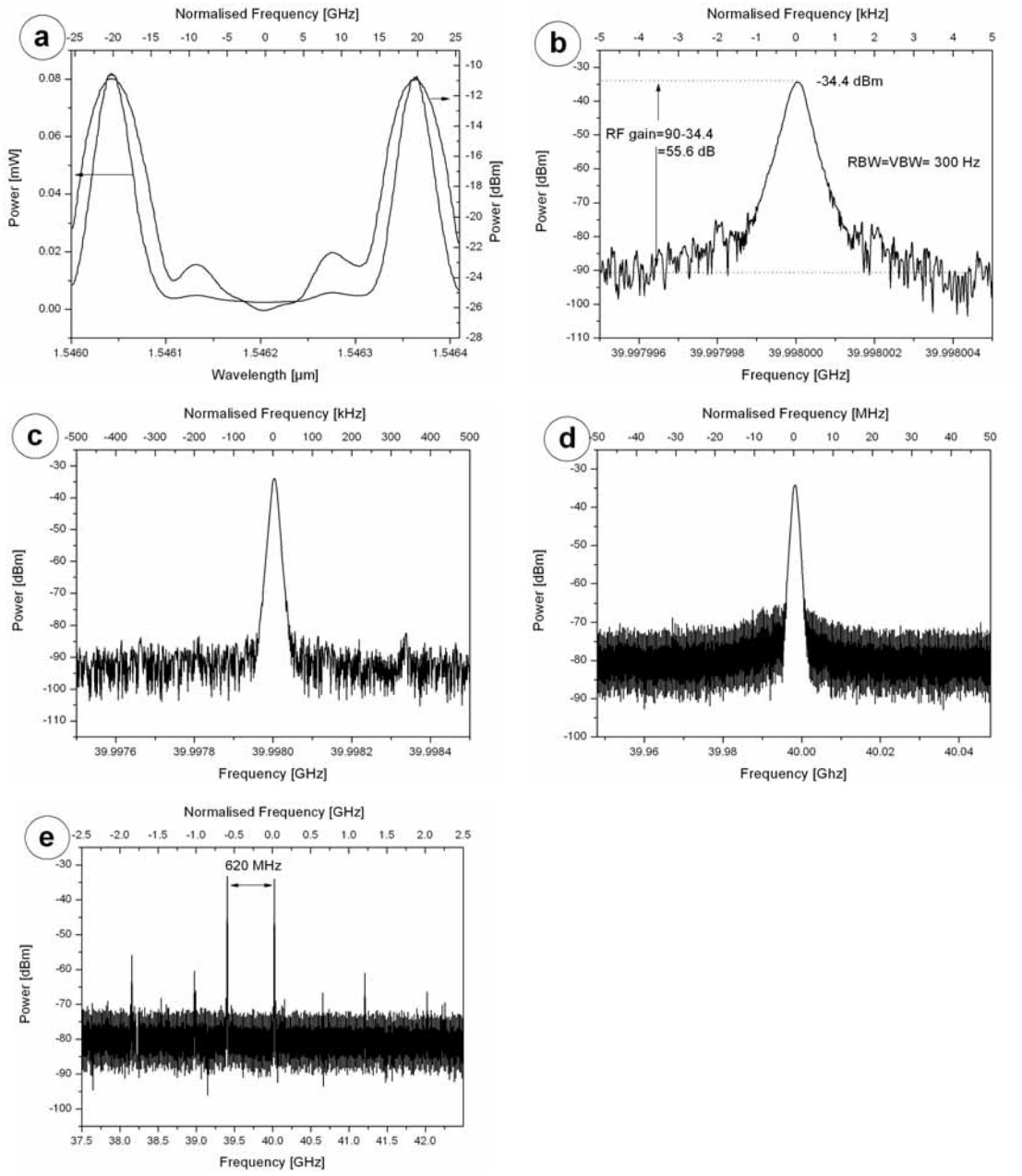

G6 Spectrum analysis of the 34.264 GHz signal (SBS amplified 6th order sidebands)

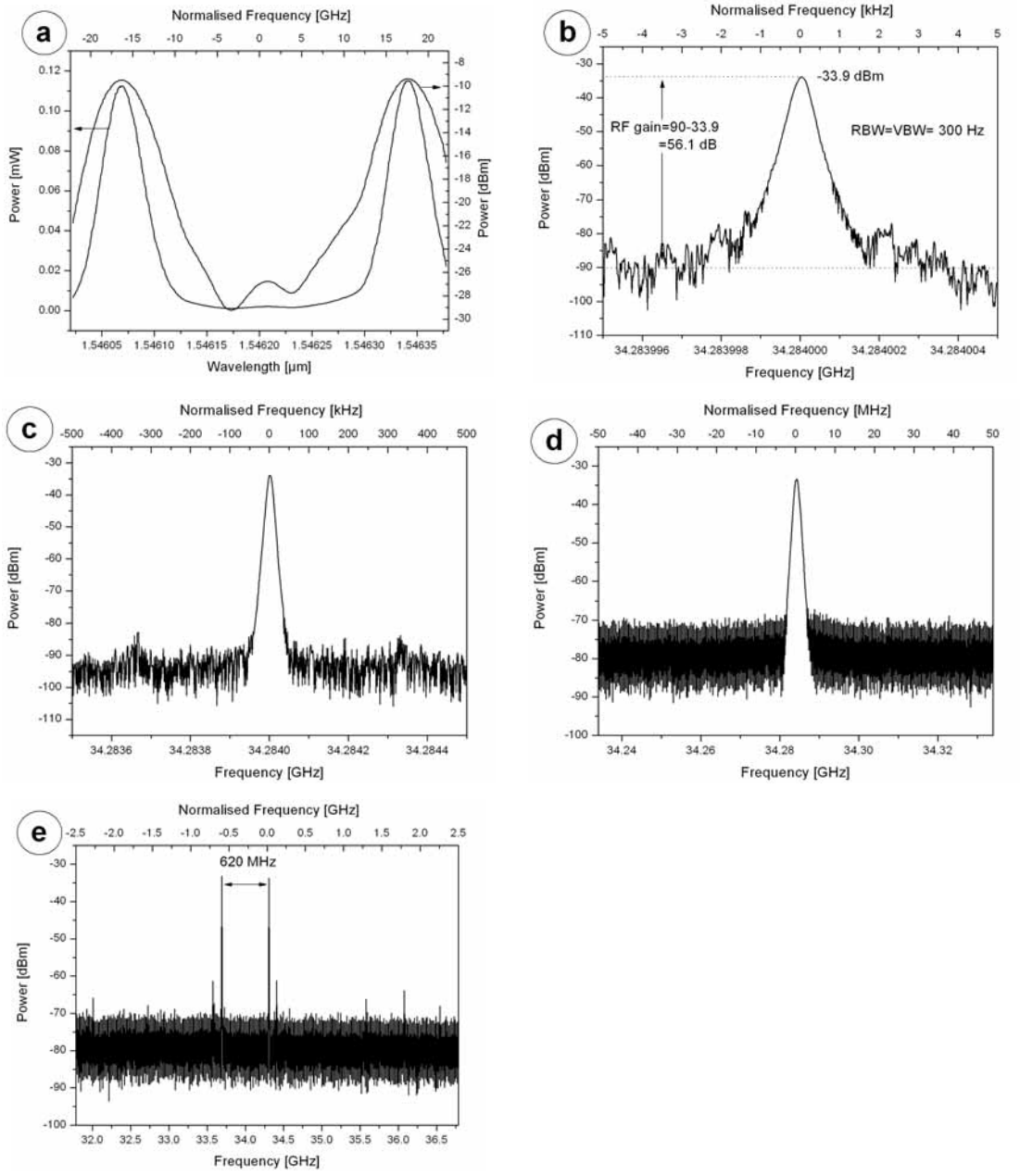

G5 Spectrum analysis of the 28.57 GHz signal (SBS amplified 5th order sidebands)

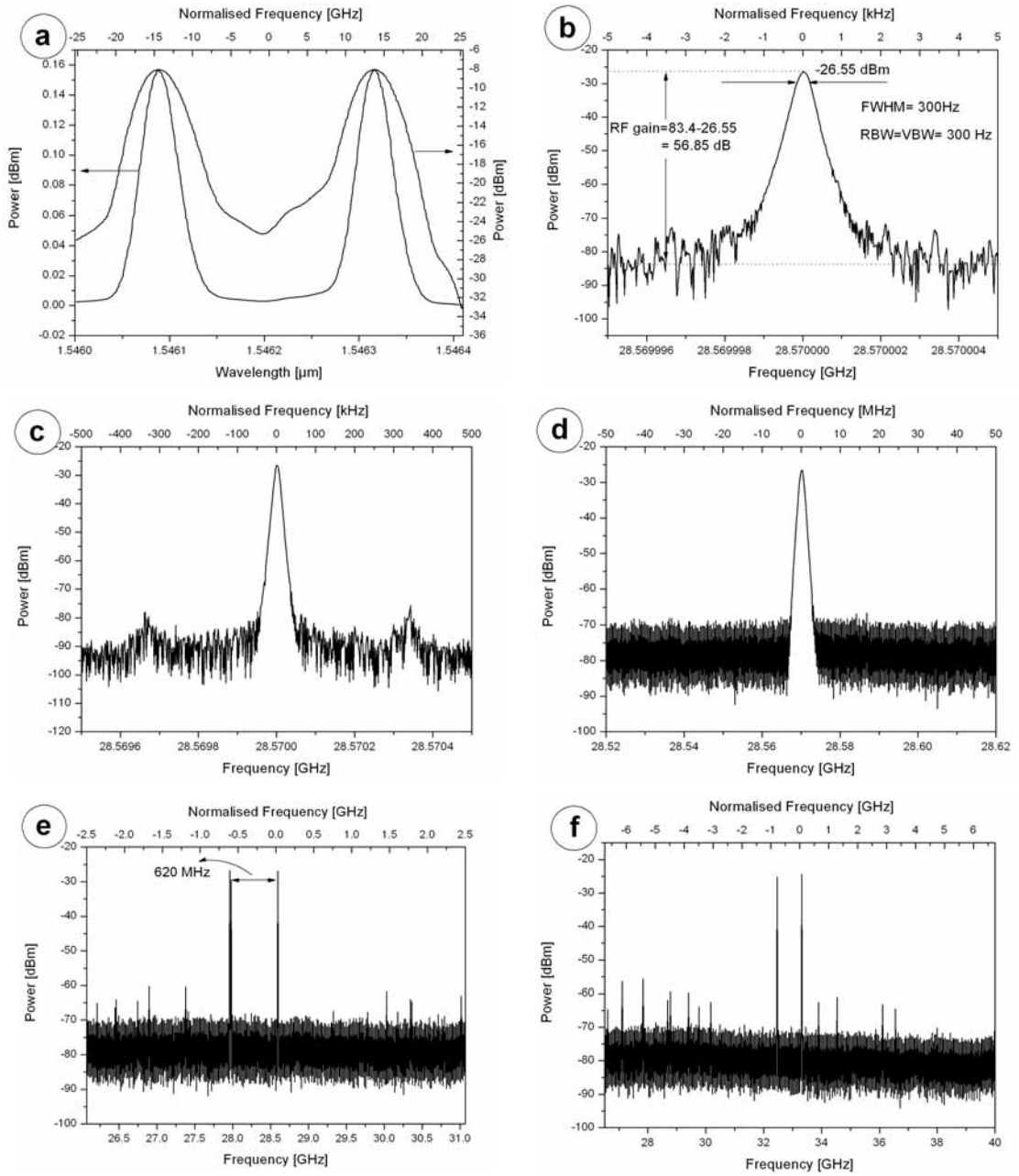

G4 Spectrum analysis of the 22.856 GHz signal (SBS amplified 4th order sidebands)

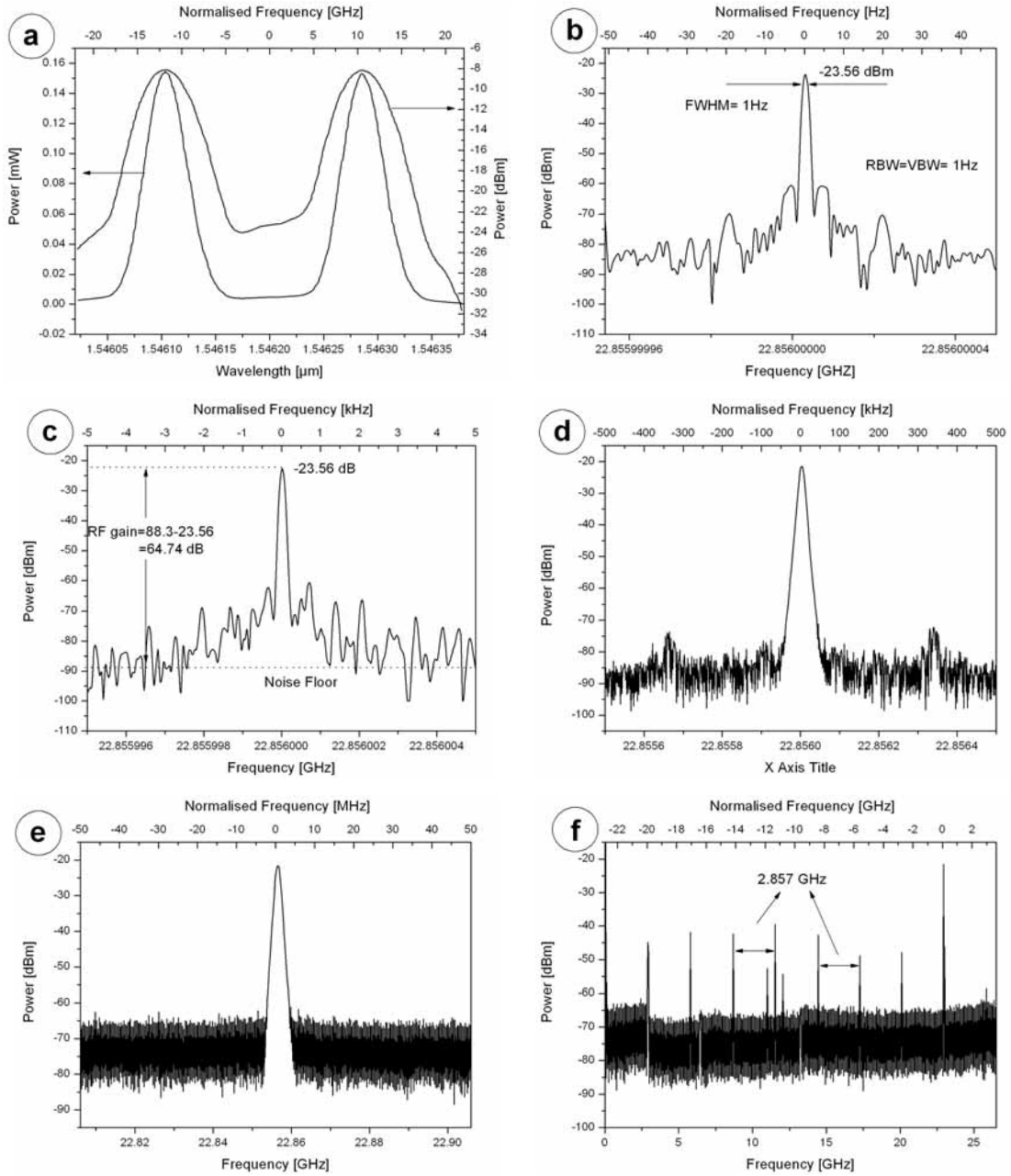

G3 Spectrum analysis of the 17.147 GHz signal (SBS amplified 3rd order sidebands)

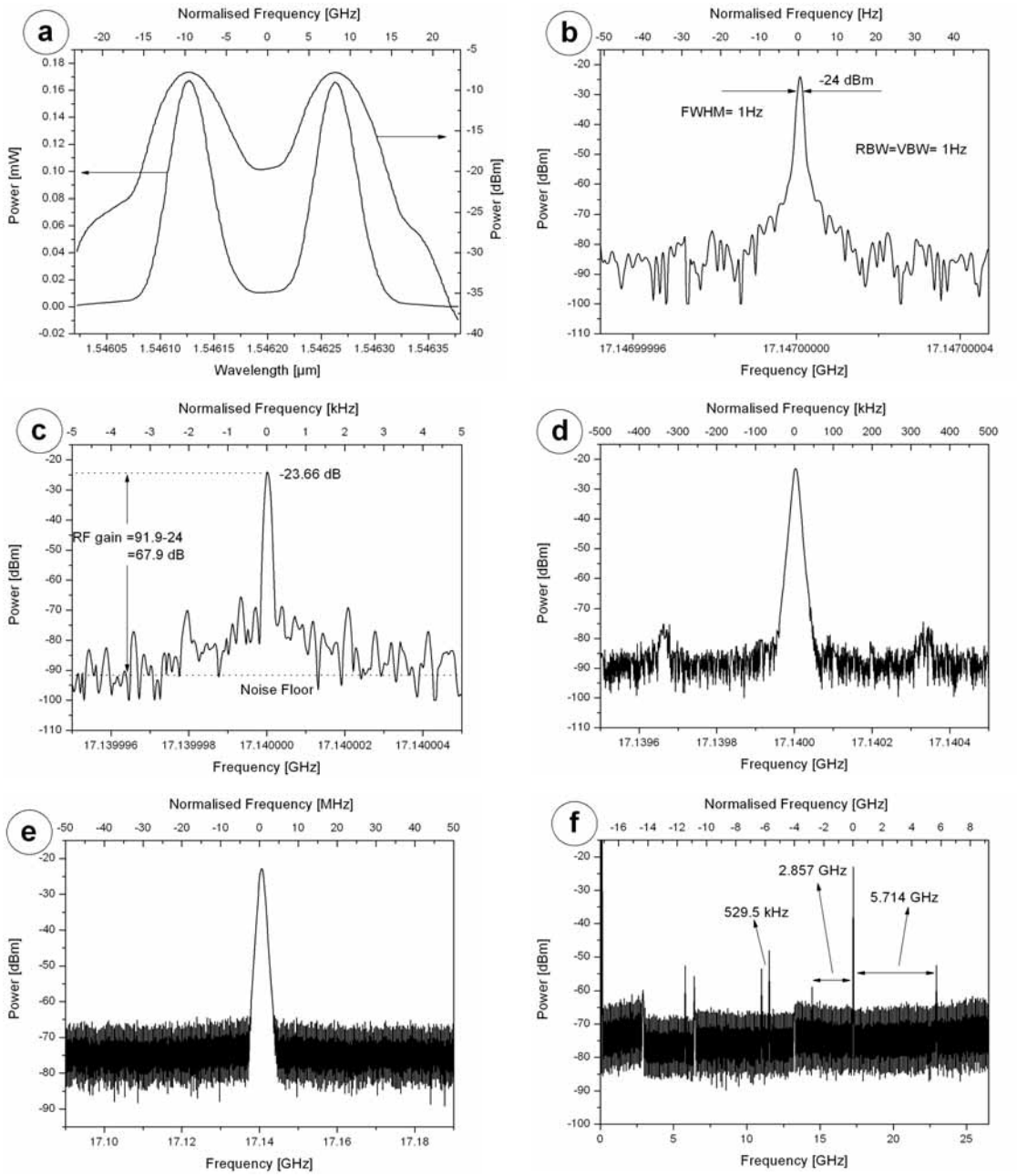

G

G2 Spectrum analysis of the 11.428 GHz signal (SBS amplified 2nd order sidebands)

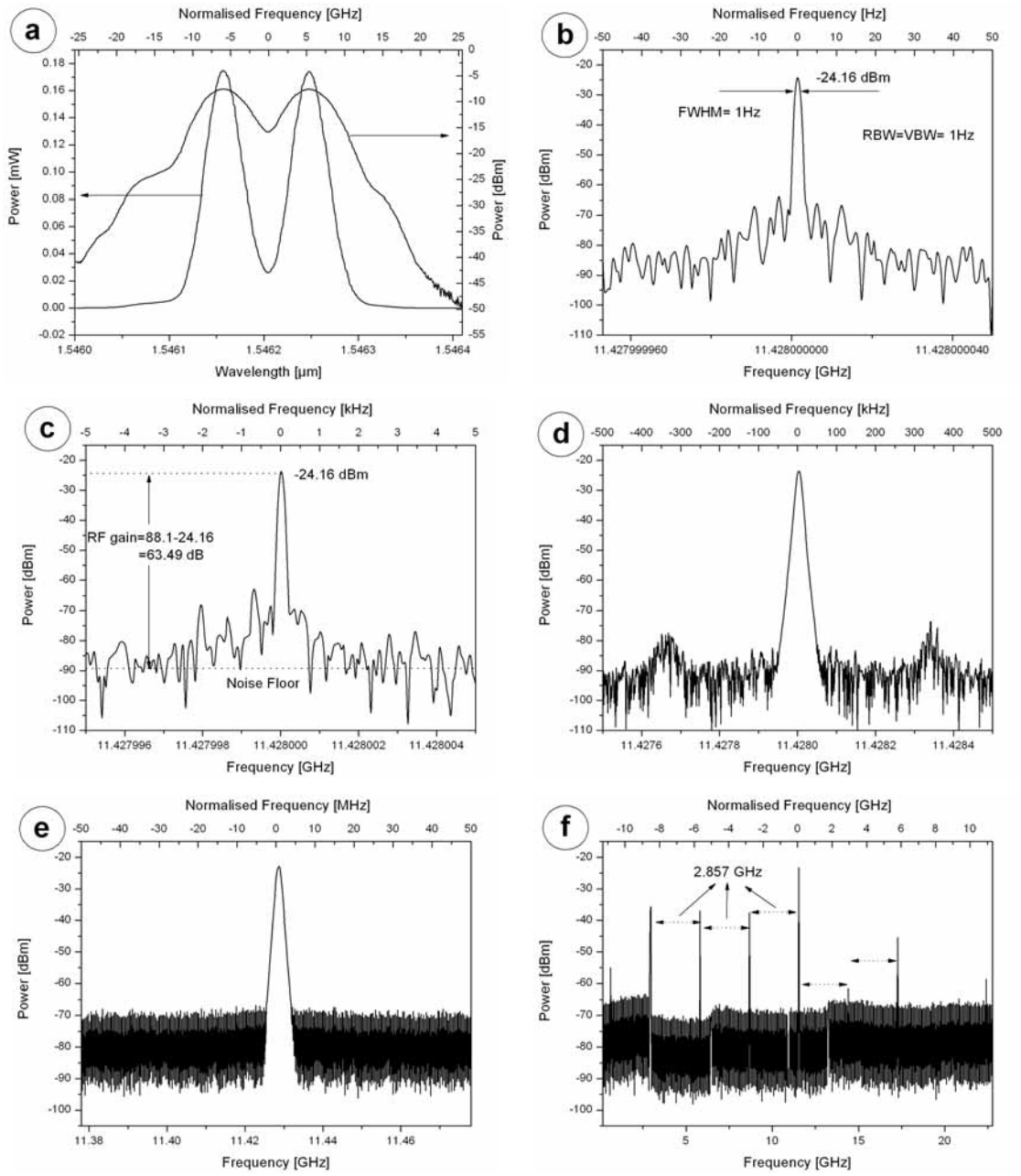

F3 S21 Parameter of the horn antennas measured at a distance of 93.4 cm.

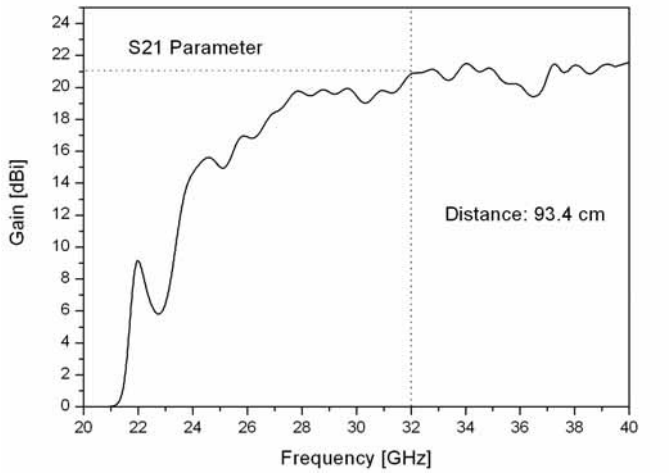

F Data sheets of the photodetector D-15ir

F1 Photodetector D-15ir.

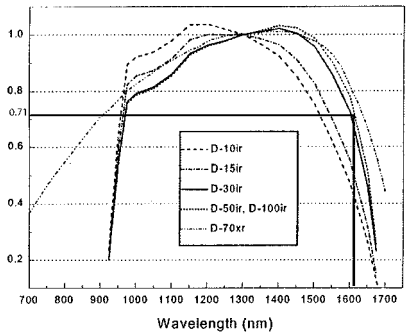

Model D-15ir

Serial No	**1357**	
Test Date	**23-Sep-04**	
Tested by	**BB**	
Responsivity	**0.72**	A/W @ 1310 nm
Pulse duration	**13.5**	ps
Risetime	**13.7**	ps

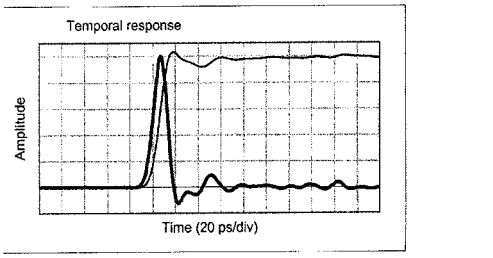

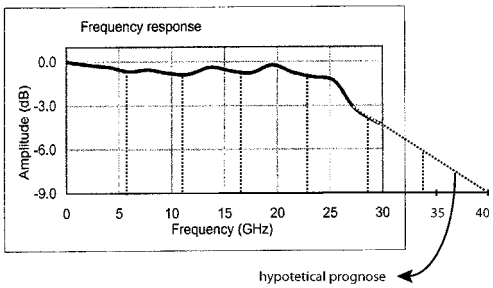

F2 S21 Amplification characteristic of the receiver unit (see Section 8.2.2).

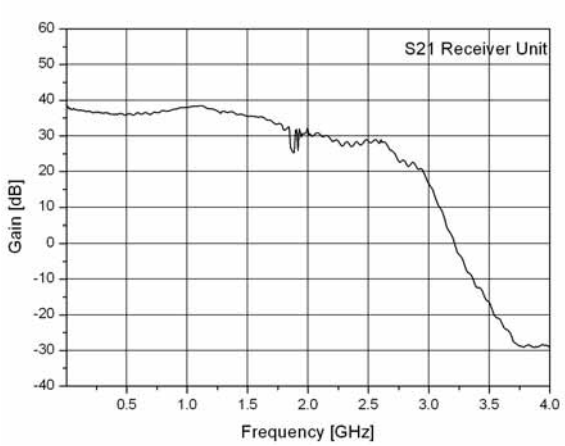

E6 (see Sections 8.1 and 8.4)

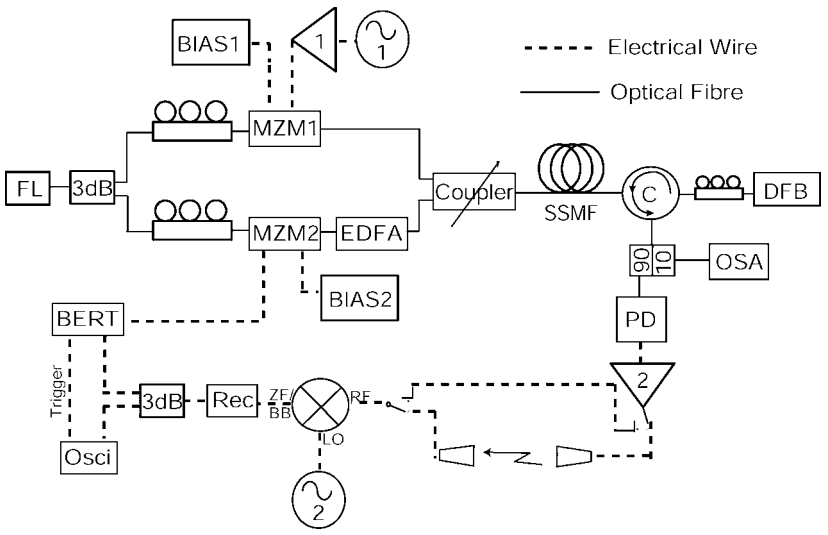

Symbol	Descriptions, comments
OSA	Optical Spectrum Analyser Agilent 86143B
BIAS1	Conventional Power Supply Voltage=4.5 V
BIAS2	Conventional Power Supply Voltage=±9 V
MZM1	Mach-Zehnder Modulator 10 Gbit/s; P_{Fin}=3.5 mW
MZM2	Mach-Zehnder Modulator with intergraed Treiber, 10 Gbit/s; P_{Fin}=3.5 mW
FL	Fibre Laser Koheras Adjustic E 15 P_{out}=16.5 mW; λ=1550 nm; Linewidth: < 1 kHz
HF Source 1	Agilent E8257C *f*=6.4 GHz
HF Amplifier 1	Quin Star QPJ 06183630 AO 6-18 GHz; P_{out}=35 dBm
HF Source 2	Agilent E8257C *f*=16 GHz, P_{out} 18 dBm
HF Amplifier 2	HP 83050A P_{out}=-7 dBm
SSMF	Standard Single Mode Fibre: L= 50.45 km (for details see app A)
PD	Photo Detector: Newport D-15ir; BW= 27 GHz, P_{in}= -1 dBm
Coupler	Tunable Coupler
DFB	Distributed Feedback Laserdiode, Bandwidth 3 MHz P_{Pump}=4.1 mW I_{LD} &=52.9, R_{Therm} 7746.3 Ω
10/90	90% 10% coupler
ESA	Electrical Spectrum Analyser HP 8563 E
MIX	External Harmonic Mixer 11790A Agilent 26.5-40 GHz
EDFA	Erbium Doped Amplifier Highwave WHT C23 G23
3 dB	Optical/ Electrical 3 dB Splitter
C	Optical Circulator
Horn Antennas	High gain (20 dB @ 32 GHz) distance: 5 cm
Rec	Receiver unit; low gain amplifier (g_{max} = 39.5 dB @ 1.1 GHz; $g_{6.5dB}$ @ 1.71 GHz; g_{0dB} @ 3.21 GHz)
Osci	Tectronix Oscilloscope TDS 5104; 1 GHz
BERT	Anritsu MU163220C 3.2G PPG

E5 (see sections 7.3.3 and 7.3.4.1)

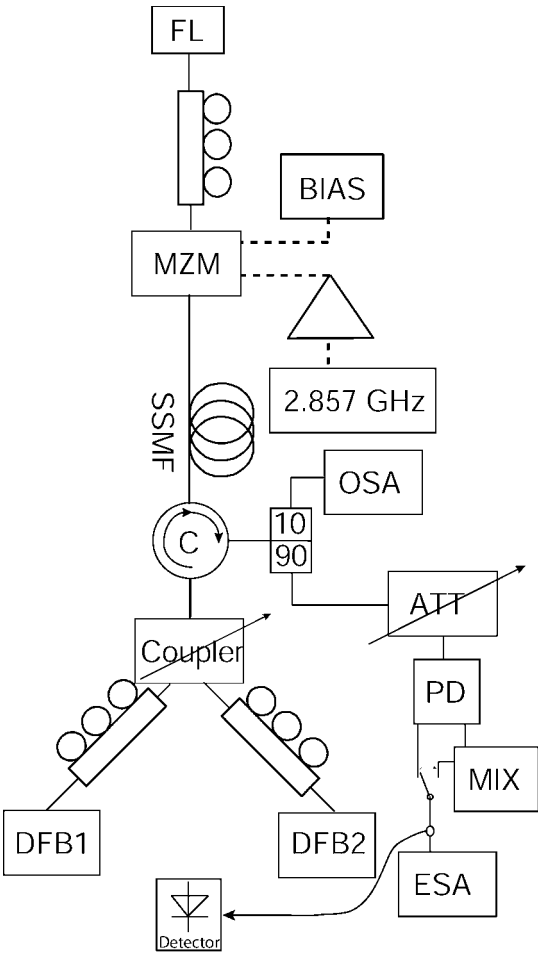

Symbol (Bold Sym. are explained in the setting table)	**Descriptions, comments**
OSA	Optical Spectrum Analyser Agilent 86143B
BIAS	Conventional Power Supply Voltage=see table
MZM	Mach-Zehnder Modulator 10 Gbit/s; P_{Fin}=see table
FL	Fibre Laser Koheras Adjustic E 15 P_{out}=17 mW; λ=1550 nm; Linewidth: < 1 kHz
2.875GHz	HF source Agilent E8257C
HF Amplifier	Bonn BLMA OB42-3
SSMF	Standard Single Mode Fibre: L= 50.45 km (for details see app A)
PD	Photo Detector: Newport D-15ir; BW= 27 GHz, P_{inMAX}= 0 dBm
Coupler	Tunable Coupler P_{out}= 5 mW/ Pump Laser
Att	Tunable Attanuator α= see table
DFB	Distributed Feedback Laserdiode Bandwidth 3 MHz P_{outMAX}=20 mW I_{LD} &R_{Therm} see table
10/90	90% 10% coupler
ESA	Electrical Spectrum Analyser HP 8563 E
MIX	External Harmonic Mixer 11790A Agilent 26.5-40 GHz See table
Detector	Detector Diode Agilent 8473B 0.01-18 GHz Inserted between PD/MIX and ESA for amplitude noise measurements
C	Optical Circulator

Settings: I_{LD}= Injection Current

R_{Therm}= Thermistor Resistor Value

Sideband	**Frequency [GHz]**	**U_{Bias} [V]**	**P_{MZM} [W]**	**Att**	**MIX**	**DFB1**		**DFB2**	
						I_{LD} [mA]	R_{Therm} [Ω]	I_{LD} [mA]	R_{Therm} [Ω]
1	5.714	0	0.273	4.6	no	121	6231.0	109	9390.0
2	11.428	-4.3	1.096	4.6	no	121	6295.5	109	9288.3
3	17.142	0	1.096	4.4	no	121	6361.4	109	9188.9
4	22.856	-4.06	2.041	3.9	no	121	6427.9	109	9090.1
5	28.57	0.1	2.958	3.9	yes	121	6495.0	109	8992.2
6	34.284	+3.9	2.958	3.7	yes	121	6561.4	109	8893.1
7	39.998	-0.1	2.958	2.6	yes	121	6630.8	109	8798.7

E3 (see Section 7.3)

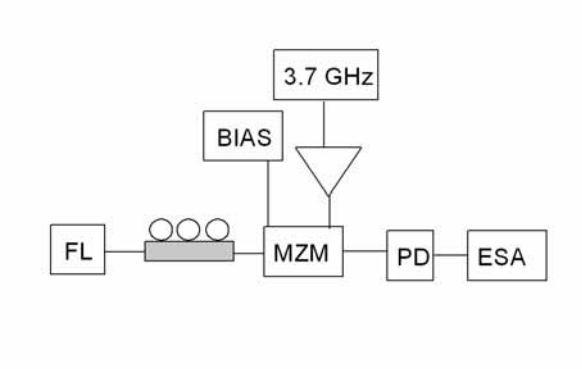

Symbol	Descriptions, comments
ESA	Electrical Spectrum Analyser HP 8563 E
PD	Photo Detector: Newport D-15ir; BW= 27 GHz, P_{inMAX}= 0 dBm
MZM	Mach-Zehnder Modulator 10 Gbit/s; P_{Fin}=3 W
FL	Fibre Laser Koheras Adjustic E 15 P_{out}=17 mW; λ=1550 nm; Linewidth: < 1 kHz
3.7 GHz	HF source Agilent E8257C
HF Amplifier	Bonn BLMA OB42-3

E4 (see Section 7.3.1)

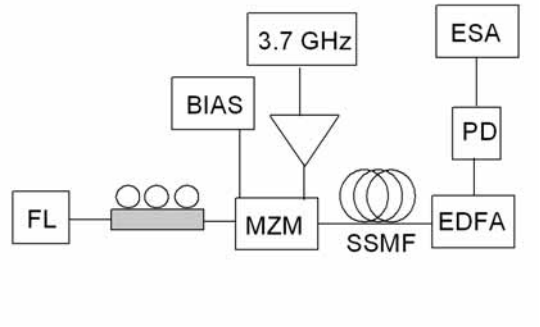

Symbol	Descriptions, comments
ESA	Electrical Spectrum Analyser HP 8563 E
PD	Photo Detector: Newport D-15ir; BW= 27 GHz P_{inMAX}= 0 dBm
MZM	Mach-Zehnder Modulator 10 Gbit/s; P_{Fin}=3 W
FL	Fibre Laser Koheras Adjustic E 15 P_{out}=17 mW; λ=1550 nm; Linewidth: < 1 kHz
3.7 GHz	HF source Agilent E8257C
HF Amplifier	Bonn BLMA OB42-3
SSMF	Standard Single Mode Fibre: L= 50.45 km (for details see app A)
EDFA	Erbium Doped Fibre Amplifier: Gain = 30 dB

E Experiments

E1 (see Section 7.1)

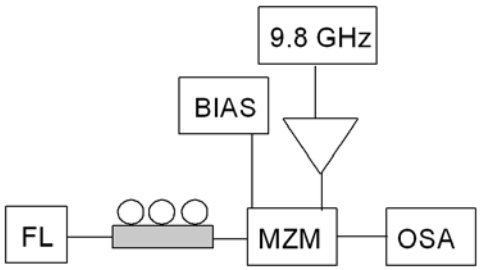

Symbol	Descriptions, comments							
	SB	1	2	3	4	5	6	7
BIAS	Conventional Power Supply Voltage=[V]	1.578	6.964	-4.22	1.108	8.058	1.17	-6.65
MZM	Mach-Zehnder Modulator 10 Gbit/s; P_{Fin}=[dBm]	25.47	32.32	35.94	36.3	36.3	36.3	36.3
FL	Fibre Laser Koheras Adjustic E 15 P_{out}=18 mW; λ=1550.3 nm; Linewidth: < 1 kHz							
10 GHz	HF source Agilent E8257C							
HF Amp-lifier	Bonn BLMA OB42-3							
OSA	Optical Spectrum Analyser Agilent 86143B							

E2 (see Section 7.2)

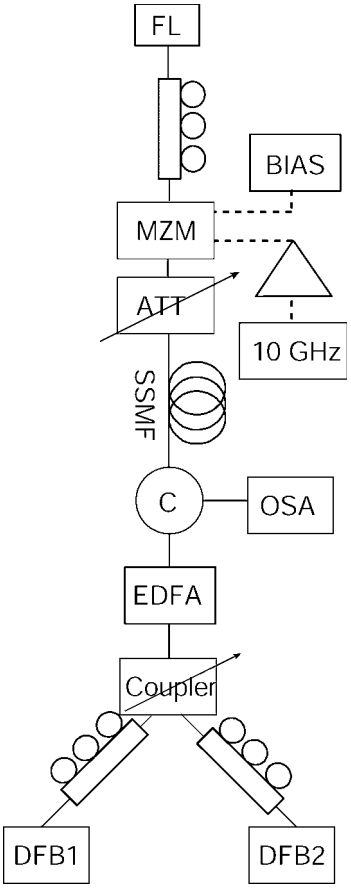

Symbol	Descriptions, comments
OSA	Optical Spectrum Analyser Agilent 86143B
BIAS	Conventional Power Supply Voltage=0.3 V
MZM	Mach-Zehnder Modulator 10 Gbit/s; P_{Fin}=0.346 W
FL	Fibre Laser Koheras Adjustic E 15 P_{out}=17 mW; λ=1550 nm; Linewidth: < 1 kHz
10 GHz	HF source Agilent E8257C
HF Amplifier	Bonn BLMA OB42-3
SSMF	Standard Single Mode Fibre: L= 50.45 km (for details see app A)
EDFA	Erbium Doped Fibre Amplifier: P_{out}/Pumpsignal=2,3,4,5,6,7,8 m W
Coupler	Tunable Coupler
Att	Tunable Attanuator P_{oui}/Sideband=0.7,7.2,52.9,244.3, 585,621.4,740.7 µW
DFB	Distributed Feedback Laserdiode Bandwidth 3 MHz
C	Optical Circulator

D Characteristics for the definition of the optimum fibre length (relationship between SBS amplified sidebands 1-5 and the undesired sidebands (left column) and the corresponding derivatives (right column)).

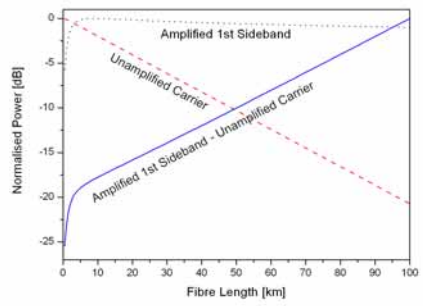

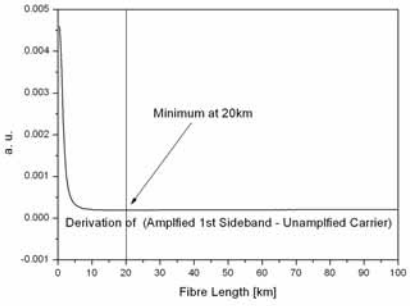

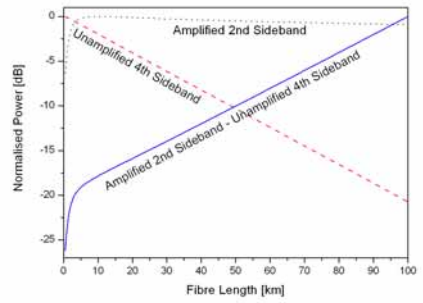

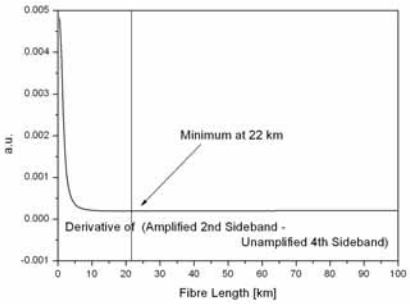

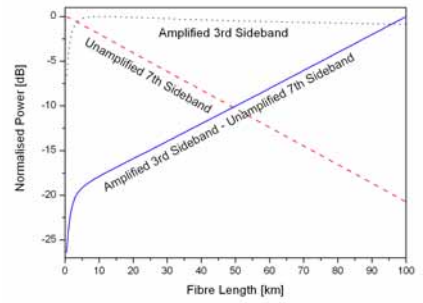

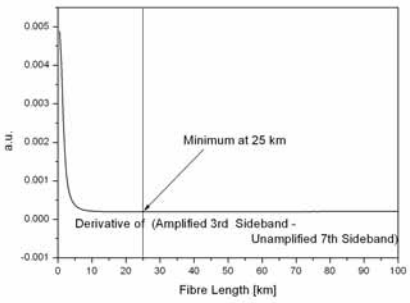

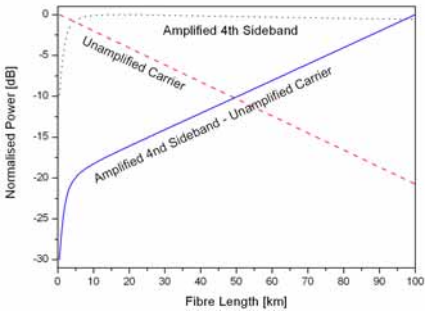

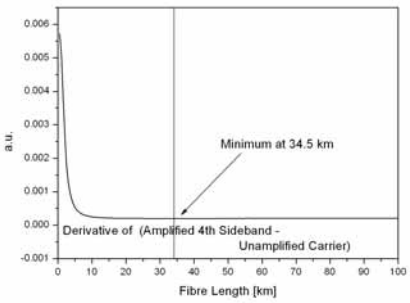

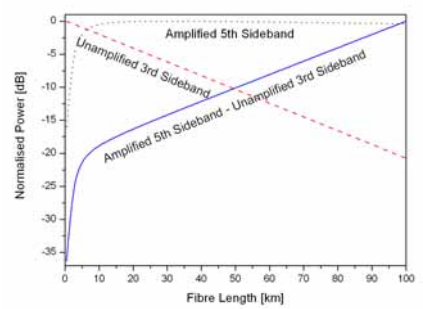

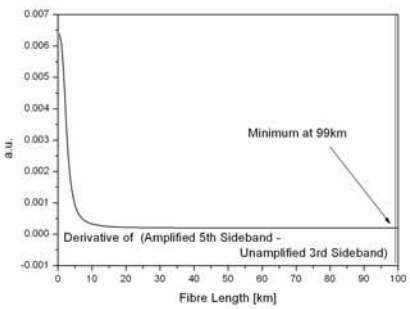

C

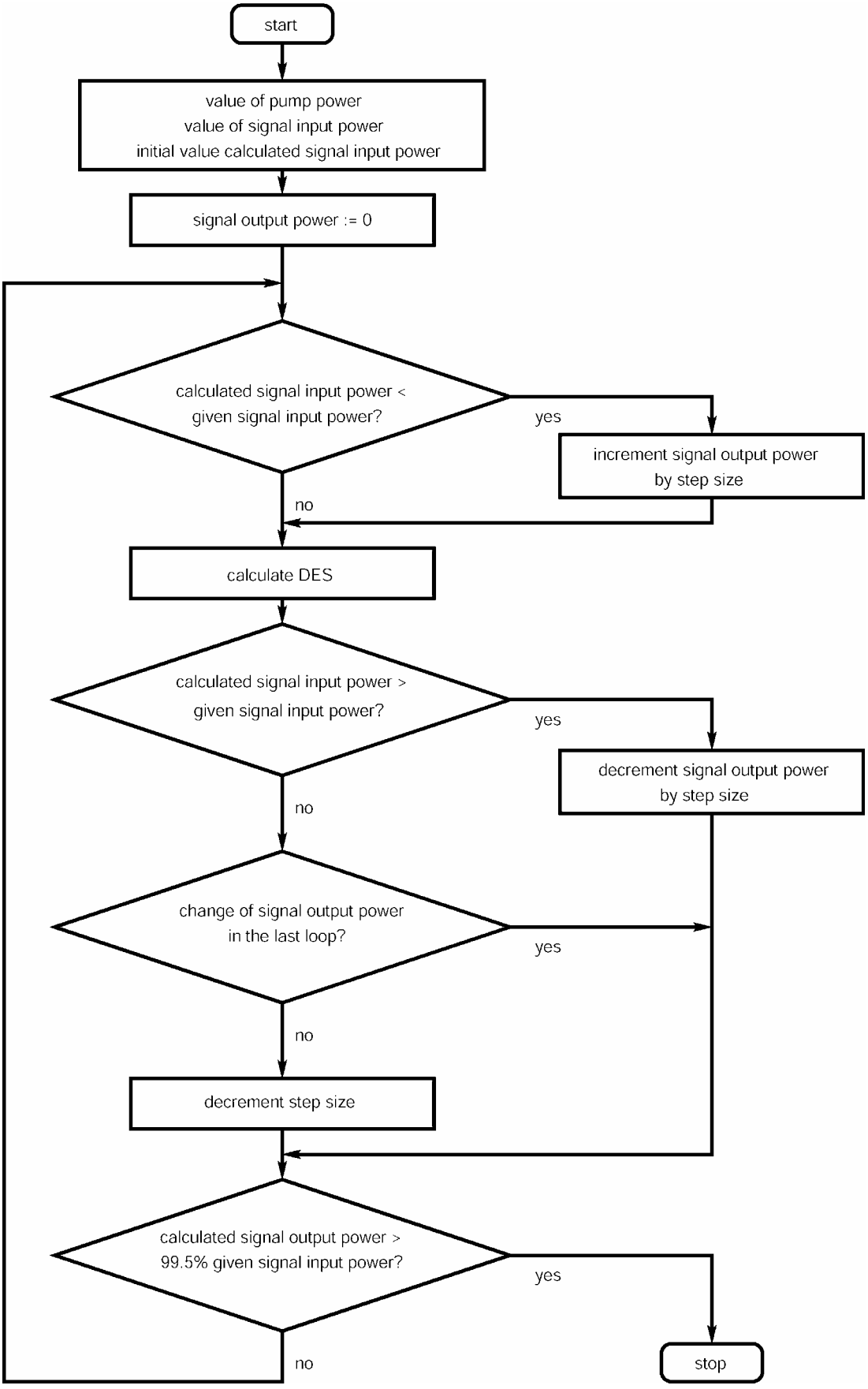
start
value of pump power
value of signal input power
initial value calculated signal input power
signal output power := 0
calculated signal input power <
given signal input power?
yes
increment signal output power
by step size
no
calculate DES
calculated signal input power >
given signal input power?
yes
decrement signal output power
by step size
no
change of signal output power
in the last loop?
yes
no
decrement step size
calculated signal output power >
99.5% given signal input power?
yes
no
stop

B

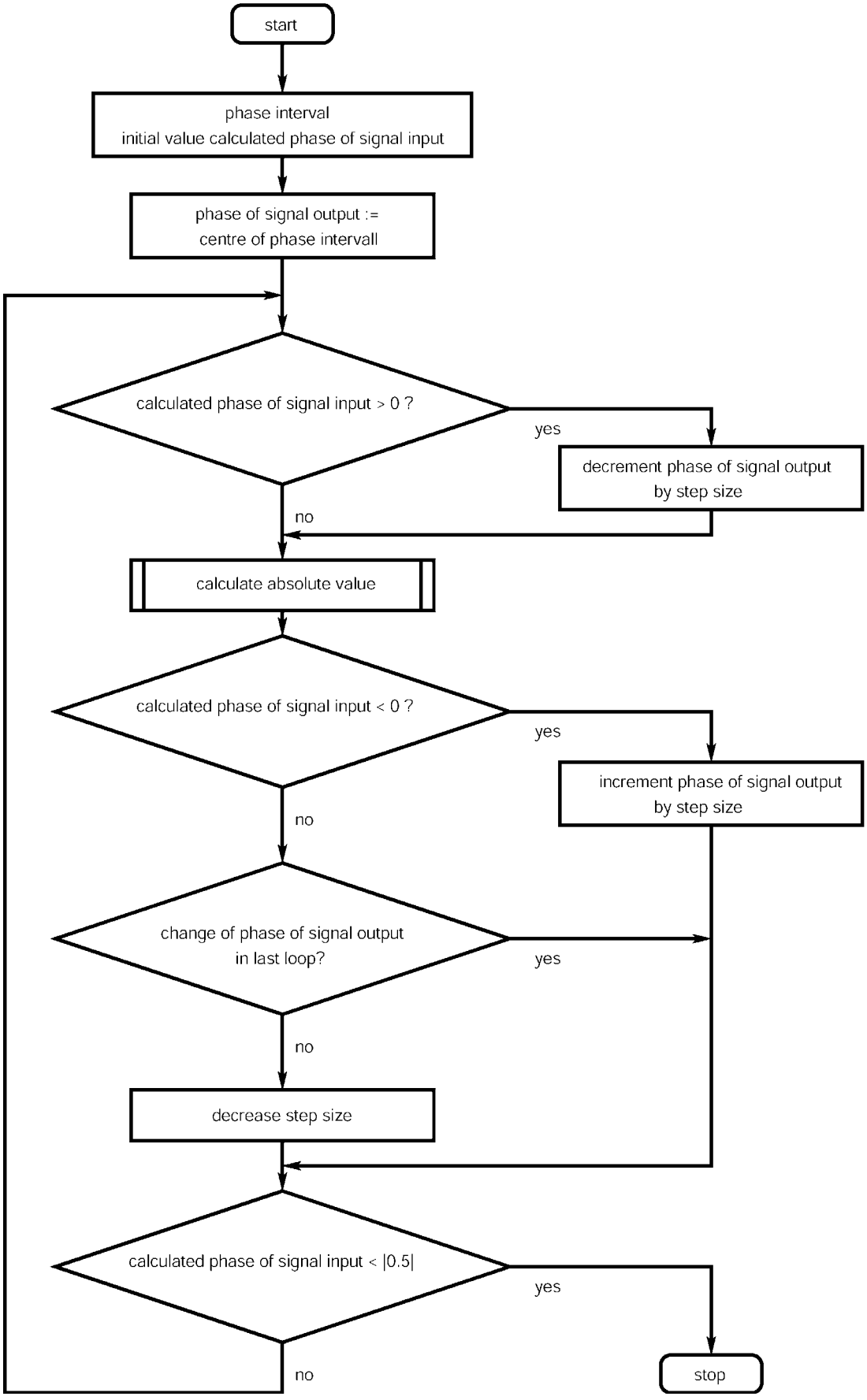
start
phase interval
initial value calculated phase of signal input
phase of signal output :=
centre of phase intervall
calculated phase of signal input > 0 ?
yes
decrement phase of signal output
by step size
no
calculate absolute value
calculated phase of signal input < 0 ?
yes
increment phase of signal output
by step size
no
change of phase of signal output
in last loop?
yes
no
decrease step size
calculated phase of signal input < |0.5|
yes
no
stop

14 Appendix

A

Since the experimental set-ups of this thesis always use the same SSMF fibre, the most important parameters are given here as an overview. Also calculated properties of Chapter 4 are included. As a reference value the wavelength is set to be 1550 nm.

Property of the used SSMF	**Symbol**	**Value**
Length	L	50.45 km
Effective length	L_{eff}	18.94 km
Attenuation	α	0.209 dB
Effective core area	A_{eff}	86 μm^2
Brillouin shift (measured)	f_a	10.727 GHz
Refractive index	n	1.44
Brillouin threshold	P_0^S	6.35 mW
Maximum Brillouin gain	g_{Bmax}	$2.25 \cdot 10^{-11}$ m/W
Natural Brillouin gain bandwidth	Δf_a	28 MHz
Dispersion	D	16.87 ps/km·nm
Speed of light in the fibre	c	207.6 Mm/s

[32] R. Henker, T. Schneider, A. Wiatrek, K.-U. Lauterbach, **M. Junker**, M.J. Ammann, A.T. Schwarzbacher, "Optimisation of optical signal delay in slow-light systems based on stimulated Brillouin scattering," *IET Irish Signals and Systems Conference 2008,* paper PS-2.5, Galway, Ireland, June 2008.

[33] K.-U. Lauterbach, R. Henker, **M. Junker**, A. Wiatrek, A.T. Schwarzbacher, M.J. Ammann, and T. Schneider, "High resolution spectroscopy on optical signals in fiber communication systems," *IEEE 2008 International Students and Young Scientists Workshop "Photonics and Microsystems", Wroclaw/Szklarska Poreba, Poland, June 2008, in press.*

[34] A. Wiatrek, T. Schneider, **M. Junker**, R. Henker, K.-U. Lauterbach, A.T. Schwarzbacher, M.J. Ammann, "Numerical investigation of Brillouin based double sideband amplification for millimeter-wave generation," *IEEE 2008 International Students and Young Scientists Workshop "Photonics and Microsystems", Wroclaw/Szklarska Poreba, Poland, June 2008, in press.*

[35] T. Schneider, R. Henker, K.-U. Lauterbach, **M. Junker**, "Delay limits of SBS based slow light," *Slow and Fast Light Topical Meeting and Tabletop Exhibit (SL) '08,* paper (STuC4), Boston, Massachusetts, USA, July 2008 (Optical Society of America, Wash., D.C., 2008), accepted for publication.

[36] **M. Junker**, T. Schneider, K.-U. Lauterbach, R. Henker, M.J. Ammann, A.T. Schwarzbacher, "1 Gbit/s radio over fiber downlink at a 32 GHz carrier," *34rd European Conference and Exhibition on Optical Communication (ECOC) '08,* paper Tu.3.F.2, Brussels, Belgium, Sept. 2008, accepted for publication.

[37] **M. Junker**, T. Schneider, K.-U. Lauterbach, R. Henker, M.J. Ammann, A.T. Schwarzbacher, "1 Gb/s Ka-band 50 km radio over fiber downlink," submitted to *IEEE Transaction on Mircowave Theory and Techniques*.

[24] T. Schneider, R. Henker, K.-U. Lauterbach, **M. Junker**, "Adapting the Brillouin spectrum for slow light delays," *Electronics Letters*, Vol. 43, No. 12, pp. 682 – 683, July 2007.

[25] T. Schneider, R. Henker, K.-U. Lauterbach, **M. Junker**, "Adapting the slow light spectrum in optical fibers for delay enhancement," *33rd European Conference and Exhibition on Optical Communication*, Berlin, P001, Sept. 2007.

[26] **M. Junker**, T. Schneider, K.-U. Lauterbach, R. Henker, M. J. Ammann, A. T. Schwarzbacher, "1 Gbit/s Übertragung von optisch erzeugten Millimeterwellen für Radio Over Fibre Anwendungen," *9. ITG-Fachtagung Photonische Netze, Leipzig,* Vol. 207, pp. 231 – 235, Apr. 2008.

[27] R. Henker, A. Wiatrek, K.-U. Lauterbach, **M. Junker**, T. Schneider, M. J. Ammann, A. T. Schwarzbacher, "Optimierung des Brillouin Spektrums für Slow-Light Systeme in faserbasierten optischen Netzen," *9. ITG-Fachtagung Photonische Netze, Leipzig,* Vol. 207, pp. 217 – 222, Apr. 2008.

[28] T. Schneider, R. Henker, A. Wiatrek, K.-U. Lauterbach, **M. Junker**, "Grenzen von Slow-Light in photonischen Netzen," *9. ITG-Fachtagung Photonische Netze, Leipzig,* Vol. 207, pp. 131 – 136, Apr. 2008.

[29] A. Wiatrek, T. Schneider, R. Henker, K.-U. Lauterbach, **M. Junker**, "Minimierung der Gruppengeschwindigkeits-Dispersion in faserbasierenden Slow-Light-Systemen," *9. ITG-Fachtagung Photonische Netze, Leipzig,* Vol. 207, pp. 223 – 226, Apr. 2008.

[29] K.-U. Lauterbach, T. Schneider, R. Henker, **M. Junker**, M.J. Ammann, A.T. Schwarzbacher, "Schnelle hochauflösende optische Spektrumanalyse," *9. ITG-Fachtagung Photonische Netze, Leipzig,* Vol. 207, pp. 227 – 230, Apr. 2008.

[30] T. Schneider, R. Henker, K.-U. Lauterbach, **M. Junker**, "Distortion reduction in Slow Light systems based on stimulated Brillouin scattering," *Optics Express*, Vol. 16, No. 11, pp. 8280 – 8285, May 2008.

[32] **M. Junker**, T. Schneider, M.J. Ammann, A.T. Schwarzbacher, K.-U. Lauterbach, R. Henker, S. Neidhardt, "32 GHz Carrier Generation and 200 Mbit/s Error Free Data Transmission in a Radio Over Fibre System," *IEE Irish Signals and Systems Conference*, Galway, Ireland, paper OS-6A.2, Galway, Ireland, June 2008.

[16] T. Schneider, **M. Junker**, K.-U. Lauterbach, Ronny Henker, "Gain-independent SBS based slow light in optical fibers," *Optical Fiber Conference*, JWA14, Mar. 2007.

[17] T. Schneider, R. Henker, K.-U. Lauterbach, **M. Junker**, "Slow und Fast Light in photonischen Netzen – ein Überblick," *8. ITG-Fachtagung Photonische Netze, Leipzig,* Vol. 201, pp. 17 – 24, May 2007.

[18] R. Henker, T. Schneider, **M. Junker**, K.-U. Lauterbach, M.J. Ammann, A.T. Schwarzbacher, "Enhancement of maximum time delay in one fiber segment slow light systems based on stimulated Brillouin scattering," *Conference on Lasers and Electrooptics/ Quantum Electronics and Laser Science and Photonic Applications, Systems and Technologies*, Optical Society of America, Washington D.C., CFD4, May 2007.

[19] **M. Junker**, T. Schneider, K.-U. Lauterbach, R. Henker, M.J. Ammann, A.T. Scharzbacher, "High quality millimeter wave carrier generation via stimulated Brillouin scattering," *Conference on Lasers and Electrooptics/ Quantum Electronics and Laser Science and Photonic Applications, Systems and Technologies*, Optical Society of America, Washington D.C. CFD2, May 2007.

[20] K.-U. Lauterbach, T. Schneider, R. Henker, **M. Junker**, M.J. Ammann, A.T. Schwarzbacher, "Investigation of fast light in long optical fibers based on stimulated Brillouin scattering," *Conference on Lasers and Electrooptics/ Quantum Electronics and Laser Science and Photonic Applications, Systems and Technologies*, Optical Society of America, Washington D.C., JWA48, May 2007.

[21] R. Henker, T. Schneider, K.-U. Lauterbach, **M. Junker**, M.J. Ammann, A.T. Schwarzbacher, "Slow and fast-light in optical fibers – an overview" *Proc. of the IEEE International Students and Young Scientists Workshop "Photonics and Microsystems"*, Dresden, July 2007.

[22] T. Schneider, R. Henker, K.-U. Lauterbach, **M. Junker**, "Adjusting the Brillouin spectrum in optical fibers for slow and fast light applications," *Slow and Fast Light Conference*, SWC3, July 2007.

[23] T. Schneider, R. Henker, K.-U. Lauterbach, **M. Junker**, "Comparison of delay enhancement mechanisms for SBS-based slow light systems," *Optics Express*, Vol. 15, No. 15, pp. 9606 – 9613, July 2007.

[8] T. Schneider, **M. Junker**, K.-U. Lauterbach, "Theoretical and experimental investigation of Brillouin scattering for the generation of millimeter waves," *Journal of the Optical Society of America B*, Vol. 23, Issue 6, pp. 1012 – 1019, June 2006.

[9] **M. Junker**, T. Schneider, M.J. Ammann, A.T. Schwarzbacher, K.-U. Lauterbach, "Carrier generation in the millimetre wave range based on stimulated Brillouin scattering for radio over fibre downlink systems," *IEE Irish Signals and Systems Conference*, Dublin, Ireland, pp. 191-194, June 2006.

[10] **M. Junker**, T. Schneider, K.-U. Lauterbach, M.J. Ammann, A.T. Schwarzbacher, "Flexible Brillouin bandwidth broadening for an amplification, filtering or millimeter wave generation systems," *Optical Amplifiers and Their Applications Topical Meeting* on CD-ROM, The Optical Society of America, Washington DC, JWB42, June 2006.

[11] T. Schneider, K.-U. Lauterbach, **M. Junker**, "Brillouin amplification for wavelength and linewidth measurement with femtometer resolution," *Optical Amplifiers and Their Applications Topical Meeting* on CD-ROM, The Optical Society of America, Washington DC, OtuB4, June 2006.

[12] T. Schneider, **M. Junker**, K.-U. Lauterbach, R. Henker, "Distortion reduction in cascaded slow light delays," Electronics Letters, Vol. 42, Issue 19, pp. 1110 – 1111, Sept. 2006.

[13] **M. Junker**, T. Schneider, K.-U. Lauterbach, M.J. Ammann, A.T. Schwarzbacher, "Millimeterwellengeneration mit Hilfe von Brillouin Verstärkung durch Modulation erzeugter Seitenbänder für Radio Over Fiber Systeme," *VDE-Kongress Innovations in Europe, Aachen*, Vol. 1, pp. 219 – 224, Oct. 2006.

[14] T. Schneider, **M. Junker**, K.-U. Lauterbach, "Potential ultra wide slow-light bandwidth enhancement," *Optics Express*, Vol. 14, No. 23, pp. 11082 – 11087, Nov. 2006.

[15] T. Schneider, **M. Junker**, K.-U. Lauterbach, "Time delay enhancement in stimulated-Brillouin-scattering-based slow-light systems," *Optics Letters*, Vol. 32, No. 3, pp.220 – 222, Feb. 2007.

13 Authors Publications

[1] T. Schneider, **M. Junker**, D. Hannover, "Generation of millimetre-wave signals by stimulated Brillouin scattering for radio over fibre systems," *Electronics Letters*, Vol. 40, pp. 1500 – 1501, Nov. 2004.

[2] T. Schneider, **M. Junker**, D. Hannover, "Nonlinear optical effects for the generation of millimeter wave signals," *Conference on Lasers and Electrooptics/ Quantum Electronics and Laser Science and Photonic Applications, Systems and Technologies*, Optical Society of America, Washington D.C., Vol. 2, pp. 1464 – 1466, CWM6, May 2005.

[3] **M. Junker**, T. Schneider, M.J. Ammann, A.T. Schwarzbacher, "Brillouin amplification of harmonics generated by external modulation for radio over fiber applications with ultra low phase noise properties," *Optical Amplifiers and Their Applications Topical Meeting* on CD-ROM, The Optical Society of America, Washington DC, WC3, 2005.

[4] T. Schneider, D. Hannover, **M. Junker**, "Investigation of Brillouin scattering in optical fibers for the generation of millimeter waves," *Journal of Lightwave Technology*, Vol. 24, Issue 1, pp. 295 – 304, Jan. 2006.

[5] **M. Junker**, M.J. Ammann, A.T. Schwarzbacher, J. Klinger, K.-U. Lauterbach, T. Schneider, "A comparative test of Brillouin amplification and erbium doped fiber amplification for the generation of millimeter waves with low phase noise properties," *IEEE Transactions on Microwave Theory and Techniques*, Vol. 54, No.4, pp. 1576 – 1581, June 2006.

[6] **M. Junker**, T. Schneider, "Brillouin Bandbreitenerweiterung als variabler Verstärker und Filter für WDM Systeme," *7. ITG-Fachtagung Photonische Netze, Leipzig,* Vol. 193, pp. 215 – 217, Apr. 2006.

[7] T. Schneider, K.-U. Lauterbach, **M. Junker**, "Optical spectrum analyzer with femtometer resolution," *Conference on Lasers and Electrooptics/ Quantum Electronics and Laser Science and Photonic Applications, Systems and Technologies*, Optical Society of America, Washington D.C., CMU1, May 2006.

für Radio Over Fibre Anwendungen," *9. ITG-Fachtagung Photonische Netze, Leipzig,* Vol. 207, pp. 231 – 235, Apr. 2008.

[205] M. Junker, T. Schneider, M.J. Ammann, A.T. Schwarzbacher, K.-U. Lauterbach, R. Henker, S. Neidhardt, "32 GHz carrier generation and 200 Mbit/s error free data transmission in a Radio Over Fibre system," *IEE Irish Signals and Systems Conference*, Galway, Ireland, paper OS-6A.2, Galway, Ireland, June 2008.

[206] M. Junker, T. Schneider, K.-U. Lauterbach, R. Henker, M.J. Ammann, A.T. Schwarzbacher, "1 Gbit/s Radio Over Fiber downlink at a 32 GHz carrier," *34rd European Conference and Exhibition on Optical Communication (ECOC) '08,* paper Tu.3.F.2, Brussels, Belgium, Sept. 2008, accepted for publication.

[207] S. Neidhardt, M. Rößler, M. Fischer, "Design of 40 GHz pyramidal horn antennas for Radio Over Fibre link," Master project work, Dublin Institute of Technology, Jan. 2008.

[208] R. Kiefer, P. Winterling, *DWDM, SDH & Co.*. Hüthig, 2002.

[209] G. Janzen, *Kurze Antennen*. Chapter 2, pg. 40, Franckh, Stuttgart, 1986

[210] W.L. Stunzman, G.A. Thiele, *Antenna Theory and Design*. Chapter 1, pg. 24, John Wiley & Sons, New York, 1981.

[211] A.R. Beaumont, B.E. Daymond-John, R.C. Booth, "Effect of ambient water vapour on stability of lithium niobate electro-optic waveguide devices," *Electronics Letters*, Vol. 22, Issue 5, pp. 262 – 263, Feb. 1986.

[212] G.L. Tangonan, D.L. Persechini, J.F. Lotspeich, M.K. Barnoski, "Electro-optic diffraction modulation in Ti-diffused $LiTaO_3$," *Applied Optics*, Vol. 17. pp. 3259 – 3263, 1978.

[213] C.M. Gee, G.D. Blauvelt, H.W. Yen, "Minimising DC drift in $LiNbO_3$ waveguide devices," *Applied Physics Letters*, Vol. 47, pp. 211 – 213, 1985.

[214] S. Yamada, M. Minkata, "DC drift phenomena in $LiNbO_3$ optical waveguide devices," *Japan. Journal of Applied Physics*, Vol. 20, pp. 733 – 737, 1981.

[215] M. Nikles, L. Thevenaz, P.A. Robert, "Brillouin gain spectrum characterization in single-mode optical fibers," *Journal of Lightwave Technology*, Vol. 15, No. 10, pp. 1842 – 1851, Oct. 1997.

fibre gratings," *International Topical Meeting on Microwave Photonics,* MWP '99., Vol. 11, pp.181 – 184, Nov. 1999.

[196] G.Qi, J. Yao, J. Seregelyi, S. Paquet, C. Bélisle, X. Zhang, K. Wu, R. Kashyap, "Phase-noise analysis of optically generated Millimeter-Wave signals with external optical modulation techniques," *Journal of Lightwave Technology*, Vol. 24, No. 12, pp. 4861 – 4875, Dec. 2006.

[197] M. Junker, T. Schneider, M.J. Ammann, A.T. Schwarzbacher, "Brillouin amplification of harmonics generated by external modulation for radio over fiber applications with ultra low phase noise properties," *Optical Amplifiers and Their Applications* Topical Meeting on CD-ROM (The Optical Society of America, Washington, DC), WC3. 2005.

[198] M. Junker, M.J. Ammann, A.T. Schwarzbacher, J. Klinger, K.-U. Lauterbach, T. Schneider, "A comparative test of Brillouin amplification and erbium doped fiber amplification for the generation of Millimeter Waves with low phase noise properties," *IEEE Transactions on Microwave Theory and Techniques*, Vol. 54, No.4, pp. 1576 – 1581, June 2006.

[199] M. Thumm, W. Wiesbeck, S. Kern, *Hochfrequenzmesstechnik*. 2nd Edn., Teubner, Stuttgart, 1998.

[200] Data Sheet of HF Source - Agilent E8247C Analog Signal Generator

[201] T. Ismail, C.P. Liu, A.J. Seeds, "Millimetre-wave Gigabit/s wireless-over-fibre transmission using low cost uncooled devices with remote local oscillator delivery," *Optical Fibre Conference*, OWN3, Mar. 2007.

[202] C.S. Park, C.G. Lee, C.-S. Park, "Photonic frequency upconversion based on stimulated Brillouin scattering," *IEEE Photonics Technology Letters*, Vol. 19, Issue 10, pp. 777 – 779, May 2007.

[203] M. Junker, T. Schneider, K.-U. Lauterbach, R. Henker, M.J. Ammann, A.T. Scharzbacher, "High quality Millimeter Wave carrier generation via stimulated Brillouin scattering," *Conference on Lasers and Electrooptics/ Quantum Electronics and Laser Science and Photonic Applications, Systems and Technologies*, Optical Society of America, Washington D.C. (2007), CFD2, May 2007.

[204] M. Junker, T. Schneider, K.-U. Lauterbach, R. Henker, M.J. Ammann, A.T. Schwarzbacher, "1 Gbit/s Übertragung von optisch erzeugten Millimeterwellen

[183] M. Herrmann, *Numerik gewöhnlicher Differentialgleichungen Anfangs- und Randwertprobleme*. Oldenbourg Wissenschaftsverlag, Oldenbourg, 2004.

[184] T. Schneider, *Nonlinear Optics in Telecommunications*. Springer, Berlin, Chapter 6, 2004.

[185] A. Wiberg, P.O. Hedekvist, "Photonic microwave generator utilizing narrowband brillouin amplification and fibre-based oscillator," *Microwave and Terahertz Photonics*, Vol. 5466, 148 – 156, Sept. 2004.

[186] J.O'Reilly, P. Lane, "Remote delivery of video services using mm-Waves and optics," *Journal of Lightwave Technology*, Vol. 12, pp. 369 – 375, 1994.

[187] S. Fukushima, C.F.C. Silva, Y. Muramoto, A.J. Seeds, "Optoelectronic millimeter-wave synthesis using an optical frequency comb generator, optically injection locked lasers, and a unitraveling-carrier photodiode," *Journal of Lightwave Technology*, Vol. 21, Issue 12, pp. 3043 – 3051, Dec. 2003.

[188] T. Kawanishi, T. Sakamoto, S. Shinada, M. Izutsu, S. Oikawa, K. Yoshiara, "Low phase noise photonic millimeter-wave generation by using a reciprocating optical modulator," *Optical Fiber Communication Conference*, Vol. 1, Feb. 2004.

[189] M.O. van Deventer, "Fundamentals of bidirectional transmission over a single optical fibre," Ph. D. dissertation, University of Eindhoven, 1994.

[190] H. Schmuck, "Comparison of optical millimetre-wave system concepts with regard to chromatic dispersion," *Electronics Letters*, Vol. 31, Issue 21, pp. 1848 – 1849, Oct. 1995.

[191] J.W. Shi, C.K. Sun, "Theory and design of a tapered linedistributed photodetector," *Journal of Lightwave Technology*, Vol. 20, No. 11, pp. 1942 – 1950, Nov. 2002.

[192] As per manufacturer information

[193] B. Schiek, H.-J. Siweris, *Rauschen in Hochfrequenzschaltungen*. Hüthig, 1990.

[194] M. Iqbal, L. Jeongseon, K. Kiseon, "Performance comparison of digital modulation schemes with respect to phase noise spectral shape," *Canadian Conference on Electrical and Computer Engineering*, Vol. 2, pp. 856 – 860, Mar. 2000.

[195] J. Marti, F. Ramos, V. Polo, J.M. Fuster, J.L. Corra, "Millimetre-wave signal generation and harmonic upconversion through PM-IM conversion in chirped

[170] M. Junker, T. Schneider, M.J. Ammann, A.T. Schwarzbacher, K.-U. Lauterbach, "Carrier generation in the Millimetre Wave range based on stimulated Brillouin scattering for Radio Over Fibre downlink systems," *IEE Irish Signals and Systems Conference*, Dublin, Ireland, pp. 191 – 194, June 2006.

[171] T. Schneider, M. Junker, D. Hannover, "Generation of millimetre-wave signals by stimulated Brillouin scattering for Radio Over Fibre systems," *Electronics Letters,* Vol. 40, pp. 1500 – 1501, 2004.

[172] T. Horiguchi, M. Tateda, N. Shibata, Y. Azuma, "Brillouin gain variation due to a polarization-state change of the pump or Stokes fields in standard single-mode fibers," *Optics Letters*, Vol. 14, pp. 329 – 331, 1989.

[173] G.A. Reider, *Photonik. Eine Einführung in die Grundlagen*. Springer, Wien, Chapter 8, 1997.

[174] G.S. He, S.H. Liu, *Physics of Nonlinear Optics*, World Scientific, Chapter 8, pg. 229, 1999.

[175] G.S. He, S.H. Liu, *Physics of Nonlinear Optics*, World Scientific, Chapter 6, 1999.

[176] T. Schneider, *Nonlinear Optics in Telecommunications*. Springer, Berlin, Chapter 7, pg.172, 2004.

[177] C.L. Tang, "Saturation and spectral characteristics of the Stokes emission in the stimulated Brillouin process," *Journal of Applied Physics*, Vol. 37, No. 8, 2945 – 2955, July 1966.

[178] T. Schneider, *Nonlinear Optics in Telecommunications*. Springer, Berlin, Chapter 2, pg. 19, 2004.

[179] G.S. He, S.H. Liu, *Physics of Nonlinear Optics*, World Scientific, Chapter 8, pg. 233, 1999.

[180] T. Schneider, *Nonlinear Optics in Telecommunications*. Springer, Berlin, Chapter 4, 2004.

[181] A. Wiatrek, "Numerische Untersuchung einer Zweiseitenband-Verstärkung zur Millimeterwellenerzeugung," Diploma Thesis at the Hochschule fuer Telekommunikation, Leipzig, University of Applied Sciences, Mar. 2008.

[182] H.R. Schwarz, N. Köckler, *Numerische Mathematik*. 6th Edn., Teubner, Wiesbaden, 2006.

[159] T. Schneider, K.-U. Lauterbach, M. Junker, "Brillouin amplification for wavelength and linewidth measurement with femtometer resolution," *Optical Amplifiers and Their Applications Topical Meeting* (The Optical Society of America, Washington, DC), OtuB4, June 2006.

[160] T. Schneider, M. Junker, K.-U. Lauterbach, "Potential ultra wide Slow-Light bandwidth enhancement," *Optics Express*, Vol. 14, No. 23, pp. 11082 – 11087, Nov. 2006.

[161] K. Yong, K. Hotate, "25 GHz bandwidth Brillouin Slow Light in optical fibers," *Optics Letters*, Vol. 32, No. 3, pp. 217 – 219, Feb. 2007.

[162] T. Schneider, R. Henker, K.-U. Lauterbach, M. Junker, "Adjusting the Brillouin spectrum in optical fibers for Slow and Fast Light applications," *Slow and Fast Light conference,* SWC3, July 2007.

[163] T. Schneider, R. Henker, K.-U. Lauterbach, M. Junker, "Comparison of delay enhancement mechanisms for SBS-based Slow Light systems," *Optics Express*, Vol. 15, No. 15, pp. 9606 – 9613, July 2007

[164] T. Schneider, R. Henker, K.-U. Lauterbach, M. Junker, "Adapting the Brillouin spectrum for Slow Light delays," *Electronics Letters*, Vol. 43, No. 12, pp. 682 – 683, July 2007.

[165] T. Schneider, R. Henker, K.-U. Lauterbach, M. Junker, "Adapting the Slow Light spectrum in optical fibers for delay enhancement," *33rd European Conference on Optical Communication*, Berlin, P001, Sept. 2007.

[166] T. Schneider, D. Hannover, M. Junker, "Investigation of Brillouin scattering in optical fibers for the generation of Millimeter Waves," *Journal of Lightwave Technologies*, Vol. 24, Issue 1, pp. 295 – 304, Jan. 2006.

[167] X.S. Yao, "Brillouin selective sideband amplification of microwave photonic signals," *IEEE Photonics Technology Letters*, Vol. 10, No. 1, pp. 138 – 40, Jan. 1998.

[168] A. Loayssa, D. Benito, M.J. Garde, "Applications of optical carrier Brillouin processing to microwave photonics", *Optical Fiber Technology*, pp. 24 – 42, 2002.

[169] T. Schneider, M. Junker, K.-U. Lauterbach, "Theoretical and experimental investigation of Brillouin scattering for the generation of millimeter waves," *Journal of the Optical Society of America B*, Vol. 23, Issue 6, pp. 1012 – 1019, Jun. 2006.

[149] K. Shiraki, M. Ohashi, M. Tateda, "SBS threshold of a fiber with a Brillouin frequency shift distribution," *Journal of Lightwave Technology*, Vol. 14, Issue 1, pp. 50 – 57, Jan. 1996.

[150] N. Uesugi, M. Ikeda, Y. Sasaki, "Maximum single frequency input power in a long optical fibre determined by stimulated Brillouin scattering," *Electronics Letters*, Vol. 17, No. 11, pp. 379 – 380, May 1981.

[151] M.O. van Deventer, A.J. Boot, "Polarization properties of stimulated Brillouin scattering in single-mode fibers," *Journal of Lightwave Technology*," Vol. 12, Issue 4, pp. 585 – 590, Apr. 1994.

[152] N. Olsson, J.P. Van der Ziel, "Characteristics of a semiconductor laser pumped brillouin amplifier with electronically controlled bandwidth," *Journal of Lightwave Technology*, Vol. 5, Issue 1, pp. 147 – 153, Jan. 1987.

[153] M.F. Ferreira, J.F. Rocha, J.L. Pinto, "Analysis of the gain and noise characteristics of fibre Brillouin amplifiers," *Optical and Quantum Electronics*, Vol. 26, pp. 35 – 44, 1994.

[154] N.A. Olsson, J.P. Van der Ziel, "Fibre Brillouin amplifier with electronically controlled bandwidth," *Electronics Letters*, Vol. 22, No. 9, pp. 488 – 490, Apr. 1986.

[155] M. González-Herráez, K.Y. Song, L. Thévenaz, "Arbitrary-bandwidth Brillouin Slow Light in optical fibers," *Optics Express*, Vol. 14, No. 4, pp. 1395 – 1400, Feb. 2006.

[156] A.M.C. Dawes, Z. Zhu, D.J. Gauthier, "Improving the bandwidth of SBS-based Slow-Light delay," *Conference on Lasers and Electrooptics/ Quantum Electronics and Laser Science and Photonic Applications, Systems and Technologies*, Optical Society of America, Washington D.C. (2006), CThW1, May 2006.

[157] Z. Zhu, A.M.C. Dawes, D.J. Gauthier, J. Zhang, A.E. Willner, "12-GHz-bandwidth SBS Slow Light in optical fibers," *Proc. of Optical Fiber Conference*, PDP1, 2006.

[158] M. Junker, T. Schneider, K.-U. Lauterbach, M.J. Ammann, A.T. Schwarzbacher, "Flexible Brillouin bandwidth broadening for an amplification, filtering or Millimeter Wave generation systems," *Optical Amplifiers and Their Applications* Topical Meeting (The Optical Society of America, Washington, DC), JWB42, June 2006.

[138] G.P. Agrawal, *Nonlinear Fibre Optics*. 3rd Edn., Academic Press, San Diego, Chapter 9, 2001.

[139] M. Niklès, L. Thévenaz, R.A. Robert, "Brillouin gain spectrum characterization in single-mode optical fibers," *Journal of Lightwave Technology*, Vol. 15, No. 10, 1842 – 1851, 1997.

[140] D. Cotter, "Observation of stimulated Brillouin scattering in low loss silica fibre at 1.3 μm," *Electronics Letters*, Vol. 18, No. 12, pp. 495 – 496, June 1982.

[141] T. Schneider, *Nonlinear Optics in Telecommunications*. Springer, Berlin, Chapter 11, 2004.

[142] R.G. Smith, "Optical power handling capacity of low loss optical fibers as determined by stimulated Raman and Brillouin scattering," *Applied Optics*, Vol. 11, Issue 11, pp. 2489 – 2494, Nov.1972.

[143] G.P. Agrawal, *Nonlinear Fibre Optics*. 3rd Edn., Academic Press, San Diego, Chapter 1, 2001.

[144] T. Schneider, K.-U. Lauterbach, M. Junker, "Optical spectrum analyzer with femtometer resolution," *Proc. Conference on Lasers and Electrooptics/ Quantum Electronics and Laser Science and Photonic Applications, Systems and Technologies*, Optical Society of America, Washington D.C. (2006), CMU1, May 2006.

[145] M. Junker, T. Schneider, "Brillouin Bandbreitenerweiterung als variabler Verstärker und Filter für WDM Systeme," *Proc. 7. ITG-Fachtagung Photonische Netze*, Leipzig, Vol. 193, pp. 215 – 217, Apr. 2006.

[146] T. Schneider, K.-U. Lauterbach, M. Junker, "Brillouin amplification for wavelength and linewidth measurement with femtometer resolution," *Optical Amplifiers and Their Applications Topical Meeting* (The Optical Society of America, Washington, DC), OtuB4, June 2006.

[147] A. Loayssa, D. Benito, M.J. Garde, "Narrow-bandwidth technique for stimulated Brillouin scattering spectral characterisation," *Electronics Letters*, Vol. 37, Issue 6, pp. 367 – 368, Mar. 2001.

[148] P. Bayvel, P.M Radmore, "Solutions of the SBS equations in single mode optical fibres and implications for fibre transmission systems," *Electronics Letters*, Vol. 26, Issue 7, pp. 435 – 436, Mar. 1990.

[129] R. Henker, T. Schneider, M. Junker, K.-U. Lauterbach, M.J. Ammann, A.T. Schwarzbacher, "Enhancement of maximum time delay in one fiber segment Slow Light systems based on stimulated Brillouin scattering," *Conference on Lasers and Electrooptics/ Quantum Electronics and Laser Science and Photonic Applications, Systems and Technologies*, Optical Society of America, Washington D.C. (2007), CFD4, May 2007.

[130] R. Henker, T. Schneider, K.-U. Lauterbach, M. Junker, M.J. Ammann, A.T. Schwarzbacher, "Slow and Fast-Light in optical fibers – An Overview," *Proc. of the IEEE International Students and Young Scientists Workshop „Photonics and Microsystems"*, Dresden, July 2007.

[131] K.-U. Lauterbach, T. Schneider, R. Henker, M. Junker, M.J. Ammann, A.T. Schwarzbacher, "Investigation of Fast Light in long optical fibers based on stimulated Brillouin scattering," *Conference on Lasers and Electrooptics/ Quantum Electronics and Laser Science and Photonic Applications, Systems and Technologies*, Optical Society of America, Washington D.C. (2007), JWA48, May 2007.

[132] T. Schneider, M. Junker, D. Hannover, "Nonlinear optical effects for the generation of Millimeter Wave signals," *Conference on Lasers and Electrooptics/ Quantum Electronics and Laser Science and Photonic Applications, Systems and Technologies*, Optical Society of America, Washington D.C., Vol. 2, pp. 1464 – 1466, CWM6, May 2005.

[133] D. Hannover, "Untersuchung der Brillouin Streuung in optischen Fasern für die Erzeugung von Millimeterwellen," Diploma Thesis, Deutsche Telekom Hochschule für Telekommunikation Leipzig, Aug. 2004.

[134] V.G. Szymonski, J.E. Bryan, J. Seyed-Yagoobi, "Theoretical study of an electrostriction pump," *Proc. of International Conference on Conduction and Breakdown in Dielectric Liquids*, pp. 393 – 396, July 1996.

[135] E. Voges, K. Petermann, *Optische Kommunikationstechnik: Handbuch für Wissenschaft und Industrie*. Springer, Berlin, Chapter 4, 2002.

[136] R.W. Boyd, *Nonlinear Optics*. 2nd Edn., Academic Press, San Diego, Chapter 9, 2003.

[137] C. Elachi, "Waves in active and passive periodic structures: A review," *Proceedings of the IEEE*, Vol. 64, Issue 12, pp. 1666 – 1698, Dec. 1976.

[118] A.R. Chraplyvy, R.W. Tkach, "Narrowband tunable optical filter for channel selection in densely packed WDM systems," *Electronics Letters*, Vol. 22, pp. 1084 – 1085, 1986.

[119] C.G. Atkins, D. Cotter, D.W. Smith, R. Wyatt, "Application of Brillouin amplification in coherent optical transmission," *Electronics Letters*, Vol. 22, pp. 556 – 558, 1986.

[120] N.A. Olsson, J. van der Ziel, "Cancellation of fiber loss by semiconductor laser pumped Brillouin amplification at 1.5 μm," *Applied Physics Letters*, Vol. 48, pp. 1328 – 1330, 1986.

[121] S.J. Strutz, K.J. Williams, R.D. Esman, "Polarization-maintaining hybrid erbium-Brillouin amplifier for high-power low-noise sources," *IEEE Photonics Technology Letters*, Vol. 13, Issue 9, pp. 936 – 938, Sept. 2001.

[122] A.S. Siddiqui, S. Andronikidis, "Transfer characteristics of Brillouin fibre amplifiers for use in self-homodyne coherent optical transmission systems," *Electronics Letters*, Vol. 25, Issue 4, pp. 264 – 266, Feb. 1989.

[123] A. Loayssa, F.J. Fahoz, "Broad-Band RF Photonic Phase Shifter Based on Stimulated Brillouin Scattering and Single-Sideband Modulation," *IEEE Photonics Technology Letters*, Vol. 18, Issue 1, pp. 208 – 210, Jan. 2006.

[124] A. Loayssa, J. Capmany, "Incoherent microwave photonic filters with complex coefficients using stimulated Brillouin scattering," *Optical Fiber Conference*, OFB2, Optical Society of America, Washington D.C., 2006.

[125] T. Schneider, M. Junker, K.-U. Lauterbach, "Time delay enhancement in stimulated-Brillouin-scattering-based slow-light systems," *Optics Letters*, Vol. 32, No. 3, pp. 220 – 222, Feb. 2007.

[126] T. Schneider, M. Junker, K.-U. Lauterbach, R. Henker, "Gain-independent SBS based Slow Light in optical fibers," *Optical Fiber Conference*, JWA14, Mar. 2007.

[127] T. Schneider, M. Junker, K.-U. Lauterbach, R. Henker, "Distortion reduction in cascaded slow light delays," *Electronics Letters*, Vol. 42, Issue 19, pp. 1110 – 1111, Sept. 2006.

[128] T. Schneider, R. Henker, K.-U. Lauterbach, M. Junker, "Slow und Fast Light in photonischen Netzen – ein Überblick," *Proc. 8. ITG-Fachtagung Photonische Netze*, Leipzig, Vol. 201, pp. 14 – 17, May. 2007.

[108] Y. Shen, Z. Xianmin, C. Kangsheng, "All-optical generation of microwave and Millimeter Wave using a two-frequency Bragg grating-based Brillouin fiber laser," *Journal of Lightwave Technology*, Vol. 23, Issue 5, pp. 1860 – 1865, May 2005.

[109] Y. Lai, W. Zhang, J.A.R. Williams, I. Bennion, "An optical Millimetre Wave fiber laser," *Proc. of the Conference on Optical Fiber Communications*, Vol. 1, pp. 238 – 239, Mar. 2003.

[110] A. Wiberg, P. Perez-Millan, M.V. Andres, P.O. Hedekvist, "Microwave-photonic frequency multiplication utilizing optical four-wave mixing and fiber Bragg gratings," *Journal of Lightwave Technology*, Vol. 24, Issue 1, pp. 329 – 334, Jan. 2006.

[111] H. Ling, A. Kaszubowska, L.P. Barry, "Investigations of stimulated Brillouin scattering effects in radio-over-fibre distribution networks," *Optics Communications*, Vol. 255, Issue 4-6, pp. 253 – 260, Nov. 2005.

[112] J.M.S. Domingo, J. Pelayo, F. Villuendas, C.D. Heras, E. Pellejer, "Very high resolution optical spectrometry by stimulated Brillouin scattering," *IEEE Photonics Technology Letters*, Vol. 17, Issue 4, pp. 855 – 857, Apr. 2005.

[113] T. Schneider, "Wavelength and line width measurement of optical sources with femtometre resolution," *Electronics Letters*, Vol. 41, Issue 22, pp. 1234 – 1235, Oct. 2005.

[114] K.-U. Lauterbach, T. Schneider, "Optische Bandbreiten- und Wellenlängenmessung im Femtometerbereich," *Proc. 7th ITG-Fachtagung Photonische Netze*, Leipzig, Vol. 193, pp. 207 – 210, Apr. 2006.

[115] K.-U. Lauterbach, T. Schneider, "Brillouin scattering in optical fibers for high resolution wavelength and line width measurements," *Optical Fiber Conference*, Anaheim, OWI11, Mar. 2006.

[116] R.W. Tkach, A.R. Chraplyvy, R.M. Derosier, H.Z. Shang, "Optical demodulation and amplification of FSK signals using AlGaAs lasers," *Electronics Letters*, Vol. 24, Issue 5, pp. 260 – 262, Mar. 1988.

[117] R.W. Tkach, A.R. Chraplyvy, R.M. Derosier, "Performance of a WDM network based on stimulated Brillouin scattering," *IEEE Photonics Technology Letters*, Vol. 1, Issue 5, pp. 111 – 113, May 1989.

[97] A. Wiberg, P. Perez-Millan, M.V. Andres, P.A. Andrekson, P.O. Hedekvist, "Fiber-optic 40-GHz mm-Wave link with 2.5-Gb/s data transmission," *IEEE Photonics Technology Letters*, Vol. 17, Issue 9, pp.1938 – 1940, Sept. 2005.

[98] M. Sauer, W. Nowak, "Simultaneous upconversion by phase modulation for dispersion-independent optical mm-Wave transmission," *Proc. of 24th European Conference on Optical Communication*, Vol. 1, pp. 347 – 348, Sept. 1998.

[99] K. Wakita, I. Kotaka, H. Asai, S. Nojima, O. Mikami, "High-efficiency electroabsorption in quaternary AlGaInAs quantum-well optical modulators," *Electronics Letters*, Vol. 24, Issue 21, pp. 1324 – 1325, Oct. 1988.

[100] European Patent: EP1315025, available: http://www.freepatentsonline.com/EP1315025.html (Feb./03/07).

[101] T. Kuri, K. Kitayama, A. Stohr, Y. Ogawa, "Fiber-optic Millimetre-Wave downlink system using 60 GHz-band external modulation," *IEEE Journal of Lightwave Technology*, Vol. 17, Issue 5, pp. 799 – 806, May 1999.

[102] A. Stähr, T. Kuri, K. Kitayama, R. Heizelmann, D. Jäger, "Full-duplex 60 GHz fibre optic transmission," *Electronics Letters*, Vol. 35, No. 19, pp. 1653 – 1655, 1999.

[103] D.G. Moodie, D. Wake, N.G. Walker, D. Nesset, "Efficient harmonic generation using an electroabsorption modulator," *IEEE Photonics Technology Letters*, Vol. 7, Issue 3, pp. 312 – 314, Mar. 1995.

[104] S. Pajarola, G. Guekos, H. Kawaguchi, "Optical millimetre-wave transmission using a dual-polarization external cavity diode laser," *IEEE Photonics Technology Letters,* Vol. 10, Issue 7, pp. 1021 – 1023, July 1998.

[105] E. Vergnol, F. Devaux, D. Jahan, A. Carenco, "Fully integrated millimetric single-sideband Millimeter source," *Electronics Letters*, Vol. 33, No. 23, pp. 1961 – 1963, Nov. 1997.

[106] X.S. Yao, "High quality microwave signal generation by use of Brillouin scattering in optical fibers," *Optics Letters*, Vol. 22, No. 17, pp. 1329 – 1331, 1997.

[107] K. Kitayama, "Highly stabilized millimetre-waves generation and transport by using fiber-optic four-wave mixing," *Proc. of the Conference on Optical Fiber Communications,* pp. 338 – 339, Feb. 1997.

[88] M. Hyodo, M. Watanabe, "Optical generation of Millimetre-Wave signals up to 330 GHz by means of cascadingly phase locking three semiconductor lasers," *IEEE Photonics Technology Letters*, Vol. 15, Issue 3, pp. 458 – 460, Mar. 2003.

[89] A.C. Davidson, F.W. Wise, R.C. Compton, "Low phase noise 33-40-GHz signal generation using multilaser phase-locked loops," *IEEE Photonics Technology Letters*, Vol. 10, Issue 9, pp. 1304 – 1306, Sept. 1998.

[90] M. Musha, K. Nakagawa, K. Ueda, A. Ueda, M. Ishiguro, "Optical generation of a highly stable Millimetre wave by heterodyning of two phase-locked diode lasers with an optical comb generator," *Proc. of Conference on Lasers and Electro-Optics*, Vol. 1, pp. 2, 2004.

[91] M. Junker, T. Schneider, K.-U. Lauterbach, M.J. Ammann, A.T. Schwarzbacher, "Millimeterwellengeneration mit Hilfe von Brillouin Verstärkung durch Modulation erzeugter Seitenbänder für Radio Over Fiber Systeme," *Proc. VDE-Kongress Innovations in Europe*, Aachen, Vol. 1, pp. 219 – 224, Oct. 2006.

[92] G.H. Smith, D. Novak, "Broadband millimetre-wave (38 GHz) fiber-wireless transmission system using electrical and optical SSB modulation to overcome dispersion effects," *IEEE Photonics Technology Letters*, Vol. 10, No. 1, pp. 1 – 3, Jan. 1998.

[93] G.H. Smith, D. Novak, C. Lim, K. Wu, "Full-cuplex broadband millimetre wave optical transport system for fibre-wireless access," *Electronics Letters*, Vol. 33, No. 13, pp. 1159 – 1160, June 1997.

[94] G.H. Smith, D. Novak, Z. Ahmed, "Technique for optical SSB generation to overcome dispersion penalties in fibre-radio systems," *Electronics Letters*, Vol. 33, No. 1, pp. 74 – 75, Jan. 1997.

[95] J.J. O'Reilly, P.M. Lane, R. Heidemann, R. Hoktetter, "Optical generation of very narrow linewidth millimeter wave signals," *Electronics Letters*, Vol. 28, pp. 2309 – 2311, 1992.

[96] R. Hofstetter, H. Schmuck, R. Heidemann, "Dispersion effects in optical millimetre-wave systems using self-heterodyne method for transport and generation," *IEEE Transactions on Microwave Theory and Techniques*, Vol. 43, Issue 9, pp. 2263 – 2269, Sept. 1995.

[78] D. Zhichao, Y. Jianping, "Photonic generation of microwave signal using a rational harmonic mode-locked fiber ring laser," *IEEE Transactions on Microwave Theory and Techniques*, Vol. 54, Issue 2, pp. 763 – 767, Feb. 2006.

[79] L. Goldberg, H.F. Taylor, J.F. Weller, D.M. Bloom, "Microwave signal generation with injection-locked laser diodes," *Electronics Letters*, Vol. 19, No. 13, pp. 491 – 493, June 1983.

[80] M. Bhattacharya, B. Sarkar, T. Chattopadhyay, "Optical generation of Millimeter and Submillimeter-Waves through optical side-band injection locking of semiconductor lasers," *IEEE Photonics Technology Letters*, Vol. 14, No. 11, pp. 1611 – 1613, 2002.

[81] L. Noël, D. Marcenac, D. Wake, "120 Mbit/s QPSK radio-fibre transmission over 100 km of standard fibre at 60 GHz using a master/slave injection-locked DFB laser source," *Electronics Letters*, Vol. 32, No. 20, pp. 1895 – 1897, Sept. 1996.

[82] R.-P. Braun, G. Grosskopf, R. Meschenmoser, D. Rohde, F. Schmidt, G. Villino, "Microwave generation for bidirectional broadband mobile communications using optical sideband injection locking," *Electronics Letters*, Vol. 33, No. 16, pp. 1395 – 1396, July 1997.

[83] L.A. Johansson, A.J. Seeds, "Generation and transmission of Millimetre-wave data-modulated optical signals using an optical injection phase-lock loop," *Journal of Lightwave Technology*, Vol. 21, Issue 2, pp. 511 – 520, Feb. 2003.

[84] R.C. Steele, "Optical phase-locked loop using semiconductor laser diodes," *Electronics Letters*, Vol. 19, No. 2, pp. 69 – 71, Jan. 1983.

[85] U. Gliese, T.N. Nielsen, M. Bruun, E. Lintz Christensen, K.E. Stubkjaer, S. Lindgren, B. Broberg, "A wideband heterodyne optical phase-locked loop for generation of 3-18 GHz microwave carriers," *IEEE Photonics Technology Letters*, Vol. 4, Issue 8, pp. 936 – 938, Aug. 1992.

[86] R.T. Ramos, A.J. Seeds, "Fast heterodyne optical phase-lock loop using double quantum well laser diodes," *Electronics Letters*, Vol. 28, Issue 1, pp. 82 – 83, Jan. 1992.

[87] R.T. Ramos, A.J. Seeds, "Delay, linewidth and bandwidth limitations in optical phase locked loop design," *Electronics Letters*, Vol. 28, Issue 1, pp. 389 – 391, 1990.

[67] P.W. Smith, "Mode-locking of lasers," *Proceedings of the IEEE*, Vol. 58, No. 9, pp. 1342 – 1357, Sept. 1970.

[68] J. Park, L.A. Buckmann, K.Y. Lau, "Compact optical millimetre-wave source modulator using a passively modelocked semiconductor laser with phase noise compensation," *IEEE Photonics Technology Letters*, Vol. 9, No. 5, pp. 619 – 612, 1997.

[69] D.Y. Kim, M. Pelusi, Z. Ahmed, D. Novak, H.F. Lui, Y. Ogawa, "Ultrastable millimetre-wave signal generation using hybrid mode locking of a monolithic DBR laser," *Electronics Letters*, Vol. 31, Issue 9, pp. 733 – 734, Apr. 1995.

[70] C. Schmidt, E. Dietrich, S. Diez, H.J. Ehrke, U. Feiste, L. Kuller, R. Ludwig, H.G. Weber, "Mode-locked semiconductor lasers and their applications for optical signal processing," *Proc. of Conference of Lasers and Electrooptics*, pp. 348 – 349, May 1999.

[71] Z. Ahmed, D. Novak, R.B. Waterhouse, H.F. Liu, "Optically fed millimetre-wave (37 GHz) transmission system incorporating a hybrid mode-locked semiconductor laser," *Electronics Letters*, Vol. 32, No. 19, pp. 1790 – 1792, 1996.

[72] A.E. Siegmann, *Lasers*. University Science Press, 1986.

[73] D. Wake, C.R. Lima, P.A. Davis, "Optical generation of millimetre-wave signals for fiber-radio systems using a dual mode DFB semiconductor laser," *IEEE Transactions on Microwave Theory and Techniques*, Vol. 43, No. 9, pp. 2270 – 2276, Oct. 1996.

[74] D. Wake, C. R. Lima, P. A. Davies, "Transmission of 60-GHz signals over 60 km of optical fibre using a dual-mode semiconductor laser source," *IEEE Photonics Technology Letters*, Vol. 8, No. 4, pp. 578 – 580, 1997.

[75] T. Ohno, F. Nakajima, T. Furuta, H. Ito, "240 GHz active mode locked laser diode," *Electronics Letters*, Vol. 41, No. 19, pp. 1057 – 1059, Sept. 2005.

[76] F. Nakajima, T. Ohno, K. Yoshino, T. Furuta, T. Sato, Y. Kondo, H. Ito, "Generation of 10-Gbit/s optical Millimeter-Wave signal using a 125-GHz mode-locked laser diode integrated with an Electro-Absorption modulator," *Int. Topical Meeting of Microwave Photonics*, pp. 33 – 36, Oct. 2005.

[77] K. Sato, A. Hirano, N. Shimizu, T. Ohno, H. Ishii, "Optical millimetre-wave generation by dual-mode operation of semiconductor modelocked lasers," *Electronics Letters*, Vol. 36, No. 4, pp. 340 – 342, Feb. 2000.

[55] K. Lange, K.-H. Löcherer, *Taschenbuch der Hochfrequenztechnik*. Springer, Berlin, 5th Edn., Vol. 1, Chapter G, 1992.

[56] C.E. Cox, G.E. Bett, L.M. Johnson, "An analytic and experimental comparison of direct and external modulation in analog fiber-optic links," *IEEE Transactions on Microwave Theory and Techniques,* Vol. 38, Issue 5, pp. 501 – 509, May 1990.

[57] R. Lewén, S. Irmscher, U. Westergren, L. Thylén, U. Ericsson, "Ultra high-speed segmented travelling-wave electroabsorbtion modulators," *Proc. of the Optical Fiber Communication*, post-deadline paper, PD38, 2003.

[58] U. Gliese, S. Nørskov, T.N. Nielsen, "Chromatic dispersion in fiber-optic microwave and millimetre-wave links," *IEEE Transaction on Microwave Theory and Techniques*, Vol. 44, No. 10, pp. 1716 – 1724, Oct. 1996.

[59] A. Stöhr, M. Weiß, M. Huchard, B. Charbonier, S. Fedderwitz, D. Jäger, "60 GHz wireless photonic link system for 12.5 Gb/s data transmission," *9. ITG-Fachtagung Photonische Netze, Leipzig,* Vol. 207, pp. 101 – 104, Apr. 2008.

[60] K. Kitayama, "Ultimate performance of optical DSB signal-based millimetre-wave fiber-radio system: effect of laser noise," *Journal of Lightwave Technology*, Vol. 17, No. 10, pp. 1774 – 1781, 1999.

[61] A. Kaszubowska, P. Anandarajah, L.P. Barry, "Improved performance of a hybrid radio/fibre system using a directly modulated laser transmitter with external injection," *IEEE Photonics Technology Letters,* Vol. 14, Issue 2, pp. 233 – 235, Feb. 2002.

[62] E. Voges, K. Petermann, *Optische Kommunikationstechnik: Handbuch für Wissenschaft und Industrie*. Springer, Berlin, Chapter 24, 2002.

[63] M. C. Teich, "Infrared heterodyne detection," *Proceedings of the IEEE*, Vol. 56, No. 1, pp. 37 – 50, Jan. 1968.

[64] R. Mäusl, *Analoge Modulationsverfahren*. 2nd Edn., Hüthig, Heidelberg, Chapter 2, 1992.

[65] Stöcker, *Taschenbuch Mathematischer Formeln und Moderner Verfahren*. 2nd Ed., Harry Deutsch, Thun, Chapter 12, 1993

[66] H. Schmuck, R. Heidemann, "Faseroptische mm-Wellen Übertragungstechnik und ihre Anwendung," *Telekom Praxis*, Vol. 7, pp. 9 – 15, 1997.

[43] H. Eisele, R. Kamoua, "High-performance oscillators and power combiners with InP Gunn devices at 260-330 GHz," *IEEE Microwave and Wireless Components Letters*, Vol. 16, Issue 5, pp. 284 – 286, May 2006.

[44] F. Kuroki, H. Shimoi, K. Yamaoka, T. Yoneyama, "NRD guide Gunn oscillator with medium power and low phase noise at 60 GHz," *Technical Digest IEEE International Microwave Symposium*, Vol. 3, pp. 1337 – 1340, June 2004.

[45] M.K. Sung, K.Y. Mun, J.P. Sang, H.K. Kyung, "Design of low phase noise K-band Gunn oscillator by using bias filter," *Asia-Pacific Microwave Conference*, Vol. 3, pp. 1283 – 1286, Dec. 2001.

[46] H. Eisele, A. Rydberg, G.I. Haddad, "Recent advances in the performance of InP gunn devices for the 100-300-GHz frequency range," *Proceedings of IEEE 6th International Conference on Terahertz Electronics*, pp. 66 – 68, Sept. 1998.

[47] Y. Kaneko, K. Kimura, K. Sekine, "Stability of Gunn oscillators," *International Electron Devices Meeting*, Vol. 16, pp. 56 – 56, 1970.

[48] E. Voges, *Hochfrequenztechnik*. Hüthig, Heidelberg, Vol. 2, Chapter 14, 1987.

[49] E. Pehl, *Mikrowellentechnik – Band 2: Antennen und aktive Bauteile*. Hüthig, Heidelberg, Vol. 2, 1984.

[50] A.G. Litvak, V.E. Myasnikov, S.V. Usachev, L.G. Popov, M.V. Agapova, et al. "Development of 170 GHz/1 MW/ 50%/CW gyrotron for ITER," *Conference Digest of the International Conference on Infrared and Millimetre Waves and 12th International Conference on Terahertz Electronics*, pp. 111 – 112, Sept. 2004.

[51] N.R. Erickson, "A 200-350-GHz heterodyne receiver," *IEEE Transactions on Microwave Theory and Techniques*, Vol. 29, Issue 6, pp. 557 – 561, June 1981.

[52] B. Piosczyk, G. Dammhertz, O. Dumbrajs, S. Illy, J. Jin, et al. "A 2 MW, 170 GHz coaxial cavity gyrotron – experimental verification of the design of main components," *Journal of Physics: Conference Series*, Vol. 25, Issue 1, pp. 24 – 32, Jan. 2005.

[53] R.H. Johnston, A.R. Boothroyd, "Charge storage frequency multipliers," *Proceedings of the IEEE*, Vol. 56, Issue 2, pp. 167 – 176, Feb. 1968.

[54] D.J. Roulston, "Frequency multiplication using storage effect: An analysis for high efficiency, high power operation," *International Journal of Electronics*, Vol. 18, pp. 73 – 86, Jan. 1965.

[32] K. Fazel, C. Decanis, J. Klein, G. Licitra, L. Lindh, Y.Y. Lebret, "An overview of the ETSI-BRAN HIPERACCESS physical layer air interface specification," *13th IEEE International Symposium on Personal, Indoor and Mobile Radio Communications*, Vol. 1, pp. 49 – 53, Sept. 2002.

[33] J. Haine, "HIPERACCESS: an access system for the information age," *Journal of Electronics & Communication Engineering*, Vol. 10, Issue 5, pp. 229 – 235, Oct. 1998.

[34] A. Kaszubowska, L. Hu, L.P. Barry, "Remote downconversion with wavelength reuse for the radio/fiber uplink connection," *IEEE Photonics Technology Letters,* Vol. 18, Issue 4, pp. 562 – 564, Feb. 2007.

[35] Recommendation ITU-R F1.1332-1, "Radio-frequency signal transport through optical fibers," 1997-1999.

[36] D. Wake, D. Hohansson, D.G. Moodie, "Passive picocell: a new concept in wireless network infrastructure," *Electronics Letters*, Vol. 33, Issue 5, pp. 404 – 406, Feb. 1997.

[37] X.S. Yao, "Phase-to-amplitude modulation conversion using Brillouin selective sideband amplification," *IEEE Photonics Technology Letters*, Vol. 10, Issue 2, pp. 264 – 266, Feb. 1998.

[38] A. Meier, "Die Ansteuerung von YIG-Oszillatoren," available: http://www.ame-engineering.de/pdf/yig_osc_rev1.pdf (Feb./03/07).

[39] S.C. Michelson, S.J. Fouche, N.J. Bornman, W.D. van Niekerk, "The design of a modular microwave frequency synthesiser: synthesisers for an 8 GHz and 23 GHz digital radio," *4th IEEE Conference in Africa, Africon*, Vol. 2, pp. 734 – 738, Sept. 1996.

[40] S.J. Prasad, C. Haynes, "First demonstration of a GaInP/GaAs HBT microwave oscillator," *IEEE MTT-S International Microwave Symposium Digest*, Vol. 1, TUID-3, pp. 87 – 90, May 1994.

[41] G. Gronau, *Höchstfrequenztechnik – Grundlagen, Schaltungstechnik, Messtechnik, Planare Antennen*. Springer, Berlin, Chapter 7, 2001.

[42] H. Eisele, G.I. Haddad, "D-band InP Gunn devices with second-harmonic power extraction up to 290 GHz," *Electronics Letters*, Vol. 30, Issue 23, pp. 1950 – 1951, Nov. 1994.

[21] Frequency Usage Plan of the German "Bundesnetzagentur für Elektrizität, Gas, Telekommunikation, Post und Eisenbahn," available: http://bundesnetzagentur.de, (Feb./03/07).

[22] M. Engl, "Characterization techniques and evaluation of a plastic Package for mm-Wave applications," Dissertation, available: http://www.opus.ub.unierlangen.de/opus/volltexte/2006/351/, (Jan./01/07).

[23] R.E. Schuh, D. Wake, B. Vern, M. Mateescu, "Hybrid fibre radio access: a network operators approach and requirements," *Proc. 10th Microcoll Conference*, Budapest, Hungary, pp. 211 – 214, Mar. 1999.

[24] IEEE Standard 802.16-2004 (Revision of IEEE Std 802.16-2001), Standard for local and metropolitan area networks, *IEEE Computer Society and IEEE Microwave Theory and Techniques Society*, Oct. 2004.

[25] M.I. Skolnik, *Introduction to radar systems*. 2nd Edn., McGraw-Hill, New York, pp. 410 – 411, 1980.

[26] D.G. Macfarlane, D.A. Robertson, "Long range, high resolution 94 GHz FMCW imaging radar (AVTIS)," *Conference on Infrared and Millimetre Waves and 13th International Conference on Terahertz Electronics*, Vol. 1, pp. 201 – 202, Sept. 2005.

[27] J.B. Mead, A.L. Pazmany, S.M. Sekelsky, R. Bambha, R.E. McIntosh, "Millimeter-wave radars for remotely sensing clouds and precipitation," *Geoscience and Remote Sensing Symposium*, Vol. 3, pp. 1553 – 1555, May 1996.

[28] United States Patent 5920813, available: http://www.freepatentsonline.com/5920813.html (Feb./03/07).

[29] R. Bose, G. Bauer, R. Jakoby, "Two-dimensional line of sight interference analysis of LMDS networks for the downlink and uplink," *Transactions on Antennas and Propagation*, Vol. 52, Issue 9, pp. 2464 – 2473, Sept. 2004.

[30] A. Nordbotten, "LMDS systems and their application," *IEEE Communications Magazine*, Vol. 38, Issue 6, pp. 150 – 154, June 2000.

[31] M. Dinis, J. Fernandes, "Provision of sufficient transmission capacity for broadband mobile multimedia: a step toward 4G," *IEEE Communications Magazine*, Vol. 39, Issue 8, pp. 46 – 54, Aug. 2001.

[11] A. Hirata, M. Harada, T. Nagatsuma, "120-GHz wireless link using photonic techniques for generation, modulation, and emission of Millimetre-wave signals," *Journal of Lightwave Technology*, Vol. 21, Issue 10, pp. 2145 – 2153, Oct. 2003.

[12] Federal Communications Commission, Office of Engineering and Technology "Millimeter Wave propagation: Spectrum Management Implications," Bulletin Nr. 70, July 1997.

[13] P816 EURESCOM study group "Implementation frameworks for integrated wireless – optical access networks," http://www.eurescom.de/~pub-deliveables/P800-series/P816/D4/p816d4.pdf, Feb. 2000, (Feb./30/06).

[14] E. Voges, K. Petermann, *Optische Kommunikationstechnik: Handbuch für Wissenschaft und Industrie*. Springer, Berlin, Chapter 30, 2002.

[15] G. Gronau, *Höchstfrequenztechnik – Grundlagen, Schaltungstechnik, Messtechnik, Planare Antennen*. Springer, Berlin, Chapter 1, 2001.

[16] G.J. Foschini, G.D. Golden, R.A. Valenzuela, T.W. Wolniansky, "Simplified processing for high spectral efficiency wireless communication employing multi-element arrays," *IEEE Journal on Selected Areas in Communications*, Vol. 17, No. 11, pp.1841 – 1852, Nov. 1999.

[17] K. Ohata, K. Maruhashi, M. Ito, S. Kishimoto, K. Ikuina, T. Hashiguchi, N. Takahashi, S. Iwanaga, "Wireless 1.25Gb/s transceiver module at 60GHz. band," *Tech. Dig. ISSCC 2002*, pp. 298 – 299, 2002.

[18] C.S. Park, C.G. Lee, C.-S. Park, "Experimental demonstration of 1.25-Gb/s Radio-Over-Fiber downlink using SBS-based photonic upconversion," *IEEE Photonics Technology Letters*, Vol. 19, Issue 22, pp. 1828 – 1830, Nov. 2007.

[19] A. Hirata, T. Kosugi, H. Takahashi, R. Yamaguchi, F. Nakajima, et al., "120-GHz-Band Millimeter-Wave photonic wireless link for 10-Gb/s data transmission," *IEEE Transactions on Microwave Theory and Techniques*, Vol. 54, No. 5, pp. 1937 – 1944, May 2006.

[20] Georgia Institute of Technology "Multi-gigabit wireless research could soon make wired computers and peripherals obsolete," *Science Daily*, 19 July 2007, available: http://www.sciencedaily.com /releases/2007/07/070719100232 .htm/ (Jan./22/08).

12 References

[1] L. Boithias, *Radio wave propagation*. North Oxford Academic Publishers Ltd., London, 1987.

[2] P.F.M. Smulders, "Exploiting the 60 GHz band for local wireless multimedia access: prospects and future directions," *IEEE Communications Magazine*, Vol. 40, No. 1, pp. 140 – 147, 2002.

[3] T.H. Maiman, "Stimulated optical radiation in ruby," *Nature*, Vol. 187, 493 – 494, 1960.

[4] F.P. Kapron, D.B. Keck, R.D. Maurer, "Radiation losses in glass optical waveguides," *Applied Physical Letters*, Vol. 17, No. 10, pp. 423 – 425, Nov. 1970.

[5] I. Hayashi, M.B. Panish, P.W. Foy, S. Sumski, "Junction lasers which operate continuously at room temperature," *Applied Physical Letters*, Vol. 17, No. 3, pp. 109 – 111, Aug. 1970.

[6] V. Brückner, "DWDM – Bandbreite ohne Ende?," *Proc. 5th ITG-Fachtagung Photonische Netze*, Leipzig, Vol. 182, pp. 13 – 18, May 2004.

[7] H. Masuda, A. Sano, T. Kobayashi, E. Yoshida, Y. Miyamoto, Y. Hibino, et al.,"20.4-Tb/s (204 × 111 Gb/s) Transmission over 240 km using bandwidth-maximized hybrid Raman/EDFAs," *Optical Fiber Conference*, Anaheim, PDP20, Mar. 2007.

[8] C.R.S. Fludger, T. Duthel, D. van den Borne, C. Schulien, E-D. Schmidt, T. Wuth, et al., "10 x 111 Gbit/s, 50 GHz spaced, POLMUX-RZ-DQPSK transmission over 2375 km employing coherent equalisation," *Optical Fiber Conference*, Anaheim, PDP22, Mar. 2007.

[9] A.H. Gnauk, C.R. Doerr, P.J. Winzer, T. Kawanishi, "Optical equalization of 42.7-Gbaud bandlimited RZ-DQPSK signals," *IEEE Photonics Technology Letters*, Vol. 19, Issue 19, pp. 1442 – 1444, Oct. 2007.

[10] A. Ng'oma, T. Koonen, I.T. Monroy, H. van den Boom, P. Smulders, G.-D. Khoe, "Distributing Microwave Signals via Polymer Optical Fiber (POF) Systems," *Proc. 6th Ann. Symposium IEEE/LEOS* Benelux Chapter, Amsterdam, 2002.

Furthermore, other types of fibre such as Allwave™ fibres are recommended to be investigated as a non-linear gain and transmission media. Since other fibre types impact the ASEN of the Brillouin amplification process in a different way, further system enhancements can be expected.

A second avenue worth investigation is the optimisation of the frequency comb generation technique. In this work, a non-linear amplitude modulation has been applied in order to be flexible in the generated frequency comb. On the other hand, amplitude modulation limits the power stability by the bias drift that induces power fluctuations in the sidebands. This disadvantage can be circumvented by the use of other frequency comb generation techniques. For instance, phase modulation or the application of FWM can replace the amplitude modulation part in the set-up. Although these techniques could lead to other limitations in the system, they should be considered in the future work.

Another possible direction would be to improve the stability performance of the system by an enhanced temperature and wavelength control. Due to the long term wavelength fluctuations of the fibre laser the pump lasers have to be tuned in temperature in order to follow the wavelength shifting sidebands. This can be realised by a suppression of environmental impacts such as air flows or room temperature fluctuations. On the other hand, if the spectrum distortions, explained in Section 9.3 can be circumvented, a more wavelength stable DFB laser can be used as a signal laser.

A further option to improve system functionality would be the integration of broadband RF-amplifiers in order to boost the modulated carrier. The main limitation of the data transmission experiments was the low power level of the RF-signal. This was caused by the conversion loss of the PD and the external mixer. On the other hand, an optical pre-amplifier located before the PD and the use of a high power PD with a higher optic-electric conversion can increase the power of the RF-signal as well. Low pass filters that are adapted to the modulation bandwidth would also increase the transmission quality. Thus, radio propagation experiments in the far field can be carried out.

11 Future Work

Future work for this project consists of the full implementation of all necessary components in order to set-up a high bit-rate Radio Over Fibre downlink transmission system. The current status of the project is a laboratory experimental set-up. It allows a flexible change of the components in order to investigate all necessary parameters of the system. The next step is an optimisation of the set-up based on the results proposed in this work. With a compact full automatic prototype the system applicability under real environmental conditions can be investigated in detail. Moreover, an automatic computer control of the system would increase the convenience of the set-up operation. The application of equipment with "device-to-computer" interfaces such as GPIB or Ethernet for instance, is a precondition. A booting algorithm where all devices are remote controlled can boot up the system without any manual settings of the user. Furthermore, a graphical operating interface of a PC provides a more convenient way to handle the system.

By using the prototype, higher data transmission rates at different carrier frequencies can be tested. The state of the art is an error free transmission of a 1 Gbit/s PRBS 23 signal. Therefore, limitations described in Section 9.4 and their impact on the transmission have to be detailed. By using higher data rates, other limitations such as chromatic dispersion in the optical fibre have to be considered. Furthermore, the transmission of a real data signal such as a video stream and its quality properties should be investigated. The system operating frequency band that should be used depends on the propagation condition in the atmosphere and the allocation of the frequency spectrum in the desired range. These circumstances have to be investigated as well.

Before the step of building a prototype can be realised, there are some avenues for future work which may be considered. A proposal to investigate the system for different fibre lengths in order to analyse ASEN influences on the phase noise of the mm-Wave signal is under way. This property has only been discussed in theory [153], and no experimental work has been conducted to date. It is assumed that the ASEN can be reduced, if shorter fibre lengths are used. For an experimental investigation, spools of optical fibre with different lengths are necessary.

The comparison of theory and experiment show that both are in agreement with one another. The phase noises of all generated carrier frequencies[1] are low (approx. -90 dBc/Hz @ 10 kHz offset frequency). Dispersion effects and amplitude noise are negligibly small. FWHM bandwidths are measured to be 1 Hz, and are assumed to be even lower. The corresponding RF gains lie between 55.6 and 66.46 dB depending on the level of up conversion. The measured RF powers are in the range of -23.66 dBm and -34.4 dBm. This power degradation occurs due to the inefficient optic-electric conversion in the PD at higher frequencies. A stability analysis of the generated RF signals showed a short term fluctuation of ± 0.29 dB and a long term fluctuation of ± 1.65 dB over 27 h.

Investigations on data modulation showed that an implementation of the presented set-up is complex and the modulation bandwidth is limited by the gain bandwidth of SBS. Therefore, the modulation set-up has been changed in order to be independent of the bandwidth of the Brillouin amplifiers. Bit error measurements have been carried out at 200, 500 and 1000 Mbit/s PRBS 23 signals. In the back to back case, an error free transmission was observed whereas the BER increases in the case of radio propagation due to the loss of power.

The main limitations of the system lie in the frequency comb generation technique employed, in polarisation penalties, stabilisation, the Brillouin amplified induced ASEN and in the location of the pump sources that have to be adapted in order to fulfil the requirements of Radio Over Fibre.

[1] 5.714, 11.428, 17.142, 22.856, 28.57, 34.284 and 39.998 GHz

10 Conclusion

This thesis has presented a new and simple method for the generation of mm-Waves in paritucular with regard to Radio Over Fibre applications. The merging of broadband optical communications and the flexible wireless radio access provides a very high potential future transmission system. Millimetre Waves as carrier frequencies are used in order to overcome the congested lower frequency bands. Beside techniques that rely on the electrical generation of high frequencies, the optical creation of carrier signals seems to be a more convenient and effective way.

The heterodyning of two phase correlated optical signals in a photodetector has been selected to be analysed in detail. These components are generated by amplitude modulation and are amplified in a transmission line by optical amplifiers. For the selection of the desired frequency components, the non-linear effect of stimulated Brillouin scattering as a narrow band amplifier was used. The effect was described in detail including preliminary simulations.

A theoretical analysis in the form of a derivation of a differential equation system allowed predictions concerning the phase properties of the amplified frequency components and the heterodyned signal. The influence of phase decorrelation of two waves derived from one source is negligible. A high signal power, a low detuning, a short fibre length and the regime of driving the amplifier into saturation, can reduce the noise significantly. If the power of both sidebands are nearly equal, the phase change due to self and cross phase modulation is the same. If the detuning between the pump and the signal wave is minimal, the phase shifts for both sidebands are also equal. Hence, the SBS influence on the mm-wave is small. All theoretically derived systems and settings have been considered except the use of a short fibre length.

A numerical solution of the DES has been carried out by a simulation in order to obtain information about the behaviour of the system in different scenarios. Besides the saturation effect, which is typical for an SBS amplification process, low phase noise influences due to amplification have also been calculated. A phase alternation of the heterodyned signal occurs when the detuning of the sidebands and the Brillouin gains are opposite. This distortion is assumed to be negligible, as the detuning has its origin in the frequency alternation of the signal laser. Hence, the sidebands drift in the same direction.

Brillouin threshold increases and higher pump powers are necessary. This effect is not a dramatic one, as the threshold depends upon the effective length of the fibre according to Equation (4.8). The characteristic of the Brillouin threshold versus the fibre length according to Equations (4.8), (4.9) and (4.14) and the parameters of Section 4.4 can be described as shown in Fig. 9-2. Thus, for a 20 km fibre the Brillouin threshold increases by 3.02 mW. It should be noted that for this optimisation the simulation results of Section 6.2.3 have to be considered.

9.6 Location of Pump Sources

As can be seen in Fig. 8-2 the pump source is located within the Central Station. That means the Brillouin gain medium that is an optical fibre cannot be used for data transmission since the CS is located at one point. At the output of the CS the optical mm-Wave has to be amplified again and further transmissions to the RAUs are required.

Another possibility is to locate the pump source within the RAU unit, although this solution is not in line with ROF principles. The complexity of the RAU would increase, which is not acceptable.

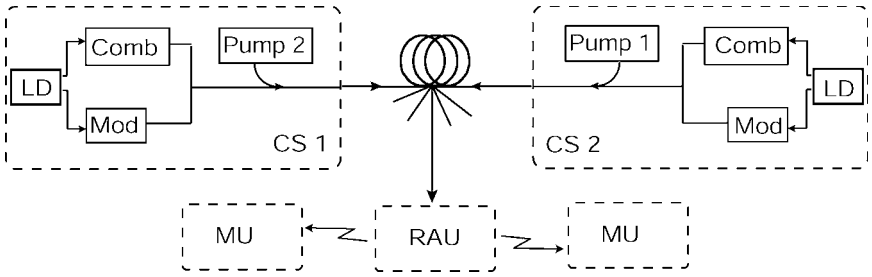

Fig. 9-3 Alternative location of pump sources.

As the Brillouin gain medium is also used as a transmission line it can be the physical link between several Central Stations as shown in Fig. 9-3. Each CS includes the pump sources for another CS in order to amplify the desired frequency component. By decoupling the desired mm-Wave at a certain point of the fibre the signal can be separated and transmitted to the RAU. Naturally, this alternative can also be applied to the modulation scheme of the proposed method in Fig. 8-1.

9.4 Modulation Bandwidth

In Chapter 8, a possible and easy way for the mm-Wave carrier modulation was shown. This solution was given under the aspect of modulating the optical carrier with data whereas one sideband is SBS amplified.

In order to modulate the RF carrier that is generated by the amplification of two sidebands there are several limitations in the system. On the one hand the Brillouin gain bandwidth has to be adapted. Several methods were described in Section 4.5, with the conclusion that there is in principle no bandwidth limitation, considering high optical pump powers.

On the other hand, the modulation bandwidth is limited by the modulation frequency of the frequency comb generator. Although all undesired sidebands are either suppressed by the MZM operation mode or by the natural attenuation of the fibre their impact can not be ignored. These components limit the modulation bandwidth and can influence the carrier, as some of them have the same frequency separation. This effect can be seen in the spectral analysis of the mm-Wave signal in Section 7.3.3.

9.5 Brillouin Amplifier Noise

As described in Section 7.3.4.1, the main noise introduction to the mm-Wave carrier originates from the Brillouin amplifiers. According to [153] the application of long fibres increase the spontaneous emission noise of the Brillouin amplifier. Thus it is

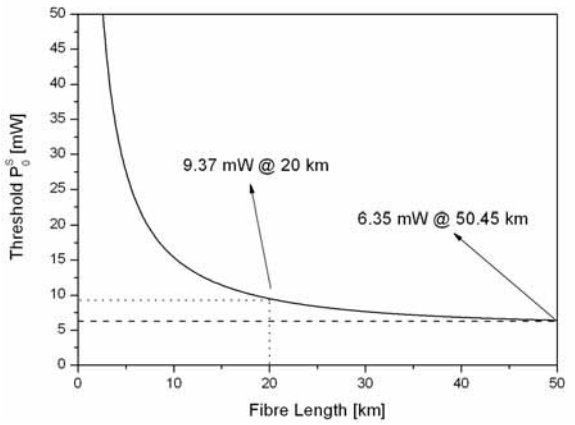

Fig. 9-2 Brillouin threshold vs. fibre length.

assumed that a shorter fibre also reduces the noise of the sideband amplification and therefore the mm-Wave signal. On the other hand, with a shorter fibre length, the

involved. In case the Brillouin amplifiers enhance the signals a dramatic increase in spectral distortion is observed. Further spectral components with a frequency separation of 92 kHz are generated, as can be seen in Fig. 9-1a. They are very strong, with a magnitude of 15 dB lower than the carrier. The same effect was also observed in phase noise measurements which can be seen in Fig. 9-1b. This distortion occurs within a range of approximately 30 MHz, which corresponds to the Brillouin bandwidth. The modulator drive signal can be excluded as the source of distortion since it includes no raised spectral component at 92 kHz[3].

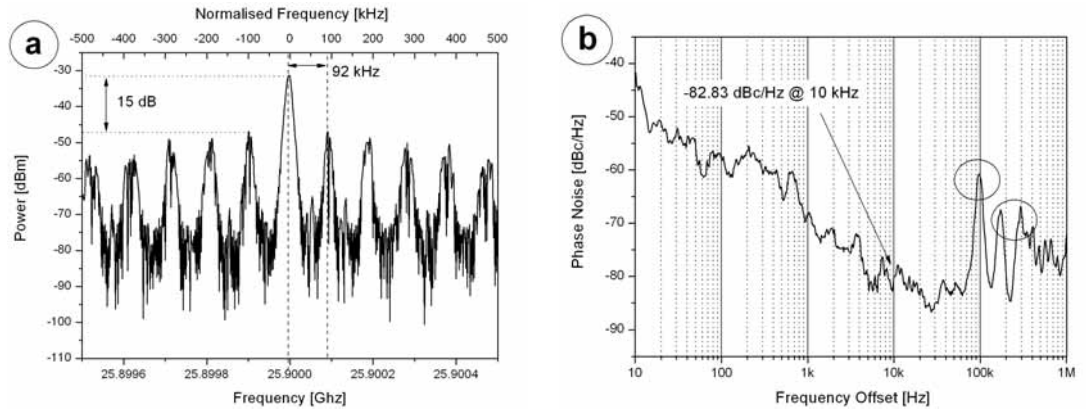

Fig. 9-1 a: spectrum and b: phase noise of 25.9 GHz carrier generated by a DSSC modulated DFB LD as a signal laser with SBS amplification.

An explanation for this phenomenon is described in the following.

Although a detuning is attempted to be avoided as much as possible, this effect can not be neglected. Therefore, the two sidebands can lie out of the centre line width of the Brillouin gains and are amplified in a different way. Whereas the fibre laser has a line width of < 1 kHz that is much lower than the Brillouin bandwidth, the sidebands generated by a DFB have a bandwidth (3 MHz) in the Brillouin bandwidth range. Hence, a detuning effect leads to a different amplification of each spectral part of the sidebands. In case the laser spectrum includes a 92 kHz signal, these ripples are amplified in a different way. Thus, during the heterodyning process in the PD these frequency separations are detected. This effect can be avoided by using either a narrow band laser source or a broadband laser (bandwidth lies in the Brillouin gain bandwidth range) that has an evenly distributed spectrum.

[3] See reference phase noise (dashed lines) @ 92 kHz in Fig. 7-13.

polarisation status via an electronically controlled polarisation controller. A simple solution to circumvent polarisation penalties is a depolariser. A depolariser can distribute the waves over all states of polarisation.

9.3 Stabilisation

As described in Section 7.3.5 the system is influenced by short term power fluctuations. They can be avoided by using a biased controlled MZM[2] and a stable coupler. On the other hand, long term fluctuations are indeed a problem of the system. It can be seen in Fig. 7-18 that the preliminary control loop is slow and not able to manage the tuning of the Brillouin gains perfectly. However, the aim of this work was not to present a fully implemented Radio Over Fibre system. Moreover, it should be a further possible realisation amongst other presented methods. Thus, in the case where the method finds a real application in industry, further developments are necessary.

In [215] it was shown that the temperature influence on the Brillouin shift is 1.36 MHz/°C in a SSMF at 1.32 µm. Assuming an equal Brillouin shift of 1.55 µm and a Brillouin bandwidth of 28 MHz there is a need of ± 10.29 °C temperature change for a 3 dB detuning between the sidebands and the Brillouin gains. Under laboratory conditions no signal impacts due to temperature shift were observed. On the other hand, the temperature change in the field is probably in this range but the alternation is slow. Thus, a professional frequency control of the Brillouin gain and the sidebands can compensate for this limitation.

In order to circumvent fluctuation limitations, a standard DFB LD was used experimentally instead of the narrowband fibre laser. Because of the precision temperature control used, there is no control loop necessary in order to readjust the Brillouin gains.

Due to the fact that the phase noises, and therefore the bandwidths, are correlated in a heterodyne detection system, the spectral bandwidth of the resulting mm-Wave is independent of the bandwidth of the optical components. Hence, a broadband 5 MHz bandwidth laser diode that is DSSC modulated also generates a mm-Wave signal with a narrow bandwidth. But this is only the case if no SBS amplification is

[2] Or another frequency comb generation method.

9 Limitations

9.1 Bias Drift

In Section 7.3.5.1 a general problem with amplitude modulators was discussed. At wavelengths around 1.5 µm bias drift problems are caused by leakage currents flowing in both the $LiNbO_3$ substrate and the buffer dielectric layer [211]. These drifts induce power fluctuations[1] to the sidebands that are generated by driving the modulator into overmodulation (see Fig. 7-17). On the other hand, there are many solutions to circumvent this system limitation. Among them are the annealing of the buffer layer [212], the use of a conducting buffer layer [213] and the removal of unwanted dielectric material from between the electrodes [214]. Another possibility is the application of a fibre Bragg grating to enhance the set-up stability [97]. However, these solutions always lead to an increased complexity. Therefore, the general use of amplitude modulation for the generation of a frequency comb for mm-Wave generation always leads to difficulties due to bias drift effects.

A further way of generating a frequency comb is the application of phase modulators that have no bias drift effects. Although there are limitations on the phase of the sidebands they provide a higher up conversion grade and more stable signals. Thus a 10 times frequency up conversion from 4.4 GHz to 44 GHz was shown in [188] by using a reciprocating optical modulator. Of course, such frequency comb generation techniques are also suitable for the proposed method.

9.2 Polarisation Penalties

The alteration of the polarisation status of the pump waves and the sidebands does not lead to a total loss of signal but can reduce the absolute power of the generated mm-Wave [151]. The time frame of polarisation change was observed to be in the range of tens of minutes. This power penalty can be decreased by a temperature and stress controlled environment, which is quite complex and increases the system costs. Furthermore, a control loop can detect the amplified sidebands and can adjust the

[1] In opposite directions

radio link was investigated and a successful 1 Gbit/s data transmission was shown. However, using high performance equipment such as a high gain broadband amplifier can also increase the data rate and the signal power.

The presented results underline the simple implementation of a modulation scheme to the presented mm-Wave generation technique.

The received 1 Gbit/s signal is shown in Fig. 8-8 and the corresponding eye diagrams of the 200 and 500 Mbit/s signal can be seen in Appendix I6. It can be seen that the noise rises due to radio propagation. Due to the low transmission distance, this enhanced noise is assumed to have its origin in the reduced power (attenuation) and not by the free space transmission impacts such as reflection, scattering, deflection. The reduced power is compensated by the receiver unit. Therefore, the power of the signal is the same as without free space transmission according to Fig. 8-7. The noise is generated due to the decreased signal-to-noise ratio.

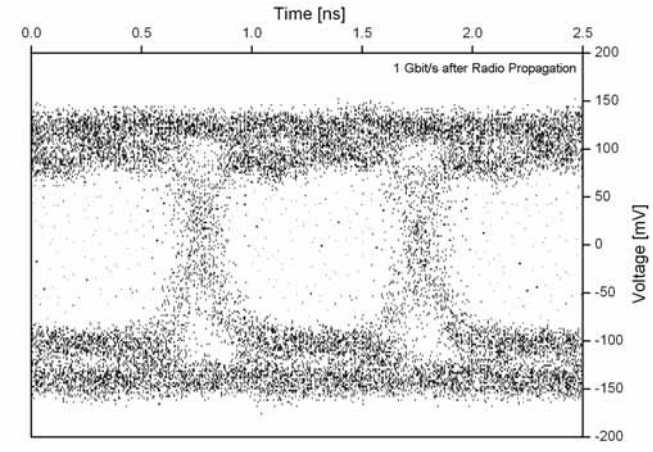

Fig. 8-8 1 Gbit/s after radio propagation.

Under the condition of radio propagation the BER tester measured error rates of up to $1 \cdot 10^{-2}$ due to the enhanced signal noise. However, although the eye was closed compared to back to back measurements, radio propagation of the 200, 500 and 1000 Mbit/s signals have been successfully realised.

8.5 Conclusion

In this chapter a successful implementation of a modulation scheme to the presented mm-Wave generation technique was illustrated. The focus was laid on a broad band downlink realisation. For simplicity the original frequency generation set-up was changed in order to simplify a modulation implementation. Several experiments with data rates of 200, 500 and 1000 Mbit/s of a PRBS 23 signal have been shown. Thus, a successful realisation of an error free transmission of a data rate of 1 Gbit/s over a 50 km optical fibre was shown. A Q-factor analysis verifies the low bit error rate measured by the BERT. Due to a very low signal power the system was very sensitive to detuning effects of the Brillouin amplification process. Furthermore, a

transmitted via several lengths of fibres at a RF frequency of 40 GHz. There were no power penalties due to chromatic dispersion measured.

Table 8-1 Important values of eye diagram analysis.

Data Rate	U_1 [mV]	U_0 [mV]	σ_1 [mV]	σ_0 [mV]	Q	BER
200 Mbit/s	125.3	-148.3	17.55	15.0	8.405	$21.6 \cdot 10^{-18}$
500 Mbit/s	117.9	-137.4	11.61	18.1	8.59	$4.4 \cdot 10^{-18}$
1 Gbit/s	92.41	-126.6	15.17	20.15	6.20	$287 \cdot 10^{-12}$

8.4 Modulation Results after Radio Propagation

The discussion in the previous chapter highlighted that a low signal power leads to an unstable set-up. Nevertheless, the experiment is extended in such a manner that two horn antennas realise radio propagation at a 32 GHz carrier frequency (see Appendix E6). The homemade pyramidal horn antennas where developed by S. Neidhardt et al. as a Masters project work in the Antennas & High frequency Research group in the Dublin Institute of Technology [207]. They are inserted between the RF amplifier (2) and the external mixer according to Appendix E6. Due to the low transmission power and the high path loss that rises in proportion to the square of the distance or greater, and proportional to the square of the frequency, the antennas have a local separation of 5 cm. This distance is within the near field of the antennas. The distance where the far field of an antenna outweighs the near field *df* lies in the range of several wavelengths [209] and can be described as [210]

$$df = \frac{2l^2}{\lambda} \tag{8.3}$$

with λ as the wavelength of the transmitted signal and *l* as the maximum radiating linear dimension of the antenna[2], or in this case, of the horn aperture. On the one hand, the application in the near field does not exploit the full gain of the antennas. On the other hand, the path loss is reduced significantly and radio propagation can be executed. All given antenna parameters are only valid for the far field. Thus the far field range for a frequency of 32 GHz starts at 43.3 cm according to Equation (8.3). The gain characteristic for the antennas is shown in Appendix F3.

[2] The E-field linear dimension of the aperture is 4.5 cm.

unit. As can be seen, the eye is opened without any significant distortions in the centre.

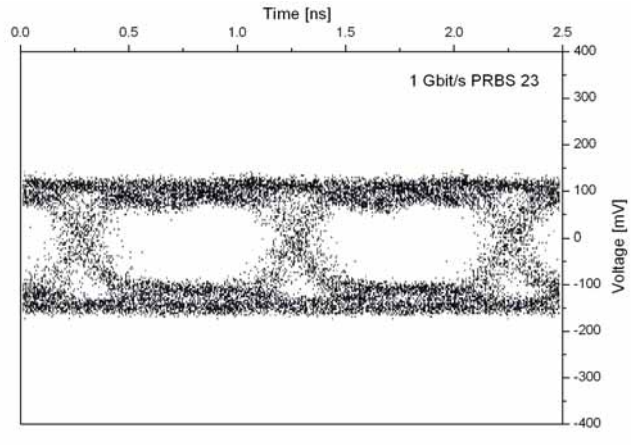

Fig. 8-7 Eye diagram of 1 Gbit/s PRBS 23 signal back to back.

In order to highlight the measurement of the BERT which results in an error free transmission, a Q-factor analysis is shown in the following. The Q-factor is a synonym for the Gaussian error integral and offers a method to investigate the probability density function (PDF) of the two signal states ("0" and "1") at a certain time. This time slot is commonly at the centre of the eye. For the analysis of the presented eye diagrams the Q-factor is calculated according to [208]

$$Q = \frac{U_1 - U_0}{\sigma_1 + \sigma_0}. \tag{8.1}$$

U_1, U_0 and σ_1, σ_2 are the averaged voltage values of "0", "1" and the standard deviation of the PDFs, respectively. In Appendix I5 an overview of the definition of the standard deviation σ is provided. Over the relation [208]

$$BER = \frac{1}{Q \cdot \sqrt{2\pi}} \cdot e^{-\frac{Q^2}{2}} \tag{8.2}$$

the BER can be calculated. It is noted that the Q-factor analysis should be seen as an approximation, since the low sample rate of the oscilloscope provided only few measurement values (compare Appendix I5). In Table 8-1 an overview of the parameters used for the calculation of the BER is provided. According to the bit error rates of the 200, 500 and 1000 Mbit/s it can be said that all eyes are open and able to transmit error free data signals. However, it is assumed that the power behaviour of the signal is not affected by chromatic dispersion. This assumption is based on the experiment of A. Wiberg et al. [110]. In this work, a data rate of 2.5 Gbit/s was

At all spectra the typical peak at the zero points that occurs due to NRZ coding can be seen. Although the RF amplifier (2) enhances the modulated signal the powers of the modulation sidebands lie at around -40 dBm according to Fig. 8-6a and Appendix I2. Due to the fact that the mixer has a high conversion loss, the base band signal is attenuated. This power penalty is balanced by the receiver module which has a zero gain bandwidth of 3.21 GHz. According to Fig. 8-6b and Appendix I4, the powers of the first sidebands of the 200, 500 and 1000 Mbit/s down converted signals are -25, -30 and -35 dBm, respectively,

8.3 Modulation Results Back to Back

This chapter analyses the data transmission from the MZM2 via an optical fibre to the photodetector. Again, data rates of 200 and 500 MHz are shown in Appendix I4. Due to the low power of the data signals the detection on the oscilloscope and the BERT was very crucial. During the measurements it was observed that there is a threshold at which the receiver unit starts amplifying. In case the optical power is high enough to drive the system, the eye became clear and the bit error rate decreased down to an error free transmission. In the case that the optical power decreases slightly due to a slow detuning of the amplification process, the power of the RF signal decreases logarithmically. Therefore, the eye got closed and the BER increases dramatically up to values of $1 \cdot 10^{-4}$. Measurements that describe the BER versus the optical power at the PD do not work due to the described non-linear property of the receiver unit. However, this problem can be circumvented by using a PD with a higher responsivity in the desired frequency range, optical amplifier, and RF amplifiers to boost the heterodyned signal, or due to a more efficient down conversion of the RF signal. Furthermore, the combination of a low noise final amplifier from DC to the desired range and a low pass filter that reduces undesired spectral frequency distortions can significantly enhance the system performance of the presented approach.

The verification of the successful error free transmission of a 1 Gbit/s data signal via a 32 GHz carrier over a 50 km standard optical fibre is shown in Fig. 8-7. The peak to peak voltage was measured to be 250 mV. This result was achieved after optimising all possible parameters to achieve the highest power level at the receiver

As can be seen, there is an overshoot in the range of 0.48 V which is a negative property of the signal. Furthermore, the edge is very flat in comparison to a 200 Mbit/s signal. The lower the bit rate, the better the signal performance of the pattern generator. However, due to the limited bandwidth of the oscilloscope (1 GHz) and the gain bandwidth of the receiver unit, a data rate of 1 Gbit/s was chosen as the upper limit for the experiments.

8.2.2 Frequency Domain

For the graphical demonstration of the modulated RF signal the mixer is not driven by an external LO source as described in Appendix E6 but by the internal LO of the ESA which is 310.7 MHz. The advantage of this measurement method is that the ESA recalculates the conversion loss of the external mixer. Thus, the actual power spectrum can be analysed. On the other hand, the spectrum is mirrored at the LO of the ESA as can be seen in Fig. 8-6a. Whereas the spectrum of the 200 Mbit/s modulated carrier can be detected without distortion (see Appendix I2) higher modulation rates lead to a falsed display at the ESA. Since this effect is just a measuring error it does not impact the experiment and can be neglected.

The modulated and amplified RF signal is down-converted via an external harmonic mixer. The LO frequency is 16 GHz in order to use the second LO harmonics to mix the 32 GHz signal into base band. After down mixing, the signal is enhanced by a receiver unit which acts as an amplifier and a band pass filter at the same time (see Appendix F2). The gain of the device enhances the base band signal of the 1 Gbit/s signal, as can be seen in Fig. 8-6b. Base band signals of 200 and 500 Mbit/s at different spans are illustrated in Appendix I3.

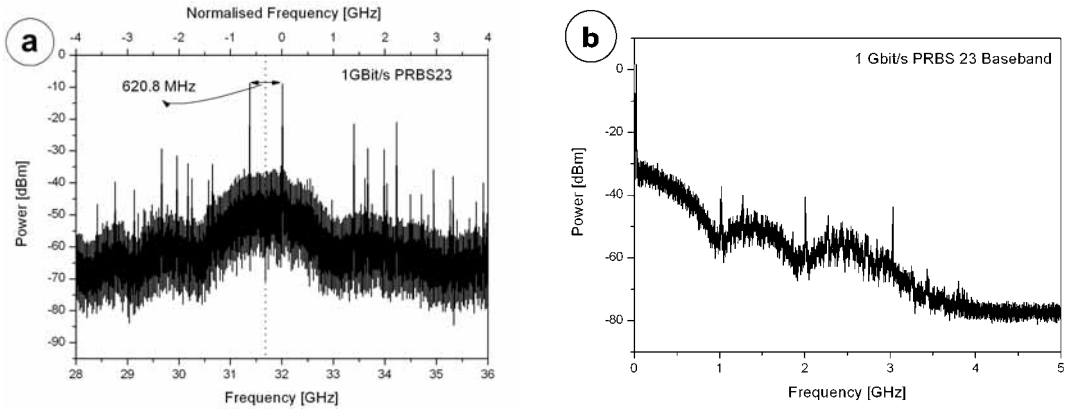

Fig. 8-6 a: 1 GBit/s modulated 32 GHz carrier signal. The spectrum is mirrored at the local frequency (310.4 MHz) of the ESA. b: 1 Gbit/s down converted into base band.

After the heterodyning process the signal was amplified by a 2-50 GHz amplifier to a power level of -10 dBm (dashed line in Fig. 8-4). Several experiments have been carried out to analyse the system at different modulation rates with and without radio propagation. However, in both cases the modulated carrier is down-converted into base band and enhanced by a receiver unit which acts as an amplifier (see Appendix E6 and F2). After a 50/50 splitting, the signal is recorded on the oscilloscope and analysed by the bit error rate tester (BERT).

8.2 Modulation Format

For the modulation, data rates of 200, 500 and 1000 Mbit/s were chosen. In this chapter all characteristics show the signal performances of a 1 Gbit/s data rate transmission. The corresponding graphs for each measurement of 200 and 500 Mbit/s are shown in Appendix I.

8.2.1 Time Domain

In order to simulate a realistic data stream a PRBS data signal with a pattern length of $1 \cdot 10^{23}$-1 bits is used with non-return-to-zero code (NRZ coding). This is one of the simplest coding mechanisms as the "transmitted bits" are converted directly to the line signal. On the one hand, NRZ signals have higher bandwidth efficiency, however, on the other an external clock is required. In Fig. 8-5 the output signal of the pulse pattern generator is shown at a data rate of 1 Gbit/s. The corresponding eye diagrams of the 200 and 500 Mbit/s signals are shown in Appendix I1.

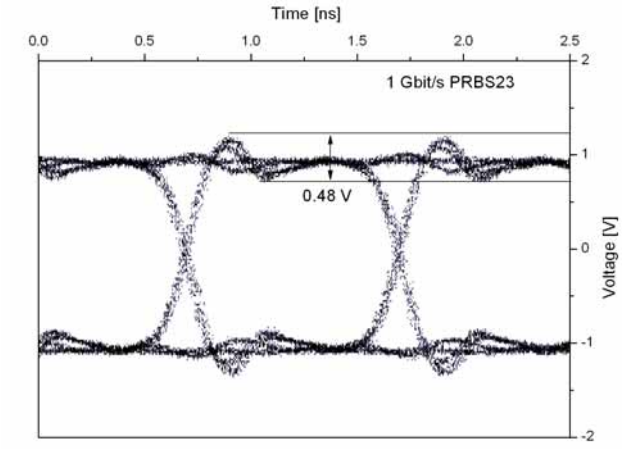

Fig. 8-5 Eye diagram of the output signal of the pulse pattern generator at 1 Gbit/s.

As can be seen, the carrier is suppressed by an adaptation of the MZM operation point in order to avoid beating signals at the same wavelength. In Fig. 8-3b the optical spectrum at the output of the circulator after SBS amplification is shown. The tunable coupler is adjusted in such a manner that both frequency components have the same power. It should be noted that the two optical carriers travel different optical paths. These paths can have different lengths, and the signal, therefore, experiences a differential propagation delay. The effect of this is described in detail in [58], and could induce a power penalty. However, due to an application of a narrowband laser source this effect becomes negligibly small.

Due to a combination of a drive signal frequency of 6.4 GHz and the usage of the 5^{th} sideband, a frequency separation of 32 GHz is achieved. This frequency was chosen under the aspect of two conditions. On the one hand, the carrier frequency should be high to emphasise the flexibility and strengths of the method. Furthermore, the hand made horn antennas are optimised to work at frequencies from 30 GHz or higher [207]. On the other hand, the PD has a 3 dB bandwidth of 27 GHz. The responsivity decreases logarithmically with increase of frequency and induces power penalties. Thus, measurements at 32 GHz are carried out as a compromise.

At the output of the circulator the signal is divided in order to monitor the amplification process at the OSA. The main part is fed into the PD with an input power of -1 dBm where the modulated carrier is heterodyned with the amplified fifth order sideband. The bandwidth of the heterodyned carrier signal (without data modulation) is measured to be 300 Hz with a power level of -40 dBm as can be seen in Fig. 8-4 (solid line). Here again, the measurements where restricted by the RBW of the ESA.

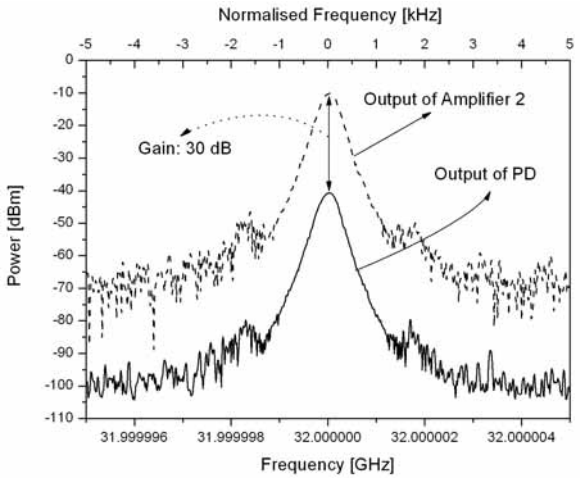

Fig. 8-4 32 GHz spectrum before (solid line) and after (dashed line) electrical amplification.

The corresponding block diagram and important measurement settings are shown in Appendix E6. Again, the light of a narrowband fibre laser is used as a signal laser. The light beam is divided into two paths. The optical carrier launched into the upper path is modulated in such a manner that only odd order sidebands are generated while the carrier is suppressed. The applied bias voltage is -4.5 V and the 6.4 GHz signal has a power of + 35 dBm at the output of the amplifier (amplifier 1). The other light beam injected into the lower path is modulated by data. Here, a 10 Gbit/s amplitude modulator with integrated driver is used. The MZM 2 is driven by an Anritsu pulse pattern generator with a Pseudorandom Binary Sequence with a pattern length of 10^{23}-1 (PRBS 23). The signal has a peak to peak voltage of 2 V with -1 V offset. An EDFA is used to boost the broadened optical carrier to a power of 10.4 dBm which is slightly under the Brillouin threshold. The generated frequency comb and the modulated carrier are coupled by a tunable coupler and are injected into the 50.45 km SSMF. A standard DFB laser diode with a pump power of 4.1 mW at the circulator output is used to amplify the upper[1] 5th order sideband. The power at the output of the fibre is 270 nW (-35.68 dBm) without and 0.46 mW (-3.37 dBm) with Brillouin amplification. Thus, an amplification of 32.31 dB for the 5th sideband is achieved. The optical spectrum at the output of the tunable coupler is shown in Fig. 8-3a. The black/dashed trace represents the spectrum when the optical carrier is injected into the system, whereas the red/solid line is the signal without the optical carrier.

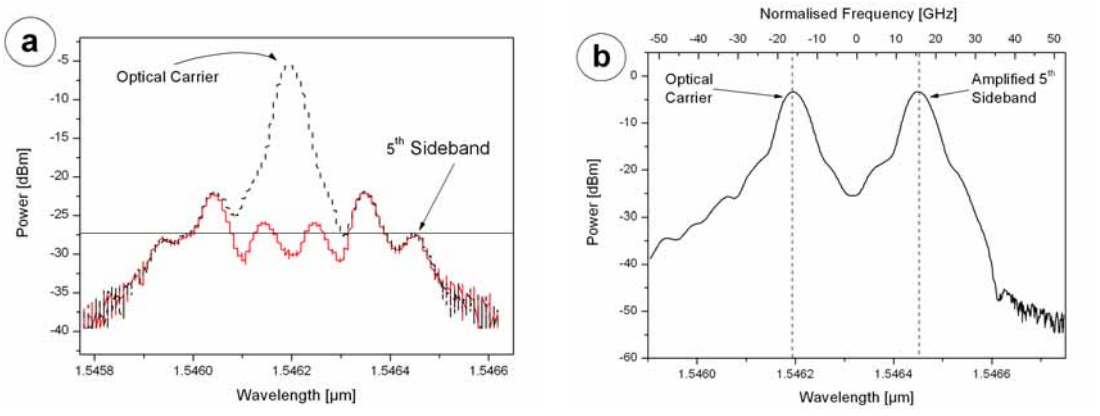

Fig. 8-3 a: Optical spectrum at the fibre input: Frequency comb without optical carrier (red/solid line) and with optical carrier (black dashed line); b: Optical spectrum at the circulator output.

[1] In regard to the wavelength

The following mm-Wave modulation method is based on the modulation of an optical carrier with data [202]. A similar idea using phase modulation for the photonic up-conversion instead of an amplitude modulation has been proposed by Yao [37]. There, a 6.4 GHz signal has been generated, but without any detailed investigations on stability, noise properties and modulation. Although phase modulation generates a large number of sidebands and, the converting factor is high, the heterodyne superposition of related sidebands may lead to distortion of the detected signal that are not discussed in the paper.

However, the principle idea of Yao is extended in this approach. Whereas preliminary results and predictions are shown in [203] and experimental results are presented in [204], [205] and [206], this chapter describes a detailed investigation of the idea and data transmission experiments.

8.1 Set-up

A principle overview of the operation of the proposed method is shown in Fig. 8-2. It relies on the separation of the optical carrier. One part is modulated by data whereas the other part is used for frequency comb generation. Only one pump source is required to amplify one sideband of the frequency comb. In Fig. 8-2 the principle Radio Over Fibre based set-up can also be seen. The set-up includes all properties described in Section 2.2.2.1. The three main components Central Station (CS), Remote Antenna Unit (RAU) and the Mobile Unit (MU) are given and can be compared to the set-up in Fig. 2-2.

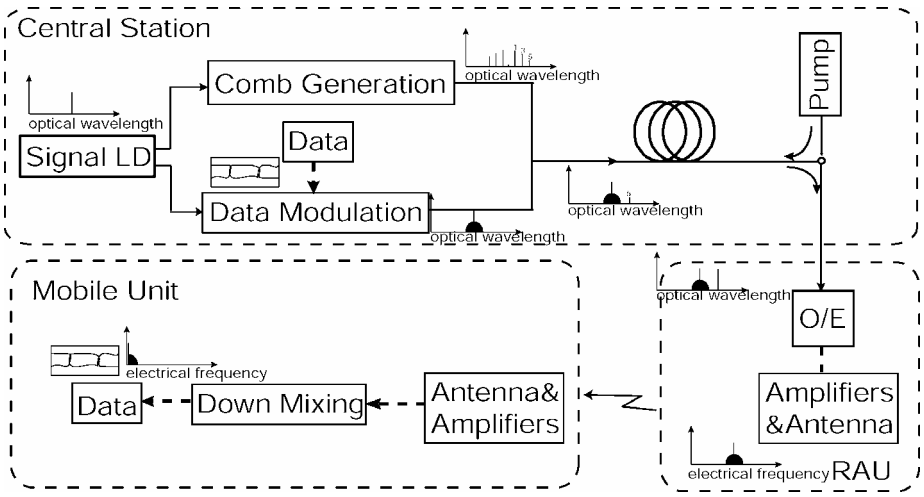

Fig. 8-2 Principle operation of modulation set-up in respect to ROF.

8 Carrier Modulation

In Chapters 5 - 7 a detailed theoretical and experimental description for the carrier generation was given. However, the main task of a transmission line in general is the transportation of data from one point to another. Therefore, it is necessary to investigate the modulation aspects of the presented set-up.

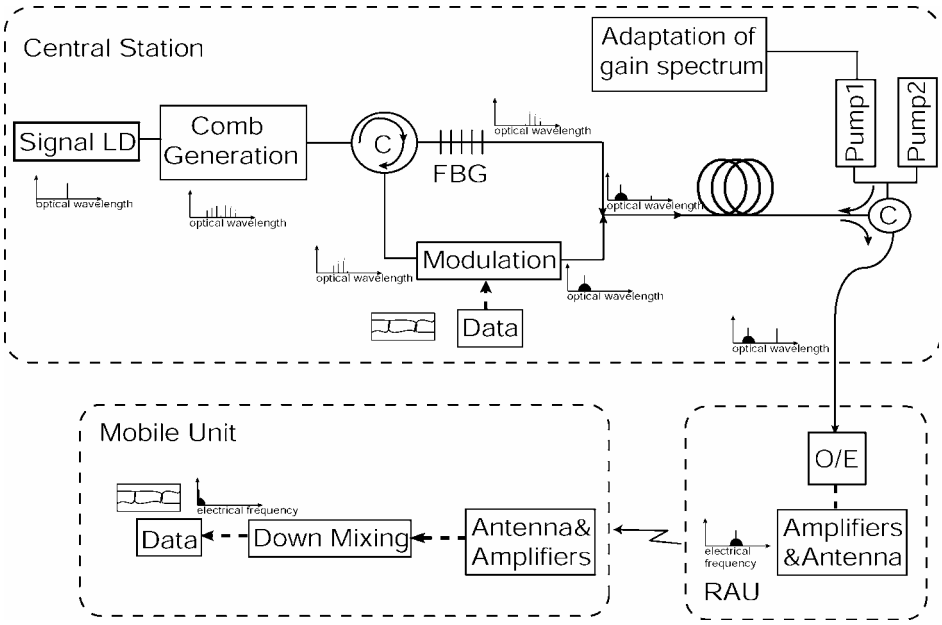

Fig. 8-1 Possible modulation scheme for the presented mm-Wave generation technique (FBG: fibre Bragg grating; C: Circulator; O/E: optic/electric converter).

There are several opportunities for the modulation of the mm-Wave carrier signal. One relies on the separation of the desired sidebands by a tunable FBG. The sidebands are separated and propagate in different optical paths. Due to the separation, one sideband can be modulated by an appropriate modulation signal and be re-injected into the system as shown in Fig. 8-1. The idea for this was also found from the analysis of [97].

On the other hand, by applying this modulation technique, the sidebands not only have to be divided into different paths but the Brillouin bandwidth also has to be adapted dynamically to the bandwidth of the data modulated sideband. Several solutions for this problem were already discussed in section 4.5, however, this would increase the system complexity and a high power EDFA is necessary to achieve a broadband Brillouin gain. Therefore, in this approach a less complex solution for the modulation of the mm-Wave carrier is shown.

sidebands[13]. Thus the generation of sidebands up to the order of 7 was shown. By altering the operation point of the MZM, the odd or even order sidebands can be generated.

The investigation of the Brillouin amplification process is accorded to the simulation in order to compare theory and practical results. It has been shown that both are in good agreement with each other. All variations from theory to experiment were explained and discussed.

The spectral analysis shows a 3 dB bandwidth of 1 Hz or lower for the carrier signals. RF gains of 55.6 dB or higher were achieved. Furthermore a phase noise of approximately -90 dBc/Hz at 10 kHz offset from the carrier was shown. The noise figure of approximately 24.5 dB at 10 kHz offset was induced by SBS amplification and multiplication processes of the frequency generation technique. The impact of chromatic dispersion is negligibly low. Power fluctuations are induced by the tunable optical coupler and the bias drift of the MZM and are enhanced by the Brillouin amplification process. The total short term power fluctuation of a 28.57 GHz signal was measured to be ± 0.29 dB and a stable 11.428 GHz was shown over a timeframe of 27 hours with a maximum power penalty peak of 3.3 dB. All in all, the experimental results prove the predicted low phase noise, high spectral quality signal generation.

[13] Odd or even order sidebands or the carrier.

up, the tuning resolution (approx. 2.5 MHz) is acceptable. This control loop detects the powers of the amplified sidebands at the OSA and readjusts the gain wavelengths by temperature tuning. The total detuning without the control loop is unavoidable. The time for this scenario depends on the environmental influences of the fibre laser and lies between minutes and hours as a coarse approximated value. However, the control loop should not produce an extremely stable signal but should show that the system is thoroughly able to generate a stable output magnitude. Advanced stability enhancements depend on further developments. In Fig. 7-18 the long term stability measurement of the 11.428 GHz signal is shown. As can be seen, there are time slots where the fibre laser altered more in wavelength than in other slots. Thus, between hour 8 and 13 the control loop was nearly active. At all other time slots the frequencies of the pump lasers are continuously adjusted in order to follow the frequency drift of the sidebands.

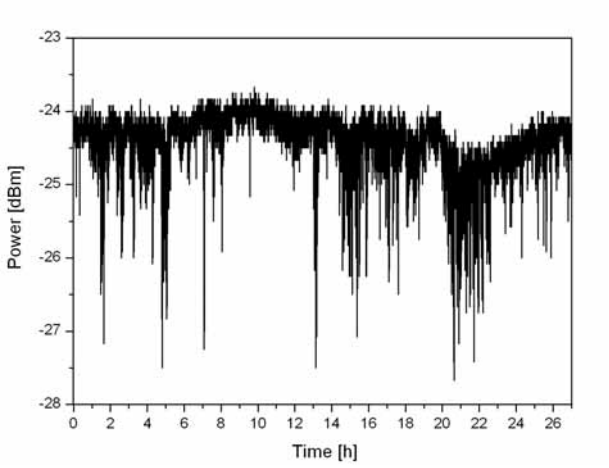

Fig. 7-18 Long term stability of the 11.428 GHz signal.

Another slowly varying power penalty was observed that was independent of any laser wavelength. Namely the alternation of the polarisation status of the pump waves and the sidebands. This effect leads not to a total loss of signal but can reduce the absolute power of the generated mm-Wave.

7.4 Conclusion

In Chapter 7 a detailed investigation of the properties of the carrier signal was shown. The tripartition of this chapter – frequency comb generation – Brillouin amplification – heterodyne detection – also represents the main processes of the experiment. An amplitude modulation was chosen in order to suppress all undesired

Table 7-7 Overview of fluctuation measurements of Fig. 7-17 and Appendix H at different points in the set-up (Fig. 7-16).

Point	Description/ Fluctuation of	Fluctuations [dB]	
		Left SB	Right SB
1	Pump laser 1 (DFB1)	0.0156	
2	Pump laser 2 (DFB 2)	0.0150	
3	Fibre laser	0.022	
4	Sidebands at the output of the MZM	0.118	0.134
5	Pump laser 1 at output of the circulator	0.176	
6	Pump laser 2 at output of the circulator	0.142	
7	Amplified left 5^{th} sideband	0.899	
8	Amplified right 5^{th} sideband	0.674	
9	28.57 GHz signal	0.58	

The development of the fluctuations is shown in Table 7-7. The first row corresponds to the points in Fig. 7-15. The actual mm-Wave features are power fluctuation of 0.58 dB at the output of the PD. The origin of the reduced variations in comparison to the heterodyned sidebands can be explained as follows. The seed waves (sidebands) that stimulate the Brillouin gains fluctuate counter wise. Hence, the amplification process is also determined by opposite fluctuations. The heterodyned signal is the superposition of the field. The sum is equal due to the bias drift induced counter wise fluctuations. This effect leads to a reduction of the power noise of the mm-Wave signal.

7.3.5.2 Long Term Power Fluctuations

Whereas short term fluctuations are measured within several minutes, long term fluctuations should deliver insight into a possible real application by the power analysis over hours. Before fluctuations are discussed, a general overview of the stability of the lasers will be given. The pump lasers (conventional DFB LDs) are controlled in wavelength with a resolution of approximately 2.5 MHz, which is very stable. On the other hand, the wavelength of the fibre laser tends to drift over time. This frequency alternation is very slow and in the range of several tens of MHz/day. According to these base conditions a control loop was induced to the system that adjusts the pump laser wavelength to set the Brillouin gain into the maximum of the corresponding sideband. Assuming a Brillouin bandwidth of 28 MHz in the used set-

sideband is plotted as a red/solid line. Furthermore, an important negative property of an amplitude modulator can be observed.

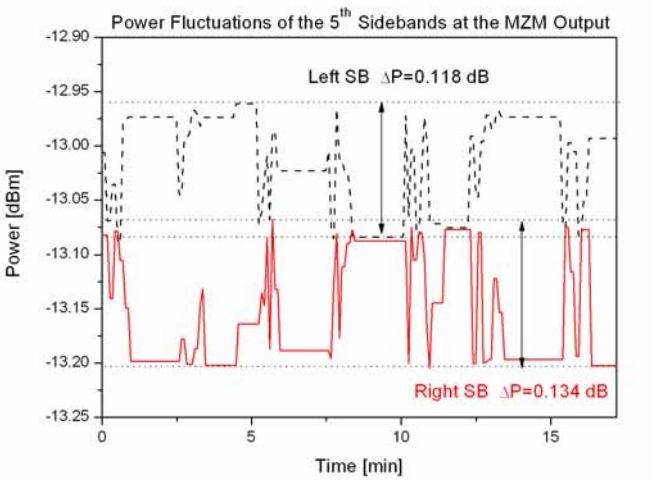

Fig. 7-17 5th order sidebands power fluctuations at the output of the MZM (point 4 in Fig. 7-16).

The power performance of the right sideband is in the opposite direction to the left one. These fluctuations are caused by the bias drift of the MZM and are a significant limitation of the system. They can be fast (min 10-11) or slow (min 1-2.5) but can be nearly suppressed. Possibilities to overcome these penalties are described in Section 9.1.

The development of total system fluctuations is determined by 3 steps. The first fluctuation increment is induced by the bias drift of the MZM according to Fig. 7-17. The second is induced by the tunable coupler that induces an additional power variety of around 0.1 dB to the pump powers. It is assumed that thermal fluctuations lead to power noise of the very coarse adjustable device. However, this property is accepted as for the measurement a tunable adjustment of the pump powers was necessary – they have to be equal. A power increment of a pump laser by increasing the injection current would also lead to a shift of wavelength and hence to a detuning effect. These fluctuations can be avoided if a fixed 50/50 coupler or a highly precise coupler is used in order to optimise the system. The third increasing of the system fluctuations has its origin in the Brillouin amplification process. Thus, the fluctuations of the left sideband (0.118 dB) and the right one (0.134 dB) increases due to Brillouin amplification processes by the fluctuating first pump wave (0.176 dB) and the second one (0.142 dB). The enhanced sidebands experience a power variation of 0.899 dB (left) and 0.675 dB (right) at the output of the circulator.

7.3.5.1 Short Term Power Fluctuations

In order to analyse the stability of the presented system it is necessary to investigate power fluctuations at a certain point of the set-up. For this investigation the amplification of the 5th sidebands and the generation of the 28.57 GHz signal were chosen. The settings of the devices are the same as for the 28.75 GHz signal measurements of sections 7.3.3 and 7.3.4 according to Appendix E5. Therefore, significant locations have been defined (points 1-9 in Fig. 7-16) to measure short term power fluctuations. These points are directly at the output of the pump lasers and the fibre laser, respectively (point 1, 2 and 3) and at the output of the MZM (point 4). Furthermore, the power fluctuation of the pump waves at the input of the fibre (point 5 and 6) and the powers of the amplified sidebands are of interest (point 7 and 8). At least the actual mm-Wave signal (point 9) is analysed in its power fluctuations. The corresponding characteristics can be found in Appendix H with the exception of point 4.

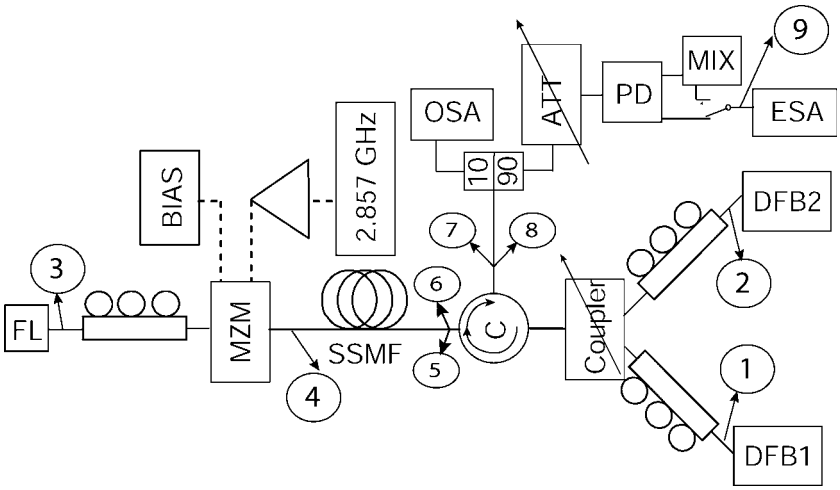

Fig. 7-16 Measurement points for short term fluctuation analysis.

The inset numbers are in agreement with the point numbers of Fig. 7-16. Point 4 is of special interest as it demonstrates the influence due to the bias drift of the MZM and is shown in Fig. 7-17. The fluctuations of each sideband are recorded simultaneously via an OSA directly at the output of the MZM. As can be seen, the variations of point 4 (see Fig. 7-17) are 0.118 dB and 0.134 dB, respectively. The fluctuations of the 5th left sideband[12] are represented by the black/dashed line, whereas the 5th right

[12] The "left" or "right sideband" refers to the wavelengths recorded by the OSA

7.3.4.2 Amplitude Noise

The noise impact on the amplitude of the mm-Wave signal can be measured by the application of a detector diode [199] according to the experimental set-up in Appendix E5. The detector converts the mm-Wave power levels applied to the input connector into proportional values of dc-voltages. Thus, the amplitude fluctuations are converted into base band and can be detected at an ESA in case the amplitude noise is higher than the noise floor of the ESA. A comparison of the ESA noise floor and the amplitude fluctuation spectrum is shown in Fig. 7-15. It can be seen that there is no detectable spectrum change between both measurements. Therefore, it can be concluded that the amplitude noise level is below the noise floor of the ESA. A comparable measurement of the 11.428 GHz signal confirms the result.

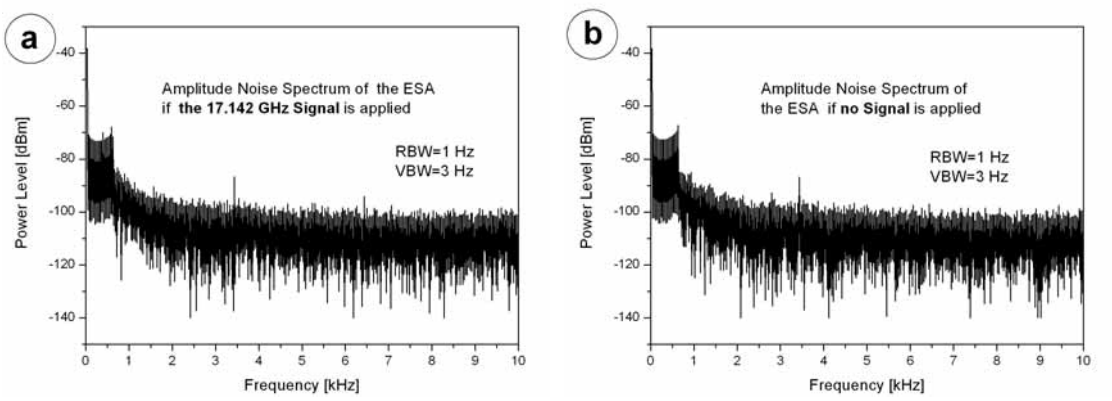

Fig. 7-15 Comparison of amplitude noise of a 17.142 GHz signal and the noise of the ESA.

7.3.5 Stability

A further property of a carrier signal is the stability of the frequency and the magnitude. The generated mm-Wave is determined by the modulator drive signal f_{mod} according to Equation (7.13). Furthermore, the frequency fluctuations are multiplied with the order of the sideband according to Equation (7.3). The base frequency fluctuation of the oscillator at 2.857 GHz is around ± 1.9375 µHz/day [200]. Assuming a frequency fluctuation multiplication of a factor of n = 1 - 7 the mm-Wave signal has a theoretical frequency variation of ± 9.0256 µHz/day for the 7th sideband. Due to the fact that this fluctuation is not measurable by the used ESA there is no experimental investigation on this. On the other hand, power fluctuations can be analysed which is done in the following section.

The scaling of the abscissas at insets (a)-(g) varies due to ESA measurement limitations. As can be seen, the phase noise of about -90 dBc/Hz is low in comparison to other mm-Wave generation techniques. As can be seen in Fig. 7-13 inset (a)-(g), the total phase noise at 10 kHz offset rises very slowly with higher frequencies. A noise variation of 1.5 dB is very small for the seven frequencies. Thus, there is no phase noise increase due to noise multiplication. The phase noise increment due to noise multiplying would be larger as shown in column 3 of Table 7-6 (PN_{HET} Calc.). This low increment proves the assumption of Equation (7.8) that the noise is a summation of the noise applied by the multiplication and the SBS amplification process. The noise figures of the SBS amplifiers at different scenarios are shown in column 6 in Table 7-6. The noise figures of the system components are illustrated in Fig. 7-14. If the order of the used sidebands and, therefore, the Brillouin gain rise, the F of the Brillouin amplifier decreases. On the other hand, a higher up-conversion grade raises the noise figure ($F_{Freq.Mod.[dB]}$). The origin of SBS noise ($F_{SBS[dB]}$) can be the amplified spontaneous emission noise (ASEN) which rises at high fibre lengths (50.45 km) [153].

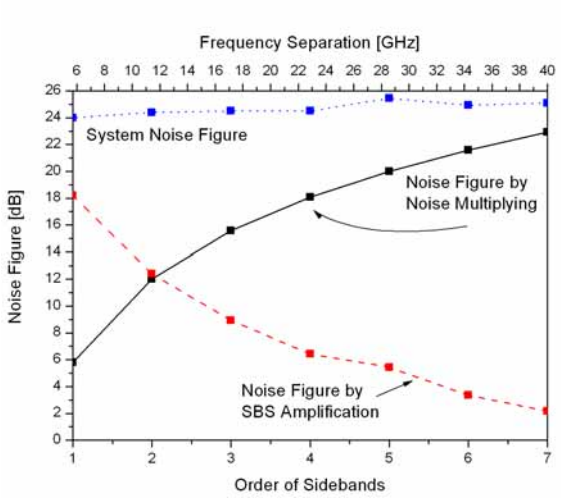

Fig. 7-14 System noise figure (blue/dotted line), noise figure induced by frequency multiplying (black/solid line) and noise figure induced by SBS amplification (red/dashed line).

It should be noted that the noise induced to the signal due to SBS amplification is almost equal to that of a conventional EDFA. Their noise figures are comparable. Detailed information about a comparison test of two different ways of mm-Wave generation under the aspect of phase noise induction is shown in [198].

For a phase noise of the 2.857 GHz driving signal of -114.5 dBc/Hz, a minimum phase noise of the heterodyned signal is calculated (PN_{HET} Calc) in Table 7-6. Note that these values are only valid for conventional frequency multipliers without any amplification processes. They are the basis for calculations that describe the noise figure of the Brillouin amplification part. For this approach it is assumed that the total noise figure consists of the enhanced noise by upconversion and the noise induced by SBS interactions

$$F_{Total[dB]} = F_{Freq.Mod.[dB]} + F_{SBS[dB]}. \tag{7.18}$$

Whereas preliminary predictions toward the low phase noise properties of the system are presented in [197], phase noise measurements of the mm-Wave signals are shown in Fig. 7-13. At all insets the RIN peak of the fibre laser at 342 kHz can be seen. On the other hand, this noise peak is reduced in power when the frequency rises. The dashed lines represent the phase noise of the MZM drive signal, which is -114.5 dBc/Hz at 10 kHz frequency offset.

Table 7-6 Overview of the phase noise measurements. The reference oscillator has a phase noise of -114.5 dBc/Hz @ 10 kHz offset.

Nr.	Sideband	1	2	3	4	5	6	7
1	f_{RF} [GHz]	5.714	11.428	17.142	22.856	28.57	34.284	39.998
2	Fig. 7-13 inset	(a)	(b)	(c)	(d)	(e)	(f)	(g)
3	PN_{HET} Calc. [7]	-108.7	-102.5	-98.93	-96.43	-94.5	-92.91	-91.57
4	PN_{HET} SBS [8]	-90.5	-90.1	-90	-90	89.06	-89.56	-89.40
5	F[9]	5.8	12	15.57	18.07	20	21.59	22.93
6	F[10]	18.2	12.4	8.93	6.43	5.44	3.35	2.17
7	F[11]	24	24.4	24.5	24.5	25.44	24.94	25.1

[7] Phase noise of the heterodyned signal @ 10 kHz offset calculated according to Equation (7.16) [dBc/Hz].

[8] Phase noise of the heterodyned signal @ 10 kHz offset generated by SBS amplification [dBc/Hz].

[9] Noise figure induced by frequency multiplication according to (7.16) and (7.17) (-114.5dBc/Hz- PN_{HET} Calc)

[10] Noise figure of SBS amplifiers (PN_{HET} Calc.- PN_{HET} SBS) [dB].

[11] Noise figure of the whole system according to Fig. 7-13 [dB].

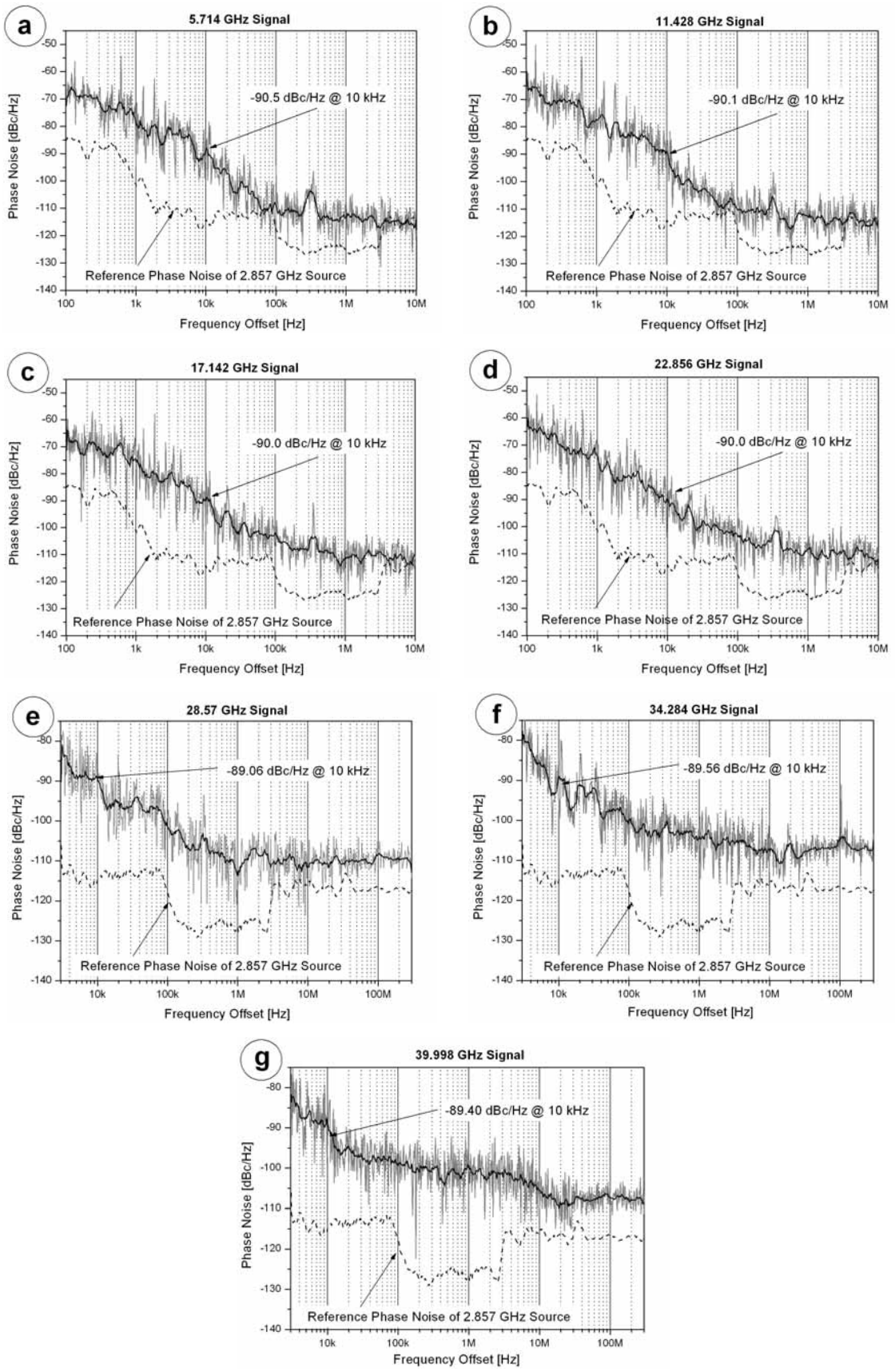

Fig. 7-13 Phase noise characteristics of mm-Wave signals according to the set-up shown in Appendix E5.

$$f = \frac{\partial(\varphi(t))}{\partial t} \tag{7.15}$$

with $\varphi(t)$ as the phase noise of a signal. The phase noise is measured in a bandwidth of one Hertz related to the **c**arrier and has the unit dB**c**/Hz. The phase noise is determined at a certain offset frequency from the carrier. A common reference value for an offset frequency is 10 kHz in order to make different phase noises comparable. This noise limits the application of carrier signals and is an important criterion for the use of different modulation formats in communication systems [194]. Phase noise degrades millimetre and microwave systems introducing a significant irreducible error rate.

In [60] the 60 GHz region phase noise of –59 dBc/Hz and –85 dBc/Hz at 10 kHz and 100 kHz respectively, offset from the carrier were measured. A mm-Wave generation of 42 GHz was shown in [73] where the phase noise was –80 dBc/Hz at 10 kHz offset. By using the method of PM-IM conversion in chirped fibre gratings, a phase noise of –87 dBc/Hz at 10 kHz offset at a frequency of 28 GHz was measured [195]. Recently, Kiwanishi et al. [188] reported a 44 GHz signal generated by an integrated reciprocating optical modulator with a phase noise property of –88.5 dBc/Hz at 10 kHz offset from the carrier. In [69] a mm-Wave generation of 33.87 GHz was realised by using hybrid mode locking of a monolithic DBR laser. The phase noise was –70 dBc/Hz at the presented method.

Using frequency multipliers that rely on optical modulation, the lower theoretical limit of the phase noise of the heterodyned signal (PN_{HET}) is defined as [196]

$$PN_{HET} = 20 \cdot \log(2n) + PN_{Source} \tag{7.16}$$

with n as the order of the sidebands and PN_{Source} as the phase noise of the MZM driving signal. The noise figure (F) of a system can be described as the phase noise ratio between the driving signal and the mm-Wave [188].

$$F_{[dB]} = PN_{Source[dBc/Hz]} - PN_{HET[dBc/Hz]} \tag{7.17}$$

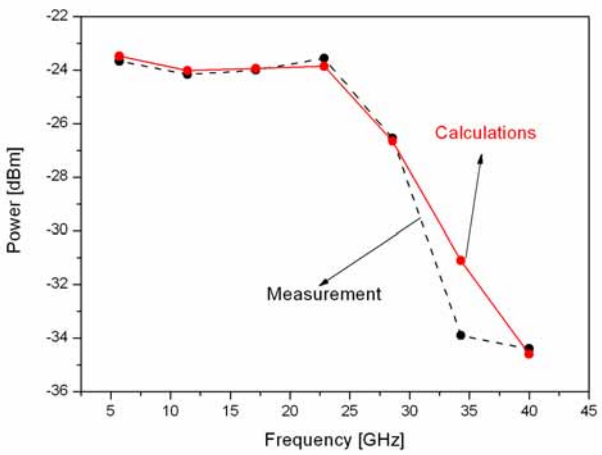

Fig. 7-12 Comparison of experimental results and calculations.

The noise floor is at around -90 dBm. The only limitation concerning modulation lies in the superposition of undesired sidebands according to inset (f) in Fig. 7-11. These occur at a separation that corresponds to the MZM modulation frequency f_{mod}. If f_{mod} rises also the modulation data rate can rise proportionally. On the other hand, optical filtering can be used to suppress sidebands that lead to this kind of spectral distortions.

7.3.4 Noise Measurements

The noise that is induced to a signal is either described by the noise of the phase or the amplitude. By expanding the equation for a sinusoidal wave (3.1) by $\Delta E(t)$ and $\Delta\varphi(t)$, as the statistical time dependent fluctuation of the amplitude and the phase, respectively it follows that

$$E_1(t) = [E + \Delta E(t)] \cdot \cos(\omega t + \varphi + \Delta\varphi(t)). \tag{7.14}$$

Due to the general assumption that a signal's amplitude noise is much lower than the noise of the phase [193] here the focus will be set on the investigation of the phase fluctuations.

7.3.4.1 Phase Noise

In wireless communications the requirements for carrier frequencies are very high. Besides frequency stability, magnitude and a narrow bandwidth the most important property of a carrier signal is the phase noise. Phase noise describes the alteration of the phase of a signal. It can be measured in the frequency domain via

Table 7-5 Important values of spectral measurements taken out of Fig. 7-11 and Appendix G

Sideband	**1**	**2**	**3**	**4**	**5**	**6**	**7**
f_{RF} [GHz]	5.714	11.428	17.142	22.856	28.57	34.284	39.998
$P_{RF\text{-}MEAS}$ [dBm] Insets (b)	-23.66	-24.16	-24.00	-23.56	-26.55	-33.90	-34.40
$P_{RF\text{-}CALC}$ [dBm]	-23.48	-24.02	-23.94	-23.86	-26.66	-31.10	-34.6
P_{opt} [mW] Insets (a)	-7.37	-7.59	-7.80	-8.16	-8.06	-9.38	-10.88
α [dB]	4.1	4.1	3.9	3.4	3.4	3.2	2.1
AFR [dB] App F	0.7	0.8	0.7	0.9	3.9	6.1	8.8
Noise Floor [dBm] App G	-90	-88.1	-91.97	-88.3	-83.4	-90	-90
RF gain @ 3.5 kHz [dB]	66.64	63.49	67.9	64.74	56.85	56.1	55.6
FWHM Bandwidth [Hz]	1	1	1	1	300	300	300

The direct comparison of experiments and calculations are also shown in Fig. 7-12 with the red/solid characteristic for the calculated values and the black/dashed line for the measured values. As can be seen, both traces are in good compliance with one another. Only the power of the heterodyned 6th amplified sidebands (28.57 GHz) has a power separation of 2.8 dB to the calculated value. A reason for this irregularity can be the frequency response value AFR that is assumed to be only 6.1 dBm. Note that a comparison of the mm-Wave signal to the simulated results of Chapter 6 is not possible as all simulations are based on a known signal power (power of sidebands). For the settings in Chapter 7 the powers of the sidebands are not detectable due to the restriction of the OSA RBW.

In conclusion the carrier signal is - with a FWHM bandwidth of 1 Hz or even lower - very pure. There are no significant perturbations in the spectrum. The RF gains are at all signals higher than 55.6 dB.

Due to this resolution the bandwidth of the mm-Wave signal was measured to be 1 Hz but is assumed to be even lower because of resolution restrictions. The noise level is calculated by an averaging of the spectrum of 60 points at an offset frequency of approximately 3 kHz. The signal to noise ratio (SNR) is 66.64 dB (see inset c in Fig. 7-11). As can be seen, the carrier signal is very pure in its spectral distribution. Only in inset (d) spectral distortions at 342 kHz can be seen. These peaks have their origin in the relative intensity noise (RIN) of the fibre laser that occurs at around 300 kHz [192]. Measurements have verified this assumption but are not described here. Inset (f) in Fig. 7-11 shows spectral distortions due to the heterodyning of other sidebands or the carrier. Due to the OSA – RBW the operation point of the MZM was only optimised in order to get a maximum amplification but not to suppress undesired frequency components. By using modulation frequencies - higher than the OSA RBW – or an OSA with a lower RBW these distortions can be optimised. The verification of the heterodyning of the SBS amplified sidebands of the order 2-7 is shown in appendices G2 - G7 at different frequency spans. There, mm-Wave signals with frequencies of 5.714, 11.428, 17.142, 22.856, 28.57, 34.284, 39.998 GHz are presented. At all signals the RIN peak of the fibre laser at 342 kHz can be observed. Frequencies higher than 26.5 GHz are measured via an external harmonic mixer (see Appendix E5). Due to this application the RBW of the ESA was limited to 300 Hz. Therefore, FWHM bandwidths of 300 Hz were measured. A comparison measurement, in which the 7^{th} amplified sidebands with a frequency separation of 25.9 GHz are heterodyned, shows a spectral bandwidth of 1 Hz.

Thus the bandwidths of the signals that are down converted via the external mixer, are assumed to have a bandwidth of 1 Hz or even lower. There are strong frequency components observed in inset (e) of Appendices G5, G6 and G7 (28.57, 34.284, 39.998 GHz). The frequency separation of 620 MHz is twice that of the local frequency (LF = 310.7 MHz) of the ESA applied to the mixer. Hence, these frequencies are measurement errors and can be neglected. Table 7-5 gives an overview of the significant results of the mm-Wave signals. The light grey coloured fields represent the direct comparison between measurement results $P_{RF\text{-}MEAS}$ and calculations $P_{RF\text{-}CALC}$ according to Equation (7.11) and the values given in the table. The dark grey coloured fields are based on the assumption that the frequency response decreases logarithmically as shown in Appendix F1 and have to be considered critically.

instance, commercially available photodetectors with a bandwidth of 170 GHz are offered by “NTT Electronics”.

The optical spectrum as a linear and logarithmical distribution at the 10 % output of the 90/10 coupler according to Appendix E5 is shown in Fig. 7-11 inset (a). At a wavelength of 1.5462 µm the spectral separation between the first order SBS amplified sidebands is 5.71 GHz. Inset (b)-(f) shows the mm-Wave spectrum at 5.71 GHz at different frequency spans: b: 100 Hz, c: 10 kHz, d: 1 MHz, e: 100 MHz and f: 11.43 GHz. Inset (b) shows the highest resolution with an RBW and video bandwidth (VBW) of 1 Hz.

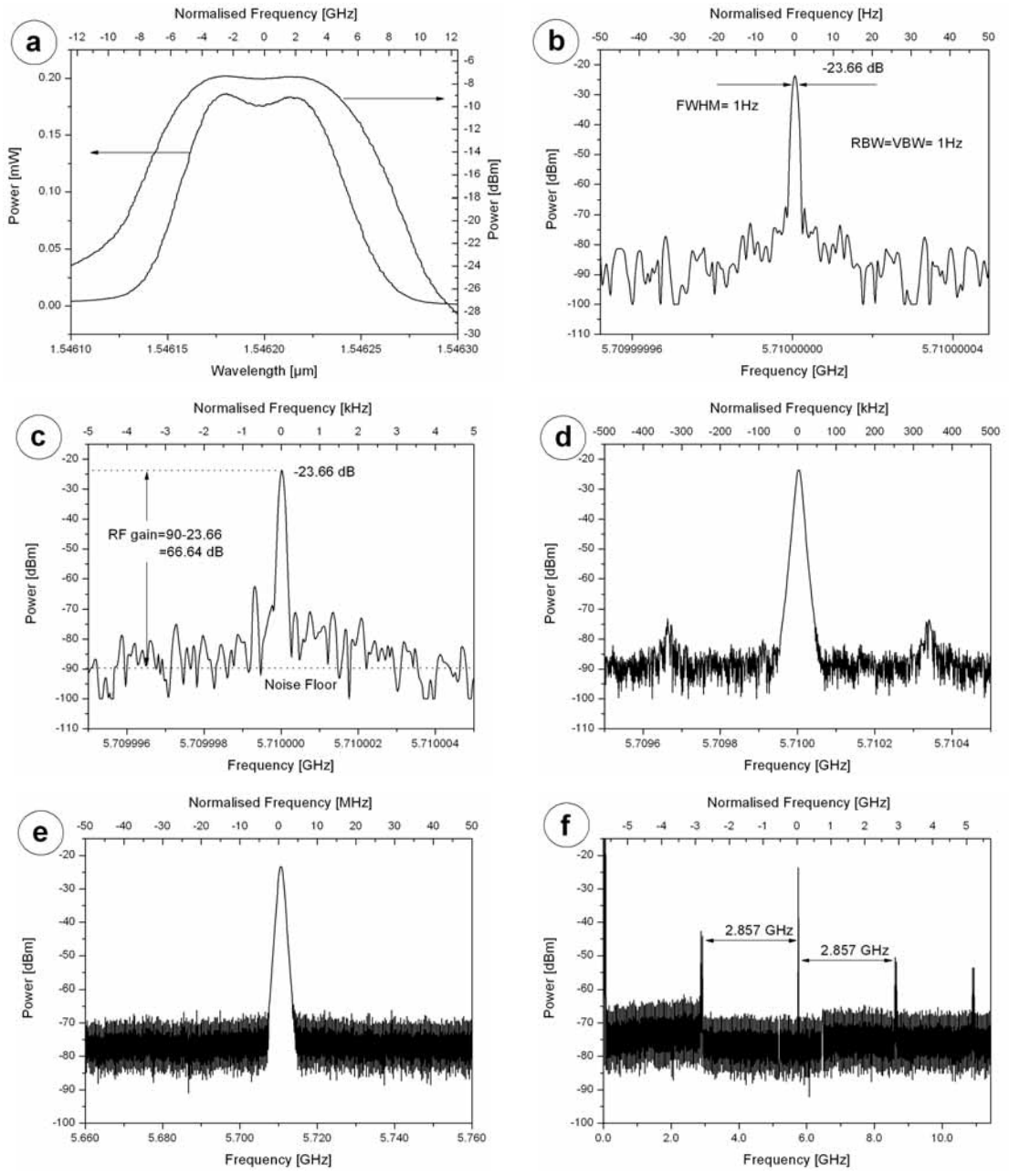

Fig. 7-11 Spectral properties of the 5.71 GHz signal.

signal power according to Fig. 7-10. A comparison of theory[6] and a measurement is shown by the black/dashed and the red/solid line.

The decrease of the negative slope of the red/solid line occurs because of the noise level of the ESA. However, theory and experiment are in good compliance with each other.

7.3.3 Spectral Properties

In Sections 7.1 and 7.2 the generation of two sidebands with a frequency separation of

$$f_{mm} = n \cdot 2 \cdot f_{\mathrm{mod}}\,, \tag{7.13}$$

with n as the order of the sidebands, was shown. Owing to the resolution of the optical spectrum analyser (0.06 nm = 7.492 GHz) the modulation frequency was chosen to be higher than this resolution, namely 10 GHz (see Fig. 7-4). On the other hand, the PD has a frequency response bandwidth (-3 dB) of 27 GHz. Therefore, investigations of the mm-Wave are done up to a frequency of 40 GHz.

In the following, a detailed investigation of the heterodyned optical frequency components is described. In this section the superposition of the first sidebands is shown whereas the spectrum analysis of the mm-Wave signals generated by higher order sidebands (order 2-7) is shown in Appendix G. The signal applied to the MZM is a sinusoidal wave with a frequency of 2.857 GHz. According to Equation (7.13) this corresponds to a maximum frequency of 39.998 GHz if the 7th order sidebands are used.

The presented measurements are examples to describe the basic performance of the system. Of course, using a higher modulation frequency such as 10 GHz for instance higher carrier frequencies can be generated. Furthermore, by the application of other frequency comb generation methods, the up conversion factor can be enhanced and the system efficiency improved. It can be said that the generatable frequency is only limited by the bandwidth of the PD. Thus in [191] about the theory and design of a photodetector with a bandwidth of 330 GHz was reported. For

[6] The calculation is done according to Equation (7.11).

7.3.2 Optic-Electric Conversion

The power of the mm-Wave depends strongly on the responsivity of the PD and the input power of the amplified sidebands. Therefore, the mathematical description of the relationship of the optical sidebands and the carrier signal can be described with $P_{mm} = I^2_{pd} \cdot R$ as

$$P_{mm}[dBm] = 10 \cdot \log\left(R \cdot \left(\frac{RESP \cdot P_{optPD}}{1000} \right)^2 \cdot 1000 \right) - AFR \,. \tag{7.11}$$

The responsivity *RESP* at 1550 nm is $0.71 \cdot 0.72\ A/W = 0.511\ A/W$ (see Appendix F). The optical power at the input of the PD, P_{optPD}, can be described as the relation of the optical power measured at the OSA (inset (a) in Fig. 7-11) and the attenuation α of the tunable attenuator.

$$P_{optPD} = \frac{P_{optOSA} \cdot 10}{\alpha} \tag{7.12}$$

The attenuator is used in order to protect the PD against high optical powers. The factor "*10*" describes the 90/10 coupler at the output of the circulator (compare set-up in Appendix E5). The resistor value *R* is 50 Ω and *AFR* stands for the attenuation due to the frequency response at a certain frequency [dB]. As the PD frequency response is measured only up to 30 GHz an approximated extension of the logarithmic characteristic is assumed (see Appendix F). Note that this extension is only an assumption.

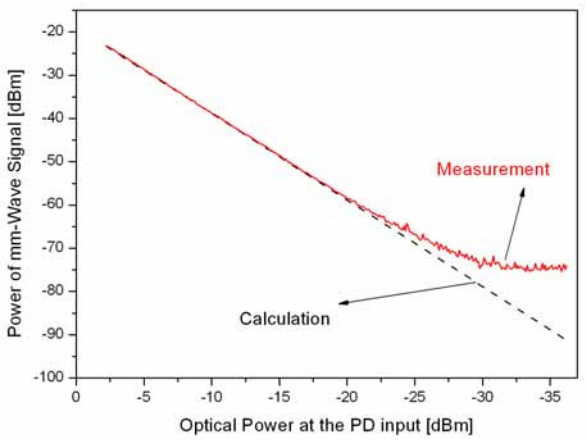

Fig. 7-10 Optic-electronic power conversion in theory and practice.

A graphical demonstration of Equation (7.11) is given in Fig. 7-10 (black/dashed line). A reduced optical input power at the PD also leads to a decay of the mm-Wave

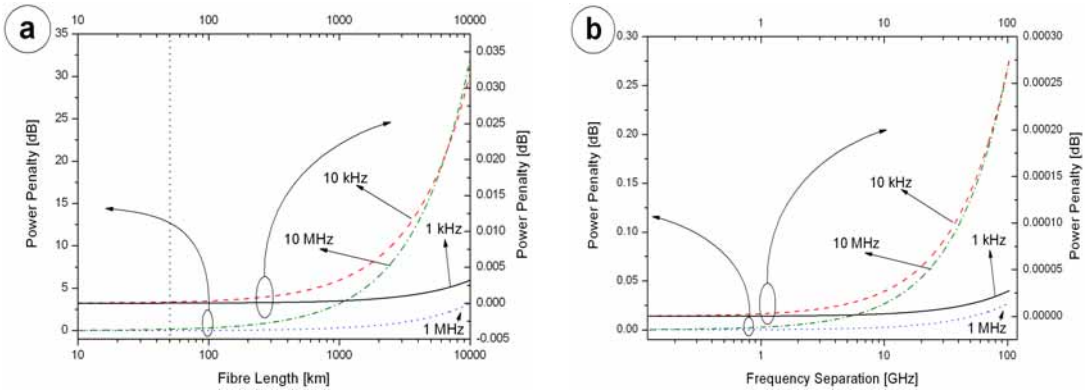

Fig. 7-9 Power penalty due to chromatic dispersion vs. fibre length; a: - at 60 GHz frequency separation and b: frequency separation - at 50.45 km fibre length.

The power penalty $P_{penalty}$ of the heterodyned signal due to chromatic dispersion is according to [58]

$$P_{penalty} = 10 \cdot \log\left(\frac{1}{e^{-2\pi \cdot \Delta\nu \cdot \tau_{disp}}}\right). \tag{7.10}$$

In Fig. 7-9 Equation (7.9) is shown. The parameter $\Delta\nu$ is the FWHM bandwidth of the power spectrum of the sidebands. The black/solid lines represent a laser line width of 1 kHz, the red/dashed lines of 10 kHz, the blue/dotted lines of 1 MHz and the green/dashed dotted line a band width of 10 MHz. It can be seen that for sidebands with a line width of even 10 MHz the power penalty for short fibre length is negligibly small (see Fig. 7-9a). Furthermore, the influence of the frequency separation of the sidebands has a very slight impact to the power of the heterodyned signal.

An experiment according to Appendix E4 verifies that the dispersion has a negligible impact on the bandwidth of the signal. The dashed line in Fig. 7-8 shows the spectrum of the 22.2 GHz signal where the two optical components are propagated via a 50.45 km long SSMF. In order to compare the SBS generated mm-Wave signal with a "non-SBS" generated mm-Wave signal the desired frequency components are heterodyned directly at the output of the MZM. However, the optical power at the input of the PD is in both cases ("back to back" and "50 km SSMF") approximately 1 mW. As can be seen in Fig. 7-8 (a-blue/dashed line) the bandwidth has not exceeded the 1 Hz border.

7.3.1 Chromatic Dispersion Effects

In contrast to the direct detection link where dispersion has a very high impact (see Section 3.2.1), the heterodyne superposition of two frequency components is insensitive to dispersion influences [190]. In the past chapters all signals have been assumed to be monochromatic waves. In reality the used signals (sidebands) are not monochromatic but have a line width in the range of the line width of the fibre laser.

In a dispersive medium the group velocity is not constant, and therefore the sidebands have different propagation times in the fibre t_1 and t_2. The result is a decorrelation of the sidebands, since the phase noises $\Delta\varphi_{opt}(t)$ of both sidebands become independent. This decorrelation effect increases with higher frequency separations and higher fibre lengths. Furthermore, the line width of the electrical signal is broadened, which results in peak power degradation due to a decreased spectral density. The time delay of the sidebands τ_{disp} can be derived as follows:

$$\tau_{disp} = t_2 - t_1 = L \cdot \left(\frac{1}{v_{g2}} - \frac{1}{v_{g1}} \right) \tag{7.7}$$

with t_1 and t_2 as the propagation time and v_{g1} and v_{g2} as the group velocity of the first and the second sideband, respectively. L reflects the fibre length. The group velocity depends on the wavelength λ and can be expressed as

$$\frac{\partial t_g}{\partial \lambda} = L \cdot \frac{\partial}{\partial \lambda} \left(\frac{1}{v_g} \right) = L \cdot D \tag{7.8}$$

with D as the dispersion parameter. As the wavelengths λ_1 and λ_2 are closely separated the characteristic of the group velocity can be assumed to be linear. Hence, the time delay τ_{disp} between the sidebands corresponds to the differential group velocity ∂t_g [58]:

$$\tau_{disp} = \partial t_g = D \cdot L \cdot (\lambda_1 - \lambda_2) \approx D \cdot L \frac{\lambda^2}{c} \cdot f_{mm} \,. \tag{7.9}$$

The time delay is directly proportional to the fibre length L and the mm-Wave frequency f_{mm}. If the wavelength separation is small in comparison to the transmission bandwidth the right term in (7.9) can be used. For f_{mm}=60 GHz it follows that the wavelength separation is $\Delta\lambda$=0.48 nm « 1550 nm and the condition is fulfilled.

This quotation gives the main point of the idea of the heterodyning of two optical components derived from one source in a PD. The phase noise is a statistical distribution that describes the location of the carrier at a certain time. Due to the DSSC modulation the spectrum of the carrier is transferred to the upper sideband and the lower sideband. The noise remains equal because an amplitude modulation is applied. Due to the fact that the PD always detects the same mix frequency, the spectral purity of the signal is extremely high. It is determined by the order of harmonics and the phase noise of the modulator drive signal according to Equation (7.6). To prove the purity of the signal an experiment according to Appendix E3 has been made.

The light of a fibre laser source was externally modulated in amplitude in such a manner that only the upper and lower third order sidebands are generated. All other components have been suppressed by applying the right bias voltage. The modulation signal was a 3.7 GHz sinusoidal signal with a spectral line width < 1 Hz. The sidebands have a frequency separation of 22.2 GHz (3 x 2 x 3.7 GHz) and are detected by a PD. The spectrum of the 22.2 GHz carrier signal can be seen in Fig. 7-8 ((a), solid line) with a bandwidth of 1 Hz measured by an electrical spectrum analyser (ESA). The real bandwidth is assumed to be even lower because the measurement is limited by the resolution bandwidth (RBW=1 Hz) of the ESA. The corresponding phase noise of the 22.2 GHz signal is shown in Fig. 7-8b. It can be seen that the phase noise is -93 dBc/Hz at an offset frequency of 10 kHz. The dashed line in Fig. 7-8b is the phase noise of the 3.7 GHz modulator drive signal.

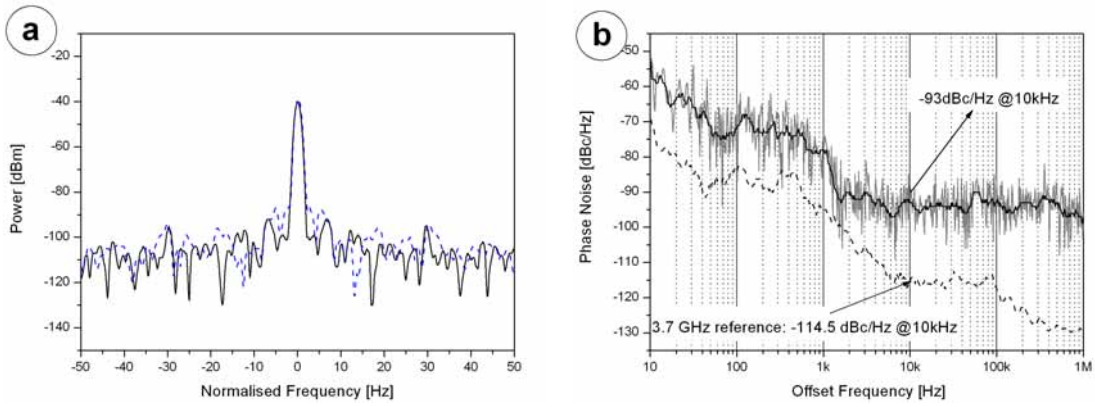

Fig. 7-8 a: 22.2 GHz signal spectrum; solid line: back to back; dashed line: after propagation in a 50.45 km SSMF; b: Phase noise of the 22.2 GHz signal back to back.

Introducing the equation for the bandwidth or the phase noise of one source (7.4) into the equation for the heterodyne superposition (3.5), leads to the intensity of the mm-Wave,

$$I_{HET}(t) = E_1 E_2 \cdot \cos\begin{pmatrix} \omega_{RF} t + \Delta\varphi_{opt1}(t) + |k| \cdot \Delta\varphi_{\mathrm{mod}}(t) \\ -\Delta\varphi_{opt2}(t) + |k| \cdot \Delta\varphi_{\mathrm{mod}}(t) + \varphi_1 - \varphi_2 \end{pmatrix} \tag{7.5}$$

including phase noise properties. $\omega_{RF}t$ is the angular frequency of the RF signal, k is the order of the sideband, $\varphi_{opt}(t)$ is the phase noise of the optical signal and $\Delta\varphi_{mod}(t)$ represents the phase noise of the modulation signal.

Assuming no decorrelation[5], the phase noise induced by the optical laser source $\Delta\varphi_{opt}(t)$ can be ignored, as the algebraic signs are equal for the sidebands in Equation (7.3). On the other hand, the phase noise caused by the electrical modulation signal $\Delta\varphi_{mod}(t)$ multiplied by the order of the sidebands is doubled during the heterodyning in the PD. This is because the algebraic signs of the phase noise $k \cdot \Delta\varphi_{mod}(t)$ for the sidebands with positive order is the reverse of the algebraic signs of the phase noise $k \cdot \Delta\varphi_{mod}(t)$ for the sidebands with negative order. After adding the components of Equation (7.5) it can be written that:

$$I_{HET}(t) = E_1 E_2 \cdot \cos\left(\omega_{RF} t + 2|k| \cdot \Delta\varphi_{\mathrm{mod}}(t) + \varphi_1 - \varphi_2\right). \tag{7.6}$$

Therefore, the magnitude of the mm-Wave carrier depends only on the magnitude of the frequency components. The frequency spectrum is determined by a multiple of the phase noise of the electrical signal.

However, J.J. O´Reilly et al. wrote about the heterodyne superposition of two sidebands in [95]: “Because both optical components are derived from a single source the phase noise of each component is totally correlated at the source and the electrical signal therefore has a line width governed by the line width of the electrical signal used to drive the modulator. Fibre dispersion reduces the correlation but the effect is negligibly small for optical component separations in the tens of gigahertz and fibre lengths of many tens of kilometres.”.

[5] The decorrelation effects of frequency components that are derived from one source and propagate in optical fibres due to chromatic dispersion are negligibly small for the presented set-up (for details see section 7.3.1).

The graphical comparison of simulations and experiment is given in Fig. 7-7. The dashed lines represent the experimental results of the sideband power and the gain, respectively, and the solid lines the simulation results. Again, it can be seen at lower signal powers that the separation between simulation calculations and experimental results is higher (7.46 dB at 0.7 µW - averaged) as for higher signal powers (3.09 dB at 740.7 µW - averaged). Furthermore, the experimental results converge to the simulation results if the pump power increases.

Considering the same error analysis as in section 7.2.1 the simulation and experimental results are in agreement with each other. A comparison of both measurements with each other can only be done in one case. This is the case if the pump power is 6 mW and the signal power is 52.9 µW. In both scenarios there are equal calculation parameters as well as experimental conditions. Comparing the results of experiment and simulation of the third row (52.9 µW) of The detailed experimental set-up is shown in Appendix E2. Fig. 7-6 shows the amplification process at signal input powers according to Table 7-1. It should be noted that the gains in Fig. 7-6 are related to the signal power after propagation in a 50.45 km long SSMF. The red/solid lines represent the amplified signals whereas the black/dashed lines follow the spectrum of the signal wave at the fibre output. The dotted line in inset 7 corresponds to the signal power at the output of the MZM or the input of the fibre, respectively. An overview of the measured values and the calculated simulations is given in Table 7-4.

Table 7-4 with the results of experiment and simulation of the 5th row (6 mW) of Table 7-3, it can be seen that the difference between both measurements is only 0.56 dB.

As a conclusion it can be said that the measurements both confirm each other and the simulation in the same manner.

7.3 Heterodyne Detection of Optical Frequency Components

Here, the third part of the experimental set-up, namely the optic-electric conversion is proposed. Among others, the main objects in which a carrier signal is determined is the magnitude and the induced noise. Hence, this section discusses several properties of the actual millimetre wave signal that is generated in the PD.

The detailed experimental set-up is shown in Appendix E2. Fig. 7-6 shows the amplification process at signal input powers according to Table 7-1. It should be noted that the gains in Fig. 7-6 are related to the signal power after propagation in a 50.45 km long SSMF. The red/solid lines represent the amplified signals whereas the black/dashed lines follow the spectrum of the signal wave at the fibre output. The dotted line in inset 7 corresponds to the signal power at the output of the MZM or the input of the fibre, respectively. An overview of the measured values and the calculated simulations is given in Table 7-4.

Table 7-4 Comparison of simulated and experimentally verified Brillouin amplification processes – Constant pump power (6 mW) at different signal powers.

Signal Power [µW]	P_{out} Simulation Fig. 6-9 @ 50 km		Gain Simulation [dB]	P_{out} Experiment [dBm]	Gain Experiment [dB]
	[mW]	[dBm]			
0.7	3.66	5.63	47.64	-2.13	40.47
7.2	4.03	6.05	37.93	0.36	32.96
52.9	4.35	6.38	29.63	1.81	25.89
244.3	4.62	6.64	23.35	2.82	20.31
585	4.81	6.82	20.05	3.37	17.42
621.4	4.82	6.83	19.83	3.50	16.89
740.7	4.85	6.85	19.18	3.56	16.29

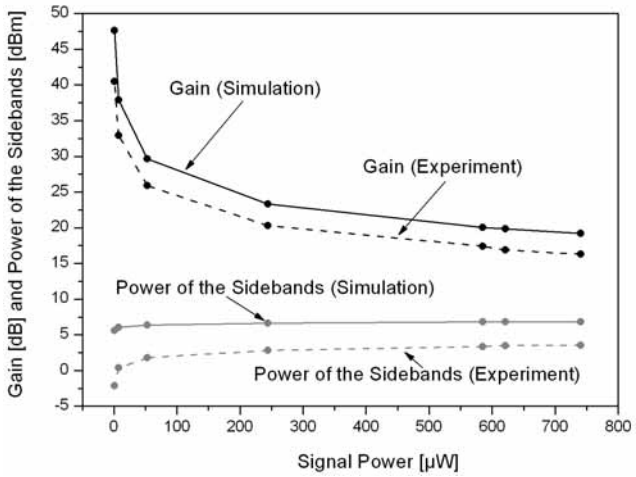

Fig. 7-7 Comparison between simulation and experiment according to Table 7-4.

This leads to the assumption that the pump power attenuation causes the altering difference between simulated values and experimental measurements. A further reason for the differences between simulation and experiment can lie in the calculations of the Brillouin gain. The maximum Brillouin gain g_{Bmax} depends on the gain bandwidth Δf_a according to Equation (4.11). This bandwidth is measured to be 28 MHz. On the other hand, there is no standardised bandwidth measurement technique. For example, a bandwidth of 40 ± 3 MHz was measured by heterodyning the backward scattered wave with the incident light wave [189]. Assuming a bandwidth measurement error, the real bandwidth can differ, hence, the calculations for the simulation. Taking these facts into account, the simulation results reflect the experimental data.

7.2.2 Different Signal Powers at Constant Pump Power

In contrast to the previous chapter here the signal power is changed whereas the pump power is fixed. The pump power constitutes 6 mW for each pump wave and the signal waves have powers that correspond to the power of the sidebands (see Table 7-1).

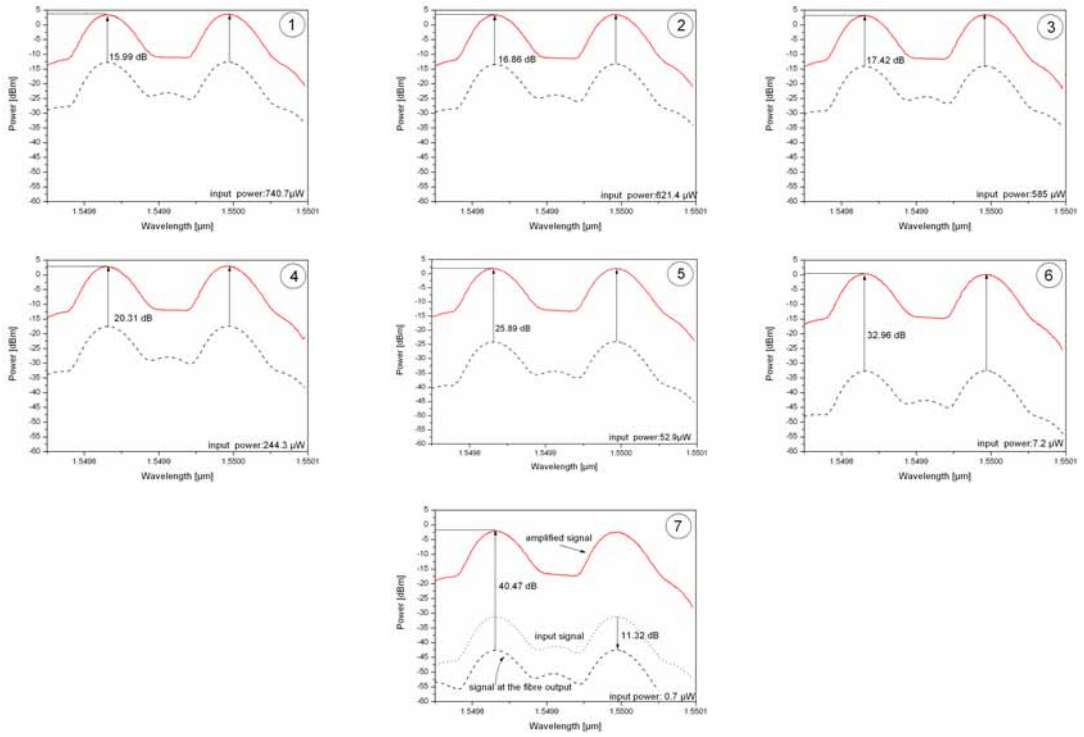

Fig. 7-6 Amplification at different signal powers and a constant pump power (6 mW); Red/solid line: amplified signal; Black/dashed line: Signal at the fibre output. The inset numbers match to the order of the sidebands that correspond to the signal powers.

The dotted line represents the same signal after propagating in the 50.45 km SSMF. The amplified signals at different pump powers are reflected by the solid lines. As can be seen in the plot, saturation occurs with higher pump powers. The calculated powers of the sidebands and the corresponding gains are shown in Table 7-3 and in Fig. 7-5b (solid lines). The dashed lines represent experimental results of the sideband power and the gain, respectively. As can be seen at lower pump powers (< 4 mW), the separation between simulation and experimental results is bigger (10.615 dB @ 2 mW - averaged) as for higher pump powers (3.51 dB @ 8 mW - averaged). Furthermore, the experimental results converge to the simulation results if the pump power increases.

However, the simulation does not consider attenuations of the optical connections and the splice losses of the fibre plugs. The losses are suppressed as much as possible by cleaning the connection devices, but can not be neglected. For example, the measured fibre attenuation in Fig. 7-6 (inset 7) is 11.32 dB whereas the calculated fibre attenuation is 10.54 dB. Furthermore, the loss of the circulator (that is approximately 0.53 dB) has to be considered as well. Hence, there is an unknown loss of pump power (at least 0.87 dB + 0.53 dB = 1.4 dB) and signal power that lead to a decreased Brillouin gain. The gain shift at lower pump powers is higher as at high pump powers (saturation effect).

Table 7-3 Comparison of simulated (section 6.2.2) and experimentally verified Brillouin amplification processes – Constant signal power (52.9 mW) at different pump powers.

Pump Power [mW]	P_{out} Simulation Fig. 6-5 @ 50 km		Gain Simulation [dB]	P_{out} Experiment [dBm]	Gain Experiment [dB]
	[mW]	[dBm]			
2	0.84	-0.76	22.45	-11.67	12.13
3	1.65	1.93	25.14	-6.16	17.64
4	2.52	4.00	27.21	-1.63	22.17
5	3.43	5.35	28.56	-0.12	23.86
6	4.35	6.38	29.62	1.52	25.32
7	5.29	7.23	30.44	2.96	26.76
8	6.24	7.95	31.16	4.13	27.93

of the OSA the MZM modulation frequency was chosen to be 10 GHz. An EDFA was used to change pump powers without impact to the pump wavelength. In order to compare theory and experiment the same scenarios as in the simulation sections 6.2.2 and 6.2.2.2 have been carried out. They are described in the following two chapters.

During the experiments a polarisation dependency of approximately 3 dB was observed. At a pump power of 2 mW and a signal power of 740 µW a difference of 2.7 dB was measured between orthogonal and parallel polarised pump and signal waves. In order to cancel these effects, the polarisation for SBS amplification was optimised before each measurement. It has been carried out by the application of polarisation controllers behind the pump sources.

A detailed analysis of the dependency of SBS on polarisation is given by M. O. Deventer in [189]. The impact of polarisation distortions to the amplified signal can be avoided by applying a depolarised pump source. This can be done by adding a commercially available depolariser behind the source. Thus the pump is evenly distributed over all states of polarisation.

7.2.1 Different Pump Powers at Constant Signal Power

In this section the scenario of different pump powers at a signal power of 53 µW for each signal will be shown. A comparison between the results of simulation and experiment is shown in Fig. 7-5b. The experimental results are presented in Fig. 7-5a. The dashed line corresponds to the input signal at the output of the MZM or the input of the fibre, respectively.

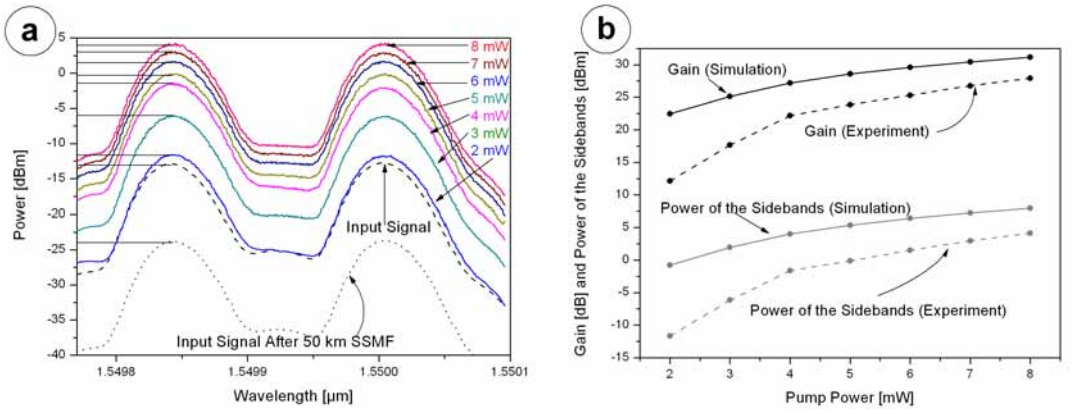

Fig. 7-5 a: Amplification at different pump powers and a constant signal power (52.9µW); b: Comparison between simulation and experiment according to Table 7-3.

The abbreviations in Table 7-2 stand for "im": **im**measurable – which means that these values could not be measured due to the resolution of the OSA. The term "n.f." means, that these sidebands have a power level below the **n**oise **f**loor of the OSA. The experimental verification showed the behaviour of the MZM at different applied HF voltages (Fig. 7-3). In order to achieve a high up conversion of the base frequency the order of attainable sidebands has to be a maximum. Therefore, the modulation index has to rise. Hence, by raising the HF drive level ("*a*") in Equation (7.1), the amplitudes of the higher order harmonics can also be increased as can be seen in Equation (7.3). According to this, the power applied to the MZM reached values of up to 12.75 V which corresponds to an RF power of 3.25 W or 35.11 dBm, respectively. It should be noted, that the data sheet sets the upper limit of electrical input power to a maximum of 30 dBm (1 W).

However, the frequency comb generation by a nonlinear amplitude modulation has several disadvantages. For instance, the order of generated sidebands is not as high as it is at a phase modulation. Thus, sidebands up to the order of 50 can be generated by a phase modulation [187]. Furthermore, the literature reports a bias drift as a negative property of MZMs. This effect was also observed in our set-up and is described later in more detail. However, the comb generation by amplitude modulation enables the user to generate a defined frequency spectrum. Another fact is that undesired sidebands[4] can be suppressed by altering the operation point of the MZM (see section 3.2.2.4). This reduces distortions due to the superposition of undesired frequency components with the same separation. On the other hand, the output spectrum of phase modulated signals can be designed by the usage of specially designed reciprocating optical modulators [188] or by optical filters.

7.2 Brillouin Amplification Properties

The principle explanation of stimulated Brillouin scattering was given in Chapter 4. Here the practical application of the amplification process to the system will be analysed in detail. Therefore, it is necessary to determine the gain and the power of the Brillouin amplified sidebands at the circulator output according to Fig. 7-1. For measurement details see Appendix E2. In order to overcome the resolution penalties

[4] Either odd or even order sidebands.

Table 7-1 Measured MZM output powers of different sidebands.

Order of sideband	f_{RF} [GHz]	Power [µW]	Power [dBm]
1	19.6	740.7	-1.30
2	39.2	621.4	-2.07
3	58.8	585.0	-2.33
4	78.4	244.3	-6.12
5	98.0	52.94	-12.76
6	117.6	7.212	-21.42
7	137.2	0.7008	-31.54

For a better characterisation of the emitted frequency comb it is necessary to compare the powers of the desired sidebands with the undesired frequency components. An overview of the most important values is summarised in Table 7-2. Here, in each row (1-7), the powers of the carrier and all wanted and not wanted harmonics are shown. The settings were optimised in such a manner that the desired sidebands are maxima whereas all other frequencies are suppressed as much as possible. Table 7-2 can be read as follows: For a generation of the 3rd order harmonics (third row) the power is -2.33 dBm whereas the carrier reaches a power of -20.1 dBm and the first order sidebands have a power of -26.8 dBm.

Table 7-2 Power relations between the sidebands [dBm].

3 \ 2	Carrier	1	2	3	4	5	6	7
1	-14.26	**-1.30**	im	-25.7	us	n.f.	n.f.	n.f.
2	-20.8	im	**-2.07**	us	-17.7	im	n.f.	n.f.
3	-20.1	-26.8	im	**-2.33**	us	-14.4	n.f.	n.f.
4	-2.8	im	-3.3	im	**-6.12**	im	-21.5	im
5	-26.4	-21.4	im	-2.29	im	**-12.76**	im	-31.7
6	-2.9	im	-3.6	im	-6.3	us	**-21.42**	im
7	-17.6	-21.1	im	-2.5	im	-13.0	im	**-31.54**

[2] Power of undesired sidebands and the carrier [dBm]

[3] Order of sideband for which the frequency comb is optimised.

On the other hand, the odd order sidebands are measured in the lower operation point while the carrier is suppressed (see Fig. 7-3a black/dashed lines). Thus, it is possible to generate a variety of optical spectra with frequency components having a defined separation to each other. For the measurements of the frequency comb generation a modulation frequency of 10 GHz was chosen (see Appendix E1). The optical input power of the light waves ($\lambda = 1550.3$ nm) at the input of the MZM was set to be 18 mW. In Fig. 7-4 all possible scenarios are shown. The 1st (solid line), 2nd (dashed line) and 3rd (dashed-dotted line) sidebands can be verified while the carrier is suppressed (Fig. 7-4a).

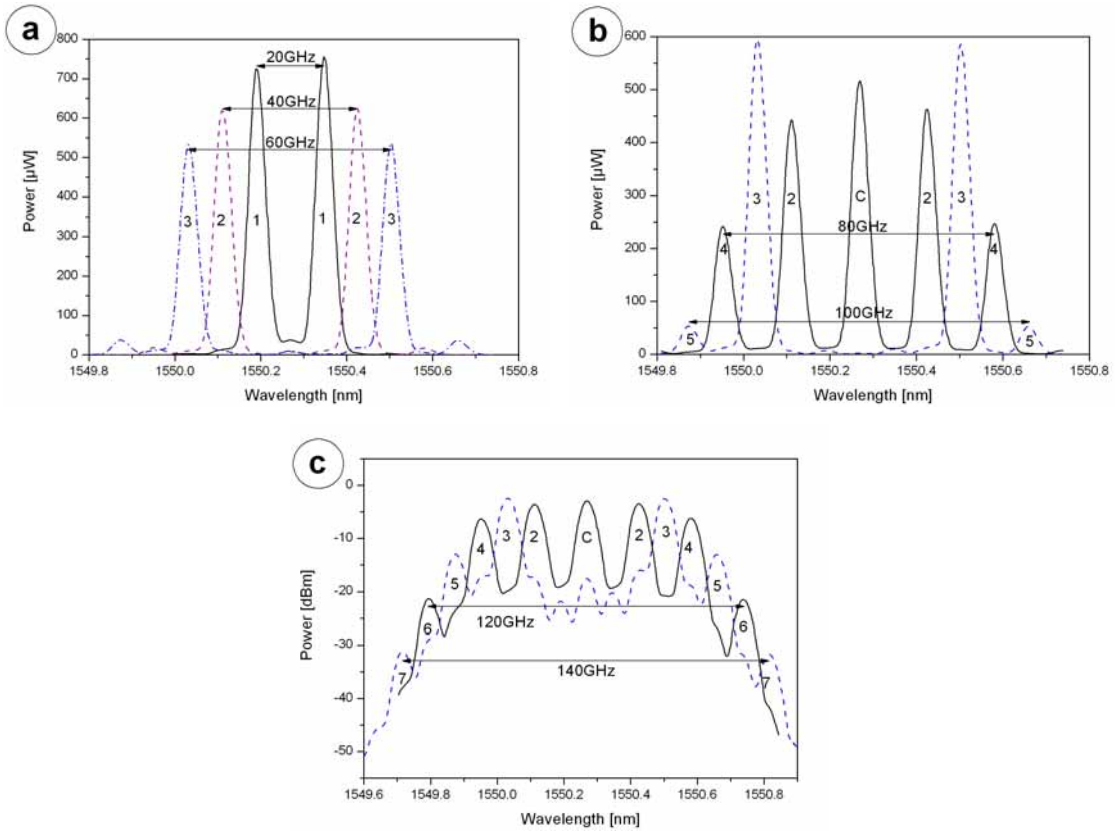

Fig. 7-4 Optical frequency components at upper and lower operating points; a: SB 1-3; b: SB 4, 5; c: SB 6,7.

On the other hand, the 4th (black/solid line) and 5th (blue/dashed line) order sidebands are obtained if the operating point alters (Fig. 7-4b). Furthermore, the 6th (black/solid line) and 7th (blue/dashed line) sidebands at a further altered bias voltage (Fig. 7-4c) can be detected. Note that the frequency separations in the graphs are approximated (20, 40 …140 GHz). Table 7-1 reflects the most important values of the characteristics in Fig. 7-4.

In Fig. 7-2 a plot of the Bessel Equation (7.3) is shown. As can be seen, the carrier (J_0) can also be suppressed at a modulation index of 2.4, for instance. The second and third order harmonics then have an enhanced magnitude. A performance demonstration of the MZM is shown in the following. The input power of the MZM was chosen to be 23 mW, the frequency of the HF generator was 10 GHz and the optical noise floor at the optical spectrum analyser (OSA) was -47 dBm.

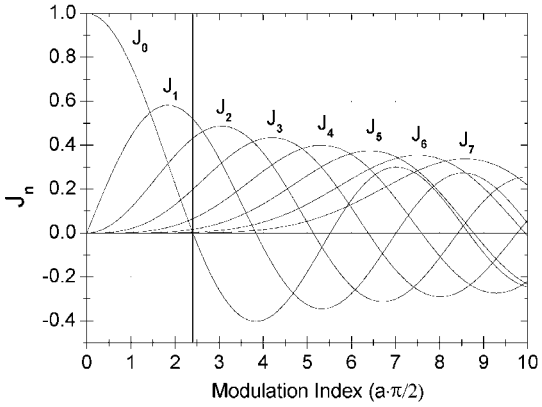

Fig. 7-2 Bessel coefficients versus modulation index.

The used MZM was a 10 Gbit/s Lithium Niobate amplitude modulator. The experimental results are shown in Fig. 7-3a. As can be seen, the amplitudes of the sidebands follow a Bessel function. The optical powers of the carrier and the sidebands were recorded by an OSA as a function of the applied HF voltage. The corresponding bias voltage versus HF voltage is verified in Fig. 7-3b with the upper OP (grey/red/solid lines) and the lower OP (black/dashed lines). As can be seen in Fig. 7-3a, while operating the MZM in the upper OP, the carrier and all even order sidebands are generated (grey/red lines).

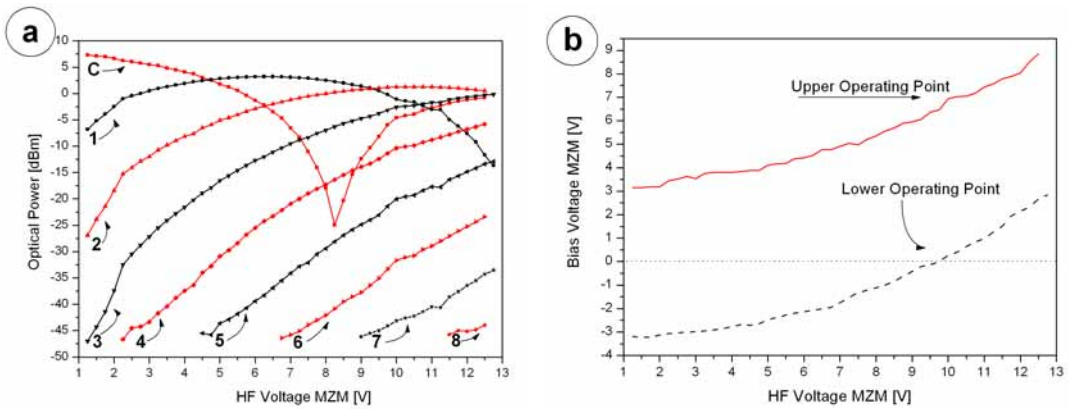

Fig. 7-3 a: Measured dependency of the power of the carrier and the sidebands on the HF voltage and b: bias voltage versus HF voltage. Grey/red lines: Upper OP; Black/dashed lines: Lower OP.

$$V_m(t) = V_\pi(1+\varepsilon) + a\,V_\pi \cos\left(\omega_{\mathrm{mod}}\, t + \Delta\varphi_{\mathrm{mod}}(t)\right) \tag{7.1}$$

with a as the drive and ε as the bias level normalised to V_π[1] and ω_{mod} as the angular modulation frequency. The function $\Delta\varphi_{mod}(t)$ corresponds to the phase noise of the modulation signal. The output field of the modulator (inset (a) of Fig. 7-1) can be described by

$$V_{out}(t) = \cos\left[\frac{\pi}{2}\left[(1+\varepsilon) + a\cdot\cos\left(\omega_{\mathrm{mod}}\, t + \Delta\varphi_{\mathrm{mod}}(t)\right)\right]\right]\cos\left(\omega_{opt}\, t + \Delta\varphi_{opt}(t)\right). \tag{7.2}$$

The angular frequency of the optical signal is ω_{opt} and the phase noise is represented by $\Delta\varphi_{opt}(t)$. After a Bessel function expansion of the output field for the spectral components it follows [186]

$$\begin{aligned} E_{out}(t) = {} & \frac{1}{2}J_0\left(a\frac{\pi}{2}\right)\cos\left(\frac{\pi}{2}(1+\varepsilon)\right)\cos\left(\omega_{opt}t + \Delta\varphi_{opt}(t)\right) \\ & - J_1\left(a\frac{\pi}{2}\right)\sin\left(\frac{\pi}{2}(1+\varepsilon)\right)\left(\cos\left(\omega_{opt}t + \Delta\varphi_{opt}(t) \pm \omega_{\mathrm{mod}}\, t + \Delta\varphi_{\mathrm{mod}}(t)\right)\right) \\ & - J_2\left(a\frac{\pi}{2}\right)\cos\left(\frac{\pi}{2}(1+\varepsilon)\right)\left(\cos\left(\omega_{opt}t + \Delta\varphi_{opt}(t) \pm 2\omega_{\mathrm{mod}}\, t + 2\Delta\varphi_{\mathrm{mod}}(t)\right)\right) \\ & + J_3\left(a\frac{\pi}{2}\right)\sin\left(\frac{\pi}{2}(1+\varepsilon)\right)\left(\cos\left(\omega_{opt}t + \Delta\varphi_{opt}(t) \pm 3\omega_{\mathrm{mod}}\, t + 3\Delta\varphi_{\mathrm{mod}}(t)\right)\right) \\ & + \ldots \end{aligned} \tag{7.3}$$

With J_i as the i^{th} Bessel function of the first kind. The term $a\cdot\pi/2$ represents the modulation index. For the case that the applied bias voltage is V_π ($\varepsilon = 0$), the frequency component at ω_{opt} (optical carrier) will be suppressed as well as all even order sidebands. On the other hand, all odd order sidebands appear at $2\cdot k\cdot\omega_{mod}$ with $k = 1,3,5\ldots$ and are centered at ω_0. The factor k represents the order of the sidebands. As can be seen, not only the modulation frequency is multiplied but also the phase noise $\Delta\varphi_{mod}(t)$. Due to the fact that the electrical phase noise is independent from the optical, the entire phase noise and hence the bandwidth of the optical field of one sideband $\Delta\nu_{SB}$ corresponds to

$$\Delta\nu_{SB} = \Delta\nu_{opt} + |k|\cdot\Delta\nu_{\mathrm{mod}}. \tag{7.4}$$

[1] V_π corresponds to the voltage that has to be applied to the modulator to achieve a phase shift of π in one interference path.

Thus either odd order sidebands or the even order sidebands including the carrier are generated. In the literature, the first method is called double sideband suppressed carrier (DSSC). Due to the fact that an extremely high electrical power is applied to the MZM, harmonics up to the order of 8 are produced during the experiments. The frequency comb, schematised in inset (a) in Fig. 7-1, is launched into a 50.45 km long SSMF. The fibre acts as a Brillouin gain medium and a transmission line at the same time. From the other side, two pump waves combined in a 3 dB coupler are injected via an optical circulator into the same fibre. The counter propagating pump waves are precisely adjusted in frequency in such a manner that their backward scattered Brillouin gains fit exactly to the wavelengths of the sideband that should be amplified. This should be the upper and the lower sideband of the same order, in order to have the same seed signal powers for SBS amplification. The strong frequency components are extracted via the circulator into a PD, schematised in Fig. 7-1 inset b. All other frequency components are attenuated owing to the natural loss in the fibre. In the PD the two amplified sidebands are heterodyned and the millimetre wave signal is generated (Fig. 7-1 inset c). The output frequency corresponds to the frequency separation of the sidebands. This can easily be adjusted by altering the MZM modulation drive signal and the emission wavelength of the pump sources.

A similar method was developed at the same time but independently by A. Wiberg [185]. There a complex fibre based oscillator is used for the generation of the base frequency and the comb. The method provides for a frequency of 10 GHz a phase noise of -61 dBc/Hz at an offset frequency of 10 kHz and instable frequency components with a frequency drift of 120 kHz for the second harmonics. The presented set-up of Fig. 7-1 can be separated into three major parts: frequency comb generation, Brillouin amplification and heterodyne detection in a PD. These parts are explained in detail in the following sub sections.

7.1 Frequency Comb Generation

In Section 3.2.2 the common ways to generate two phase correlated signals were shown. Here an amplitude modulation was applied for the generation of a frequency comb. The modulation signal $V_m(t)$ is a sinusoid with a frequency ω. Summed with the bias voltage it can be written as [186]

7 Experimental Verifications

The theory of mm-Wave generation was already discussed in the previous chapters. In this section, the practical generation of mm-Waves by stimulated Brillouin scattering for ROF systems is described in detail. The results of the theoretical investigation of Chapter 5 and the predictions of the simulation are confirmed by analysing and comparing practical results. Whereas a principle overview about the experimental set-up is presented in the following, a detailed analysis of each part is described in the sub-sections of Chapter 7.

The experimental part of this thesis describes the majority of the work carried out by the author. The experimental set-up was designed step by step from scratch to until the final design of the overall system described in this chapter was operational. In the process each component was individually investigated towards its interaction with the remainder of the system. This ensured that the system presented was able to generate high quality signals as the basis for the further carrier modulation.

The experimental set-up is shown in Fig. 7-1. The light of a narrow band fibre laser (line width < 1 kHz) acts as a signal laser. Its polarisation controlled light is externally modulated by a MZM that is driven by a high power 10 GHz sinusoidal microwave signal. The MZM is operated in the over modulation mode due to an appropriate application of bias voltage. Due to this, it is possible to switch between the upper quadratic OP and the lower quadratic OP.

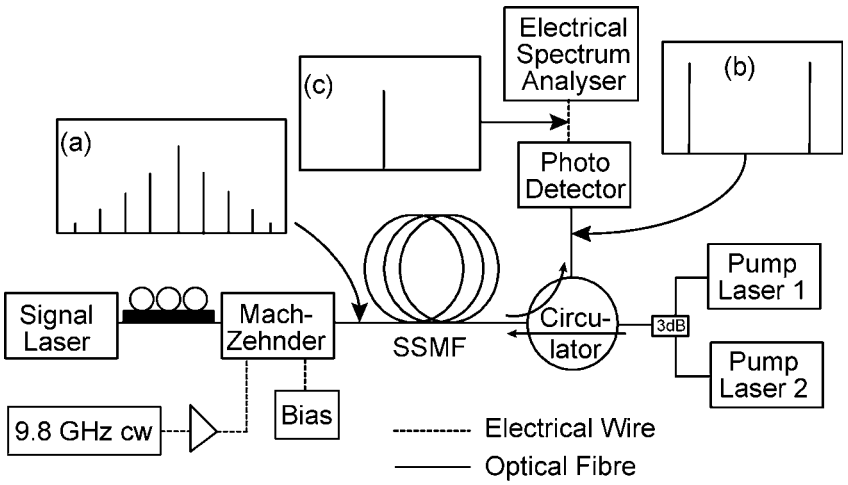

Fig. 7-1 Experimental set-up for the generation of Millimetre Waves by Brillouin scattering.

the gain and the phase behaviour at different fibre lengths, and signal and pump powers. The saturation effect that occurs for higher signal powers which is reported in the literature was confirmed. The absolute phase change due to SBS amplification of one sideband for a fibre length of 50 km is below 13 °. The highest powers of the amplified signals have been calculated to be for fibre lengths between 26.5 and 30 km (see Table 6-1).

Simulations that give information about the optimum fibre length showed that the suitable fibre length depends on the power of the signal wave. For a 50 km SSMF a signal power of 113.7 µW is ideal. On the other hand, for the signal powers used in the set-up (0.7 µW – 740 µW) a fibre length of 50.45 km is calculated to be a good compromise. Calculations, demonstrated in Sections 6.2.4 and 6.2.5, consider pump power fluctuations and frequency detuning effects on the sidebands and the heterodyned signal. Pump power fluctuations can be directly transferred to the fluctuations in the heterodyned signal power. On the other hand, the phase of the heterodyned signal is fairly insensitive to pump power variations. This shift is caused by SPM and lies in the range of $\pm 1 \cdot 10^{-14}$ °.

At the end of chapter 6, detuning effects in the heterodyned signal where discussed. Although the absolute phase change for one sideband is high, the phase difference of both sidebands remains low due to the same detuning direction of the signal laser. Thus the phases of both sidebands where changed in the same manner and the phase of the heterodyned signal remained stable.

As a general conclusion to Chapter 6 it can be said that the simulations of the complex DES (Equations (5.88)-(5.91)) show identical results for the power calculations as the simulation of the DES in Chapter 4 (Equations (4.5) and (4.6)).

14 MHz (blue/dashed dotted line) and 25 MHz (green/dotted line) have been chosen. Due to the fact that the heterodyned signal is a superposition of the fields of the amplified sidebands the detuning impact on the power of the mm-Wave is divided in halves.

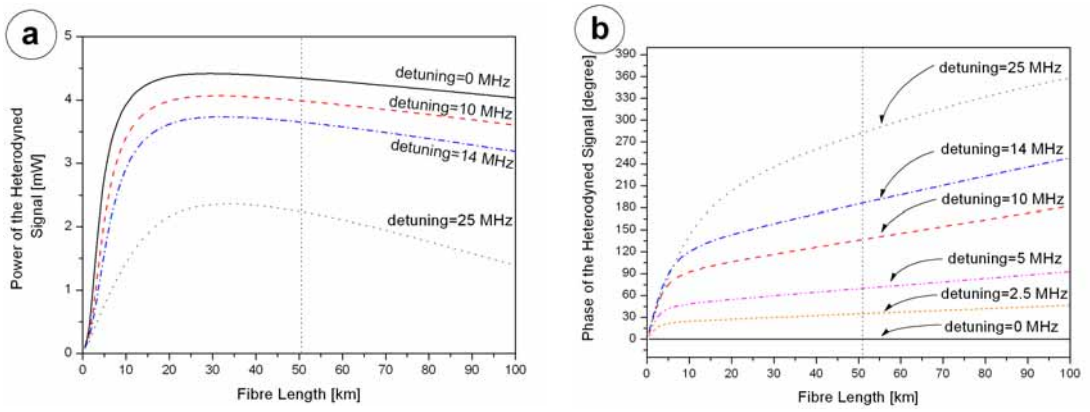

Fig. 6-15 Power (a) and phase (b) of the heterodyned signal under detuning impacts.

The phase characteristic of the heterodyned signal shows that a detuning effect has an enormous impact on the absolute phase. Thus, a detuning of 10 MHz causes a phase change of 136 ° in the mm-Wave carrier. In case that both pump lasers are detuned in the opposite direction, the absolute phase change would be doubled. This is the worst case scenario. On the other hand, the pump lasers are very stable in their emission wavelength and the setting resolution is high (approximately 2.5 MHz). Thus, a detuning of 2.5 MHz leads to a phase shift of 34.8 ° as can be seen for a fibre length of 50.45 km (Fig. 6-15b, yellow/short dotted line). In case the signal laser is tuned in wavelength (i.e. due to temperature instabilities) the detuning follows the same direction for both Brillouin gains. Hence, the phases of the sidebands are altered in the same manner and the phase difference that determines the phase of the mm-Wave is constant. Another opportunity to circumvent detuning problems is Brillouin bandwidth enhancement, which is described in Section 4.5. Due to this, the Brillouin gain can be adapted in order to significantly reduce detuning effects.

6.2.6 Conclusion

Chapter 6 described the simulated results for the differential equation system derived in Chapter 5. It has been shown that there are no power impacts of the amplified sidebands on one another. In Sections 6.2.2 and 6.2.2.2 diverse amplification scenarios have been proposed such as the amplified sideband, the heterodyned signal,

6.2.5 Simulation of Frequency Detuning

The investigation of the Brillouin gain characteristic with the phase matching terms in (5.95) and (5.96) requires an analysis of the impact of the frequency detuning to the gain maximum. For this approach, the natural Brillouin gain bandwidth is measured to be 28 MHz at room temperature. As can be seen in Fig. 5-2, the largest impact to the phase is induced at the maximum of the imaginary part. The investigation of frequency detuning is done within and outside of the gain bandwidth. The impact of the detuning is shown in Fig. 6-14 where four cases are simulated. Thus, in the graph the powers of the signal wave are shown for detuning values of 0, 10, 14 and 25 MHz, respectively.

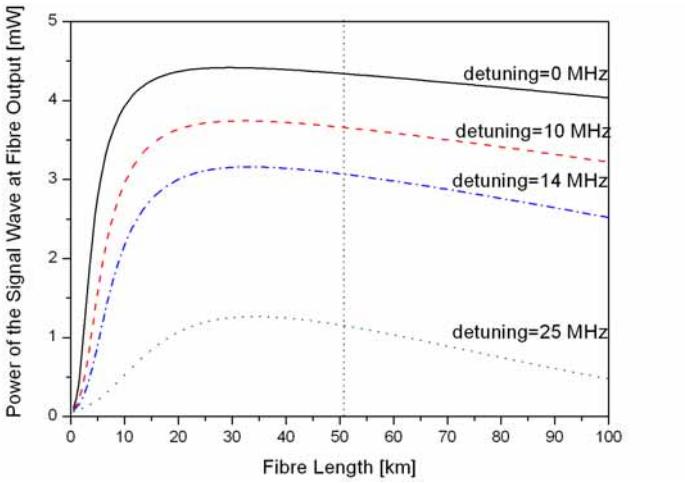

Fig. 6-14 Signal power at fibre output for different frequency detuning values.

The pump power is assumed to be 6 mW and the signal power to be 52.94 µW. On the one hand, if the detuning is within the natural Brillouin gain bandwidth (10 MHz red/dashed line) the impact to the signal power is low. On the other hand, the influences become greater if the detuning is increased (14 MHz blue/dashed dotted line). A detuning of 14 MHz corresponds to the 3 dB bandwidth where the phase change due to SBS is maximum (compare Fig. 5-2). For a detuning of 25 MHz (green/dotted line) the signal wave is attenuated drastically due to the low Brillouin gain.

The impact of detuning on the heterodyned signal is shown in Fig. 6-15 with respect to the power (a) and the absolute phase (b). Here, only one pump source is detuned whereas the second is assumed to be stable at the maximum Brillouin gain. Again, detuning scenarios of 0 Hz (black/solid line), 10 MHz (red/dashed line),

effects the first signal (P_{S1}) - first pump (P_{P1}) amplification process. The increase in one pump power over 1 mW leads to a phase shift of $\approx \pm 0.05°$ whereas the change of the pump power of both pump lasers leads to a phase shift of $\approx \pm 0.1°$. These effects have also been observed in simulations where the phase of the second signal wave was calculated. Furthermore, it has been noted that the directions of the phase alterations are in the same direction. The steps in Fig. 6-12b are due to the limited resolution of the numerical simulation method.

The corresponding power of the heterodyned signal is shown in Fig. 6-13a. As also described in section 6.2.2, the optical powers are converted into the electrical field via (5.76) and (5.77) and are multiplied with each other.

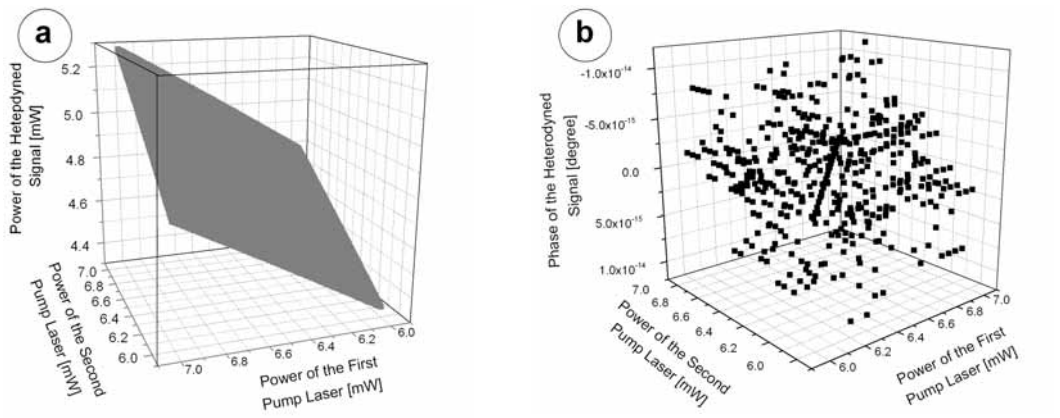

Fig. 6-13 Power (a) and phase (b) of the heterodyned signal wave for drifting pump powers.

The power of the electrical signal can be calculated using the same equations. Thus, Fig. 6-13a shows the multiplication of the fields of signal wave 1 and signal wave 2 of Fig. 6-12. It can be seen that the power of the heterodyned signal is directly proportional to the powers of the sidebands that are superimposed in the PD. Due to the fact that the phase development of both amplified sidebands is almost the same according to Fig. 6-12b; the phase difference is also very low. The phase noise lies in the range of $\pm 1 \cdot 10^{-14}$ °. The phase change due to SBS is assumed to be the same for both amplified sidebands according to Fig. 6-12b. Hence, the imaginary parts of Equations (5.89) and (5.91) show that the difference between the two waves lies in the power of the signal waves P_{S2} and P_{S1} and corresponds to the SPM.

Concluding this section, it can be said that the used fibre length is a good compromise for the usage of high and low signal powers. However, as can be seen in Appendix D (right column), the rise characteristics (derivative) increase very slowly for fibre lengths longer than the minimum. Hence, the impact of the undesired sidebands will still be low, even outside of the optimum fibre length.

6.2.4 Simulation of Pump Power Drifts

Due to fluctuations in the pump laser diode powers, there can be variations in the powers and the phases of the signal wave. This effect on the amplified signals is analysed in detail in the following section. For the simulation, a pump power drift of $\Delta P = 1$ mW[3] and a fibre length of 50.45 km were assumed. As can be seen in Fig. 6-12a, the alteration of power of the second pump laser has no impact on the power of the amplified first sideband (light grey curve). The power of the first signal wave increases linearly with the power of the first pump laser. This effect can also be observed for the second signal wave (dark grey curve). The second signal wave increases linearly from 4.2 mW to 5.3 mW as the second pump laser power increases from 6 to 7 mW. The simultaneous increase of the first pump power has no effect on the power of the second signal wave.

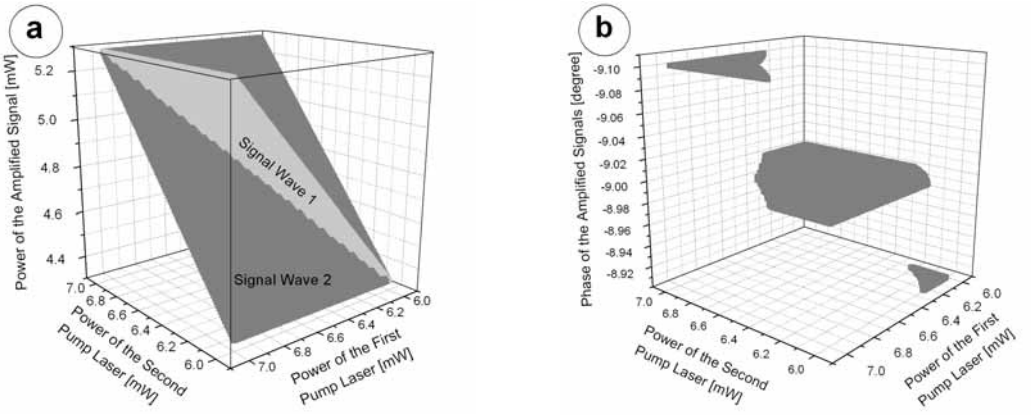

Fig. 6-12 a: Power of the first (light grey curve) and second (dark grey curve) signal wave for the fibre output at drifting pump powers; b: Phase of both amplified signal waves at different pump powers.

The relationship between the phase of the amplified signal and the pump power is shown in Fig. 6-12b. As shown, a change in the second pump wave power (P_{P2}) also

[3] The power was increased from 6 to 7 mW.

maximum value for any fibre length. The greater the fibre length the higher the power separation of the sidebands. Therefore, the definition of the optimum fibre length has to change.

It is adapted in such a manner that the optimum fibre length occurs when the rise of the relationship curve (blue/solid lines in Appendix D) is negligible. At this point on the graph, the rise in power hits saturation.

This optimum can be expressed via the minimum of the derived relationship characteristic. The simulation results can be seen in the right column of Appendix D. Although the minima can not be seen by the eye due to the very low change, the calculation program has found minimum values marked in the figures. A review of the optimum fibre lengths is given in Fig. 6-11. It shows the characteristic of the optimum fibre length versus the order of the sideband and the corresponding signal power, respectively. Due to the fact that all simulations have been carried out within a range of 0-100 km, only optima for the sidebands 1-5 are shown. As can be seen for lower signal powers, the optimum fibre length rises, whereas with higher power levels shorter fibre lengths show a better performance according to the definition. It should be noted that in the "optimum fibre length" definition, no other circumstances, such as dependency of the pump power or the ASEN, are considered. Therefore, according to [153] the ASEN can rise in Brillouin amplifiers if the fibre length increases. Thus, the real characteristic can vary from the presented one.

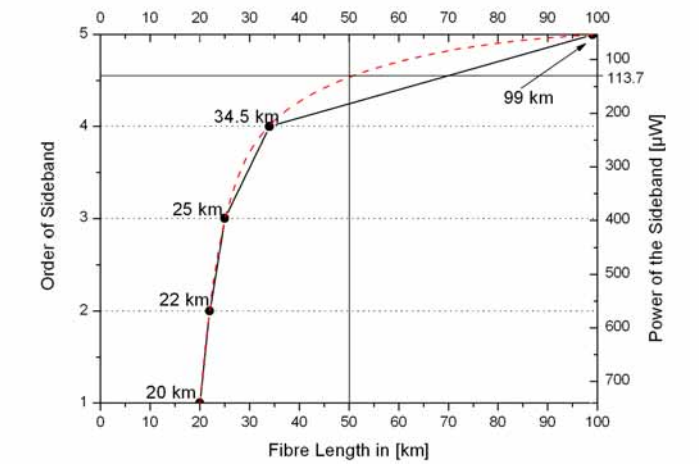

Fig. 6-11 Order of amplified sidebands vs. optimum fibre length (black/solid line); Exponential growth fitting (red/dashed line).

For the given set-up, a 50.45 km long SSMF is used. Assuming an exponential fitting of the given values (red/dashed line in Fig. 6-11) an optimum signal power of 113.7 µW can be seen.

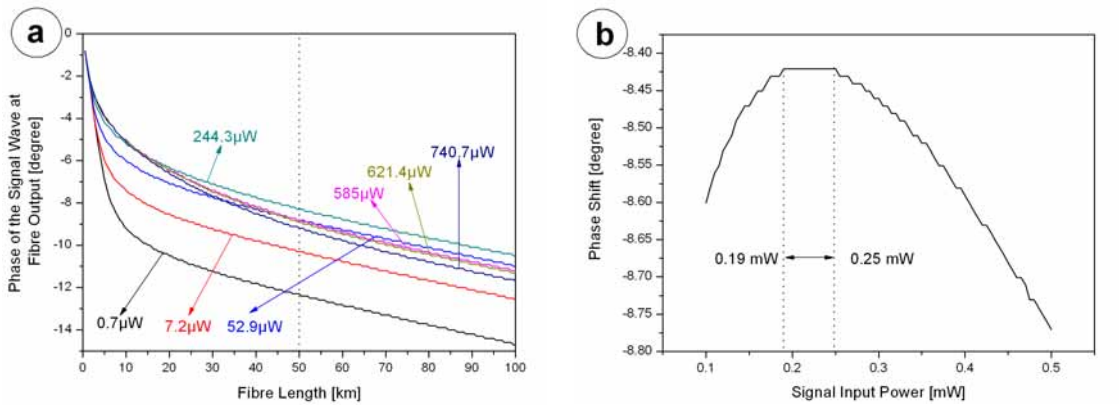

Fig. 6-10 a: Fibre output phase dependence on signal powers; b: Optimum signal input power vs. phase shift for a 50 km long fibre.

are shown in Fig. 6-10b. For this case, within a range of 0.19 µW and 0.25 µW, the absolute phase change is minimal**.** An explanation for this behaviour lies in the imaginary part of Equations (5.89) and (5.91). With the increasing signal wave power P_{S1} and P_{S2}, the impact of SPM becomes more significant. Then, P_{S1} and P_{S2} are in the same power range as the pump powers P_{P1} and P_{P2}.

6.2.3 Optimum Fibre Length

The optimum fibre length of the system can be defined as the maximum power separation of the amplified sidebands to the highest power non-amplified sidebands. This definition is based on the assumption that when the power ratio of the desired sidebands to the undesired sidebands is greatest, the impact on the millimetre wave signal becomes negligible. The frequency separations between the undesired sidebands are nearly the same as for the desired ones. Therefore, distortions can occur in the PD due to a superposition and interaction of equal frequencies.

The graphs in Appendix D show simulations relating to the optimum fibre length. In the left column the relationships of the amplified sidebands (pump power = 6 mW) to the highest unamplified sidebands are given. The power relationships of each sideband, summarised in Table 7-2 on page 86, are the basis for the simulations. The graphs in the left column of Appendix D show the power variation of the amplified sidebands (black/dotted lines), the behaviour of the powers of the maximum undesired sidebands (red/dashed lines) and the separation of both (blue/solid line). The difference represents the normalised relationship. Due to the fact that the power of the desired sidebands decreases slowly with higher fibre lengths but the power of the undesired sidebands drops off sharply, there is no

Table 6-2 Maximum values at different signal powers.

Power of signal wave		Fibre length [km] where signal is maximal	Maximum powers of the amplified signals		Gain [dB]
[µW]	[dBm]		[mW]	[dBm]	
0.7	-31.55	50	3.66	5.63	47.62
7.2	-21.43	42.4	4.04	6.06	37.93
52.9	-12.77	28.5	4.42	6.45	29.66
244.3	-6.12	16	4.87	6.87	23.35
585	-2.33	12	5.35	7.28	20.05
621.4	-2.07	10	5.40	7.32	19.83
740.7	-1.30	9	5.54	7.43	19.18

Fig. 6-9a shows the gain with respect to the signal power at the input of the fibre, whereas Fig. 6-9b demonstrates the gain with respect to the signal power at the fibre output. It can be seen in the second case that there is no maximum gain. This is due to the fact that the fibre attenuation also impacts the gain calculations. Fig. 6-9b reflects the same result as for Fig. 6-9a, but from a different point of view.

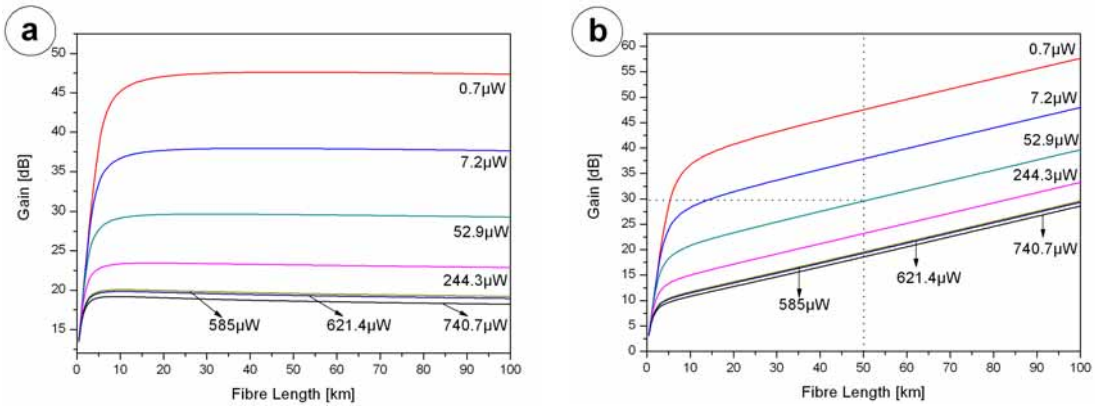

Fig. 6-9 Gain for different signal powers. a: Related to the input power; b: Related to the output power.

The phase characteristics in Fig. 6-10 also show similarities to Fig. 6-7. On the other hand, Fig. 6-10a shows that the phase change depends heavily upon the signal power. Furthermore, it can be seen that for higher signal powers (585, 621.4 and 740.7 µW) the phase change is lower than for lower signal powers. Hence, there is a maximum signal power for a minimal phase shift. It can be seen that the optimum signal input power depends on the length of the fibre. Calculation results for a 50 km long fibre

change of the phases. This can be due to the large power change due to pump depletion which results in XPM or the increase in signal power which causes SPM and XPM, respectively. Due to the fact that the impact of XPM is twice as large as the impact due to SPM, these nonlinear effects seem to be the reason for the phase shift [184].

6.2.2.2 Different Signal Powers and Constant Pump Power

For this simulation, different signal powers (as marked in the figures) were chosen. These values correspond to the measured powers of the sidebands at the input of the 50 km SSMF at different operation points according to Table 7-1. The pump power is assumed to be 6 mW. The change of signal power has a similar impact on the absolute value of the signal output power as the variation of the pump power (see Fig. 6-8). On the other hand, the maximum of the signal power has moved to shorter fibre lengths while the input power has increased. Along with the power of the amplified sidebands, Fig. 6-8 also shows the power of the heterodyned signal.

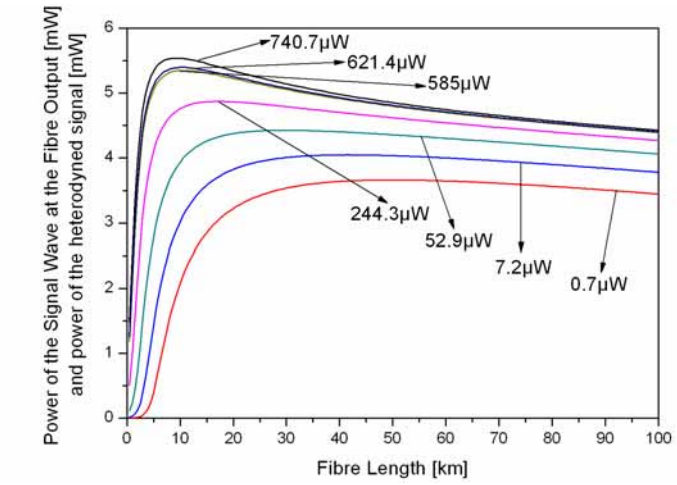

Fig. 6-8 Fibre output power and power of the heterodyned signal for different input signal powers.

A comparison of the amplification characteristics of each simulation scheme (Fig. 6-6 and Fig. 6-9) shows that the gain for low signal powers is higher than for high signal powers.

Table 6-2 gives an overview of the most important values taken out of Fig. 6-8 and Fig. 6-9b. The gain in Table 6-2 is calculated as a relationship of the fibre output power with and without amplification, assuming a SSM Fibre with an attenuation of 10.45 dB (50.45 km).

In Sections 6.2.4 and 6.2.5 the behaviour of the heterodyned signal due to pump power drifts and frequency detuning is discussed. The corresponding gains relating to the fibre input power characteristics at different pump powers are shown in Fig. 6-6. Here again, the signal power is 52.94 µW.

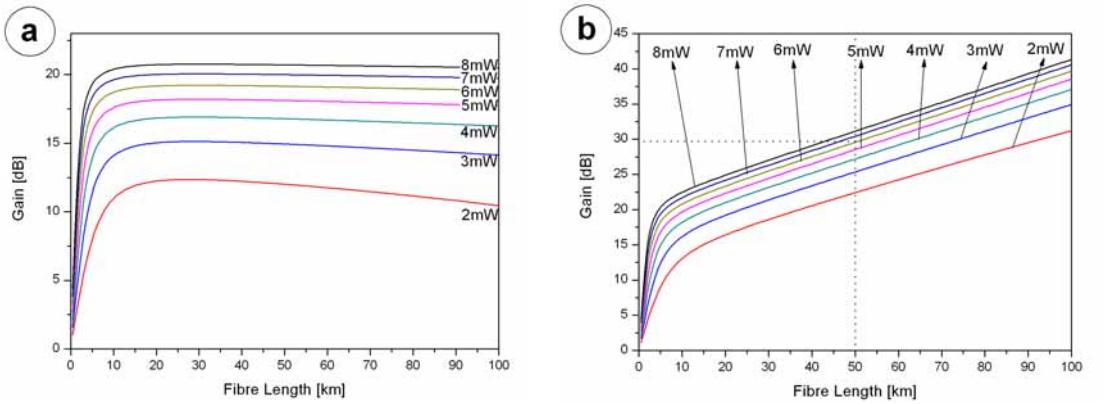

Fig. 6-6 Gain at different pump powers; a: Related to the input power; b: Related to the output power.

Fig. 6-6b shows the gain in relation to the signal power at the output of the fibre. It can be seen that there is no maximum gain, as the fibre attenuation also influences the gain calculations. Fig. 6-6b reflects the same result as Fig. 6-6a but under different points of view.

The investigation of the phase as a function of the fibre length is shown in Fig. 6-7. It can be seen that the phase shift at low pump powers and at high fibre lengths (> 20 km) reaches a maximum value. With growing pump power a higher phase alteration is observed. Again this influence is induced by SPM and XPM effects at higher power levels. For fibre length less than 10 km the simulation shows a large

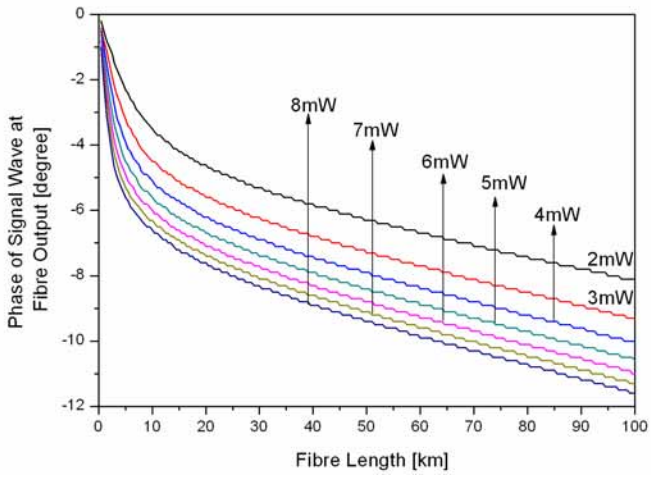

Fig. 6-7 Phase of the signal wave at the fibre output for different pump powers.

signal power of 52.94 µW the optimum fibre length for a maximum Brillouin amplification is 31 km with a power of the amplified signal of 2.6 mW. All graphs in Fig. 6-5 show approximately the same progress. The main difference lies in the absolute power of the amplified sidebands and the fibre length where the power is maximum. The maximum of each graph is only slightly shifted up in the length of the fibre. Table 6-1 gives an overview of the most important values taken out of Fig. 6-5.

Table 6-1 Maximum values at different pump powers.

Power of pump signal		**Fibre length [km] where signal is maximal**	**Maximum powers of the amplified signals**		**Gain [dB]**
[mW]	**[dBm]**		**[mW]**	**[dBm]**	
2	3.01	26.5	0.911	-0.4	22.80
3	4.77	28.0	1.723	2.36	25.57
4	6.02	28.5	2.597	4.14	27.35
5	6.99	28.0	3.503	5.44	28.56
6	7.78	28.5	4.428	6.46	29.67
7	8.45	28.5	5.366	7.29	30.50
8	9.03	30	6.313	8.00	31.20

The gain in Table 6-1 is calculated as the relationship of the fibre output power with and without amplification. For this calculation, a fibre length of 50.45 km is assumed with an attenuation of 0.209 dB/km. Thus, the total attenuation is 10.54 dB.

In Sections 6.2.2 and 6.2.2.2 it is assumed that there are no fluctuations either due to frequency detuning or to pump power instabilities. Therefore, it is assumed that the phase changes impact both amplified sidebands in the same manner. Since both shifts are equal the heterodyned signal that is described by Equation (3.5) has no influences through the phases. Hence, all simulation results that concern the power of the amplified sidebands can be transformed directly into the power characteristic of the heterodyned signal. The power can be computed into the electrical field via (5.76) and (5.77). By calculating the power from the intensity field according to the same equations, the same power for the heterodyned signal as for one single amplified sideband is obtained.

As can be seen, the phase shift increases with an increased amplification by SBS over the fibre. On the other hand, SBS can not be the cause of this phase shift because the imaginary part is zero for an amplification process when the Brillouin gain maximum (no detuning) is considered. However, the power increase due to SBS amplification also raises the impact of SPM and XPM. Hence the impact to the phase. Therefore, assuming zero detuning, the phase is only impacted by SPM and XPM effects.

6.2.2 Diverse Amplification Scenarios

In the following two sub-sections simulation results of diverse amplification scenarios are proposed. In Section 6.2.2.1 the pump power is altered and the signal power is kept constant. In Section 6.2.2.2 the signal power is changed whereas the pump power is unchanged.

6.2.2.1 Different Pump Powers and Constant Signal Power

This section gives information about the amplification processes for different pump powers at a constant signal power. Note that for the simulations in Section 6.2.2 and 6.2.2.2 the characteristics for the amplified sidebands (P_{S1} and P_{S2}) are equal.

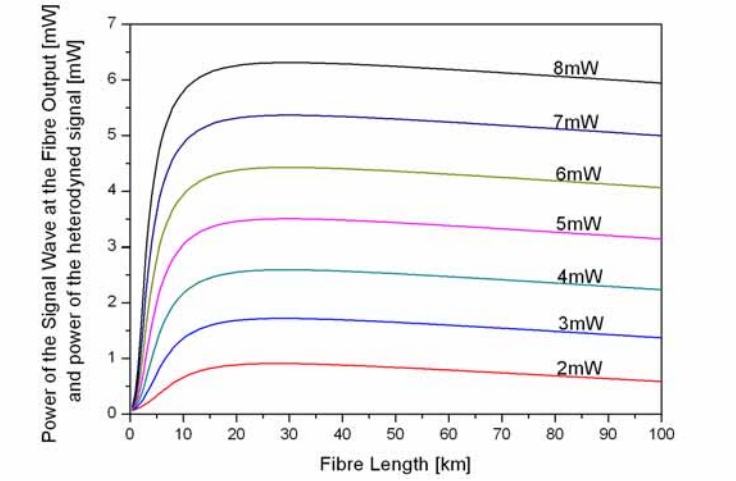

Fig. 6-5 Signal power at the fibre output and heterodyned signal power at different pump powers.

The pump powers are chosen to be below and slightly above the Brillouin threshold for the SSMF used, namely 2, 3 …8 mW. The power of the signal waves P_{Sig} is 52.94 µW. As can be seen in Fig. 6-5 the signal output power rises if the pump power increases. The graph can be read as follows: At a pump power of 4 mW and a

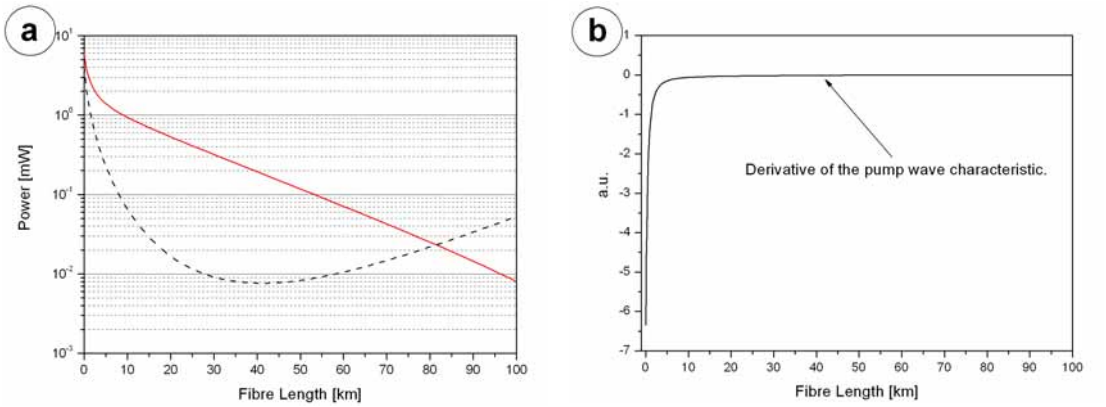

Fig. 6-3 a: Power of the amplified signal wave (black dashed line) and of the pump wave (red solid line) along the fibre; b: Rise (derivative) of the pump wave.

rise of the pump wave power is much bigger than at higher fibre segments. The power of the signal wave reaches values that are in the order of the pump wave, which can be seen as pump depletion[2] [136].

The signal wave (dashed line in Fig. 6-3a) is coupled in at point "100 km". Naturally, it also depends on the attenuation in the fibre, however, its influence decreases with increased fibre length (negative "z"). At the point "40 km" (namely after a propagation of 60 km) the Brillouin amplification corresponds to the attenuation in the fibre. For the further propagation in the fibre, the amplification process dominates over the attenuation. Hence, the power of the signal wave increases exponentially.

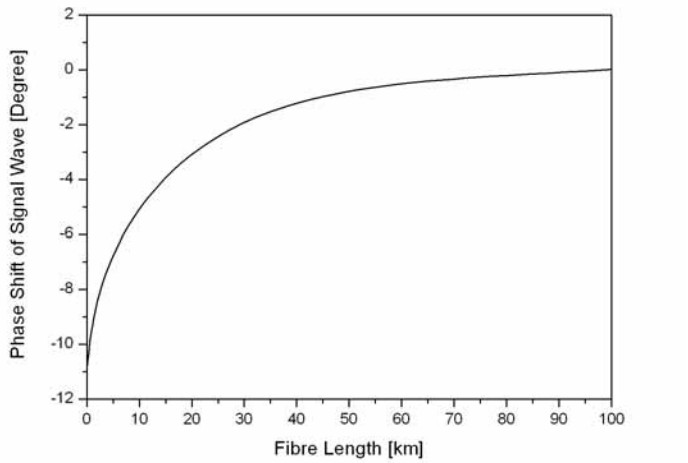

Fig. 6-4 Phase shift along the fibre.

The corresponding increase of the phase of the amplified signal is shown in Fig. 6-4. For the calculation of this graph, again the signal wave is injected at point "100 km".

[2] Pump depletion: The major part of the pump power is transferred to the signal wave.

chosen to reduce computation time. This means that the shooting method searches for the right value within this interval (± 5° and ± 2.5°).

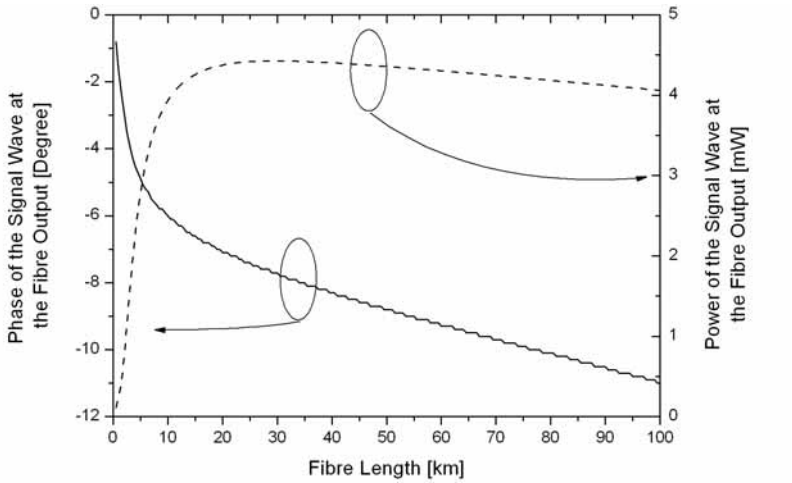

Fig. 6-2 Dashed line: Power of the signal wave as a function of the fibre length; Solid line: Phase of the signal vs. fibre length.

Simulation results for the amplification process of the signal wave by SBS are demonstrated in Fig. 6-2. The parameters used for the simulation can be found in Appendix A. For the approach in this chapter a pump power of 6 mW and a signal power of 52.94 µW have been chosen. Thus, the pump power lies just below the Brillouin threshold and the signal power corresponds to the measured power of the 5^{th} sideband of the generated frequency comb. The values for the amplified first and second signal wave are identical because the influence of equal pump powers to the absolute value and phase has to be the same as it is reported in [169]. The dashed line in Fig. 6-2 shows the power of the signal at different Brillouin medium lengths. A saturation effect can be observed for a fibre length of 29 km which is similar to the simulation results in Fig. 4-6. The solid line in Fig. 6-2 represents the phase change of the signal wave for a certain fibre length. As can be seen, the largest phase change occurs in the first 20 km of optical fibre. On the other hand, the absolute phase shift is with -8.85° (at 50.45 km) small. In Fig. 6-3 the power of the signal and the pump wave along a 100 km long optical fibre is shown. The fibre output corresponds to the point "0 km" where the pump waves are coupled in and the signal waves are coupled out. As can be seen in Fig. 6-3, the pump power (solid line) decreases steadily at an exponential rate (logarithm view) over the largest part of the fibre (approx. 4-100 km). This is due to the mainly constant attenuation in the fibre [136]. On the other hand, it can be observed in Fig. 6-3b that within the range of 0 and 4 km the

A possible method for the analysis of the DES is the application of the shooting method where the BVC is traced back to an initial value condition. Hence, the initial values are evaluated in such a manner that the BVC is fulfilled. The condition for this method is the existence of a unique solution and proportionality between the input and output power. That means that an increment of the initial value follows an increment of the boundary value. At the beginning the shooting algorithm is executed on a large scale whereas the increment is reduced if the absolute value of the boundary value is reached.

The shooting algorithm for the calculation of the Brillouin amplified signal is schematised in Appendix B. The internal loop "calculate absolute value" is a further shooting algorithm shown in appendix C. Both loops represent the calculation of the amplification process at a certain length of the fibre.

6.2 Results

While the simulation in section 4.6 is based on Equations (4.5) and (4.6) the following simulations are based on the coupled equation system of Chapter 5. Thus, in these simulations, the amplification processes of two signal waves by two pump waves instead of one signal and one pump wave is given. Due to the fact that the imaginary part of the wave equations is considered, the DES is able to describe the change of the phase of the signal wave due to SBS interactions. Furthermore, nonlinear interactions due to SPM and XPM are also considered.

6.2.1 Simulation of Basic Brillouin Interactions

This chapter should give an extended overview of the SBS[1] by simulations of the principal interactions including phase analysis. Due to the fact that the phase formation over the entire fibre has to be known for the investigations, it is necessary to start the simulation at a short fibre length. For the calculations of the next value, the phase interval is tracked on the basis of the result of the last value. The searching interval is ± 5° around the last calculated value up to a fibre length of 20 km. For the calculation of lengths of 20 km or even higher a searching interval of ± 2.5° has been

[1] In contrast to section 4.6

6 Simulations

The presented simulations of the DES were carried out by Andrzej Wiatrek [181]. The DES in chapter 5 ((5.88) - (5.91)) is coupled in such a manner that the solution of one equation depends always on the solutions of the other equations. The condition $\delta P(z)/\ \delta z = f(z,P(z))$ verifies that the system is a first order DES [182] which is only in a few cases solvable by analytic methods [183]. Hence, numerical methods are often used for the solution of such systems. Another fact is that the given parameters, namely the power of the pump waves at the fibre output and the power of the signal waves at the fibre input, can be seen as a boundary value condition (BVC).

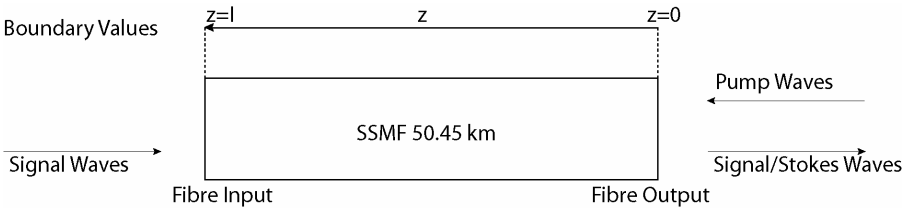

Fig. 6-1 Principal system model.

The arrows in Fig. 6-1 illustrating “Signal Waves” and “Pump Waves” represent the input parameters of the system. The “Signal/Stokes Waves” are the unknown parameters in the system. The direction “z” defines the integration direction which shows that the signal waves are calculated in the opposite direction to their propagation direction.

The application of the Runge-Kutta-Method for the investigation of the stability of the DES shows a very high performance and high accuracy. Detailed information about the rigidity of the DES can be found in [181].

6.1 Shooting Method

Since the algorithm of the DES is a BVC there is no standardised theory for the solution, as there are for initial value conditions. This is due to the fact that the calculations can only be executed in one direction, as is illustrated in Fig. 6-1. Since the solution depends on arbitrary parameters [182] the boundary value conditions that are based on non-linear DES are not solvable by analytic methods.

- As can be seen**,** the phase change term due to SBS interaction in (5.89) and (5.91) shows that also the pump wave itself can lead to an additional phase noise. However, this noise can be ignored if the pump powers are chosen to be equal and thus the signal waves are influenced in the same manner.
- This chapter gave a theoretical description of the wave interactions in the Brillouin gain medium. Due to the proposed results, it is possible to optimise the experimental set-up. Preliminary forecast or tendencies can be made in respect of the noise properties of the generated mm-Wave signal. The mathematical description provides the basis for a simulation of different scenarios. Therefore, more information about the behaviour of the system is obtained. This simulation is presented in the following chapter.

with $\omega_{S1,2max}$ as the frequency shift between the pump and the sideband where the maximum Brillouin gain occurs. Introducing (5.94) into (5.86) it follows that [169]

$$\Delta k_{eR1,2} = \frac{v_a^2 \alpha_a / 2}{(v_a \alpha_a / 2)^2 + (\omega_{S1,2} - \omega_{S1,2\max})^2} \tag{5.95}$$

and (5.94) into the imaginary part (5.87) [169]

$$\Delta k_{eI1,2} = \frac{v_a (\omega_{S1,2} - \omega_{S1,2\max})}{(v_a \alpha_a / 2)^2 + (\omega_{S1,2} - \omega_{S1,2\max})^2} \,. \tag{5.96}$$

According to equations (5.88) - (5.91), the mismatch factor $\Delta k_{1,2}$ impacts the Brillouin gain directly. In Fig. 5-2 the real and the imaginary part of the Brillouin gain is shown. The simulation has been executed with v_a =5.95 km/s, a Brillouin gain bandwidth of 28 MHz and an acoustic field attenuation of $\alpha_a \approx 29518$ km^{-1}.

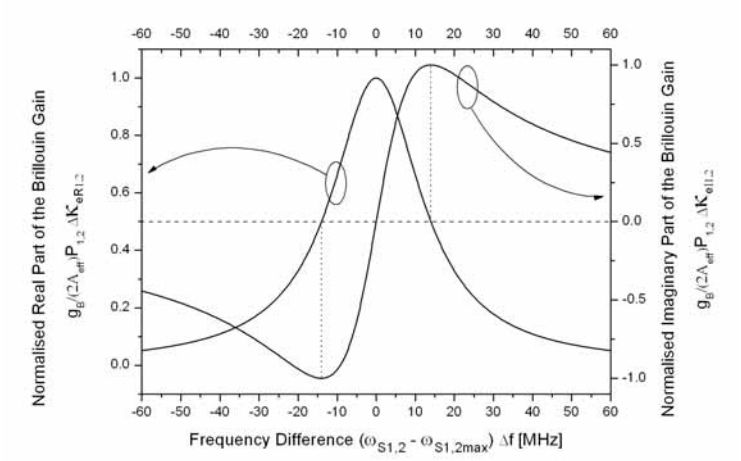

Fig. 5-2 Normalised real (left) and imaginary part (right) of the Brillouin gain (FHWM=28 MHz) depending on the frequency difference ($\omega_{S1,2}$ - $\omega_{S1,2max}$) according to (5.95) and (5.96) [169].

The real part (5.95) describes the Brillouin gain characteristic whereas the imaginary part (5.96) corresponds to the phase shift. As can be seen in Fig. 5-2 the minimum and the maximum of the phase shift occurs at a frequency detuning which corresponds to the half bandwidth of the gain characteristic. The phase change is the same if the detuning of both gain curves and sidebands is equal. On the other hand, the frequency shift is zero if the sideband is in the centre frequency of the gain bandwidth. Hence, in this case there would be no influence on the phase by SBS interactions.

the attenuation in the fibre. The main differences from Equation (4.5) and (4.6) are, that also nonlinear effects such as SPM, XPM and FWM are considered here and that there are four equations. Furthermore, there are no calculations feasible that analyse the phase of the amplified signal by using (4.5) and (4.6).

- The terms in the brackets, accompanied with the nonlinear coefficient γ represent the interaction owing to SPM (first term) and XPM (second to fourth term) between the waves. A comparison of (5.89) and (5.91) demonstrates that the pump power P_{P1} and P_{P2} have the same influence on both sidebands E_{S1} and E_{S2}. Because of this, the phase change due to XPM and SPM is equal for both in the case of their power being equal. Equation (5.91) for instance shows that power fluctuations of the pump source can lead to XPM with the other pump wave which could induce a phase noise to the generated mm-Wave carrier. But, due to the fact that both sidebands and both pump waves propagate in the same fibre and hence the pump waves affect the sidebands in the same manner, a phase correlated maintaining status during the Brillouin amplification process can be expected.
- The phase influences due to Brillouin scattering are described by the first term in the brackets of (5.88) - (5.91). Owing to the fact that the attenuation is a constant, the variable parameter $\Delta k_{eI1,2}$ can be reduced to the average phase mismatch $\Delta k_{1,2}$. According to (5.46), $k_{S1} = (n_0 \cdot \omega_{S1})/c$ and (5.4) the mismatch factor can be written as

$$\Delta k_{1,2} = k_{P1,2} + k_{S1,2} - k_a = \frac{\omega_{P1,2} n}{c} + \frac{\omega_{S1,2} n}{c} - \frac{\omega_a}{v_a}. \tag{5.92}$$

With $\omega_a = \omega_P - \omega_S$ and the assumption that the frequency of the pump and the Stokes wave is almost the same it can be simplified further to

$$\Delta k_{1,2} \approx 2\frac{\omega_{P1,2} n}{c} - \frac{\omega_{P1,2} - \omega_{S1,2}}{v_a} = \frac{1}{v_a}\left[\frac{2\omega_{P1,2} n v_a}{c} - \left(\omega_{P1,2} - \omega_{S1,2}\right)\right] \tag{5.93}$$

and accordingly (4.4) to [169]

$$\Delta k_{1,2} = \frac{1}{v_a}\left[\omega_{S1,2} - \omega_{S1,2\max}\right] \tag{5.94}$$

simplification: The differential equation system of the Brillouin amplification processes of two waves by two independent pump sources in an optical fibre[169]:

$$\frac{\delta E_{P1}}{\delta z} = -\left[\frac{g_B}{2A_{eff}}\Delta k_{eR1}P_{S1} + \frac{\alpha}{2}\right]E_{P1} - j\left\{\frac{g_B}{2A_{eff}}\Delta k_{eI1}P_{S1} + \gamma\left(P_{P1} + 2P_{S1} + 2P_{P2} + 2P_{S2}\right)\right\}E_{P1} \tag{5.88}$$

$$\frac{\delta E_{S1}}{\delta z} = -\left[\frac{g_B}{2A_{eff}}\Delta k_{eR1}P_{P1} - \frac{\alpha}{2}\right]E_{S1} + j\left\{\frac{g_B}{2A_{eff}}\Delta k_{eI1}P_{P1} + \gamma\left(P_{S1} + 2P_{P1} + 2P_{P2} + 2P_{S2}\right)\right\}E_{S1} \tag{5.89}$$

$$\frac{\delta E_{P2}}{\delta z} = -\left[\frac{g_B}{2A_{eff}}\Delta k_{eR2}P_{S2} + \frac{\alpha}{2}\right]E_{P2} - j\left\{\frac{g_B}{2A_{eff}}\Delta k_{eI2}P_{S2} + \gamma\left(P_{P2} + 2P_{P1} + 2P_{S1} + 2P_{S2}\right)\right\}E_{P2} \tag{5.90}$$

$$\frac{\delta E_{S2}}{\delta z} = -\left[\frac{g_B}{2A_{eff}}\Delta k_{eR2}P_{P2} - \frac{\alpha}{2}\right]E_{S2} + j\left\{\frac{g_B}{2A_{eff}}\Delta k_{eI2}P_{P2} + \gamma\left(P_{S2} + 2P_{P1} + 2P_{P2} + 2P_{S1}\right)\right\}E_{S2} \tag{5.91}$$

5.3 Analysis

In this chapter a detailed analysis of the resultant equations is given. As described at the beginning of Chapter 5, the two sidebands that should be heterodyned in a PD, are totally phase correlated at the output of the MZM. The equation system gives information about the impact of SBS amplification to the mm-Wave generation system in special respect to the phase influences.

- The differential equation system (5.88) - (5.91) with its parameters Δk_{eR} and Δk_{eI} describe the local change of the two pump waves and the two sidebands. The first term in the square brackets of (5.88) - (5.91) represents the real part and describes the exchange of power between the pump waves and the sidebands due to Brillouin interactions. It can be seen that the amplitudes of the pump waves ((5.88) and (5.90)) decrease with positive z. On the other hand, the amplitudes of the amplified sidebands ((5.89) and (5.91)) increase with negative z. The second term ($\alpha/2$) in the square brackets in all four equations ((5.88) - (5.91)) represents

On the other hand, the constants $C_{P,S,1,2}$ (5.44) and C_3 (5.63) can be merged to:

$$C_{S,P;1,2} \cdot C_3 = \frac{\gamma_e \omega_{S,P;1,2}}{\rho_0 c 4n} \frac{\varepsilon_0 \gamma_e}{4 v_a^2} k_a \tag{5.80}$$

Where $k_{P,S;1,2}=n\omega_{P,S;1,2}/c$ and $v_a^2=\beta/\rho_0$ with β as the adiabatic modulus of elasticity [174] the equation can be simplified to [169]

$$C_{P,S;1,2} \cdot C_3 = \frac{\varepsilon_0 \gamma_e^2 \omega_{P,S;1,2}}{16 c^2 \beta} \frac{k_a}{k_{P,S;1,2}} \tag{5.81}$$

After inserting (5.77) and (5.81) into (5.70) - (5.73), neglecting the terms including the phase mismatch differences and summarising the appropriate parameters to the Brillouin gain factor g_B (5.78) it follows that [169]

$$\frac{\delta E_{P1}}{\delta z} + \frac{a}{2} E_{P1} = -\frac{g_B}{2} A_{eff} \Delta k_{e1} E_{P1} P_{S1} - jD_{P1}\left[SPM_{P1} + XPM_{P1}\right] \tag{5.82}$$

$$\frac{\delta E_{S1}}{\delta z} - \frac{a}{2} E_{S1} = -\frac{g_B}{2} A_{eff} \Delta k_{e1} E_{S1} P_{P1} - jD_{S1}\left[SPM_{S1} + XPM_{S1}\right] \tag{5.83}$$

$$\frac{\delta E_{P2}}{\delta z} + \frac{a}{2} E_{P2} = -\frac{g_B}{2} A_{eff} \Delta k_{e2} E_{P2} P_{S2} - jD_{P2}\left[SPM_{P2} + XPM_{P2}\right] \tag{5.84}$$

$$\frac{\delta E_{S2}}{\delta z} - \frac{a}{2} E_{S2} = -\frac{g_B}{2} A_{eff} \Delta k_{e2} E_{S2} P_{P2} - jD_{S2}\left[SPM_{S2} + XPM_{S2}\right]. \tag{5.85}$$

According to (5.67) the conjugate complex expansion of the factor $\Delta k_{e1,2}$ towards the real Δk_{eR} and imaginary part Δk_{eI} leads to [169]

$$\Delta k_{eR1,2} = \frac{\alpha_a / 2}{(\alpha_a / 2)^2 + (\Delta k_{1,2})^2} \tag{5.86}$$

$$\Delta k_{eI1,2} = \frac{\Delta k}{(\alpha_a / 2)^2 + (\Delta k_{1,2})^2} \cdot \tag{5.87}$$

Under consideration of (5.77), the introduction of (5.79), (5.45) and (5.38) - (5.41) into (5.82) - (5.85) and the assumption that the Brillouin gain coefficients g_B and the nonlinear coefficients γ are equal[6] for all four waves lead to an additional

[6] due to the small frequency difference of the waves

$$\frac{\delta E_{S1}}{\delta z} - \frac{a}{2} E_{S1} = -C_{S1} C_3 \left[\Delta k_{e1} \left| E_{P1} \right|^2 E_{S1} + \Delta k_{e2} E_{P1} E_{P2}^* E_{S2} e^{j(\Delta k_2 - \Delta k_1) z} \right] - jD_{S1} \left[SPM_{S1} + XPM_{S1} \right]. \tag{5.71}$$

With (5.66) into (5.36) for the second pump wave $E_{P2}(z)$ it can be written that

$$\frac{\delta E_{P2}}{\delta z} + \frac{a}{2} E_{P2} = -C_{P2} C_3 \left[\Delta k_{e1} E_{P1} E_{S1}^* E_{S2} e^{j(\Delta k_2 - \Delta k_1) z} + \Delta k_{e2} E_{P2} \left| E_{S2} \right|^2 \right] - jD_{P2} \left[SPM_{P2} + XPM_{P2} \right] \tag{5.72}$$

and finally with (5.68) into (5.37) it follows for the second sideband $E_{S2}(z)$

$$\frac{\delta E_{S2}}{\delta z} - \frac{a}{2} E_{S2} = -C_{S2} C_3 \left[\Delta k_{e1} E_{P1}^* E_{S1} E_{P2} e^{j(\Delta k_1 - \Delta k_2) z} + \Delta k_{e2} \left| E_{P2} \right|^2 E_{S2} \right] - jD_{S2} \left[SPM_{S2} + XPM_{S2} \right] \tag{5.73}$$

with $E_{P1,2}, E^*_{P1,2} = E_{P1,2}(z), E^*_{P1,2}(z)$. According to (5.47) and (5.48) the phase mismatching differences in (5.70) - (5.73)

$$\Delta k_1 - \Delta k_2 = k_{P1} + k_{S1} - k_a - \left(k_{P2} + k_{S2} - k_a \right) \tag{5.74}$$

and

$$\Delta k_2 - \Delta k_1 = k_{P2} + k_{S2} - k_a - \left(k_{P1} + k_{S1} - k_a \right) \tag{5.75}$$

lead to a very low coherence length. Hence, these terms can be neglected. The intensity of the waves is [178]

$$I = \frac{1}{2} \varepsilon_0 cn \left| E \right|^2 \tag{5.76}$$

and their input power is described by $P = I \cdot A_{eff}$. Hence, the square of the absolute value of E can be described by

$$\left| E_{P,S;1,2} \right|^2 = P_{P,S;1,2} \frac{2}{\varepsilon_0 cn A_{eff}}. \tag{5.77}$$

Furthermore, the Brillouin gain coefficient for a pump wave can be written as [179]

$$g_{BP} = \frac{\omega_P^2 \gamma_e^2 k_a}{4nc^3 \rho_0 v_a^2 k_P} \tag{5.78}$$

and according to [180] the nonlinear coefficient γ can be described by

$$\gamma_{P,S} = \frac{3 \chi^{(3)} \omega_{P,S}}{4 c^2 n^2 \varepsilon_0 A_{eff}}. \tag{5.79}$$

pump waves and the sidebands can be ignored. Hence, the product of these amplitude functions can be moved outside the integrals. Equation (5.64) then becomes[169]

$$Q(z) = -jC_3 \cdot \left[\begin{array}{l} E_{P1}E_{S1}^{*} \dfrac{1}{\alpha_a/2 - j\Delta k_1}\left(e^{-j\Delta k_1 z} - e^{-\alpha_a \frac{z}{2}} \right) \\ + E_{P2}E_{S2}^{*} \dfrac{1}{\alpha_a/2 - j\Delta k_2}\left(e^{-j\Delta k_2 z} - e^{-\alpha_a \frac{z}{2}} \right) \end{array} \right] + Q_{(0)} e^{-\alpha_a \frac{z}{2}} \tag{5.65}$$

with $E_{P1,2}, E^{*}_{P1,2} = E_{P1,2}(z), E^{*}_{P1,2}(z)$.

With $v_a = 5.96$ km/s, a Brillouin gain bandwidth of $\Delta f_a = 28$ MHz and the relationship $\Delta\omega_a = \alpha_a \cdot v_a$ [177] an attenuation of the acoustic wave of $\alpha_a \approx 29518$ km^{-1} can be calculated. On the other hand, the interaction length ($z \approx 50$ km) of the optical field and the scattering medium is much greater than the attenuation length of the phonon *($z \gg 2/\alpha_a$)*. Thus, by neglecting the term $e^{-\alpha_a z/2}$ Equation (5.65) becomes

$$Q(z) = -jC_3 \cdot \left(\Delta k_{e1} E_{P1} E_{S1}^{*} e^{-j\Delta k_1 z} + \Delta k_{e2} E_{P2} E_{S2}^{*} e^{-j\Delta k_2 z} \right) \tag{5.66}$$

with

$$\Delta k_{e1} = \frac{1}{\alpha_a/2 - j\Delta k_1} \quad \text{and} \quad \Delta k_{e2} = \frac{1}{\alpha_a/2 - j\Delta k_2}. \tag{5.67}$$

The conjugate complex function of *Q(z)* is

$$Q^{*}(z) = -jC_3 \cdot \left(\Delta k_{e1} E_{P1}^{*} E_{S1} e^{j\Delta k_1 z} + \Delta k_{e2} E_{P2}^{*} E_{S2} e^{j\Delta k_2 z} \right) \tag{5.68}$$

with

$$\Delta k_{e1}^{*} = \frac{1}{\alpha_a/2 + j\Delta k_1} \quad \text{and} \quad \Delta k_{e2}^{*} = \frac{1}{\alpha_a/2 + j\Delta k_2}. \tag{5.69}$$

5.2.3 The Complete Differential Equation System

All components that have been derived in this chapter have to be introduced into the equation system (5.34) to (5.37). Thus, for the first pump wave $E_{P1}(z)$ Equation (5.66) is inserted into (5.34)

$$\begin{aligned} \frac{\delta E_{P1}}{\delta z} + \frac{a}{2} E_{P1} = -C_{P1}C_3 \Big[\Delta k_{e1} E_{P1} \left| E_{S1} \right|^2 + \Delta k_{e2} E_{P2} E_{S2}^{*} E_{S1} e^{j(\Delta k_1 - \Delta k_2)z} \Big]. \\ - jD_{P1}\left[SPM_{P1} + XPM_{P1} \right] \end{aligned} \tag{5.70}$$

By introducing (5.68) into (5.35) for the first sideband $E_{S1}(z)$ it follows that

$$\frac{\delta^2\rho}{\delta z^2}-\frac{\alpha_a}{\upsilon_a}\frac{\delta\rho}{\delta t}-\frac{1}{\upsilon_a^2}\frac{\delta^2\rho}{\delta t^2}=\left[-jk_a\frac{\delta Q(z)}{\delta z}-\frac{1}{2}jk_a\alpha_a Q(z)\right]e^{j(\omega_a t-k_a z)}, \tag{5.59}$$

respectively.

Complete Equation

The combination of the solved left (5.59) and right (5.53) part leads to

$$\left[-jk_a\frac{\delta Q(z)}{\delta z}-\frac{1}{2}jk_a\alpha_a Q(z)\right]e^{j(\omega_a t-k_a z)}= -\frac{\varepsilon_0\gamma_e}{2v_a^2}\frac{1}{2}k_a^2\left(E_{P1}E_{S1}^*e^{-j(k_{P1}+k_{S1})z}+E_{P2}E_{S2}^*e^{-j(k_{P2}+k_{S2})z}e^{j\omega_a t}\right). \tag{5.60}$$

After eliminating $e^{j\omega_a t}$ and the division by $e^{-jk_a z}$ it follows that

$$-jk_a\frac{\delta Q(z)}{\delta z}-\frac{1}{2}jk_a\alpha_a Q(z)= -\frac{\varepsilon_0\gamma_e}{4v_a^2}k_a^2\cdot\left(E_{P1}E_{S1}^*e^{-j(k_{P1}+k_{S1}-k_a)z}+E_{P2}E_{S2}^*e^{-j(k_{P2}+k_{S2}-k_a)z}\right). \tag{5.61}$$

After the division by $-jk_a$ and the introduction of (5.46) the complete equation for the acoustic phonons can be written as

$$\frac{\delta Q(z)}{\delta z}+\frac{\alpha_a}{2}Q(z)=-jC_3\cdot\left(E_{P1}E_{S1}^*e^{-j\Delta k_1 z}+E_{P2}E_{S2}^*e^{-j\Delta k_2 z}\right) \tag{5.62}$$

where C_3 is defined as

$$C_3=\frac{\varepsilon_0\gamma_e}{4v_a^2}k_a. \tag{5.63}$$

Integral Form

According to [177], Equation (5.62) can be expressed in the integral form

$$Q(z)=-jC_3\cdot\left[\begin{array}{l}\int_0^z E_{P1}(z')E_{S1}^*(z')e^{-j\Delta k_1 z'-\alpha_a\frac{z-z'}{2}}dz' \\ +\int_0^z E_{P2}(z')E_{S2}^*(z')e^{-j\Delta k_2 z'-\alpha_a\frac{z-z'}{2}}dz'\end{array}\right]+Q_{(0)}e^{-\alpha_a\frac{z}{2}}. \tag{5.64}$$

Only in the range of $(z - z') \leq 2 / \alpha_a$ significant contributions of the integrals in (5.64) influence the equation. Furthermore, the rate of the acoustic loss α_a is usually much larger than the rates of change of $E_P(z)$ and $E_S(z)$ due to stimulated scattering or optical losses. Thus, within the range of $(z - z') \leq 2 / \alpha_a$ the spatial variations of the

$$\begin{aligned}\frac{\delta^2(E)}{\delta z^2} &= \frac{\delta^2}{\delta z^2}\frac{1}{2}\left(E_{P1}e^{j(\omega_{P1}t-k_{P1}z)}\cdot E_{S1}^{*}e^{-j(\omega_{S1}t-k_{S1}z)}+E_{P2}e^{j(\omega_{P2}t-k_{P2}z)}\cdot E_{S2}^{*}e^{-j(\omega_{S2}t-k_{S2}z)}\right)\\ &= \frac{\delta^2}{\delta z^2}\frac{1}{2}\left(E_{P1}E_{S1}^{*}e^{-j(k_{P1}+k_{S1})z}+E_{P2}E_{S2}^{*}e^{-j(k_{P2}+k_{S2})z}\right)e^{j\omega_a t}\end{aligned} \tag{5.51}$$

with $E_{P1,2},E^{*}_{P1,2} = E_{P1,2}(z),E^{*}_{P1,2}(z)$. If

$$k_a^2 \approx (k_P + k_S)^2, \tag{5.52}$$

ε_0, γ_e and v_a are introduced into the right term of (5.11) and by the execution of the differentiation process it can be written that [169]

$$\frac{\varepsilon_0\gamma_e}{2v_a^2}\frac{\delta^2(E)}{\delta z^2} = -\frac{\varepsilon_0\gamma_e}{2v_a^2}\frac{1}{2}k_a^2\left(E_{P1}E_{S1}^{*}e^{-j(k_{P1}+k_{S1})z}+E_{P2}E_{S2}^{*}e^{-j(k_{P2}+k_{S2})z}e^{j\omega_a t}\right). \tag{5.53}$$

Left Part

Considering the SVE approximation the local derivatives (δz) of (5.6) can be written as

$$\frac{\delta\rho}{\delta z} = \frac{1}{2}\left[\frac{\delta Q(z)}{\delta z}e^{j(\omega_a t-k_a z)} - Q(z)jk_a e^{j(\omega_a t-k_a z)}\right] \tag{5.54}$$

$$\frac{\delta^2\rho}{\delta z^2} = \frac{1}{2}\left[-2\frac{\delta Q_a(z)}{\delta z}jk_a - k_a^2 Q(z)\right]\cdot e^{j(\omega_a t-k_a z)}. \tag{5.55}$$

By expanding the first and second time derivative (δt) with α_a/v_a and $1/v_a$, respectively it follows that

$$\frac{\alpha_a}{v_a}\frac{\delta\rho}{\delta t} = \frac{1}{2}\frac{\alpha_a}{v_a}j\omega_a Q(z)e^{j(\omega_a t-k_a z)} \tag{5.56}$$

$$\frac{1}{v_a}\frac{\delta^2\rho}{\delta t^2} = -\frac{1}{2}\frac{\omega_a^2}{v_a}Q(z)e^{j(\omega_a t-k_a z)}. \tag{5.57}$$

With $k_a=\omega_a/v_a$ the left hand side of (5.11) can be written as

$$-jk_a\frac{\delta Q(z)}{\delta z}e^{j(\omega_a t-k_a z)} + \frac{1}{2}Q(z)k_a^2 e^{j(\omega_a t-k_a z)} - \frac{1}{2}\frac{\alpha_a}{v_a}j\omega_a Q(z)e^{j(\omega_a t-k_a z)} - \frac{1}{2}Q(z)k_a^2 e^{j(\omega_a t-k_a z)} \tag{5.58}$$

or

The phase mismatch condition terms can be written as

$$\Delta k_{1,2} = k_{P1,2} + k_{S1,2} - k_a \tag{5.46}$$

$$\Delta k_{FWM} = k_{S1} - k_{P2} - k_{S2} + k_{P1}\,. \tag{5.47}$$

Since the two pump waves and the two sidebands have almost the same frequency it can be assumed that the refractive index is equal for all four frequencies. Hence, according to (5.5) and (5.47) and with ω_{RF} as the angular frequency of the RF signal the phase mismatch term for FWM can be written as [169]

$$\Delta k_{FWM} = \frac{n}{c}\left(\omega_{S1} - \omega_{S2} + \omega_{P1} - \omega_{P2}\right) = 2\frac{n}{c}\omega_{RF} \tag{5.48}$$

with $n = 1.44$ for the fibre used and an RF frequency of $f = 60$ GHz the phase mismatch for FWM is 3620.52 m^{-1}. By following $L_{coh} = \pi/k_{\Delta FWM}$ a coherence length[5] of only 0.867 mm can be calculated. Therefore, the FWM terms can be neglected.

5.2.2 Investigation of the Wave Equation for the Density Modulation

Right part

As well as in chapter 5.3.1.1 there are many solutions of $(E)^2$ which are introduced into the right hand side of the wave equation for the density modulation (5.11).

$$\begin{aligned}(E)^2 = &\left(E_{P1} + E_{S1} + E_{P2} + E_{S2} + E_{P1}^* + E_{S1}^* + E_{P2}^* + E_{S2}^*\right)\cdot \\ &\left(E_{P1} + E_{S1} + E_{P2} + E_{S2} + E_{P1}^* + E_{S1}^* + E_{P2}^* + E_{S2}^*\right)\end{aligned} \tag{5.49}$$

But only few terms fulfil the condition $\omega_a = \omega_P - \omega_S$ for Q and $-\omega_a = \omega_S - \omega_P$ for Q^*. After eliminating all terms that do not fulfil the condition it can be written:

$$(E)^2 = 2E_{P1}E_{S1}^* + 2E_{P2}E_{S2}^*\,. \tag{5.50}$$

The second derivative of (5.50) with respect to z is

[5] The coherence length corresponds to the maximum optical retardation of two light waves. This maximum corresponds to the point at which a superposition of the waves is still constructive.

$$\frac{\delta E_{P1}(z)}{\delta z}+\frac{a}{2}E_{P1}(z)=-jC_{P1}Q(z)E_{S1}(z)\cdot e^{j\Delta k_1 z}-jD_{P1}\left[SPM_{P1}+XPM_{P1}+FWM_{P1}\right] \tag{5.34}$$

$$\frac{\delta E_{S1}(z)}{\delta z}-\frac{a}{2}E_{S1}(z)=jC_{S1}Q^{*}(z)E_{P1}(z)\cdot e^{-j\Delta k_1 z}+jD_{S1}\left[SPM_{S1}+XPM_{S1}+FWM_{S1}\right] \tag{5.35}$$

$$\frac{\delta E_{P2}(z)}{\delta z}+\frac{a}{2}E_{P2}(z)=-jC_{P2}Q(z)E_{S2}(z)\cdot e^{j\Delta k_2 z}-jD_{P2}\left[SPM_{P2}+XPM_{P2}+FWM_{P2}\right] \tag{5.36}$$

$$\frac{\delta E_{S2}(z)}{\delta z}-\frac{a}{2}E_{S2}(z)=jC_{S2}Q^{*}(z)E_{P2}(z)\cdot e^{-j\Delta k_2 z}+jD_{S2}\left[SPM_{S2}+XPM_{S2}+FWM_{S2}\right]. \tag{5.37}$$

with the self phase modulation terms

$$SPM_{P1,2}=\left|E_{P1,2}\right|^2\cdot E_{P1,2} \tag{5.38}$$

$$SPM_{S1,2}=\left|E_{S1,2}\right|^2\cdot E_{S1,2} \tag{5.39}$$

and the cross phase modulation terms

$$XPM_{P1,2}=\left(2\left|E_{P2,1}\right|^2+2\left|E_{S1}\right|^2+2\left|E_{S2}\right|^2\right)E_{P1,2} \tag{5.40}$$

$$XPM_{S1,2}=\left(2\left|E_{S2,1}\right|^2+2\left|E_{P1}\right|^2+2\left|E_{P2}\right|^2\right)E_{S1,2}\,. \tag{5.41}$$

The four FWM terms can be described by

$$FWM_{P1,S2}=2E_{S1}E_{P2}E^{*}_{S2,P1}e^{j\Delta k_{FWM}z} \tag{5.42}$$

$$FWM_{P2,S1}=2E_{P1}E_{S2}E^{*}_{S1,P2}e^{-j\Delta k_{FWM}z}\,. \tag{5.43}$$

The constants in (5.34) - (5.37) are[169]

$$C_{P1,2}=\frac{\gamma_e\omega_{P1,2}}{\rho_0 c4n};\ C_{S1,2}=\frac{\gamma_e\omega_{S1,2}}{\rho_0 c4n} \tag{5.44}$$

$$D_{P1,2}=\frac{3\chi^{(3)}\omega^2_{P1,2}}{8k_{P1,2}c^2};\ D_{S1,2}=\frac{3\chi^{(3)}\omega^2_{S1,2}}{8k_{S1,2}c^2} \tag{5.45}$$

$$SPM = \left|E_x\right|^2 \cdot E_x \tag{5.27}$$

$$XPM = \left|E_x\right|^2 \cdot E_y \quad ; x \neq y \tag{5.28}$$

$$FWM = E_x^t \cdot E_y^t \cdot E_z^t \quad ; x \neq y \neq z; t = * \ or \neq * \tag{5.29}$$

with the relation $E \cdot E^* = |E|^2$. All other components occur at different frequencies, their phase condition is not fulfilled or both. Hence, they can be neglected. By reducing the equation system to relevant terms the complete right side of (5.10) ($1/c^2 \cdot \delta^2/\delta t^2 \cdot (\gamma_e/\rho_0 \cdot \rho E + \chi^{(3)} EEE)$) can be written as

$$-\frac{\omega_{P1}^2}{c^2} e^{j\omega_{P1}t} \left\{ \frac{\gamma_e}{\rho_0} \frac{1}{4} Q(z) E_{S1}(z) \cdot e^{-j(k_a - k_{S1})z} + \frac{3}{8} \chi^{(3)} \begin{bmatrix} \left(\left|E_{P1}\right|^2 + 2\left|E_{S1}\right|^2 + 2\left|E_{P2}\right|^2 + 2\left|E_{S2}\right|^2 \right) E_{P1} e^{-jk_{P1}z} \\ + 2E_{S1} E_{P2} E_{S2}^* e^{j(k_{S1} - k_{P2} - k_{S2})z} \end{bmatrix} \right\} \tag{5.30}$$

$$-\frac{\omega_{S1}^2}{c^2} e^{j\omega_{S1}t} \left\{ \frac{\gamma_e}{\rho_0} \frac{1}{4} Q^*(z) E_{P1}(z) \cdot e^{-j(k_{P1} - k_a)z} + \frac{3}{8} \chi^{(3)} \begin{bmatrix} \left(\left|E_{S1}\right|^2 + 2\left|E_{P1}\right|^2 + 2\left|E_{P2}\right|^2 + 2\left|E_{S2}\right|^2 \right) E_{S1} e^{jk_{S1}z} \\ + 2E_{P1} E_{S2} E_{P2}^* e^{j(k_{P2} - k_{P1} + k_{S2})z} \end{bmatrix} \right\} \tag{5.31}$$

$$-\frac{\omega_{P2}^2}{c^2} e^{j\omega_{P2}t} \left\{ \frac{\gamma_e}{\rho_0} \frac{1}{4} Q(z) E_{S2}(z) \cdot e^{-j(k_a - k_{S2})z} + \frac{3}{8} \chi^{(3)} \begin{bmatrix} \left(\left|E_{P2}\right|^2 + 2\left|E_{P1}\right|^2 + 2\left|E_{S1}\right|^2 + 2\left|E_{S2}\right|^2 \right) E_{P2} e^{-jk_{P2}z} \\ + 2E_{P1} E_{S2} E_{S1}^* e^{j(k_{S2} - k_{P1} - k_{S1})z} \end{bmatrix} \right\} \tag{5.32}$$

$$-\frac{\omega_{S2}^2}{c^2} e^{j\omega_{S2}t} \left\{ \frac{\gamma_e}{\rho_0} \frac{1}{4} Q^*(z) E_{P2}(z) \cdot e^{-j(k_{P2} - k_a)z} + \frac{3}{8} \chi^{(3)} \begin{bmatrix} \left(\left|E_{S2}\right|^2 + 2\left|E_{P1}\right|^2 + 2\left|E_{S1}\right|^2 + 2\left|E_{P2}\right|^2 \right) E_{S2} e^{jk_{S2}z} \\ + 2E_{S1} E_{P2} E_{P1}^* e^{j(k_{S1} - k_{P2} + k_{P1})z} \end{bmatrix} \right\}. \tag{5.33}$$

The first term in the curly brace describes the acoustic phonons in the fibre. The second term in the square brackets represents the influences by FWM. The first term in the square brackets stands for SPM and the 2nd-4th summand in brackets for XPM.

Complete Equation System

The differential equation system that describes two pump waves and the two amplified sidebands in the silica fibre can be written as[169]:

$$\frac{1}{c^2}\frac{\delta^2}{\delta t^2}\frac{\gamma_e}{\rho_0}\rho E = \frac{\gamma_e \delta^2}{\rho_0 c^2 \delta t^2}\cdot\left(\begin{bmatrix}\rho+\rho^*\end{bmatrix}\cdot \begin{bmatrix}E_{S1}+E_{S1}^*+E_{S2}+E_{S2}^*+E_{P1}+E_{P1}^*+E_{P2}+E_{P2}^*\end{bmatrix}\right) \tag{5.22}$$

with E_{SPi}^* as the conjugate complex of E_{SPi}, with $i = 1,2$ representing the two pump waves and the two side bands. Under the consideration of (5.9) the insertion of (5.2) and (5.6) into (5.22) leads to a number of terms. With the help of the vector diagram of Fig. 5-1 and Equation (5.9) the equations responsible for the pump waves and the sidebands can be separated[4].

$$\begin{aligned}\frac{\gamma_e \delta^2}{\rho_0 c^2 \delta t^2}\rho\cdot E_{S1} &= \frac{1}{2}\left[Q(z)\cdot e^{j(\omega_a t - k_a z)}\right]\cdot\frac{1}{2}\left[E_{S1}(z)\cdot e^{j(\omega_{S1} t + k_{S1} z)}\right] \\ &= \frac{\gamma_e \delta^2}{\rho_0 c^2 \delta t^2 4}\left[Q(z)E_{S1}(z)\cdot e^{j(\omega_{P1} t - [k_a - k_{S1}]z)}\right]\end{aligned} \tag{5.23}$$

$$\frac{\gamma_e \delta^2}{\rho_0 c^2 \delta t^2}\rho\cdot E_{S2} = \frac{\gamma_e \delta^2}{\rho_0 c^2 \delta t^2 4}\left[Q(z)E_{S2}(z)\cdot e^{j(\omega_{P2} t - [k_a - k_{S2}]z)}\right] \tag{5.24}$$

$$\begin{aligned}\frac{\gamma_e \delta^2}{\rho_0 c^2 \delta t^2}\rho^*\cdot E_{P1} &= \frac{1}{2}\left[Q^*(z)\cdot e^{-j(\omega_a t - k_a z)}\right]\cdot\frac{1}{2}\left[E_{P1}(z)\cdot e^{j(\omega_{P1} t - k_{P1} z)}\right] \\ &= \frac{\gamma_e \delta^2}{\rho_0 c^2 \delta t^2 4}\left[Q^*(z)E_{P1}(z)\cdot e^{j(\omega_{S1} t - [k_{P1} - k_a]z)}\right]\end{aligned} \tag{5.25}$$

$$\frac{\gamma_e \delta^2}{\rho_0 c^2 \delta t^2}\rho^*\cdot E_{P2} = \frac{\gamma_e \delta^2}{\rho_0 c^2 \delta t^2 4}\left[Q^*(z)E_{P2}(z)\cdot e^{j(\omega_{S2} t - [k_{P2} - k_a]z)}\right] \tag{5.26}$$

The introduction of Equation (5.2) into the second term on the right side of (5.10) ($1/c^2\cdot\delta^2/\delta t^2\cdot\chi^{(3)}EEE$) leads to a large number of terms. Due to the multiplication with the third order susceptibility the non-linear effects SPM, XPM and FWM have to be considered. If the phase of a wave changes with the intensitiy of the wave itself, the effect is called Self Phase Modulation (SPM). If the phase is impacted by other waves the effect is described as Cross Phase Modulation (XPM). SPM and XPM lead to a phase noise of the sidebands and therefore to a broadening of the spectrum and signal distortion. Beside SPM and XPM there are also terms that represent mixing of participated waves. These terms describe the Four Wave Mixing (FWM) effect where waves interact with each other while propagating in the fibre. SPM, XPM and FWM have the form [176]

[4] For each wave there are four terms. Under consideration of Equation (5.1) only one term includes the relevant frequency. The other can be neglected.

The derivatives with respect to *t* are

$$\frac{\delta E_{P1}}{\delta t} = \frac{1}{2}\omega_{P1}E_{P1}(z)jk_{P1}e^{j(\omega_{P1}t-k_{P1}z)} \tag{5.14}$$

$$\frac{\delta^2 E_{P1}}{\delta t^2} = -\frac{1}{2}\omega_{P1}^2 E_{P1}(z)k_{P1}e^{j(\omega_{P1}t-k_{P1}z)}. \tag{5.15}$$

The insertion of the first pump wave $E_{P1}(z,t)$ and its derivative (5.12) to (5.15) into the left part of (5.10) yields

$$\left[-\frac{\delta E_{P1}(z)}{\delta z}jk_{P1} - \frac{\alpha}{2}jk_{P1}E_{P1}(z)\right]e^{j(\omega_{P1}t-k_{P1}z)} \tag{5.16}$$

with $k_{P1}^2 = (n_0^2 \cdot \omega_{P1}^2)/c^2$.

On the other hand, the derivation with respect to *z* of the first sideband $E_{S1}(z,t)$ can be written as

$$\frac{\delta E_{S1}}{\delta z} = \frac{1}{2}\left[\frac{\delta E_{S1}(z)}{\delta z}e^{j(\omega_{S1}t-k_{S1}z)} + E_{S1}(z)jk_{S1}e^{j(\omega_{S1}t-k_{S1}z)}\right] \tag{5.17}$$

$$\frac{\delta^2 E_{S1}}{\delta z^2} = \left[\frac{\delta E_{S1}(z)}{\delta z}jk_{S1} - \frac{k_{S1}^2}{2}E_{S1}(z)\right]\cdot e^{j(\omega_{S1}t-k_{S1}z)}. \tag{5.18}$$

Note, that in (5.18) the SVEA has also been applied. Whereas the derivatives with respect to *t* is

$$\frac{\delta E_{S1}}{\delta t} = \frac{j\omega_{S1}}{2}E_{S1}(z)e^{j(\omega_{S1}t-k_{S1}z)} \tag{5.19}$$

$$\frac{\delta^2 E_{S1}}{\delta t^2} = -\frac{\omega_{S1}^2}{2}E_{S1}(z)e^{j(\omega_{S1}t-k_{S1}z)}. \tag{5.20}$$

If Equations ((5.18)to (5.20)) are introduced into the left part of (5.10), it follows

$$\frac{\delta^2 E}{\delta z^2} - \frac{n^2}{c^2}\frac{\delta^2 E}{\delta t^2} - \frac{\alpha \cdot n}{c}\frac{\delta E}{\delta t} = \left[\frac{\delta E_{S1}(z)}{\delta z}jk_{S1} - \frac{\alpha}{2}jk_{S1}E_{S1}(z)\right]e^{j(\omega_{S1}t-k_{S1}z)} \tag{5.21}$$

with $k_{S1} = (n_0 \cdot \omega_{S1})/c$.

(5.17)

Right Part

The first term of the right side of (5.10) can be written as

$$\rho = \rho(z,t) \text{ and } E = E(z,t). \tag{5.9}$$

Since the threshold of stimulated Raman scattering is much higher than that for Brillouin scattering, Raman scattering is not considered here. Equation (5.2) expresses the field in the fibre whereas the density variation (acoustic phonons) is described by (5.6). By inserting (5.8) in (5.7) it follows for the electric field in the fibre that

$$\frac{\delta^2 E}{\delta z^2} - \frac{n^2}{c^2}\frac{\delta^2 E}{\delta t^2} - \frac{\alpha \cdot n}{c}\frac{\delta E}{\delta t} = \frac{1}{c^2}\frac{\delta^2}{\delta t^2}\left(\frac{\gamma_e}{\rho_0}\rho E + \chi^{(3)} EEE\right). \tag{5.10}$$

with α_a as the attenuation of the acoustic wave. The acoustic phonons follow the wave equation [174]

$$\frac{\delta^2 \rho}{\delta z^2} - \frac{\alpha_a}{\upsilon_a}\frac{\delta \rho}{\delta t} - \frac{1}{\upsilon_a^2}\frac{\delta^2 \rho}{\delta t^2} = \frac{\varepsilon_0 \gamma_e}{2\upsilon_a^2}\frac{\delta^2}{\delta z^2}(E)^2. \tag{5.11}$$

5.2.1 The Nonlinear Wave Equation

Left Part

For the derivation of the left hand side of the nonlinear wave equation (5.10), the first pump wave (E_{P1}) and the first sideband (E_{S1}) were chosen as an example. Several pre-calculations have to be done before the waves can be inserted into (5.10):

The derivations of the first pump wave $E_{P1}(z,t)$ with respect to z can be written as

$$\frac{\delta E_{P1}}{\delta z} = \frac{1}{2}\left[\frac{\delta E_{P1}(z)}{\delta z} e^{j(\omega_{P1} t - k_{P1} z)} - E_{P1}(z) j k_{P1} e^{j(\omega_{P1} t - k_{P1} z)}\right] \tag{5.12}$$

$$\frac{\delta^2 E_{P1}}{\delta z^2} = \frac{1}{2}\left[-2\frac{\delta E_{P1}(z)}{\delta z} j k_{P1} - k_{P1}^2 E_{P1}(z)\right] \cdot e^{j(\omega_{P1} t - k_{P1} z)}. \tag{5.13}$$

Note that in (5.13) the slowly varying envelope approximation[3] (SVEA) was applied.

[3] SVEA: The change of an amplitude A of a pulse (envelope) during its propagation in x-direction is low in comparison to the corresponding wave magnitude. That means that the pulse duration is much higher than the periodic time of a wave. Due to this, the absolute value of the second derivative is much lower than the absolute value of the first one. Hence the second derivative is negligible. It follows that $\left|\frac{d^2 A}{dx^2}\right| \ll \left|k\frac{dA}{dx}\right|$ [175].

with k_a as the wave vector of the acoustic wave. It can also be written as

$$k_a = \frac{2\pi}{\lambda_a} = \frac{2\pi f_a}{\upsilon_a} \tag{5.4}$$

and

$$k_{Pi,Si} = \frac{2\pi n}{\lambda_{Pi,Si}} = \frac{2\pi n f_{Pi,Si}}{c}\,. \tag{5.5}$$

where $i = 1,2$, and f_a and λ_a correspond to the frequency and the wavelength of the acoustic wave, respectively. $f_{Pi,Si}$ and $\lambda_{Pi,Si}$ are the frequencies and the wavelengths of the pump waves and the sidebands.

The acoustic phonons, the refractive index modulation, propagates in the same direction as the pump wave and follows the function

$$\rho(z,t) = \frac{1}{2}\left[Q(z)\cdot e^{j(\omega_a t - k_a z)} + c.c.\right]. \tag{5.6}$$

The wave equations that describe the interaction in the fibre are found by the deviation of Maxwells Equations[169]:

$$\frac{\delta^2 E}{\delta z^2} - \frac{n^2}{c^2}\frac{\delta^2 E}{\delta t^2} - \frac{\alpha\cdot n}{c}\frac{\delta E}{\delta t} = \frac{1}{\varepsilon_0 c^2}\frac{\delta^2 P_{NL}}{\delta t^2}\,, \tag{5.7}$$

where P_{NL} describes the nonlinear polarisation in the medium, ε_0 the permittivity in vacuum and α the attenuation in the fibre. The material of the optical fibre (silica) features an inversion symmetry[2] [173]. Therefore, the nonlinear polarisation consists on the one hand of Electrostriction (SBS) and on the other hand of the non-linear third order Susceptibility $\chi^{(3)}$. Assuming that both are independent of each other the nonlinear polarisation can be described as[169]

$$P_{NL} = P_{NL\,SBS} + P_{NL\chi^{(3)}} = \frac{\varepsilon_0 \gamma_e}{\rho_0}\rho E + \varepsilon_0 \chi^{(3)} EEE\,, \tag{5.8}$$

with γ_e as the electrostrictive coefficient, ρ_0 is the deviation of the material density from its equilibrium value and

[2] The properties of the material are unchanged under consideration of point reflection.

amplified sidebands to the non-amplified sidebands at the input of the PD. It is approximately 15 dB[1] depending on the OP of the MZM.

- A further simplification is made by neglecting the spontaneous emission noise (SEN). In [152] it was reported, that if a Brillouin amplifier is driven by high signal levels and the amplification is in the saturation regime the SEN can be significantly reduced. A small detuning of the probe signal and the gain spectrum leads to a further enhancement of the SEN performance.
- The pump waves are in the same wavelength range. Their frequency separation is defined by the frequencies of the sidebands and is in the region of several tens of GHz. This leads to the simplification that the Brillouin frequency shifts are almost the same. Hence, it can be written that:

$$\omega_a = \omega_{P1} - \omega_{S1} = \omega_{P2} - \omega_{S2}\,. \tag{5.1}$$

- For the last simplification it is assumed that amplitudes and phases are not time dependent

5.2 Derivation of the Differential Equation System

The whole electric field in the optical fibre can be written as

$$E(z,t) = \frac{1}{2}\left[\sum_{i=1,2} E_{Pi}(z)\cdot e^{j(\omega_{Pi}t - k_{Pi}z)} + c.c. + E_{Si}(z)\cdot e^{j(\omega_{Si}t + k_{Si}z)} + c.c.\right]. \tag{5.2}$$

The electric fields of the first and the second pump wave are determined by E_{Pi}, $i = 1,2$ with its frequencies ω_{Pi} and its wave vectors k_{Pi}. The fields of the amplified sidebands are represented by E_{Si}, $i = 1,2$ with ω_{Si} and k_{Si} as the corresponding frequencies and wave vectors, respectively. The conservation of energy that is required for the scattering process is proven by (5.1). On the other hand, the conservation of momentum can be described by

$$k_a = k_{P1} - k_{S1} = k_{P2} - k_{S2} \tag{5.3}$$

[1] This value depends also on the order of the amplified sidebands. 15 dB corresponds to the ratio of the amplified 7th order sidebands to the unamplified 1st order sidebands as the worst case scenario.

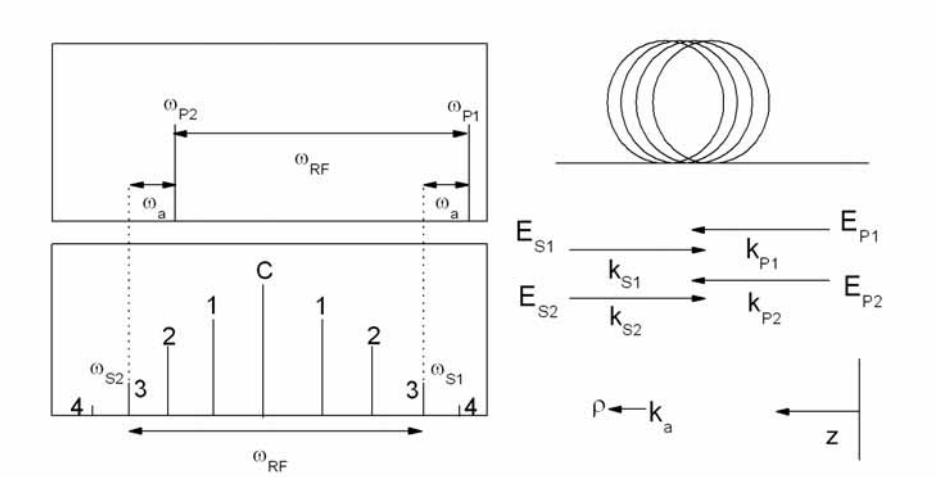

Fig. 5-1 Pump, gain and sideband arrangement in the fibre as frequencies and vectors [169].

In order for heterodyning in the PD at the fibre output, the phase correlated status has to be maintained during the amplification process and the propagation in the fibre. In case of a decorrelation the heterodyned signal will be degraded by an enhanced phase noise. The pump waves themselves can influence their own phases by self-and or the other phases by cross-phase modulation. This chapter describes the amplification processes with respect to the phase influences of the two sidebands, theoretically.

For the derivation several simplifications have been made:

- On the one hand it was shown in [151], that for orthogonally polarised pump and probe-waves the Brillouin gain is half of that which can be achieved with co-polarisation. On the other hand, the Brillouin gain reaches nearly one third of the gain that is expected for a scrambled polarisation [172] if a Brillouin gain medium of a length of several kilometres and an azimuth polarisation variation of pump and the Stokes wave is assumed. In the experiment a polarisation dependency of 2.35 dB (averaged) for parallel and orthogonal polarised pump waves has been observed. Since the amplification process was optimised by the application of polarisation controllers in the set-up, the polarisation is assumed to be negligible. Hence, the sidebands are assumed to be linearly polarised and parallel to each other.
- Due to the fact that all non-amplified sidebands are attenuated owing to the natural loss of the fibre, their influence on the heterodyning in the PD are assumed to be negligible. Measurements have shown a power difference from the

5 Backround Theory on Stimulated Brillouin Scattering

In this chapter, the theoretical background for the mm-Wave generation is proposed. The theory for the SBS amplification of two frequency components was derived by Schneider [169]. In contrast to the DES ((4.5) and (4.6)) the DES here describes not one, but two optical signals that are amplified by two independent Brillouin gains. Furthermore, it depicts the interaction between them which results in Self Phase Modulation (SPM), Cross Phase Modulation (XPM) and FWM.

This chapter is the basis for the simulation in chapter 6. Thus several scenarios are calculated for a description and an optimisation of the presented mm-Wave generation technique.

5.1 Basics

Initially, it is necessary to explain the principle operation mode for the understanding of the theoretical description. Further detailed descriptions are given in Chapter 7, Appendix E5 or can be found in [170] and [171].

The light of a fibre laser is modulated in such a manner that sidebands are generated with a separation corresponding to the modulation frequency. This frequency comb is launched into a 50.45 km long optical fibre. From the opposite direction two pump waves are injected in order to amplify two components of the frequency comb by Brillouin scattering. In Fig. 5-1 (left insets) the arrangement of frequencies for the amplification of the 3rd sidebands is shown schematically. The enhanced sidebands are coupled out via a circulator and heterodyned in a PD. The vector and frequency arrangement of pump waves and sidebands is demonstrated in Fig. 5-1 (right insets). It can be seen that the pump ($E_{P1,2}$) and signal waves ($E_{S1,2}$) propagate in opposite directions. Furthermore, the density in the fibre, i.e. the acoustic wave (ρ) moves in the same direction as the pump waves. Since the two frequency components (upper/lower sideband of the same order) have the same origin they are totally phase correlated at the input of the SSMF.

method. For this optical fibre, the Brillouin threshold and the gain bandwidth was found to be 6.35 mW and 28 MHz, respectively, from calculations and measurements. The spontaneous emission noise of a Brillouin amplifier can be significantly reduced if the saturation effect, the amplifier length, the detuning and the input signal power is considered. Preliminary simulations have shown that a Brillouin gain of 37 dB[1] can be expected. Using increased signal powers, a saturation effect has been observed in the simulations. In the following chapter a mathematical description for the amplification of two frequency components by two independent Brillouin amplifiers is proposed.

[1] For a signal power of 0.7 μW and a pump power of 6 mW.

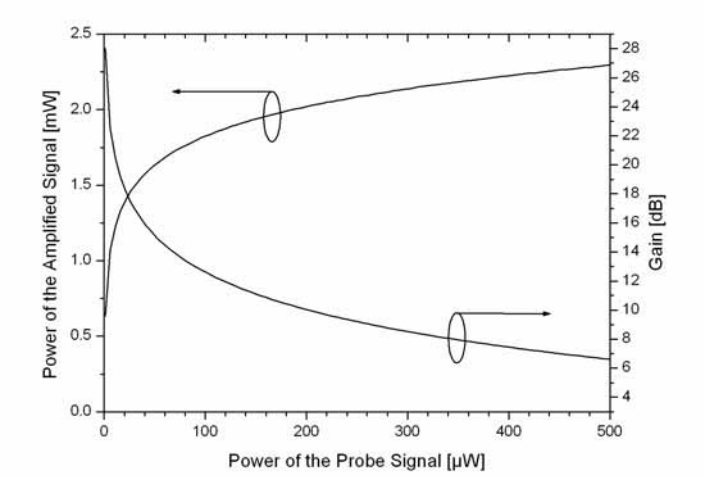

Fig. 4-7 Saturation effects in dependency of the probe signal.

Besides the power of the probe signal the Stokes power depends on the pump power also. If the pump power decreases the gain and, hence, the backward scattered power also decreases. Contrary to the scenario in Fig. 4-6 the influence of the fibre length to the maximum Stokes power remains low. Simulations at different pump powers are shown in Fig. 4-8. An input power of the probe signal of 52.9 µW is assumed for the calculations. With an input power of 52.9 µW and a pump power of 3 mW, for instance, the amplified signal (Stokes wave) reaches a power of 1.67 mW after propagation in 27.5 km optical fibre.

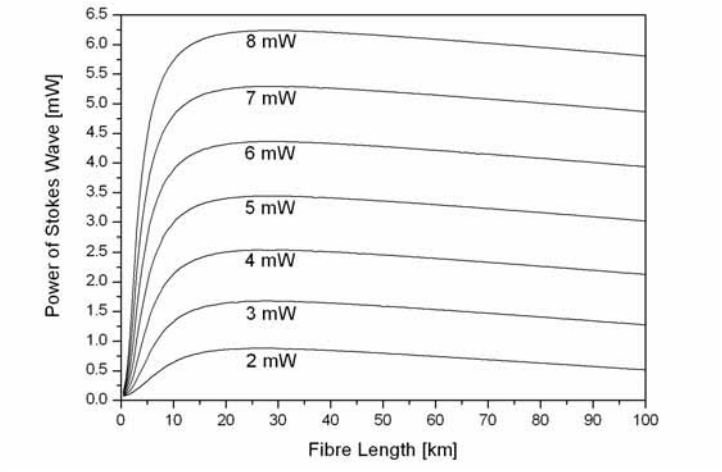

Fig. 4-8 Simulated power of different amplified probe signals depending on the fibre length at altered pump powers.

Concluding this chapter, it can be said that stimulated Brillouin scattering can be used as an effective and narrowband optical amplifier. Due to the fact that the bandwidth can be adapted to the given application and the high gain and low pump powers required, the non-linear effect is used for the proposed mm-Wave generation

power of 0.7 µW and a pump power of 6 mW the amplified signal (Stokes wave) reaches a power of 3.52 mW after propagation in 45 km optical fibre.

In case the fibre input power rises to a value of 585 µW, the backward scattered wave has an output power of 5.31 mW after propagation in a 10.5 km optical fibre. On the other hand, the figure shows an increase of the backward scattered wave up to a maximum. For low signal powers the "Stokes maximum" and, hence, the optimum fibre length is higher than for high input powers as can be seen in Fig. 4-6. According to this, the optimum fibre length depends on the power of the injected signal. An overview of the most important values is given in Table 4-1. The gain is calculated by the relationship of the power of the probe signal and the backward scattered power. It can be seen that the absolute gain rises if the power of the probe signal decreases which indicates a saturation effect. This result was also observed in [106], [167] and [168].

Table 4-1 Overview of important values of Fig. 4-6.

Power of probe signal [µW]	**Fibre length [km] where gain is maximal**	**Maximum backward scattered power [mW]**	**Gain [dB]**
740.4	9	5.506	8.7
624.4	10	5.359	9.3
585	10.5	5.312	9.6
244.3	16.5	4.823	13
52.9	28.5	4.359	19.2
7.2	40	3,95	27.4
0.7	45	3.52	37

The dependency of the Stokes power on the probe signal is demonstrated in Fig. 4-7. The saturation effect at the output of the 50.45 km optical fibre, can be seen, as the signal power increases. This is due to the fact that at high input powers the maximum of the Stokes power occurs at lower fibre lengths. Hence, the attenuation affects the amplification process. The gain characteristic in Fig. 4-7 reflects the ratio of output and input power of the fibre. A closer look at (4.5) and (4.6) leads to a further characteristic that has to be investigated.

based on the overlapping of stokes and antistokes spectra of different pumps can increase the deceleration of optical pulses [162] - [165].

The following chapter underlines the discussion about the gain bandwidth for the application of SBS as an amplifier.

4.6 Amplification Processes

The numerical solution of the differential equation system (4.5) and (4.6) demonstrates the amplification process dependency on different parameters. In the following a gain process of a probe signal $I_S(L)$ that is injected from one side of the fibre by a pump signal $I_P(L)$ is simulated. It gives clearness about the properties of the chosen equipment and the circumstances that have to be considered when working with SBS as an amplifier. Simulation results in respect to the generation of mm-Waves are given in [166]. The amplified signal is also called "Stokes wave" in this chapter.

For the simulation a Brillouin gain of $2.25 \cdot 10^{-11}$ m/W, an attenuation of 0.048 km^{-1}, an effective core area of $86 \cdot 10^{-12}$ m^2 and a pump power of 6 mW where assumed. In order to simulate the amplification of several signals, power levels of 0.7, 7.2, 52.9, 244.3, 585, 624.4 and 740.7 µW where chosen. The values correspond to measured magnitudes of the generated sidebands described in section 7.1 in Table 7-1. These powers are used as input powers $I_S(L)$.

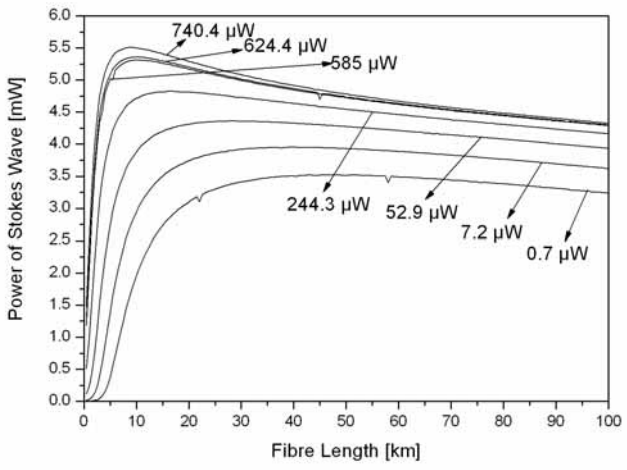

Fig. 4-6 Simulated power of different amplified probe signals depending on the fibre length at altered probe signal powers.

The output powers of the fibre that correspond to $I_S(0)$ are shown in Fig. 4-6. The trace indicated by "0.7 µW", for instance can be read as follows: With an input

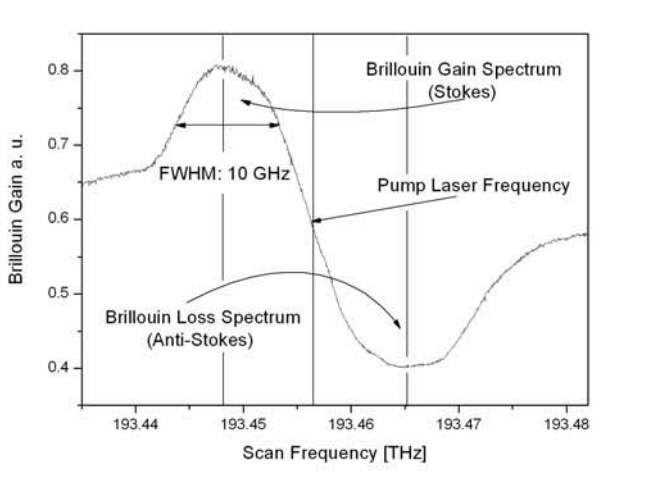

Fig. 4-5 10 GHz Brillouin gain bandwidth and its Anti-Stokes spectrum.

bandwidth broadening exceeding the Brillouin shift. By a direct modulation of a DFB LD by a 1.1 GHz noise with a power of 30 dBm we broadened the Brillouin gain spectrum up to 10 GHz as illustrated in Fig. 4-5. Any enlargement of the pump spectrum would not lead to any bandwidth broadening due to the loss spectrum of the Anti-Stokes spectrum that would get broadened as well.The spectrum was taken by using the measurement set-up of [159]. The output spectrum of a standard DFB LD is precisely altered in frequency by temperature.

To circumvent this limitation of bandwidth broadening, recently, we published the basis for an enlargement of the Brillouin gain bandwidth without any obvious theoretical restrictions [160]. The idea behind it is the following:

The Brillouin Anti-Stokes spectrum generated by one pump LD is compensated by a further Brillouin gain generated by another pump laser diode. The pump wavelength is adjusted in such a manner, that the gain spectrum is located directly at the Anti Stokes spectrum of the first pump LD. Of course, the pump power for a gain bandwidth of 10 GHz lies in the range of 500 mW in a SSMF. Hence, the compensating gain spectrum has to be even higher. Experimental investigation results show an additional gain of ≈13 dB. On the other hand, a bandwidth independent Brillouin amplifier offers new visions for slow light applications [160].

The same idea of overlapping the Brillouin gain of one and the loss spectrum of a further pump laser but in two independent fibres (6 km highly NA fibre and 2 km DSF) was realised later in [161]. Thus, a bandwidth of 25 GHz was achieved.

On the other hand, for slow light applications the Brillouin gain spectrum can be adapted as well to the given requirements. Thus, a tunable Brillouin spectrum that is

can be achieved with the pump laser. Generally it can be said that direct laser modulation has much lower limitations than external modulation due to the inertia of the laser diode controller itself. Recently, a Brillouin gain bandwidth of 12 GHz was generated by Zhu et al. [157] as an extension of [155].

However, there are many ways for the Brillouin bandwidth enhancement. We investigated a new method where the Brillouin gain remains high over the whole bandwidth; hence, additional amplifiers are not required. In the proof of concept set-up the Brillouin bandwidth was enhanced from 28 to 144 MHz with two pump sources. The number of pump sources and, therefore, the maximum amplification bandwidth is not restricted. So, with this method, the Brillouin bandwidth can be adapted to any given application. The method is based on the overlapping of six independent Brillouin gains that are generated by two 28 MHz phase modulated pump sources. The experimental set-up and experimental results are described in detail in [145] and [158]. The application of this technique generates an enhanced flatness of the Brillouin gain spectrum. Hence, a further independency of the phase to the Brillouin amplification process can be expected if the frequency detuning of the gain and the sideband can be minimised.

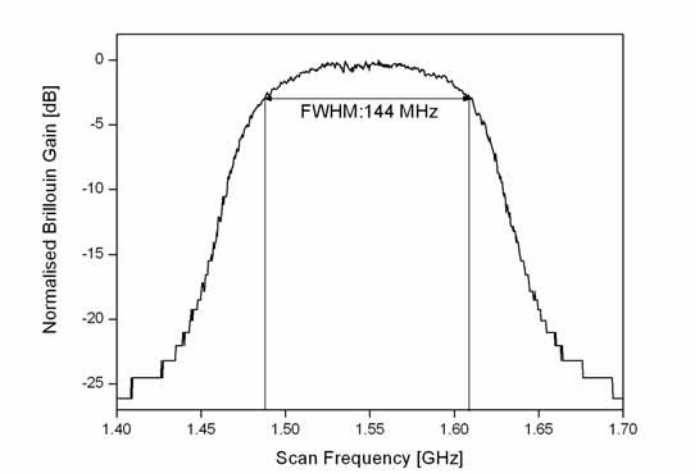

Fig. 4-4 Flat Brillouin gain characteristic.

In the past the maximum achievable bandwidth was restricted by the Anti Stokes spectrum which is up shifted in frequency unlike the Stokes wave. It is generated as a result of FWM effects between the copropagating pump and Stokes wave [138]. Since it generates not a gain but a loss spectrum it has destructive impacts to a

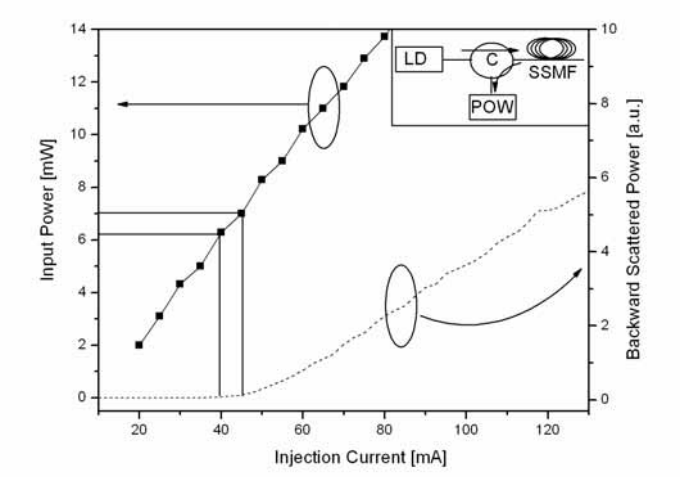

Fig. 4-3 Brillouin threshold in a 50.45 km SSMF; The inset shows the experimental set-up (LD: Laser Diode, C: Circulator, POW: Power Meter).

4.5 Gain Bandwidth Broadening

Due to the fact, that the Brillouin gain bandwidth plays a mayor role in the investigation of SBS for Radio Over Fibre systems its realisation is described in the following section.

The large spontaneous emission noise (SEN) and the very small natural Brillouin bandwidth of approximately 30 MHz limit the applicability of SBS in conventional optical communication systems and slow light systems. The SEN in a Brillouin amplifier can be 500 times larger than in Raman amplifiers [152] and the noise figure can be 20 dB higher than that of an ideal amplifier. However, in [153] it was reported that driving the amplifier in the saturation regime, using short amplifier lengths, a low signal detuning and relatively high input signal powers could significantly reduce the SEN. The other limiting factor – the bandwidth – depends on environmental influences and on the line width of the pump laser. The general principle relies on the spectral broadening of the pump which leads also to an enhancement of the Brillouin gain.

A bandwidth enhancement of 150 MHz was shown in [154] where a pump laser was directly modulated in frequency. Recently, Herráez et al. reported a bandwidth enhancement of 325 MHz by a 38 MBit/s pseudo random binary sequence pump laser modulation [155] and in [156] a 1.9 GHz large bandwidth has been achieved by a noise modulation of the pump source. Although these methods are simple, the maximum reachable bandwidth is limited by the amount of frequency derivation that

with λ_p as the wavelength of the pump signal. Considering an elasto-optical figure of merit M_2 of $1.51 \cdot 10^{-15}$ s^3/kg [142], a spectral line width Δf_a of 28 MHz, a refractive index n of 1.44 and a Brillouin shift f_a of 10.727 GHz a maximum Brillouin gain of $2.25 \cdot 10^{-11}$ m/W according (4.11) can be calculated.

4.4 Threshold

Owing to the fact that SBS occurs at very low intensities its threshold is a limiting factor for the maximum power that can be injected in conventional fibre transmission links [147]. Because of this, it is a very important property that has to be considered. In this purpose SBS is used as an amplifier. Since the Brillouin threshold is the boundary between stimulated and non-stimulated scattering, it plays a major role in the experimental set-up. If a Brillouin amplifier is driven under the threshold, the Stokes wave is stimulated by a probe signal and not by the noise in the fibre.

Although there are several definitions of the SBS threshold [140], [148], [149] at this point only one is explained in detail. The SBS threshold can be seen as the necessary input power at which the power of the Stokes wave increases dramatically or on the other hand, the output power of the pump decreases significantly [150]. Considering a localised source and a negligible decay of the pump power due to SBS a mathematical description can be given as [142]

$$P_0^S = 21 \cdot \frac{K_B \cdot A_{eff}}{g_{B\max} \cdot L_{eff}}. \tag{4.14}$$

where K_B is a polarisation dependent factor. In standard non-polarisation-maintaning fibres K_B corresponds to a factor of 1.5 [151]. With an effective core area[3] of 86 μm^2, a Brillouin gain of $2.25 \cdot 10^{-11}$ m/W and an effective fibre length of a SSMF of 18.95 km (L= 50.45 km) a Brillouin threshold of 6.35 mW is obtained. An experimental verification is shown in Fig. 4-3. The figure shows the optical input and output of an optical circulator. The pump wave is launched into the SSMF and the backward scattered Stokes power is measured at the power meter. As can be seen, the Brillouin threshold range lies between 6.2 mW and 7.1 mW.

[3] As per manufacturer information

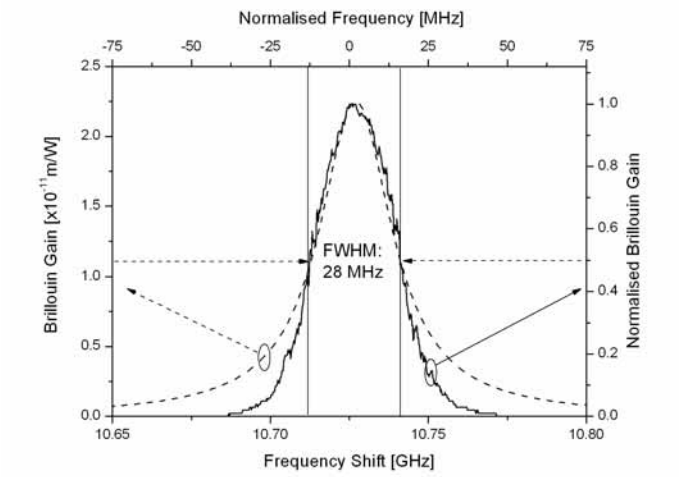

Fig. 4-2 Dashed line - Lorentzian shaped Brillouin gain distribution versus Brillouin shift f_a; Solid line - measured Gaussian shaped gain spectrum.

The natural spectral width of the Brillouin bandwidth Δf_a is very narrow and lies in the range of tens of MHz [145]. Thus, a bandwidth of 28 MHz in a 50.45 km long SSMF was measured (see Fig. 4-2). Since the SBS gain bandwidth strongly depends on the pump power and the status of saturation, its recording is not standardised. Thus, we observed a bandwidth enlargement in the range of several MHz if the pump power exceeds the threshold as it is applied to the heterodyne measurement method. In case the gain bandwidth is recorded by a scanning method [144], [146] and the pump power is in or under the threshold the resulting bandwidth depends also on the probe signal power.

The maximum amplification factor g_{Bmax} depends on several wave guide parameters such as the refractive index n or the elasto-optical figure of merit M_2 and the line width of the pump source for instance. It is described by [141]

$$g_{B\max} = \frac{\pi \cdot f_a^2 \cdot M_2}{c \cdot \Delta f_a \cdot 2 \cdot n}. \tag{4.11}$$

with p as the elasto-optic constant, ρ_{Mat} as the material density and υ_a as the velocity of the acoustic wave in the medium M_2 follows as [142]

$$M_2 = \frac{n^6 \cdot p^2}{\rho_{Mat} \cdot \upsilon_a^3}. \tag{4.12}$$

By applying (4.4) and (4.12) to (4.11) the maximum Brillouin gain can be written as

$$g_{B\max} = \frac{4 \cdot \pi \cdot n^8 \cdot p^2}{c \cdot \lambda_p^3 \cdot \Delta f_a \cdot \rho_{Mat} \cdot f_a} \tag{4.13}$$

$$\alpha_{[km^{-1}]} \approx \frac{\alpha_{[dB]}}{4.343}. \tag{4.9}$$

The effective core area, A_{eff}, and the Brillouin gain, g_B, are given by the properties of the fibre. The second term of the exponential function of equation (4.7) leads to an attenuation α along the fibre length L. As long as the amplification is higher than the loss the intensity of the Stokes wave rises. If longer fibres are used for amplification processes L_{eff} rises as well and also the amplification increases to a maximum. In case the fibre length overcomes this maximum those values keep constant but the attenuation rises further and decreases the effectiveness of SBS.

For pump powers above the Brillouin threshold Equation (4.7) becomes invalid due to the fact that the power transfer from the pump wave to the Stokes wave can not be neglected anymore.

4.3 Gain Characteristics

As described in (4.5) and (4.6) respectively the intensity of the Stokes wave and the amplification depends mainly on the Brillouin gain g_B which can also be seen as an amplification factor. The Brillouin gain characteristic itself depends on the Brillouin shift f_a, the line width of the Stokes wave Δf_a and the maximum of the amplification factor g_{Bmax}. For pump sources with a narrow emission spectrum the Brillouin gain follows a Lorentzian distribution and can be written as [140]

$$g_B(f) = \frac{1}{1+\left[\left(f-f_a\right)/\left(\frac{\Delta f_a}{2}\right)\right]^2} \cdot g_{B\max}. \tag{4.10}$$

For pump sources emitting non-quasi monochromatic waves the characteristic follows a Gaussian shape. The Brillouin gain characteristic of (4.10) is shown in Fig. 4-2 with a maximum gain g_{Bmax} of $2.25 \cdot 10^{-11}$ m/W, a Brillouin shift of 10.727 GHz and a full width at half maximum (FWHM) bandwidth of 28 MHz. The characteristics of Fig. 4-2 show clearly the difference between the theoretical Lorentzian shaped spectrum of quasi monochromatic pump waves and a practical measurement of a Gaussian shaped Brillouin gain generated by a 3 MHz broad pump source. For Brillouin gain measurement description details see [144].

4.2 Intensity Equations

The dependency of the pump wave intensity I_p and the Stokes wave intensity I_s via the distance z is governed by the following two coupled equations [141]

$$\frac{\partial I_s}{\partial z} = -g_B I_p I_s + \alpha \cdot I_s \tag{4.5}$$

$$\frac{\partial I_p}{\partial z} = -g_B I_p I_s - \alpha \cdot I_s . \tag{4.6}$$

Where g_B is the Brillouin gain which is assumed to be equal in both equations. Due to the relatively small frequency shift, $\omega_p \approx \omega_s$ the attenuation of the pump and Stokes wave is assumed to be the same $\alpha_s \approx \alpha_p \equiv \alpha$ [138].

According to (4.5) the counter propagating wave grows exponentially in intensity I_s with negative z as long as the product of I_p and I_s is bigger than the loss α in the fibre. On the other hand, the intensity of the pump wave I_p decreases due to the attenuation and the power transfer to the Stokes wave (4.6). Assuming low pump powers below the Brillouin threshold, the first term in (4.6) can be neglected. Hence, the pump intensity depends only on the attenuation in the fibre. Note that equations (4.5) and (4.6) are only valid for approximately monochromatic waves and relatively long pulses. Furthermore, polarisation effects that occur during the propagation in the fibre have not been considered in the differential equation system (DES). Considering these restrictions a solution for the Stokes wave intensity I_s at the fibre input $I_s(0)$ is represented by [142]

$$I_s(0) = I_s(L) \cdot e^{\frac{g_B P_0 L_{eff}}{A_{eff}} - \alpha L} . \tag{4.7}$$

For this solution a Stokes wave at the end of the fibre $I_s(L)$ is necessary as can be seen in (4.7). This can be a Brillouin shifted signal that should be amplified. The first term in the exponential function of (4.7) describes the amplification adjustable by the pump power P_0. The effective length is given by [143]

$$L_{eff} = \frac{1 - e^{-\alpha_{[km^{-1}]} \cdot L}}{\alpha_{[km^{-1}]}} \tag{4.8}$$

with

$$|\kappa_a| = 2 \cdot |\kappa_p| \cdot \sin\left(\frac{\theta}{2}\right). \tag{4.3}$$

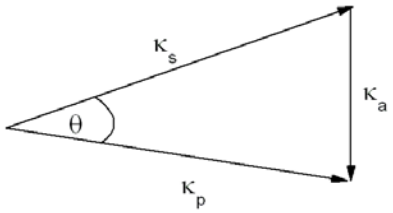

Fig. 4-1 Vector diagram analysis for the Brillouin scattering effect.

Since light can only propagate via two directions in an optical fibre, there are two possible angles for θ, namely 0° and 180°. For $\theta = 0°$ the absolute value of the acoustical wave vector is equal to zero (forward direction) whereas the value becomes maximum in case of $\theta = 180°$ (backward direction). Due to this, the Stokes wave can propagate only in the opposite direction of the pump wave [138].

The acoustic wave vector is determined by $|\kappa_a| = \omega_a / \upsilon_a$ with ω_a as the angular frequency of the acoustic wave and υ_a as the speed of sound in the material. On the other hand, the pump wave vector can be described by $|\kappa_p| = 2\,\pi\, n / \lambda_p$ with n as the refractive index in the medium and λ_p as the wavelength of the pump wave. According to (4.3) the mathematical description of the frequency of the acoustic wave f_a which is also called the Brillouin shift is described by

$$f_a = f_{S\max} = \frac{2n \cdot \upsilon_a}{\lambda_p} \tag{4.4}$$

where n is the refractive index of the medium, υ_a is the speed of sound in the material and λ_p the wavelength of the pump wave. The term *sin (θ)* can be neglected due to the fact that the pump and the Stokes wave have opposite directions (*sin (θ)=0)* . In addition to the parameters described in (4.4) the Brillouin shift depends also on the type of optical fibre, the doping, the ambient temperature (approximately 1 MHz/°C at 1300 nm [139]) and mechanical stress. According to (4.4) the Doppler shift in single mode fibres lies in the range of 10-15 GHz if optical communication relevant wavelengths are considered. Assuming a velocity of sound of $\upsilon_a = 5.96$ km/s [140] and a refractive index of silica fibre of 1.44 at a wavelength of 1.55 µm a Brillouin shift of 11.07 GHz can be calculated according to (4.4). All calculation and measurement results in this chapter are summarised in Appendix A.

which the incoming pump wave scatters. The interference of the backward scattered wave and the pump wave amplifies the acoustic wave due to Electrostriction[1] and raises the refractive index modulation. As a result of the Bragg[2] condition the generated grating structure leads to a further scattering of the injected pump wave and to an amplification of the backward scattered wave (Stokes wave) [135]. The Brillouin effect can be called "stimulated" if the density modulation is self induced. Since the grating structure (acoustic wave) propagates with the speed of sound, the backward scattered light is shifted in frequency towards the pump wave due to the Doppler Effect. The Stokes wave has a power maximum for a frequency shift of f_{Smax} (see Equation (4.4)).

Thus, SBS can be seen as a three wave interaction of the pump wave (wave vector: κ_p, frequency f_p), the acoustic wave (wave vector: κ_a, frequency f_a) and the backward scattered Stokes wave (wave vector: κ_s, frequency f_s) [136]. If the density modulation propagates in the opposite direction the relationship between the wave vectors and frequencies is

$$\boldsymbol{\kappa}_s = \boldsymbol{\kappa}_p - \boldsymbol{\kappa}_a \tag{4.1}$$

$$f_s = f_p - f_a\,. \tag{4.2}$$

Equation (4.2) describes the frequency down shifting of the Stokes wave to the pump wave.

In Fig. 4-1 the vector diagram that corresponds to (4.1) is illustrated with θ as the angle between the pump and Stokes field. If it is assumed that the wave vectors κ_p and κ_s have approximately the same absolute values ($|\kappa_p| = |\kappa_s|$) it can be written for the acoustic wave vector

[1] Electrostriction describes the dependency of the density of a medium of an applied electric field. It is converse to the piezoelectric effect [134].

[2] The Bragg condition is fulfilled if the cumulative reflection of waves from each plane in a grating structure occurs [137]. Owing to this, the phases of each wave are equal and the superposition is constructive. It depends on the angle of incidence, the retardation of the material and the wavelength of the incoming signal.

4 Stimulated Brillouin Scattering

Stimulated Brillouin scattering (SBS) is named after the French physicist Leon Brillouin who investigated the interaction of light with acoustic waves. Since non-linear effects occur only at high intensities they became relevant with the enhancement of laser and optical fibre technologies.

SBS is a non-linear effect that occurs at low pump powers. Only a few milliwatts are required to initialise Brillouin interaction in an optical fibre. SBS is generally harmful in optical communication systems since the maximum transferable signal power is limited by the SBS. This argument is also valid for ROF systems [111]. On the other hand, SBS is useful for fibre based amplifiers or high resolution spectroscopy for instance [112] - [115]. Furthermore, the effect can be used for demodulator operations in WDM systems, [116], [117] and tuneable filters for channel selection in densely packed WDM systems [118]. The properties of SBS in Brillouin lasers and amplifiers are demonstrated in [119] - [121] and the application in self-homodyned coherent optical transmission systems in [122]. An RF-photonic phase shifter based on SBS is demonstrated in [123] and an incoherent microwave photonic filter in [124]. The latest application of SBS is the slowing down [125] - [130] of optical pulses and the acceleration [131] of optical pulse maxima by changing the group refractive index and thus the group velocity of pulses. A short preview of the application of the nonlinear effect for the generation of mm-Waves is presented in [132].

All calculations in this chapter have been made with the simulation software Matlab version 6.5. They are based on the simulations by Danny Hannover. Further information about the simulating tool and scripted programs for the simulation can be found in [133]

4.1 Basics

SBS occurs due to an interaction of the incident light wave with the material. This is because high intensity thermo-elastic fluctuations of the molecules (acoustic phonons) which exist in the fibre arise and can also be seen as an acoustic wave. These periodical grating fluctuations cause a density modulation of the material at

derivations of the demonstrated techniques that can not be classified. A short excerpt will be given in the following subsection.

3.2.2.5 Unconventional Millimetre Wave Generation Techniques

Because the variety of methods is so large, only some examples for some unconventional techniques are given here. In [104] a specially designed external cavity laser diode which emits two polarisation modes is presented. The frequency separation (58 GHz) corresponds to the desired mm-Wave signal. Due to the orthogonal polarisation the carrier can simply be modulated by using a polarisation dependent external modulator. Hence, a dispersion-independent propagation can be achieved.

A very compact and flexible mm-Wave generator is presented in [105]. The source is based on SSB modulation, generates frequencies of up to 40 GHz and is very suitable as a transmitter in ROF systems owing to its consolidated set-up.

By using fibre non-linearities such as Stimulated Brillouin Scattering (SBS) [106] or Four Wave Mixing (FWM) [107] optoelectronic oscillators of up to 100 GHz and 60 GHz respectively, were presented.

In [108] an application of fibre Bragg gratings (FBG) into a Brillouin fibre laser leads to a generation of a microwave signal of 10.88 GHz.

Another use of a special designed dual, co-located phase-shifted grating that is inserted into a fibre laser configuration is verified in [109]. By this method a 32.5 GHz mm-Wave signal was generated.

Recently, a photonic frequency multiplying using FWM was applied for sixfold multiplication. FWM is achieved in HNLFs by the usage of a high power EDFA. The undesired frequency components are filtered out by FBGs and a 40 GHz carrier generation is shown [110].

In this thesis, SBS plays a major role in the system and is discussed in detail in the following section.

band pass filtering [98]. On the one hand, the number of generated sidebands is higher than at a conventional amplitude modulation. On the other hand, phase modulated optical carriers have the property that the odd order lower sidebands are in opposition to the corresponding upper sidebands [64]. Hence, odd order sidebands do not fulfil the requirements of a correlated status that is requested for heterodyne based ROF systems as a limiting factor.

- Whereas conventionally implemented modulators such as MZMs are based on Lithiumniobate ($LiNbO_3$) **Electro Absorption Modulators** gained in importance due to its fast modulation performance and low power requirements to modulation signals. EAMs are based on an absorption medium that passes light in dependency of the applied voltage. For this purpose effects of quantum mechanics are used [99]. An extension for a low chirp EAM modulator for ASK and Phase Shift Keying (PSK) is verified in [100] and an extensive investigation of a special designed EAM in the 60 GHz range for mm-Wave downlink systems is demonstrated in [101]. On the other hand, EAMs can be used as a photodetector as well since the absorbed light can be converted into an electrical signal. Due to this electro absorption modulators can be used in ROF systems as a modulator and a PD simultaneously. This leads to a further reduction of complexity in the base station [36], [102]. A comparison of EAMs and MZMs shows, that an EAM requires less modulation power for the generation of high order harmonics [103]. On the other hand, the MZMs achieve a high efficiency due to their cosines shaped dependency of the intensity to the applied voltage (see Fig. 3-7b).

A notable advantage of this generation method is that the generated optical carriers are totally phase correlated directly at the output of the modulator due to the fact, that they have the same emission source. There is neither a need for a phase control loop nor for any other unconventional super structural components in the set-up. On the other hand, the system is limited by the high frequency low noise modulation signal that is required for this method.

The presented methods typify the most common ways of generating mm-Waves by heterodyning. Of course, there is a large number of variations, combinations and

Experimental verifications are illustrated in Fig. 3-8 to emphasise the flexibility of an MZM.

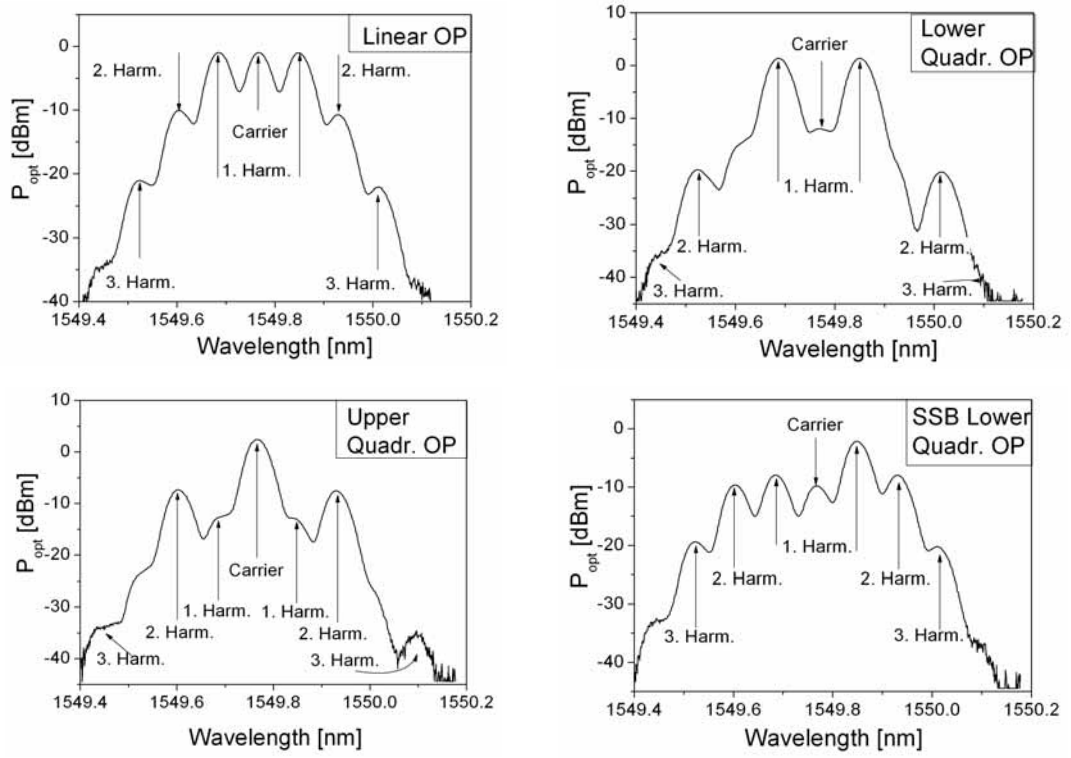

Fig. 3-8 Output spectrum of an MZM at different operation points (OP).

- An application of **Single Sideband** modulation for Radio Over Fibre systems was described in [92] where a 155 Mbit/s Binary Phase Shift Keying (BPSK) was applied to a 38 GHz carrier signal. An error free transmission was observed over a distance of 50 km SSMF and 5 m radio propagation. A full-duplex mm-Wave link at 39 GHz carrier frequency was verified in [93] and in [94] SSB modulation was investigated under the aspect of dispersion penalties.
- **Double Sideband Suppressed Carrier Modulation** was used in [95] and in [96] for the generation of two phase correlated optical carriers while considering dispersion effects. Recently, a 2.5 Gbit/s ASK modulated 40 GHz carrier transmission over 44 km optical fibre was verified [97]. It was realised by a PRBS signal modulation of one sideband generated by a DSSC modulated optical carrier. There was no power penalty observed due to chromatic dispersion.
- A further mm-Wave generation method can be realised by **Phase Modulation** where the undesired frequency components are suppressed by

phase variance. A further millimetre wave generation technique by the optical phase locking of two laser diodes is realised by the application of an optical comb generator [90]. Thus, frequencies up to 100 GHz with a phase noise of -92.5 dBc/Hz at 10 kHz offset from the carrier have been observed.

3.2.2.4 Optical Frequency Multiplying by Modulation

A very elegant generation of two phase correlated signals can be achieved by the external modulation of laser diodes. An appropriate modulation scheme is represented by the exploitation of the non-linearities of external modulators such as Mach Zehnder (amplitude) Modulators (MZM).

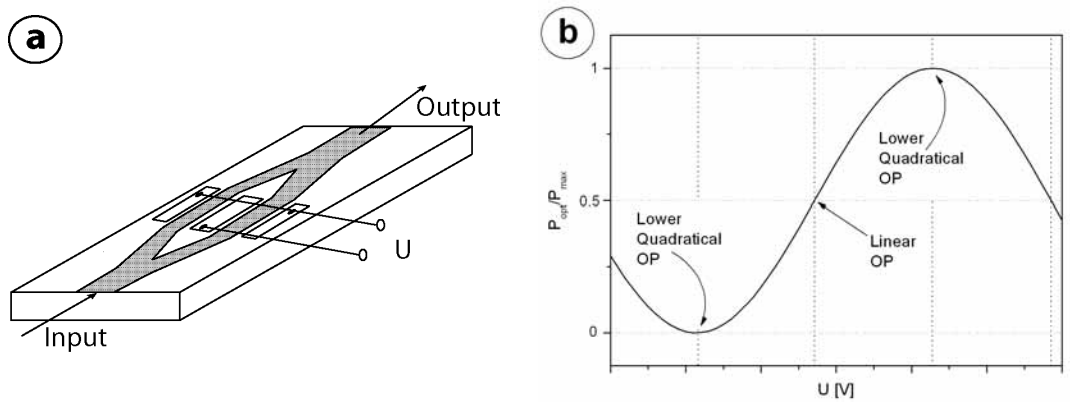

Fig. 3-7 a: Mach Zehnder Modulator configuration and b: its operation characteristic.

A MZM consists of two wave guides that separate the incoming light as can be seen in Fig. 3-7 (a). This set-up results in an interferometer. Due to an applied voltage to a control electrode located at one wave guide, the phase is changed owing to a refractive index modulation. At the output the waves interfere with each other. If the phase difference of each wave part is equal to π the superposition is destructive hence, no light (logical "0") is transmitted [56].

The other control electrode adjusts the operation point (OP) of the MZM via a bias voltage. The typical operation characteristic is illustrated in Fig. 3-7b. If the modulator is driven in the non-linear regime higher harmonics are generated. The operation in the lower quadratic OP leads to a double sideband suppressed carrier (DSSC) modulation whereas the operation in the upper quadratic OP leads to a generation of even order sidebands including the carrier [91]. A single sideband modulation (SSB) can be achieved by launching the modulation signal to the control electrode of both wave guides. Both signals have to have a phase shift of π.

environment. Thus, for optical injection locking a temperature change of a fraction of a degree leads to a fall out of lock in case of using standard DFB lasers [83].

3.2.2.3 Optical Phase Locking

A further method for the generation of two phase correlated frequency components is the heterodyne detection of the modes of two independent lasers in a PD [84]. The frequency separation corresponds to the desired mm-Wave signal as for all heterodyne methods. In case an uncorrelated reception occurs the detected signal is unstable. If an **Optical Phase Locked Loop** (OPLL) is applied to the emitted signals the phases can be varied and adapted to each other. This is done by a comparison of the beat signal of two lasers to the signal from a microwave reference oscillator with a phase noise a little lower than required for the generated carrier. The resulting phase difference signal is fed back to the slave laser that is thus forced to track the master laser [85], [86]. The principle of an OPLL is schematised in Fig. 3-6.

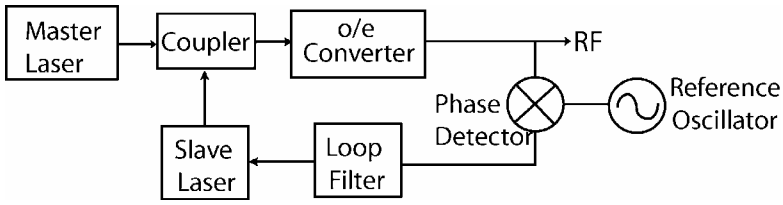

Fig. 3-6 General set-up of an optical phase locked loop.

Owing to a relative high linewidth of semiconductor lasers (several MHz) the round-trip propagation delay should be very low (typical < 1 ns) [87].

Disadvantages of the application of optical phase locking for the generation of mm-Waves are the high system complexity and the feedback channel between control station and base station. It is required for the transmission of the phase information.

In [88] mm-Waves with a frequency of 110 GHz, 220 GHz and 330.566 GHz where obtained by a cascaded phase locking of three semiconductor lasers. A 140 Mbit/s amplitude shift keying (ASK) modulation over a 65 km uncompensated SSMF at 36 GHz was verified in [83]. The carrier signal has a phase noise of -93 dBc/Hz at 10 kHz carrier offset.

By applying three external-cavity lasers constructed from commercial laser diodes to a phase locked loop Andrew et al. [89] generated 33-40.5 GHz with a low

3.2.2.2 Injection Locking

In contrast to Mode Locked LDs in which the locking is realised by an electrical modulation the **Injection Locking** method is realised by an external optical signal [79]. A narrowband laser diode (master laser) is modulated by the desired mm-Wave signal. Due to this, the emission spectrum is broadened and sidebands are generated. If the frequency comb is injected into a second laser (slave laser) one sideband of the modulated master laser can lock the emitted signal of the slave laser to have the same phase as the sideband. An alternative is the application of two slave lasers that is schematised in Fig. 3-5. Each slave laser is locked by one sideband of the master laser.

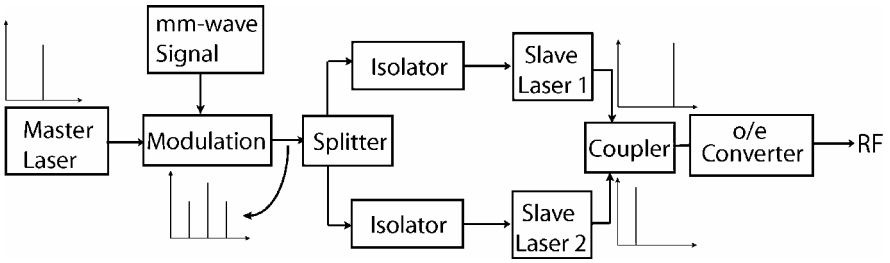

Fig. 3-5 Block diagram of the injection locking scheme with two slave lasers.

Hence, both lasers transmit two phase correlated signals with spectral separation that corresponds to the desired mm-wave signal. In [80] a 200 GHz signal and a power of 1.2 mW are predicted. The stimulated sidebands that are induced into the slave lasers are generated by a phase modulation. Noël et al. [81] presented an optical fibre link that uses a master/slave distributed feedback (DFB) arrangement to generate a 60 GHz carrier signal in an o/e converter. The authors show the transmission of a 120 Mbit/s Quadrature Phase Shift Keyed (QPSK) signal over a 100 km long SSMF and via air. A bidirectional transmission system using optical sideband injection locking was demonstrated in [82]. In that paper a 19 GHz carrier signal with a phase noise of -85 dBc/Hz at 10 kHz carrier offset and a 140 Mbit/s QPSK signal was generated and investigated.

Although many papers present different variations of Injection Locking with more or less good results the technique in general is complex in its set-up and strongly dependent on temperature influences. The wavelength detuning of master and slave spectrum has to be minimised by a temperature control of the laser and its

status is called **Locking** of laser modes [67] or Mode Locking. Active mode locking (AML) can be realised by a modulation of the laser with a frequency f_m that corresponds to the mode separation Δf. Due to the stimulation of modes, the mode oscillations become dependent and their phases correlated. In contrast to AML passive mode locking (PML) is realised by a saturable absorber [68]. Although the practical realisation of AML is more complex than PML there are more control options of this method. A combination of AML and PML is represented by Hybrid Mode locking where lower modulation power as at AML is necessary [69]. On the other hand, Hybrid Mode locking and a special arrangement of the lasers increase the production costs [70], [71]. The high number of emitted modes is a further limiting factor of the technique due to dispersion effects. Although the optical filtering of two modes can generate dispersion independent signals there is a big decrease of power due to the screening procedure. Because the very complex mode locking analysis is not the focus of this thesis it is not investigated further at this point. For detailed information see [72].

Applications of mode locked lasers are a frequency modulated (FM) laser output, a specially scanning laser beam or an output of optical pulses with variable position for optical data transmission systems [70]. For mm-Wave generation techniques the generation of two phase correlated frequency components via mode locking takes a centre stage. For its realisation semiconductor laser diodes play a major role due to their compact set-up and a mode spacing in the GHz range.

There are efforts to investigate methods that generate only two locked modes (Dual-mode Laser) that are compact, efficient and emit signals that are also dispersion independent [73], [74].

In [75] an AML diode with an integrated high-mesa EAM was presented. Owing to an external modulation by an 80 GHz signal the AML falls into the locked mode and generates a frequency comb where two modes are dominant. After a heterodyne detection a 240 GHz signal with a power level of -11 dBm and a phase noise of -86 dBc/Hz at 10 kHz offset from the carrier have been obtained. By using the same method the authors transmitted a 10 Gbit/s data signal at a carrier frequency of 125 GHz [76]. In [77] a 60 GHz carrier signal generation by using a dual laser which modes are selected by chirped gratings is described. Recently, due to the application of a mode locked fibre ring a 22.08 GHz signal with a spectral width of less than 1 Hz was recorded [78].

In (3.12) it can be seen that the spectrum consists of the carrier ω_{RF} and the summation of ω_{RF} and $2\omega_{mod}$ for the second upper harmonic and the difference of ω_{RF} and $2\omega_{mod}$ for the second lower harmonic. Apart the term "*1/8 E_1E_2"* the magnitude is determined by the frequency and the phase deviation $\Delta(\omega/\varphi)_{mod}$. Thus, it has been shown, that the modulated signal is unconverted to higher frequency. The phases act in all three modulation formats as well as the frequencies.

A special case of the heterodyne detection is known as the homodyne detection. In this case the frequency of the one wave $E_1(t)$ fits exactly to the second wave $E_2(t)$. The o/e converter detects the mix frequency that is zero. Homodyne receivers are not used for the generation of mm-Waves due to a high system complexity [66] and a high impact of dispersion to the signals [62].

There are several methods for the generation of two phase correlated signals as a basis for the heterodyne detection technique that are described in the following subsection.

3.2.2.1 Mode Locking

Classical lasers are based on an optical cavity, which consists of two mirrors and an active gain medium inside it. One of the mirrors is partially transparent. The laser beam is coupled out through this mirror. The emitted spectrum is determined by the length of the cavity and the gain medium. In practice there are several frequencies which can be generated by such a set-up. Therefore, the emitted output spectrum is described by a frequency comb consisting of closely separated frequency components (modes). The axial distribution of the longitudinal modes depends on the number of half-wavelengths along the axis of the cavity. The longitudinal mode spacing Δf corresponds to

$$\Delta f = \frac{c}{2n_L L_{\mathrm{Re}s}} \tag{3.13}$$

where n_L is the group refractive index, L_{Res} the separation distance of the resonator mirrors and c the speed of light. The number of half-wavelengths of the light for typical lasers is in the range of around 10^6 [67].

Random fluctuations and non-linear effects in the cavity affect the amplitudes, phases and frequencies of the resonator modes. If frequency spacing and phases are fixed to a certain value the modes have a special relationship to each other. This

Frequency and Phase Modulation:

The result of a frequency and a phase modulation is similar. The main difference lies in the fact, that the signal is impacted by a phase deviation or a frequency deviation. Furthermore, for a phase modulation all upper order sidebands have the opposite phase to the lower sideband of the same order [64].

A wave $E_1(t)$ that is modulated in its **frequency** or **phase** by a signal $E_{modFPM}(t) = \Delta(\omega/\varphi)_{mod}\, cos(\omega_{mod}t+\varphi_{mod})$ can be written as

$$E_{PFM}(t) = E_1 \cos\left(\omega_1 t + \Delta(\omega/\varphi)_{\mathrm{mod}} \cdot \cos(\omega_{\mathrm{mod}} t + \varphi_{\mathrm{mod}}) + \varphi_1\right) \tag{3.9}$$

with $\Delta(\omega/\varphi)_{mod}$ as the **frequency** and **phase deviation,** respectively. For the heterodyne superposition of $E_{PFM}(t)$ (3.9) and $E_2(t)$ (3.2) it follows that

$$I_{HEPFM}(t) = \begin{pmatrix} E_1 \cos\left(\omega_1 t + \Delta(\omega/\varphi)_{\mathrm{mod}} \cdot \cos(\omega_{\mathrm{mod}} t + \varphi_{\mathrm{mod}}) + \varphi_1\right) \\ + E_2 \cos(\omega_2 t + \varphi_2) \end{pmatrix}^2 \tag{3.10}$$

For the solution of a frequency/phase modulated signal it is necessary to transfer the $cos(a + cos(b))$ function in the first term of (3.10) to a Taylor row [65]. Each term of the row corresponds to the carrier and the sideband of the nth order. Theoretically the number of terms (sidebands) is unlimited. On the other hand, the power of the sidebands decrease in practice and can be neglected at higher orders. For simplification further calculations have been made with the second harmonic as a showcase. The heterodyned superposition of $E_2(t)$ with the second sideband is

$$I_{HETPFM}(t) = \begin{pmatrix} E_1 \dfrac{\left(\Delta(\omega/\varphi)_{\mathrm{mod}} \cos \omega_{\mathrm{mod}} t + \varphi_{\mathrm{mod}}\right)^2 \cdot \cos \omega_1 t + \varphi_1}{2} \\ + E_2 \cos(\omega_2 t + \varphi_2) \end{pmatrix}^2 . \tag{3.11}$$

Again, the calculations bring several terms containing DC components and frequencies at $2\omega_{mod}$ and $4\omega_{mod}$. After neglecting all solutions that are excluded due to the characteristic of the PD the spectrum of the superposition of the second harmonic of the frequency modulated signal $E_1(t)$ and $E_2(t)$ can be described as

$$\begin{aligned} I_{HETPFM}(t) = {} & \frac{1}{4} E_1 E_2 \Delta(\omega/\varphi)_{\mathrm{mod}} \cos(\omega_{RF} t + \varphi_{RF}) \\ & + \frac{1}{8} E_1 E_2 \Delta(\omega/\varphi)_{\mathrm{mod}} \cos(\omega_{RF} t + 2\omega_{\mathrm{mod}} + \varphi_{RF} + 2\varphi_{\mathrm{mod}}) \\ & + \frac{1}{8} E_1 E_2 \Delta(\omega/\varphi)_{\mathrm{mod}} \cos(\omega_{RF} t - 2\omega_{\mathrm{mod}} + \varphi_{RF} - 2\varphi_{\mathrm{mod}}). \end{aligned} \tag{3.12}$$

would lead to an increased phase noise of the heterodyned signal. Hence, the phase adjustment of both signals is one of the main objects that needs investigation.

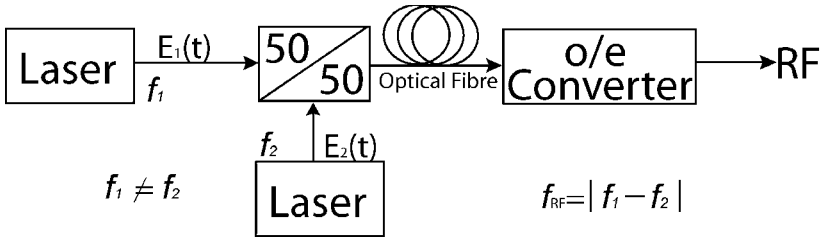

Fig. 3-4 Heterodyne superposition.

If either the field $E_1(t)$ or $E_2(t)$ is modulated the information can be detected by a demodulator behind the PD. In the following the impact of an amplitude, frequency and phase modulation to the heterodyned signal is shown.

Amplitude Modulation:

A wave $E_1(t)$ that is modulated in its **amplitude** by a signal $E_{modAM}(t) = E_{mod}\cos(\omega_{mod}t+\varphi_{mod})$ can be written as

$$E_{AM}(t) = \left(E_1 + E_{\mathrm{mod}}\cos\left(\omega_{\mathrm{mod}}t + \varphi_{\mathrm{mod}}\right)\right)\cos\left(\omega_1 t + \varphi_1\right). \tag{3.6}$$

For the heterodyne superposition of $E_{AM}(t)$ (3.6) and $E_2(t)$ (3.2) it follows that

$$I_{HETAM}(t) = \left(\left(E_1 + E_{\mathrm{mod}}\cos\left(\omega_{\mathrm{mod}}t + \varphi_{\mathrm{mod}}\right)\cos\left(\omega_1 t + \varphi_1\right)\right) + E_2\cos\left(\omega_2 t + \varphi_2\right)\right)^2. \tag{3.7}$$

The calculations result in several terms containing DC components and frequencies at ω_{mod} and $2\omega_{mod}$. After neglecting all solutions that are not possible due to the performance of the PD such as $2\omega_1$; $2\omega_2$ or $(\omega_1 + \omega_2)$ for instance, the spectrum at the output of the PD can be described as

$$\begin{aligned} I_{HETAM}(t) = {} & E_1 E_2\cos\left(\omega_{RF}t + \varphi_{RF}\right) \\ & + \frac{1}{2}E_{\mathrm{mod}}E_2\cos\left(\omega_{RF}t + \omega_{\mathrm{mod}} + \varphi_{RF} + \varphi_{\mathrm{mod}}\right) \\ & + \frac{1}{2}E_{\mathrm{mod}}E_2\cos\left(\omega_{RF}t - \omega_{\mathrm{mod}} + \varphi_{RF} - \varphi_{\mathrm{mod}}\right) \end{aligned} \tag{3.8}$$

with $\omega_{RF} = \omega_1 - \omega_2$ and $\varphi_{RF} = \varphi_1 - \varphi_2$. As can be seen in (3.8), the output signal at the PD consists of the RF carrier and the upper and the lower sideband at $\omega_{RF} + \omega_{mod}$ and $\omega_{RF} - \omega_{mod}$ respectively.

3.2.2 Heterodyne Detection

Heterodyne detection relies on the beating between two waves $E_1(t)$ and $E_2(t)$. The electric field of the one wave is given by

$$E_1(t) = E_1 \cos(\omega_1 t + \varphi_1) \tag{3.1}$$

and the field of the second wave can be written as

$$E_2(t) = E_2 \cos(\omega_2 t + \varphi_2)\,. \tag{3.2}$$

The photodiode has a response to the intensity that is injected into the detector. The intensity depends on the square of the electric field [62]. That means the output signal is proportional to the square of the absolute value of the input. It can be written as [63]

$$I(t) = \left(E_1 \cos(\omega_1 t + \varphi_1) + E_2 \cos(\omega_2 t + \varphi_2)\right)^2 \tag{3.3}$$

$$\begin{aligned} I(t) &= E_1^2 \cdot \frac{1}{2}\left(1 + \cos(2\omega_1 t + 2\varphi_1)\right) \\ &+ E_2^2 \cdot \frac{1}{2}\left(1 + \cos(2\omega_2 t + 2\varphi_2)\right) \\ &+ E_1 E_2 \cdot \left[\cos\left((\omega_1 + \omega_2)t + \varphi_1 + \varphi_2\right) + \cos\left((\omega_1 - \omega_2)t + \varphi_1 - \varphi_2\right)\right] \end{aligned} \tag{3.4}$$

The output has high frequency components ($2\omega_1$, $2\omega_2$ and $(\omega_1 + \omega_2)$) and low frequency components ($\omega_1 - \omega_2$). If operation wavelengths around 1550 nm are considered, the corresponding frequencies lie around 192.9 THz. Due to the fact that the PD is unable to follow these high frequencies these components are filtered out. Owing to this non-linear operation the PD detects a signal containing the beat frequency that is $\omega_{RF} = \omega_1 - \omega_2$ and is described by

$$I_{HET}(t) = E_1 E_2 \cdot \cos(\omega_{RF} t + \varphi_1 - \varphi_2)\,. \tag{3.5}$$

In Fig. 3-4 the principle realisation of a heterodyne receiver is shown. The phase correlation of both signals impacts the phase of the heterodyned signal directly. In case where the phases are not controlled, stochastic phase fluctuations of each wave

to the electrical signal generation mm-photonics transmit the data signal over large distances via an optical fibre to the point of use. Then the actual modulated mm-Wave carrier is generated and transmitted via air. For an overview of optical generation techniques see Fig. 3-1 on page 16.

3.2.1 Direct Detection

If the emitted light of LD is either direct or external modulated by a mm-Wave signal and detected by a PD (see Fig. 3-3) it can be classified as a directly received signal. If a direct reception is inevitable, an external modulation provides a much better performance due to a low RF-to-RF insertion loss. Furthermore, it allows suppression of the contribution of PD shot noise. Thus the noise figure of directly modulated links is substantially higher than externally modulated ones [56].

For external modulation MZMs or EAMs are useful since bandwidths up to 95 GHz can be expected [57]. This is one of the easiest ways of generating mm-Waves but there are many limitations on this technique. One restriction is a large influence of dispersion to the signal. Thus a 60 GHz signal is for instance smothered after 1 km SSMF because of dispersion [58]. This is due to the fact that the phases of the frequency components (carrier, upper/lower sideband) will change relative to each other along the fibre and interfere. Because of this, the application of direct detection for mm-Waves is not appropriate. However, a recently presented method proves that a 12.5 Gbit/s downlink can be realised in the 60 GHz band [59].

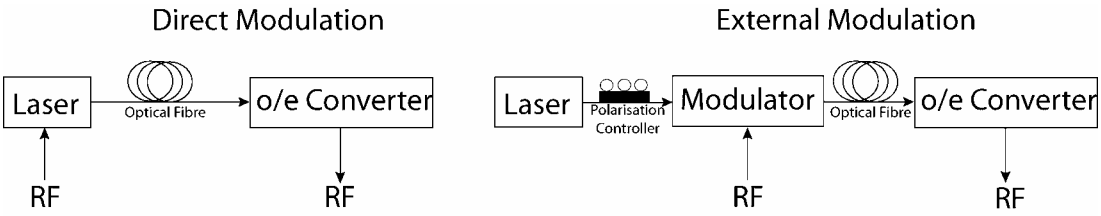

Fig. 3-3 Direct and external modulation for direct reception links.

On the other hand, dispersion can be significantly reduced by adding a dispersion compensating fibre (DCF) with a length that corresponds to the dispersion of the link. Another method is the application of a chirped [60] or conventional fibre Bragg grating, together with an optical circulator [34] or specially designed FBGs, in order to filter the optical carrier and one signal sideband [61]. This would increase the system costs and the complexity.

Here, only a short overview of the main representatives of the wide field of so called "slow wave devices" such as planar tubes, velocity-modulated tubes and Gyrotrons is given. For detailed information see ref. [49].

3.1.4 Frequency Multiplier

A further way of generating extremely high frequencies is the multiplication of the frequency of a stable, linear and low phase noise, Microwave source. This could be a YIG or Gunn oscillator for example. It can be realised by applying the base frequency to an electronic semiconductor that is driven in the non-linear regime. This can be an Impact Ionisation Avalanche Transit Time Diode (IMPATT) [26], a Schottky diode [51], a point contact diode, a PIN-diode, a varactor diode, or a backward [49] diode for instance. Semiconductor diodes that use the charge storage effect of the forward directed pn-junctions for frequency multiplying achieve high efficiencies and high output powers [52], [54]. Due to the overmodulation harmonic waves are generated. All frequency components that are not useful for high frequency generation are suppressed by a band pass filter whereas the multiplied component is coupled out [55]. Frequency multiplication is a common application in laboratory equipment such as signal generators.

Although frequency multiplication is a convenient way for generating high frequency signals the method is limited by the following restrictions: since not only the frequency but also all properties of the base signal such as phase noise, fluctuations and other distortions are multiplied as well, the base signal has to be extremely pure with very good noise properties. Owing to the fact that harmonics have lower magnitudes than the fundamental, there is a significant loss of power.

3.2 Optical Millimetre Wave Generation

In the following the termini "heterodyne reception" respectively "detection" are used as synonyms for "generation". This is due to the fact that generation relies on the optic-electrical conversion in a photo detector (PD). At the input of the PD the optical signal is "received" or "detected" and at the PD output the electrical signal is "generated". More details about the relation of "receiving" and "generation" are given in section 3.2.2. In general optical mm-Wave generation techniques are most suitable for the field of Radio Over Fibre as described in the introduction. In contrast

inserted into a resonator this property is employed for the generation of oscillations [41]. Gunn oscillators have output powers of 200 – 300 mW in the lower frequency range. For higher frequencies the emission power decreases to 0.29 mW at 289.74 GHz [42] or 1.6 mW at 329 GHz [43]. They have great potential regarding the emission frequency. Due to a high efficiency they can achieve oscillation frequencies from 1.5 GHz up to 500 GHz as the state of the art [43]. The phase noise is an important property of Gunn oscillators and is for instance: -113 dBc/Hz at 300 kHz offset from the carrier at a frequency of 60 GHz [44], -97 dBc/Hz at 100 kHz away from carrier at 24 GHz [45] or -110 dBc/Hz at 500 MHz off the oscillation frequency of 103 GHz and a power of 180 mW [46]. The limitations of Gunn oscillators lie in the low frequency tuning range and a high temperature-sensivity due to its extremely small dimensions [47].

3.1.3 Electron Tubes

Electron tubes have their main applications in Radar systems, the medical field, dielectric heaters or linear accelerators. This is due to the fact, that the transmitted signal has a high frequency and a high power at the same time. There was no reference found reporting on the phase noise measurements of electron tubes.

Table 3-1 Overview of Significant Properties of Electron Tubes (Powers correspond to Frequencies).

	Travelling Wave Tubes	**Klystron**	**Magnetron**	**Gyrotron**
Frequency Range	1 GHz, 10 GHz, 100 GHz	10 GHz, 100 GHz	30 GHz, 100 GHz, 230 GHz	170 GHz
Emission Power (cw)	100 kW, 50 kW, 1 kW	500 kW, 50 W	400 kW, 30 kW, 1 kW	1 MW and 2 MW
Main Applications	Radar, LOS-Radio or Satellite transmission	Radar, Microwave Transmitter/ Heater	Radar, Impulse Application	Generating, heating and stability control of magnetic entrapped plasmas
References	[48], [49]	[48], [49]	[48], [49]	[49], [51], [52]

3.1.1 Yttrium-Iron-Garnet Oscillators

Yttrium-Iron-Garnet (YIG) oscillators are Microwave oscillators which can be tuned over several octaves by an external magnetic field. A solid state cavity with a yttrium-iron garnet sphere as a frequency adjusting element is used. The sphere has an extremely high figure of merit and can be varied by applying an external magnetic field. A further enhancement of the frequency range can be achieved by gallium doping. The frequency range of YIG oscillators is between 0.5 and 25 GHz. Due to the high figure of merit YIG oscillators have a low phase noise property and a high adjustment linearity. To provide independency to temperature influences the cavity is located in a heated cover with a constant temperature of approximately 80 °C. Due to its relative large frequency tuning-range YIG oscillators are applied in spectrum analysers, microwave receivers or military devices [38]. Although the tuning range is very high, the 30 GHz threshold border can rarely be reached. However, YIG oscillators can be the basis for frequency multiplication systems [26], [39], [40].

3.1.2 Gunn Oscillators

The function of a Gunn-diode relies on the negative drift velocity as a function of the electrical field intensity. This causes a characteristic with a negative differential resistance. Gunn-diodes consist of n-doped GaAs. They do not have a pn-junction. Due to this the drift velocity decreases while the electrical field intensity increases as can be seen in Fig. 3-2. Owing to the negative resistance electrons accumulate and propagate in very fast packets through the Gunn element. If the Gunn element is

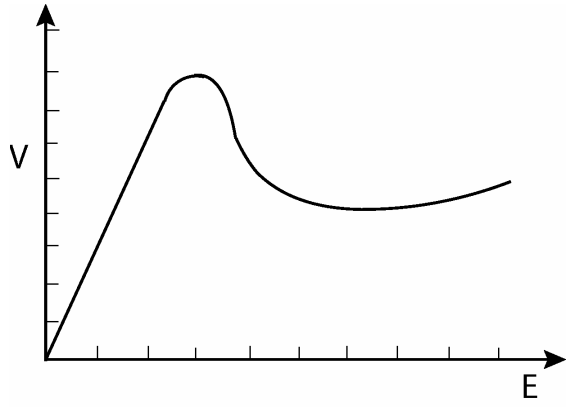

Fig. 3-2 Drift velocity versus electrical field intensity in n-GaAs.

3 Millimetre Wave Generation Systems

To classify all mm-Wave generation systems it is necessary to separate them into two fields: The electrical and the optical generation. A classification of the wide field of mm-Wave generation systems is shown in Fig. 3-1.

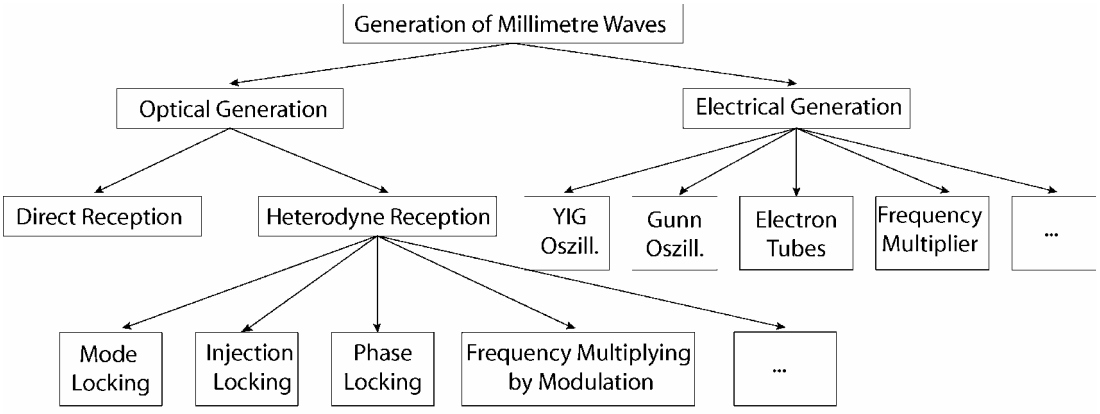

Fig. 3-1 Classification of possible mm-Wave generation techniques.

3.1 Electrical Millimetre Wave Generation

Although the electrical generation of extreme high frequencies has different applications than its optical counterpart, it is briefly explained for completeness. The propagation circumstances for electromagnetic waves in the mm-Wave range in cables, wave guides or the atmosphere are not suitable for long distance transmission. Hence, for ROF systems the oscillator has to be located directly at the transmitter. This would increase the complexity of the radio station enormously if electrical ways of carrier generation is chosen. A general drawback of electrical oscillators for telecommunication applications is the relatively small frequency tuning range.

Some common oscillators that operates in the mm-Wave range are presented here. Furthermore, a common technique for the generation of mm-Waves by frequency multiplication of signals to a higher level is explained.

BB modulation there are no possibilities for a central frequency allocation which is one interesting aspect of ROF. LMDS using OSSB modulation is more complex in its central station. But the access control consists again only of an optic-electronic converter and allows a complexity reduction as a typical property of ROF.

- Even **Satellite Communication** can be made more convenient for installation, use, and maintenance by applying ROF. The low loss optical fibre operates as the connection between service provider and the feeder station. The up/downlink channel for Digital Video Broadcasting (DVB) satellite TV uses carrier frequencies around 12 GHz and 18 GHz respectively. Fig. 2-4 demonstrates a possible feeder concept for the realisation of satellite video broadcasting. Note that polarisation is not considered.

A further possible implementation of ROF is the supplement of **UMTS.** Thus, hybrid fibre radio can also work as a connection link between the Radio Node Control (RNC) and the base stations. Due to the fact that there are no strict requirements on the dynamic range for UMTS an EAM could be used for the RAU realisation.

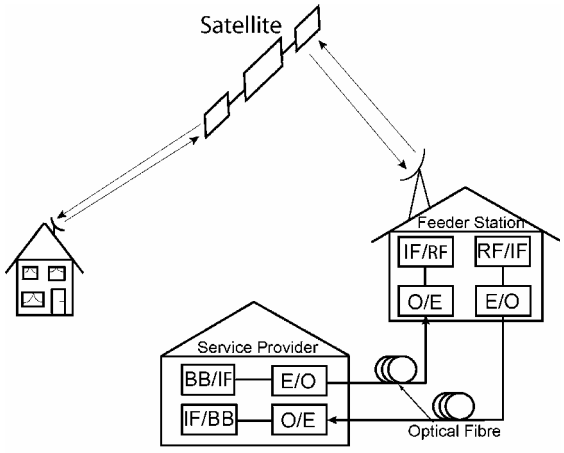

Fig. 2-4 ROF implementation into a satellite broadcast system.

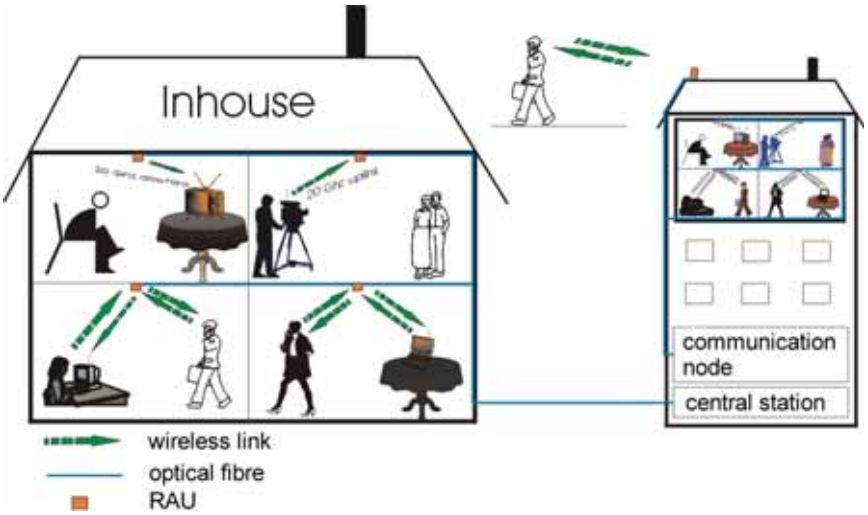

Fig. 2-3 Possible Radio Over Fibre and Millimetre Wave applications.

Besides an application as a separate radio system the ROF technology can also be implemented into current mobile communication techniques such as WLAN or HIPERLAN for instance. Such systems operate mainly in the UHF range. Of course, the simple generation of ultra high frequencies in the mm-Wave range, which is the main object in this dissertation, can be adapted to lower frequency ranges. A further decrease of costs and complexity can be expected. The following scenarios of implementing ROF and hence a Millimetre Wave generation technique are reported in [13].

- The interconnection between terrestrial networks and **WLAN** (IEEE 802.11) can be realized by ROF. The radio base station corresponds to the central station (CS) where the complex technique is centralised. The WLAN access point reflects the RAU and consists only of an optic-electric conversion. By using Hybrid Fibre Radio (HFR) with an added repeater the indoor coverage of terrestrial systems can be enhanced.
- The application of HFR to the **HIPERLAN/2** technology also allows a complexity reduction of the set-up. Thus, problems of carrying an RF or IF over cable from one device to the other would be avoided.
- Since **LMDS** operates in frequency bands above 30 GHz the attractiveness of ROF for LMDS has increased. The distribution service uses the digital base band (BB) and the analogue Optical Single Sideband (OSSB) as modulation techniques that are of interest for ROF. In respect to HFR the simple optical base band modulation has the advantage that the signal is conveyed through an optical fibre; hence a large amount of capacity is available. On the other hand, by using

used. The Millimetre Wave feeder consists of a low loss optical fibre that offers a large capacity and low production costs.

As described above, ROF uses mm-Waves as carrier frequencies. mm-Waves have the property that in the GHz range the transmission loss in the atmosphere increases with frequency. Additionally, at 24 GHz and 60 GHz the attenuation rises drastically due to the H_2O and O_2 absorption of the waves [15]. Furthermore, higher frequencies are much more affected by rain than waves in the lower frequency range [13]. This influences directly the cell diameter in the radio system. The planned cell sizes lie in the range of less than 100 m which corresponds to Pico cells. In standard mobile communication systems based on the cellular concept atmospheric loss is avoided. ROF uses this property, to reuse the carrier frequency in the next cluster. This increases the spectral efficiency and hence the transmission rate. The fact that the frequencies in the mm-Wave range have a lower penetration depth than signals with lower frequencies, has advantages for electromagnetic capability.

However, ROF can also be used for bridging the “last mile” in office buildings. The installation of optical fibres to each work place is a large cost factor in transmission networks. By offering high bandwidths via radio signals the users in overcrowded areas can be provided with any required data rates [36].

2.2.2.2 Radio Over Fibre Applications

In this chapter the variety of ROF techniques and hence the optical generation of Millimetre Waves is discussed. The properties - very high transmission rates and low cell diameters - offer great opportunities on the one hand and limit the applicability of the Radio Over Fibre technology on the other hand. Due to the fact, that cell diameters in the Pico cell range are small, planned applications in congested areas are preferred. Radio Over Fibre as a stand alone system can substitute present wireless communication systems such as GSM, UMTS, DECT, Wireless LANs, Microwave Multichannel/Video Distribution Systems (MMDS/MVDS), Local Multipoint Communication/ Distribution Service (LMCS/LMDS) etc.. Although applications are limited by the cell size, they increase in attractiveness due to their broadband transmission rate. ROF does not only provide users with mobile phone requirements. Moreover, it satisfies the demand of applications such as broadband internet access, multimedia applications of cell phones, computer networks and video on demand. A possible application scenario is demonstrated in Fig. 2-3.

- By using the **intermediate frequency (IF)** transmission concept some complexity of the RAU is shifted to the CS. However, up/down conversion to the Radio Frequency (RF) band and the amplification processes are still the functions of the RAU.

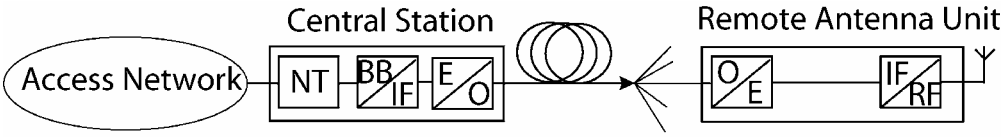

- The **Millimetre Wave feeder** concept allows transferring the whole complexity to the CS. Thus, the line termination of the digital segment, modulation/demodulation, up/down conversion to RF, multiplexing/ demultiplexing can be performed by the CS. The RAU consists of an optic/electronic converter to transform the optical signal into the actual modulated Millimetre Wave carrier. An electrical power amplifier is used to increase the signal magnitude to the required output power. The Millimetre Wave feeder concept is demonstrated in Fig. 2-2.

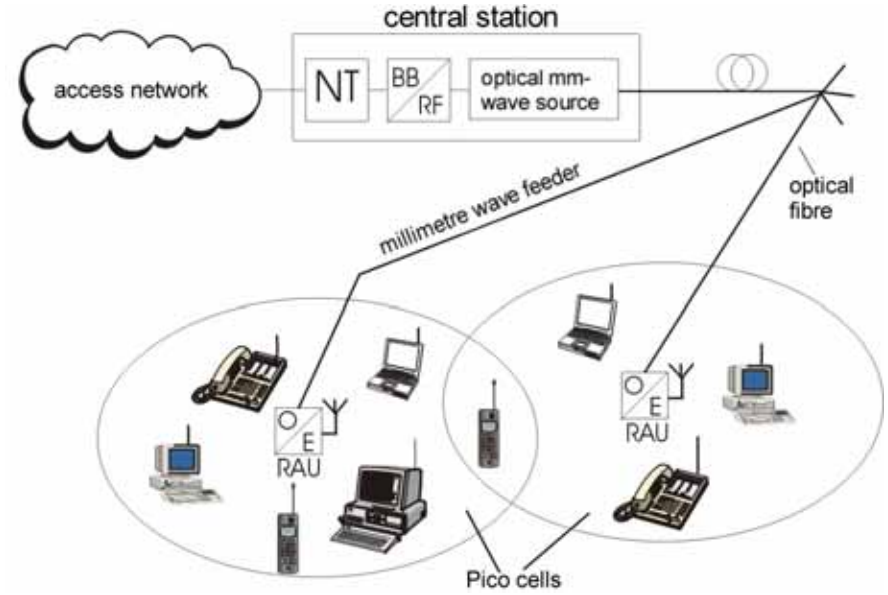

Fig. 2-2 Millimetre Wave feeder concept [13].

The Millimetre Wave feeder concept enables a significant reduction in maintenance owing to the fact that the antenna unit has a very simple set-up [35]. The antenna size is very small, low-priced and does not require an external power supply when passive electro-absorption modulators (EAM) [36] or even photo-diodes (PD) are

2.2.2 Future Mobile Communication Systems – Radio Over Fibre

As described in the introduction the merging of the wireless and fiberoptic worlds provides enormous potential regarding higher transmission rates and more local flexibility. Radio Over Fibre (ROF) represents such a combination. The main objective is to save costs while increasing the network coverage and performance.

The idea of ROF is not new. It was invented in the 1990s in order to simplify, or even replace, the mobile infrastructure. Commercial success was not obtained due to difficulties with the implementation of the feedback channel. For several years the diffusion process of broadband internet innovations such as "Video on Demand" has risen and thus the demand for a high download transmission speed for the customer has increased. This demand for high speed downlinks can be accommodated by Radio Over Fibre networks, whereas the narrowband uplink can be realised by conventional wireless cell systems or wireless LANs. Whereas recent investigations report a simple and impressive 150 Mbit/s transmission in the up link direction [34], the main research focus lies in the high speed downlink. Considering these aspects in this approach, investigations regarding the ROF-downlink have been made.

2.2.2.1 Properties of Radio Over Fibre

This aim can be achieved by centralising the system complexity to one location – the central station (CS). Due to this, the radio capacity can be allocated while considering the mobility of the subscriber. In a crowded city the requirements for a high capacity in the daytime exceeds that of the night. Since the demand in populated suburbs increases at night, the net capacity allocation can be adapted to the new situation. Moreover, congested areas can be provided with broadband radio access and employees can change their position within one office building without any restrictions.

In principal there are three feeder concepts for the realisation of ROF [13].

- The **base band feeder** concept with low transmission loss and a large bandwidth allows no complexity reduction of the remote antenna unit (RAU). NT: Network Terminal

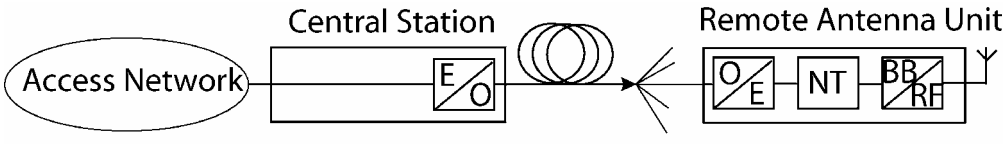

- **Local Multipoint Distribution Service** (LMDS) uses Millimetre Wave signals to transmit and receive data in the range between 26 GHz and 43 GHz having bandwidths of 0.1 up to 2 GHz. On the other hand, the area coverage is limited due to the line of sight constraints and large propagation losses [29]. The transmitter should be on the top of a tall building or on any other high platform. One transmitter covers a sector typically 60° - 90° wide. Hence, 4-6 transmitters are necessary to achieve a 360° coverage. LMDSs provide a point-to-multipoint broadcast downlink of 34–38 Mbit/s per transport stream to everybody located in the covered zone. This kind of data is typically television broadcasting, Internet applications and communications [30].
- The **Mobile Broadband System** (MBS) is a part of the "RACE" project that is supported by the European Union for the investigation of broadband networks. It belongs to the 4th mobile generation techniques and provides the terrestrial radio applications. The cellular network works in a frequency range between 40 GHz and 60 GHz and reaches data transmission rates up to 150 Mbit/s [31]. MBS provides voice, video, and high demanding data applications. The cell coverage range is 1 km for outdoor and 100 m for indoor applications. The broadband system is located in high traffic density service areas indoor as well as outdoor.
- The ETSI-BRAN **High Performance Radio Access** (Hiperaccess) standard is confined to specify radio communication systems that work with frequencies above 11 GHz. Hiperaccess supports voice and data services using frequencies between 11 GHz and 42 GHz with a large bandwidth of 2 GHz [32]. This provides "bandwidth on demand", i.e. any appropriate data rate at any time. At least 25 Mbit/s can be offered at the user-network interface in up or downstream direction. These data rates are possible due to the large bandwidth and the application of the IP (Internet Protocol) and ATM (Asynchronous Transfer Mode) in the system [33].

Overall, the impact of Millimetre Waves to communication systems will rise in the future. The performance capabilities that come with short wavelengths enable many new applications, only a few of which have been covered here.

2.2.1 Current Commercial Applications of mm-Waves

While the UHF band has a dense allocation of many types of demonstrated applications the SHF and EHF band is very transparent in its spectrum. Millimetre Waves are only used in few commercial applications.

- The term **RADAR** (Radio Detection and Ranging systems) stands for detection and distance measurement. The basic principle relies on the transmitting of electromagnetic waves by directional antenna into air. In case the waves hit an object, a part of the energy is backscattered to the receiver. Object parameters can be investigated by the analysis of the received electromagnetic field [25].

  Radar systems belong to one of the first natural applications in the area of mm-Waves due to its small antenna size and its inherent high resolution. The evolution of radar systems from X-band to 24 GHz, then 77 GHz, and to 100 GHz or 220 GHz have shown, that sub-millimetre distance resolution is possible. Recently a long range 7 km Radar system with a resolution of around l.5 m at a frequency of 94 GHz was achieved by Macfarlane et al. [26]. This high resolution has been achieved by a highly linear, low phase noise YIG oscillator[1] in the frequency-multiplied transmitter. Nowadays Radar systems can be used for long distance applications such as tornado observations for instance [27] on the one hand or for short distance applications such as anti-collision radar between vehicles on the roadway and ground penetration (mine detection).
- **Microwave Video Distribution Systems** (MVDS) operate at frequencies of around 29 GHz and 40 GHz. They rely on the cell fragmentation into different sectors. A monitor control of the signal power level in each sector allows the system to control, adapt and improve the quality of signal reception as requested by the subscribers. By minimising the transmitting power the operational life of the transmitter increases and the responsiveness to other demands for signal transmissions is enhanced [28]. Sector monitoring in MVDS may be used in a variety of scenarios. A Millimetre Wave power detector can be used to shut down or reduce the power from a particular antenna sector. Moreover, it is beneficial in improving the stability of the transmitter and its component parts due to power reduction.

[1] See chapter 3.1.1.

indoor applications to 10 km in the countryside. It can provide features like 2nd generation mobile systems but will also offer multimedia services like video telephony.

W-LAN (IEEE 802.11) uses frequencies around 2.4 and 5 GHz in an 80 MHz spectrum. The standard is designed for theoretical transmission rates from 2 Mbit/s to 600 Mbit/s indoor for up and downlink (IEEE 802.11a-n). The provided area can reach a diameter of 250 m.

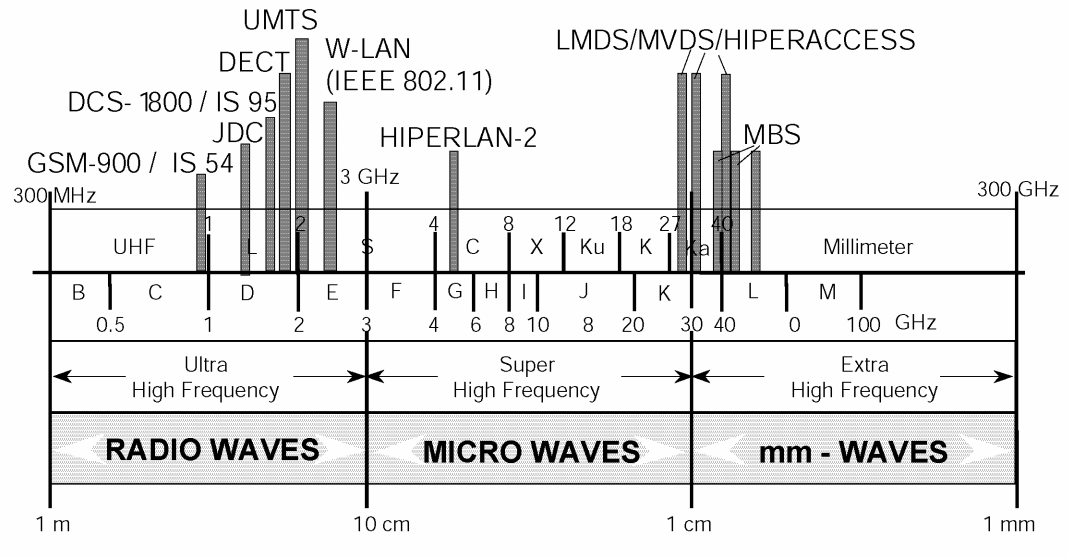

Fig. 2-1 UHF/SHF/EHF radio spectrum and its frequency allocation [23].

WiMAX is described by the IEEE 802 standard family and provides the user with data rates up to 100 Mbit/s. It is a standard for wireless networks (IEEE 802.16) and works with frequencies from 2 GHz to over 11 GHz. For data transmission between 2 GHz and 11 GHz no line-of-sight connection is necessary. Moreover, the antenna installation is easy and the modulation technique is Orthogonal Frequency Division Multiplexing (OFDM), which tolerates diversity reception and has a high spectral efficiency. The disadvantages are smaller antenna gains due to the high frequencies that are used and low transmission rates owing to lacking broadband frequency spectra. If WiMAX uses frequencies higher than 11 GHz a line-of-sight connection is required and hence mobile communication services are impossible [24].

HIPERLAN works around 5 GHz and offers data traffic up to 54 Mbit/s. The cell diameters are 30 m for indoor and 150 m for outdoor applications.

55 GHz are used for satellite radio between two satellites for speech and data transmission. For applications such as the satellite position and speed control the 66–71 GHz band is used. For traffic telematics such as distance control electromagnetic waves with frequencies of around 77 GHz are applied. Packet characterisation techniques and the evaluation of plastic package are planned at frequencies around 79 GHz. It allows impedance characterisation of enclosures, failure analysis and fault localisation [22]. The allocation of applications presented in this chapter reaches frequencies of up to 300 GHz

All verified applications are recurrent at higher frequencies up to the upper border of the mm-Wave range (300 GHz).

2.2 Public Request

Fig. 2-1 gives an overview of the operation frequencies for different radio communication systems from 0.8 GHz to 70 GHz, including the ones treated below. The most popular are Global Systems for Mobile Communications (**GSM)** 900, 1800 and 1900 MHz, which provide data rates between 9.6 and 14.4 kbit/s. The cell diameters go from 10 m in buildings and 30 km in the countryside depending on the geographical environment. Higher bit rates can be achieved by channel packing (High Speed Circuit Switched Data - **HSCSD**). Due to allocation of several GSM channels the transmission rate increases up to 57.6 kbit/s if 4 timeslots are occupied.

The General Packet Radio Service (**GPRS**) provides the timeslot packing of all 8 GSM timeslots and achieves a theoretical bandwidth of 171.2 kbit/s. The packet based “high-speed transmission” system Enhanced Data rates for Global Evolution (**EDGE**) is an extension of GPRS and is three times as fast as GPRS. All demonstrated methods relying on the basis of GSM in a 200 kHz spectrum and are called the 2nd mobile generation.

Another radio system is the Digital European Cordless Telecommunications Standard (**DECT**). It works in a 20 MHz spectrum around 1.9 GHz and supplies narrow band indoor services and cordless telephony.

The next step in developing high-speed transmission links was represented by the 3rd generation with **UMTS** as the main application. UMTS uses carrier frequencies around 2 GHz and theoretically provides data rates up to 2 Mbit/s for the case of a user density of one mobile and a low mobility. Cell diameters go from 100 m for

2 Millimetre Wave Applications

The worldwide development in wireless and fibre-optic telecommunications is a result of the availability of high quality signal generators and signal processing systems and the requirement of higher bandwidths and low cost system set-ups. While available mm-Wave generation systems are verified in Chapter 3, the application aspects of the wide field of Millimetre Waves are demonstrated here.

A classification of the main applications can be made if a distinction is made between commercial public telecommunication systems for private and business demands and non-public applications such as military, meteorological or aerospace related systems.

2.1 Closed Requests

This Chapter is based on [21] and should give an overview of the non-public applications of Extremely High Frequencies (EHF) in the range from 30 GHz to 275 GHz. It should be noted, that frequency bands in the EHF domain are indeed allocated but the use and the density of channels are much smaller than in the Very High Frequency (VHF; 30 MHz – 300 MHz) and the Ultra High Frequency band (UHF; 300 MHz – 3 GHz) for instance. Frequencies exceeding 275 GHz are not allocated to any radio channel.

Around 30 GHz the radio astronomy systems search for radio waves and radiation from outer space. Furthermore, the space radio communication research applies mm-Waves for investigations of space and natural phenomenon's on board spacecraft by passive sensors (radiometer). The data transport of technical and scientific measurement results made by spacecrafts is also completed in this frequency range. The 34 GHz band is used for the transmission of data for sea and ashore surveying.

Other uses of mmWaves in this range are e.g. speed controls, traffic counts, security services and distance detection. In the higher 40 GHz range a radio amateur band for satellite communications is provided. In addition, a digital point to multi-point line-of-sight (LOS) radio system with radio link antennas is located at a certain height in the stratosphere (High Altitude Platform Station). Frequencies of about

allocation into private (astronomy, military etc.) and public (radio communication, RADAR etc.) domains has been conducted. Special attention is given to the application of mm-Waves for Radio Over Fibre systems and is described in more detail.

Chapter 3 gives an overview of the state of the art electrical and optical techniques for the generation of Millimetre Waves. The main objective in this chapter is to discuss the heterodyne superposition of two optical phase correlated signals in a photo detector.

Since “stimulated Brillouin scattering” is applied in the system, an overview of the important properties of the non-linear effect is provided in Chapter 4, where characteristics such as gain, its bandwidth, the threshold and several amplification scenarios are presented.

In Chapter 5, the proposed Millimetre Wave generation method is briefly described followed by a detailed theoretical investigation of the system. Based on the nonlinear wave equation and the wave equation for the density modulation, a complex differential equation system is derived and analysed. This equation system is the basis for a simulation presented in Chapter 6. Several scenarios are calculated in order to optimise the experimental set-up. Furthermore, calculations concerning the optimum fibre length, as well as power and frequency drifts are illustrated in Chapter 6.

The experiment, which is verified in Chapter 7, confirms the predictions of Chapters 4 - 6. Several scenarios of Brillouin amplification are carried out in order to compare theory and experiment. Furthermore, Millimetre Wave signals at different grades of up conversion are presented. Properties such as line width, power, and stability are analysed.

In order to modulate the carrier signal with data, the set-up has been modified in Chapter 8. Thus, a simple implementation of modulation into the set-up can be provided. An error free transmission of a 1 Gbit/s data signal for a “back to back” case is shown, as well as a successful realisation of radio propagation between two antennas.

In Chapter 9, the limitations of the presented mm-Wave generation technique are described in order to analyse the method from all points of view.

A general summation of the results is provided in Chapter 10, while a forecast for future work is described in Chapter 11.

radio cells [10]. The amount of cells has to increase to guarantee full network coverage.

To make a virtue of necessity, the advantage of using high frequencies such as mm-Waves is the following. As the propagation distance via air is short [15] the same carrier frequency can be reused in the neighbouring clusters. Because of this and the fact that the electromagnetic spectrum in this frequency range is fairly unoccupied, it offers an enormously large transferable bandwidth and a high number of usable frequency bands.

Another advantage of electromagnetic waves in the mm-Wave range is that they do not penetrate into the human skin deeper than a few millimetres, whereas the penetration depth for the current mobile applications lies in the range of centimetres. In the event that electromagnetic waves are found to have some adverse biological effect other than the established thermal effects, then it can be negligible if mm-Waves are used. With the use of frequencies in the Millimetre Wave range the antenna dimensions can be very small. Hence, small antenna arrays for multiple input, multiple output (MIMO) systems can be designed to achieve a data rate enhancement [16]. The state of the art of data rates in wireless communications lie in the Giga bit range. At 10.8 GHz and in the 60 GHz band, a data transmission rate of 1.25 Gbit/s was verified [17], [18]. Hirata et al. demonstrated a 3 Gbit/s transmission link at 120 GHz [11] and a 10 Gbit/s data rate at 125 GHz [19]. Recently, a 15 Gbit/s, 10 Gbit/s and 5 Gbit/s data transmission over a 1, 2 and 5 metre radio link was performed [20].

The main objective of this work is to analyse and investigate a new and simple method for the generation of Millimetre Waves for Radio Over Fibre Systems. The increased demand for mm-Wave generation techniques has made them more attractive. This dissertation presents a new mm-Wave generation method including some obvious applications. This includes a signal generator or a base station in ROF system. The method relies on a very simple principle, achieves an excellent system performance and is variable in its application.

1.3 Outline

The thesis is divided into 11 Chapters as is detailed below. The following chapter describes typical applications of Millimetre Waves. For purposes of classification, an

subdivided into plural different wireless communication systems. On the other hand, Millimetre Waves especially the range above 100 GHz and higher, are rarely employed by radio stations or industrial services with the exception of radio astronomy applications. Therefore, it is important to investigate the applicability of Millimetre Waves in wireless communications in order to increase the data rate. The frequency region in the mm-Waves range particularly above 100 GHz remains undeveloped, mainly due to technical difficulties associated with conventional electronic systems. As the frequency is increased, the generation, modulation and amplification of electronic signals is more complicated due to the characteristics of semiconductor devices. Furthermore, the electrical channel is affected by a very high transmission loss even in case of short transmission distances. These electronic systems limitations can be overcome by combining the wireless link with photonic techniques. The **merging of the optical and the electrical** domain creates an extreme highly efficient base. It consists of the low-loss high-data rate optical transmission link on one hand, and of the flexible, user-friendly and convenient wireless communication system on the other. Such a combination is also called Microwave Photonics (MWP) or Millimetre Wave Photonics (mmWP) depending on the frequency range that is used.

1.2 Motivation and Scope

The integration of wireless and optical networks is a potential solution for increasing capacity and mobility as well as decreasing costs in the access network. The Radio Over Fibre (ROF)[2] technology with its use of Millimetre Waves (mmW) represents one of the best solutions. The attenuation of electromagnetic waves with frequencies from 30 GHz during their propagation in the atmosphere rises up to 60 GHz. Furthermore, there are attenuation maxima at the resonant frequencies of H_2O and O_2 molecules in the higher Gigahertz range [12]. Hence, the transmission distance reaches only few hundreds meters or less. This property affects the planning of future cellular communication systems. The cell diameter is adapted to the propagation conditions, i.e. the higher the attenuation of the waves the smaller the diameter of the

[2] Another expression for ROF is Hybrid Fibre Radio (HFR) [13],[14]

The theoretical bandwidth capacity of a SSMF is around 25 THz represented by the S-band, the 3rd optical window and the L-band [6]. The present optical communication systems have many advantages over electronical systems. They include reduced size, weight and cost, low dispersion, low and constant attenuation over the entire modulation frequency range, extremely wide bandwidth and high information transfer capacity. The current data rate for a multi channel transmission system is 20.4 Tbit/s and 1 Tbit/s over a distance of 240 km and 2375 km, respectively, as the state of the art [7], [8]. Recently, an RZ-DQPSK signal with a data rate of 25.6 TBit/s was generated and successfully detected [9]. On the other hand, **wireless telecommunications** can circumvent restrictions of the optical communications such as reduced flexibility and burying costs.

However, besides speech, several other applications such as data and video transmission are becoming more important in wireless communications. Hence, wireless local area computer networks (WLAN) as well as mobile radio systems have a growing demand for higher bandwidths [10]. While the cabled network systems transmission rates reach tens of Gbit/s (Gigabit Ethernet) the wireless computer networks have transmission rates of only tens of Mbit/s (54 Mbit/s for IEEE 802.11). Future trends demonstrate new applications such as video broadcasting in congested areas and airports or traffic information systems at traffic nodes. In order to meet these requirements, wireless communication systems need higher data rates of several Gbit/s to keep up with the wired network techniques [11].

A way to increase the bandwidth significantly is the use of Millimetre Waves as carrier frequencies. The Millimetre Wave range lies between 30 GHz and 300 GHz. The same frequency range is also known as extreme high frequency (EHF). This domain is followed by the terahertz region.

The bandwidth allocated to wireless links which operate in the lower frequency ranges such as Microwaves[1] is insufficient because these frequency bands are already used by many systems. For example, the Worldwide Interoperability for Microwave Access (WiMAX) works at frequencies up to 11 GHz for mobile radio networks. The Japanese and U.S. governments have allocated 5 and 7 GHz bandwidths, respectively, to the 60 GHz band wireless communication system. These bands are

[1] The Microwave range starts at 0.3 GHz and ends at 30 GHz. The Millimetre Wave range lies between 30 GHz and 300 GHz.

1 Introduction

1.1 The Merging of Optical and Wireless Telecommunications

Modern mobile broadband radio communication systems take centre stage in many research institutes all over the world. Since the first experiments in sending radio signals between two war ships in the English Channel over a distance of 119 km by Marconi in 1899 [1] the 20th century was shaped by new investigations in the field of cabled, wireless and particularly optical telecommunications. Since 1921 radio signals of wavelengths less than 200 m have been used for long distance data transmission and the first public mobile network was put into operation in 1946 in America. Due to the invention of electronic circuits and cellular structures the proliferation of mobile phones was made possible. Before the global standardisation of the mobile network in the 1990's creating the current GSM system, many countries used different standards for mobile communication systems which were incompatible with one other. The 3rd mobile generation provides a user bandwidth of up to 2 Mbit/s as the state of the art [2].

Along with the rapid development of the wireless communication systems, the **optical telecommunication** sector also flourished. The foundation was made in 1960 when the first laser was invented by Theodor Maiman [3] and the first optical fibre in 1966. Although the losses of the fibres first produced were extremely high, it was now possible to generate and transmit coherent light. In 1970 Kapron illustrated a big decrease of the attenuation in optical fibres down to 20 dB/km [4] and lasers operating continuously at room temperatures were invented by Hayashi [5]. The current range of optical fibre types for different applications has become very large. Initially, the Standard Single Mode Fibre (SSMF) was produced with a natural attenuation of approximately 0.2 dB/km at 1550 nm, followed by Dispersion Shifted Fibres (DSF), Highly Non-linear Fibres (HNLF), Photonic Crystal Fibres and others. Moreover, the development of application-based lasers has also seen rapid progress which includes Distributed Feedback Laser diodes, Fibre Lasers, Vertical-Cavity Surface-Emitting Lasers and Fabry-Perot Lasers.

List of Figures

κ_s	Vector of the Stokes wave
λ_p	Wavelength of the pump wave
$\rho(z,t)$	Field of the acoustic phonons
ρ_0	Deviation in material density from its equilibrium value
ρ_{Mat}	Material density
σ	Standard deviation
τ_{disp}	Time delay due to dispersion effects
v_a	Speed of sound in material/ Velocity of the acoustic wave
φ_c	Phase of the carrier wave
φ_{LO}	Phase of the local wave
Φ_{NLSPM}	Phase shift due to self phase modulation
$\chi^{(3)}$	Third order nonlinear susceptibility
ω_a	Angular frequency of the acoustic wave
ω_c	Angular frequency of the carrier wave
ω_{IF}	Angular frequency of intermediate signal
ω_{LO}	Angular frequency of the local wave
ω_{mod}	Angular modulation frequency
ω_{opt}	Angular frequency of the optical signal
ω_p	Angular frequency of the pump wave
ω_{RF}	Angular frequency of the RF Signal
ω_s	Angular frequency of the Stokes wave
ω_{Smax}	Angular central frequency of the Stokes wave

P	Power
p	elasto-optic constant
P_0	Pump power
$P_{0(SRS)}$	Threshold of stimulated Raman scattering
P_{Het}	Power of the heterodyned signal
P_{mm}	Power of the mm-Wave Signal
PN_{HET}	Phase noise of the heterodyned signal
P_{NL}	nonlinear polarisation
PN_{Source}	Phase noise of the source (driving signal of the MZM)
P_{optPD}	Optocal power at the input of the photo detector
$P_{Penalty}$	Power penalty of the heterodyned signal due to chromatic dispersion
P^S_0	Brillouin threshold
P_{Sig}	Power of the signal wave
Q^*	*C*onjugate complex of Q
R	Resistor
$Resp$	Responsivity of the photo detector at 1550 nm [A/W]
t	Time
v_g	Group velocity
V_π	Voltage that has to be applied to a MZM to achieve a phase shift of π in one interference arm
z	Propagation direction
z_d	Distance
α	Attenuation
α_a	Attenuation of the acoustic wave
β	Adiabatic modulus of elasticity
γ	Nonlinear coefficient
γ_e	Electrostrictive coefficient
ε	Bias level of modulator
ε_0	Vacuum permittivity
θ	Angle between pump wave vector and Stokes wave vector
κ_a	Vector of the acoustic wave
κ_p	Vector of the pump wave

E_{P1}	First pump wave
E_{P2}	Second pump wave
E_S	Field of the Stokes wave (amplified sideband)
E_{S1}	First Stokes wave
E_{S2}	Second Stokes wave
F	Noise figure
f_a	Frequency of the acoustic wave
f_c	Carrier frequency
f_{LO}	Local laser frequency
f_m	Modulation frequency
f_p	Frequency of the pump wave
f_s	Frequency of the Stokes wave
g_B	Brillouin gain
g_{Bmax}	Maximum of the amplification factor (g_B)
I	Intensity
I^2_{pd}	Photo diode current
$I_{HET}(t)$	Heterodyned signal
$I_{HETAM}(t)$	Amplitude modulated heterodyned signal
$I_{HETFM}(t)$	Frequency modulated heterodyned signal
I_p	Intensity of the pump wave
I_{pd}	Photo diode current
I_s	Intensity of the Stokes wave
$I_s(0)$	Intensity of the Stokes wave at the fibre input
k	Order of sideband
K_B	Polarisation dependency factor between pump and Stokes wave
L	Length
l	Maximum dimension of an antenna
L_{coh}	Coherence length
L_{eff}	Effective length
L_{Res}	Resonator length
M_2	Elasto-optical figure of merit
n_{eff}	refractive index
n_L	Group refractive index

List of Symbols

*	Conjugated complex
$\Delta(\omega/\varphi)_{mod}$	Frequency/ phase deviation of the modulation signal
$\Delta E(t)$	Amplitude noise
Δf	Frequency separation
Δf_a	Line width of the Stokes wave
Δk	Phase mismatch factor
Δk_{eI}	Imaginary part of the phase mismatch term
Δk_{eR}	Real part of the phase mismatch term
ΔP_{PLD}	Pump power alternation
Δ_T	Transverse component of the Laplace operator
$\Delta \nu_{mod}$	Spectral bandwidth of the modulation signal
$\Delta \nu_{opt}$	Spectral bandwidth of the optical signal
$\Delta \nu_{SB}$	Spectral bandwidth of the sideband
$\Delta\varphi(t)$	Phase noise
$\Delta\varphi_{mod}(t)$	Phase noise of the modulation signal
$\Delta\varphi_{opt}(t)$	Phase noise of the optical signal
a	Drive level of modulator
A_{eff}	Effective core area
AFR	Attenuation due to frequency response of the photodetector
c	Speed of light in the fibre
c_0	Speed of light in vaccum
D	Dispersion parameter
$E(z,t)$	Electrical field in the fibre; abbr.: E
E^*	*C*onjugate complex of E
$E_{AM}(t)$	Amplitude modulated Signal
E_c	Magnitude of the carrier wave
$E_{HET}(t)$	Heterodyned signal as a function of time
E_{LO}	Magnitude of the local wave
$E_{modAM}(t)$	Modulation signal for amplitude modulation
$E_{modPFM}(t)$	Modulation signal for phase/frequency modulation
E_P	Field of the pump wave

Table of Contents

PD	Photo Detector
PDF	Probability Density Function
PIN	Positive Intrinsic Negative
PML	Passive Mode Locking
POW	Power Meter
PRBS	Pseudo Random Binary Sequence
QPSK	Quadrature Phase Shift Keying
RACE	Research in Advanced Communications in Europe
RADAR	Radio Detection and Ranging
RAU	Remote Antenna Unit
RBW	Resolution Bandwidth
RBW	Resolution Bandwidth
RF	Radio Frequency
RHD	Remote Heterodyne Detection
RNC	Radio Node Control
SBS	Stimulated Brillouin Scattering
SEN	Spontaneous Emission Noise
SNR	Signal to Noise Ratio
SPM	Self Phase Modulation
SSB	Single Sideband Modulation
SSMF	Standard Single Mode Fibre
SVEA	Slowly Varying Envelope Approximation
TV	Television
TWT	Travelling Wave Tubes
UHF	Ultra High Frequency
UMTS	Universal Mobile Telecommunication System
VBW	Video Bandwidth
VHF	Very High Frequency
WDM	Wavelength Division Multiplex
WiMAX	Worldwide Interoperability for Microwave Access
WLAN	Wireless Local Area Network
XPM	Cross Phase Modulation
YIG	Yttrium-Iron-Garnet

FWM	Four Wave Mixing
GPIB	General Purpose Interface Bus
GPRS	General Packet Radio Service
GSM	Global System for Mobile Communications
HEMT	High Electron Mobility Transistor
HFR	Hybrid Fibre Radio
HIPERACCESS	High Performance Radio Access
HNLF	Highly Non-Linear Fibre
HSCSD	High Speed Circuit Switched Data
IMPATT	Impact Ionisation Avalanche Transit Time Diode
IP	Internet Protocol
LD	Laser Diode
LMCS	Local Multipoint Communication Service
LMDS	Local Multipoint Distribution Service
LOS	Line of Sight
MASER	Microwave Amplification by Stimulated Emission of Radiation
mmW	Millimetre Waves
mmWP	Millimetre Wave Photonic
MU	Mobile Unit
MVDS	Microwave Video Distribution System
mW	Micro Waves
mWP	Micro Wave Photonic
MZM	Mach Zehnder Modulator
NA	Numerical Aperture
NRZ	Non Return to Zero
NSE	Nonlinear Schrödinger Equation
NT	Network Terminal
O/E	Optic/Electronic
OFDM	Orthogonal Frequency Division Multiplex
OP	Operation Point
OPLL	Optical Phase Locked Loop
OSA	Optical Spectrum Analyser
OSSB	Optical Single Sideband

List of Abbreviations

AML	Active Mode Locking
ASEN	Amplified Spontaneous Emission Noise
ASK	Amplitude Shift Keying
ATM	Asynchronous Transfer Mode
BB	Base Band
BER	Bit Error Rate
BERT	Bit Error Rate Tester
BPSK	Binary Phase Shift Keying
BRAN	Broadband Radio Access Networks
BVC	Boundary Value Condition
C	Circulator
c.c.	Conjugate Complex
CS	Central Station
CW	Continuous Wave
DC	Direct Current
DCF	Dispersion Compensating Fibre
DECT	Digital European Cordless Telecommunications Standard
DES	Differential Equation System
DFB	Distributed Feedback
DSF	Dispersion Shifted Fibres
DSSC	Double Sideband Suppressed Carrier
DVB	Digital Video Broadcasting
EAM	Electro Absorption Modulators
EDFA	Erbium Doped Fibre Amplifier
EDGE	Enhanced Data Rates for Global Evolution
EHF	Extremely High Frequencies
ESA	Electrical Spectrum Analyser
ETSI	European Telecommunications Standards Institute
FBG	Fibre Bragg Grating
FM	Frequency Modulation
FWHM	Full Width at Half Maximum

Acknowledgements

First, I would like to thank my supervisor Prof. Dr. Thomas Schneider from the Hochschule für Telekommunikation, Leipzig for his inspiration to begin work on Ph.D., and for his support and help throughout. His advice and guidance was invaluable on many occasions.

Furthermore, I wish to express my gratitude to my supervisors Dr. Max Ammann, Dr. Andreas Schwarzbacher and Dr. Gerry Farrell from the School of Electronics and Communications Engineering at the Dublin Institute of Technology, for their support, and for the opportunity to work on the Ph.D..

I would also like to thank my colleagues from HfT Leipzig for all of the support that I received. They have been instrumental in providing access to building equipment, in conducting measurements and calculations, in providing explanations and reviews, and in technical discussions. I am indebted to Kai-Uwe Lauterbach, Ronny Henker, Jens Klinger, Andrzej Wiatrek and Steffen Neidhardt.

Additionally, I would like to thank the members of the academic administration of HfT Leipzig and the Deutsche Telekom AG for financial support.

I would also like to thank the research team of Prof. Dr. Ing. Schäffer of the Technical University Dresden for the use of technical equipment and for fruitful discussions.

Special thanks go to James Poborsa from the University of Toronto, who has read a major part of the dissertation and provided his comments and suggestions regarding the English translation.

Finally, I wish to thank Heidi, Clara and my parents for the moral support they have given me over the years.

Declaration

I certify that this thesis which I now submit for examination for the award of PhD, is entirely my own work and has not been taken from the work of others save and to the extent that such work has been cited and acknowledged within the text of my work.

This thesis was prepared according to the regulations for postgraduate study by research of the Dublin Institute of Technology and has not been submitted in whole or in part for an award in any other Institute or University.

The work reported on in this thesis conforms to the principles and requirements of the Institute's guidelines for ethics in research.

Signature _____ Date _____

Abstract

The rising demand for greater bandwidth and increased flexibility in modern telecommunication systems has lead to increased research activities in the field of Millimetre Wave-Photonics. The combination of an optical access network and the radio propagation of high data-rate signals provides a solution to meet these demands. Such structures are also known as Radio Over Fibre systems. They implement the optical Millimetre Wave generation in a central station and the transmission of radio waves via a remote antenna unit to the radio cell. The expected data rate is very high, due to the fact that both the optical and the radio-link provide a large transmission bandwidth.

This dissertation concerns the investigation of a new and simple method for the flexible generation of Millimetre Waves for application in Radio Over Fibre systems. The method is based on the heterodyne detection of two optical waves in a photo detector. By externally amplitude modulating the optical wave, different sidebands are generated. Two of these sidebands are selected and amplified by the non-linear effect of stimulated Brillouin scattering. As a gain medium, a standard single mode fibre is used.

According to the theoretical investigation, very good carrier performances are possible with this method, and a computer simulation shows little degradation to the signals during their propagation in the system. The measured results are in strong agreement with the theoretical analysis. Experimental results show that the system can be fully utilised as a Radio Over Fibre system.

The thesis is divided into five main parts: Introduction – Theory – Simulation – Experiment – Conclusion. In the Introduction, an overview of the current methods of Millimetre Wave generation, Radio Over Fibre and the nonlinear effect of Brillouin scattering is given. In the theoretical section, a differential equation system which mathematically describes the system is derived and also solved numerically. With a proof of the concept set-up, the simulated results are compared with the experimental data. In the last section the work is concluded and future tasks are discussed.

Investigation of Millimetre Wave Generation by Stimulated Brillouin Scattering for Radio Over Fibre Applications

Markus Junker Dipl. Ing. (FH)

Dissertation submitted in fulfilment of the requirements for candidature of the degree of

Doctor of Philosophy

Dublin Institute of Technology

Supervisors: Dr. Max J. Ammann, Prof. Dr. Thomas Schneider,

Dr. Andreas T. Schwarzbacher

School of Electronic & Communications Engineering

September 2008